THE ROLE OF A CONSERVED DNA-BINDING PROTEIN IN PRECISE POSITIONING OF THE POLAR SEPTUM DURING *BACILLUS SUBTILIS* SPORULATION

A Dissertation

by

ALLYSSA KERSTIN MILLER

Submitted to the Office of Graduate and Professional Studies of
Texas A&M University
in partial fulfillment of the requirements for the degree of

DOCTOR OF PHILOSOPHY

Chair of Committee,	Jennifer K. Herman
Co-Chair of Committee,	Paul D. Straight
Committee Members,	Sarah E. Bondos
	Jim C. Hu
Chair of Interdisciplinary Faculty,	David W. Threadgill

August 2019

Major Subject: Genetics

ABSTRACT

Bacterial chromosomes are compacted in the cytoplasm into a membrane-less structure called the nucleoid. The nucleoid is condensed and organized by a number of DNA-binding proteins that work in concert to establish its overall 3D structure. Some proteins exploit this spatial organization to localize their activities to specific subcellular regions. In this study, we focused on a developmentally-regulated DNA-binding protein, RefZ (Regulator of FtsZ), and its role in tuning septum placement during sporulation in the model bacterium, *Bacillus subtilis*.

In response to starvation, *B. subtilis* initiate a developmental program called sporulation, during which the cell division protein, FtsZ, is redeployed from midcell to a polar position. Septation then occurs over one of the cell's two chromosomes, generating a transient period of genetic asymmetry critical for sporulation. Artificial expression of *refZ* during growth disrupts FtsZ-ring assembly and blocks cell division, and during sporulation, *refZ* mutants are delayed in Z-ring shifting. We demonstrate that artificial expression of a RefZ homolog also blocks cell division, indicating that this function is conserved in other *Bacillus* species.

RefZ binds five sites, *RBM*s, arranged symmetric about the chromosomal origin. The outermost sites on the left and right chromosome arms lie at the boundary of the region reproducibly captured by the sporulation septum. In addition to the *refZ* gene, we show the position of the *RBM*s on the chromosome is also conserved across the *Bacillus* genus. Using a single cell-based fluorescence trapping assay, we find that RefZ and the

*RBM*s are required for precise capture of the chromosome in the future spore compartment.

To delineate the role of RefZ's division regulation function in chromosome capture, we performed a genetic selection-screen to isolate RefZ variants loss-of-function for inhibiting division. Analysis of the variants using our trapping assay indicates that RefZ's role in chromosome capture is mediated through modulation of cell division. In addition, we find that RefZ acts redundantly with the nucleoid occlusion protein, Noc, to prevent aberrant midcell divisions during sporulation. We propose RefZ acts as a developmentally-regulated nucleoid occlusion protein, helping to maintain the fidelity of division site selection in the early stages of sporulation.

DEDICATION

I dedicate this thesis to the late Michael Wayne Vogel, the most extraordinary human being one could ever have the honor to know and love. Thank you for bringing me to College Station and continually inspiring me from beyond to live my best life. I love you always.

ACKNOWLEDGEMENTS

I would like to thank my committee chair, Dr. Jen Herman, my committee co-chair, Dr. Paul Straight, and my committee members, Dr. Jim Hu and Dr. Sarah Bondos for their remarkable patience, guidance and support throughout the course of this research.

To my advisor Jen, thank you for believing in me enough to invest the resources and time needed to take me on a graduate student with such notice. You took a leap of faith and I can only hope that I have made you proud and glad you chose to bring me on.

To my friends old and new, near and far, you have always been family and not a day passed during my graduate career that I did not think of each of you. You were and will always be the light when my world dims.

To my incredible parents, Kelly and Karl, I dedicate my doctorate; you deserve it as much as I do. Your belief in my abilities and unconditional love and support over the last ten years is the only reason I have come this far. I owe everything to you, and I love you.

CONTRIBUTORS AND FUNDING SOURCES

This work was supervised by a dissertation committee consisting of Dr. Jennifer Herman [Graduate advisor and Chair of Committee] and Dr. Paul Straight [Co-chair of Committee] and Dr. Jim Hu [Committee Member] of the Department of Biochemistry and Biophysics, and Dr. Sarah Bondos [Committee Member] of the Department of Molecular and Cellular Medicine.

The work presented in Chapter II was published in print January 2016 in Molecular Microbiology (Vol 99 Issue 1, p111-122) and was done in collaboration with Emily E. Brown and Benjamin T. Mercado both former members of Jennifer Herman's lab. EMSA experiments characterizing the interaction between purified RefZ-His6 or SUMO-RefZ and the *RBM*s (Figure II.3, II.4, and II.5) were done by Emily E. Brown. Bioinformatics analyses as outlined in APPENDIX A Methods A.3 and as presented in Figures II.1C, II.1D, and APPENDIX A Figure A.1, and construction of the RBM_{5mu} mutant strain was performed by Benjamin T. Mercado. I am responsible for the work presented in Figures II.2, II.6, II.7, II.8, and II.9. Additional contributors: Yves Brun (IU, Department of Biology), Jim Hu, Craig Kaplan, and Ry Young (TAMU, Department of Biochemistry and Biophysics) for critical reading of the manuscript; David Rudner (HMS, Microbiology) and Xindan Wang (IU, Department of Biology) for providing FROS strains; Larry Mulcahy for making the original observation of a chromosome organization defect; Incheol Yeo (TAMU, former rotation student) for making strains and performing initial trapping experiments; Larry Dangott and the

Protein Chemistry Lab (TAMU) for helpful advice regarding protein purification; and the Texas A&M Center for Phage Technology.

The work presented in Chapter III was published in print July 2019 in Journal of Bacteriology (Vol 201, Issue 16, e00287-19) in collaboration with Emily E. Brown and Ryan M. Otto (undergraduate researcher) of Jennifer Herman's lab, and Dr. Inna V. Krieger and Dr. James C. Sacchettini of the Sacchettini lab (TAMU, Department of Biochemistry and Biophysics). Solution and refinement of the RefZ crystal structure was performed by Dr. Inna V. Krieger and Dr. James C. Sacchettini. RefZ protein crystallization and generation of structure images (Figure III.3, III.4, III.5, III.6), EMSA (Figure III.8, III.9A), size-exclusion chromatography (Figure III.11A, III.12), and differential scanning fluorimetry (Figure III.13) was performed by Emily E. Brown. rLOF variant protein purifications (Figure III.7) and Bio-layer Interferometry experiments (Figure III.8, inset table and III.9C) was performed by Ryan M. Otto and Emily E. Brown. I am responsible for the work presented in Figures III.1, III.2, III.10B, III.11B, III.11C, and III.13 and Table III.1. Additional contributors: Larry Dangott and the Protein Chemistry Lab (TAMU) for helpful advice regarding protein purification; Ann Tran (former undergraduate researcher) for her efforts toward constructing B2H plasmids and quantifying rLOF trapping data; and members of the Herman Lab for critical reading of the manuscript.

The work presented in Chapter IV was done in collaboration with Krithika Kumar (a former post-doctoral researcher). Krithika Kumar is responsible for the quantitation and imaging in Figure IV.5A. I performed the experiments described in

Figure IV.1, IV.2, IV.3. IV.4, IV.5B, IV.6, IV.7, IV.8, and IV.10, as well as the work presented in Chapter V.

This work was supported in part by start-up funding to Jennifer Herman from the Department of Biochemistry and Biophysics (02-248312) and by a grant from the National Science Foundation (Award #1514629).

TABLE OF CONTENTS

Page

LIST OF FIGURES

Page

LIST OF TABLES

Page

CHAPTER I

INTRODUCTION

I.1 BACTERIAL REPRODUCTION

Like all living organisms, bacteria propagate by transmitting copies of their genetic material to progeny. Most bacteria store genetic information in the form of a single, circular chromosome of double-stranded DNA (dsDNA) and reproduce by binary fission at the end of a cell cycle. Progression through one cell cycle entails three fundamental processes: 1) copying of the genetic material (DNA replication), 2) separation of the copied material to opposite cell halves (chromosome segregation), and 3) generation of two genetically and cytologically identical daughter cells by binary fission (cell division). Failure in any of these processes can significantly impair reproductive capacity and be detrimental to a species' survival, especially in environments where resources are scarce, or in those populated by multiple species in competition for resources, such as the human gut (Selber-Hnatiw *et al.*, 2017).

In order to fit inside a typical bacterial cell (1-3 μm) the circular chromosome is condensed nearly 1,000 times it's length into a membrane-less structure called the nucleoid (Holmes & Cozzarelli, 2000). For many bacteria, cell growth occurs prior to division and simultaneous with DNA replication and chromosome segregation. Growth occurs at the cell envelope, which is composed of a cytoplasmic membrane surrounded by a cell wall composed of peptidoglycan (PG). The layer of PG acts as a rigid, lattice-like structure around the cell that helps maintain shape and protect the cell from osmotic

lysis (Young, 2006). The thickness of the PG within the cell wall depends on the bacterium; most Gram-negatives have a single, thin PG layer ranging between 1-10 nm, whereas Gram-positives have much a thicker, multi-layered PG component ranging anywhere from 20-50 nm (Egan & Vollmer, 2013). Cell envelopes can additionally contain variable outer layers, such as an outer membrane (Gram-negatives), teichoic acids (many Gram-positives), and capsules (Silhavy *et al.*, 2010).

With some notable exceptions (Murat *et al.*, 2010, Wagstaff & Lowe, 2018), bacteria lack the internal compartmentalization and true cytoskeletal structures of their eukaryotic counterparts. However, essential processes governing survival are still spatially organized at the subcellular level. The wealth of data acquired over the last five decades from research in prokaryotic model systems has significantly contributed to our understanding of the mechanisms by which bacterial cells transmit spatio-temporal cues between cell cycle processes. Current evidence indicate that bacteria rely extensively on the two largest structures in the cell, the cell envelope and the nucleoid, to localize and spatially regulate cellular processes.

I.1.1 Cell wall dynamics during reproduction

Architectural variations in the PG component of the cell wall are responsible for dictating a bacterium's shape (Young, 2006). In rod-shaped bacteria like the model Gram-positive bacterium, *Bacillus subtilis*, and the model Gram-negative bacterium, *Escherichia coli*, reproduction occurs through alternating rounds of cell elongation and cell division, during which the cell wall is remodeled by the removal of old PG to permit

incorporation of newly synthesized cell wall material (Park & Uehara, 2008). PG is composed of linear chains of glycan comprised of repeating disaccharide units of β-(1,4)-linked *N*-acetylglucosamine and *N*-acetylmuramic acid with an attached amino acid pentapeptide side-chain [NAG-(NAM-peptide)]. In rod-shaped cells, glycan strands lie parallel to the cell surface and run circumferentially around the cylinder. Cross-linking between NAM-associated peptides of adjacent strands forms a mesh-like structure that surrounds the cytoplasmic membrane.

Numerous enzymes with specialized functions are required to synthesize and remodel PG. New PG is synthesized from Lipid II, a precursor molecule of the [NAG-(NAM-peptide)] unit that contains an attached lipid moiety (Egan & Vollmer, 2013). Lipid II is synthesized in the cytoplasm in a multi-step process before becoming flipped across the cytoplasmic membrane, where it is incorporated into a growing peptidoglycan strand by transglycosylases (Egan & Vollmer, 2013). Nascent peptidoglycan strands are incorporated into the pre-existing PG layer nearest the membrane by transpeptidases which facilitate cross-linking between the pentapeptide chains of neighboring strands. Transglycosylation and transpeptidation reactions are catalyzed by different classes of enzymes called PBPs (Penicillin Binding Proteins), some of which are capable of performing both reactions. Various autolysins and hydrolases act upstream of insertion to remodel PG, by breaking cross-links between pentapeptides, cleaving bonds within the pentapeptide, hydrolyzing within the glycan strand, or cleaving bonds between NAM residues and the associated pentapeptide (Egan & Vollmer, 2013).

During cell elongation, these enzymes are directed to the lateral walls of the cylinder as part of a multi-protein complex called the elongasome, where they direct incorporation of PG along the long axis of the cell (van Teeffelen & Renner, 2018). During division, many of these enzymes are redirected to the division site as part of a second multi-protein complex, called the divisome, where they direct PG synthesis along the short axis of the cell at the "septum" that will eventually separate the two daughter cells (van Teeffelen & Renner, 2018). The elongasome and divisome also include one or more homologs of the eukaryotic cytoskeletal proteins, actin and tubulin, that act to recruit and scaffold PG synthesis enzymes and accessory proteins (Carballido-Lopez, 2006, Jones *et al.*, 2001, van den Ent *et al.*, 2001).

I.1.1.1 Cell elongation

MreB family proteins, the predominant homologs of eukaryotic actin, are well conserved across bacteria, especially in those with rod-shapes, and play critical roles in cell shape determination (Carballido-Lopez, 2006). MreB polymerizes in an ATP-dependent manner at the membrane into anti-parallel filaments that associate with the cell wall synthesis machinery to form the elongasome, which moves dynamically around the cell circumference (Dominguez-Escobar *et al.*, 2011, Garner *et al.*, 2011, van Teeffelen *et al.*, 2011). The rod-shape is maintained as new cell wall is inserted into the lateral walls as the elongasome tracks around the cell circumference (Chang & Huang, 2014, Garner *et al.*, 2011).

Directional movement of the elongasome is dependent on the orientation of MreB filaments (Hussain et al., 2018). In *E. coli*, MreB filament orientation is influenced by the width of the rod portion of the cell (Ouzounov *et al.*, 2016), while in *B. subtilis*, orientation is stable over a range of widths and is instead dictated by the dominant curvature of the membrane along the rod circumference (Hussain *et al.*, 2018, Ursell *et al.*, 2014). In this way, the rod-shape itself is both sensed and reinforced by MreB filaments, which orient the direction of elongasome movement along the circumference, stabilizing the rod-shape as new cell wall is inserted (Hussain *et al.*, 2018).

I.1.1.2 Cell division

Division in most rod-shaped bacteria occurs at midcell, between replicated chromosomes, to ensure each progeny cell inherits a complete copy of the genome. Assembly of the divisome in *E. coli* and *B. subtilis* is a two-step process initiated by the localization and polymerization of the bacterial tubulin homolog, FtsZ, to the future site of division (Aarsman *et al.*, 2005, Gamba *et al.*, 2009). FtsZ is a self-assembling GTPase that polymerizes as protofilaments which become tethered to the cell envelope by the membrane-anchoring protein, FtsA (Pichoff & Lutkenhaus, 2005). FtsA is an actin homolog that also self-assembles into actin-like protofilaments using ATP hydrolysis (Pichoff & Lutkenhaus, 2005, Pichoff & Lutkenhaus, 2007, Szwedziak *et al.*, 2012). Together, FtsA and FtsZ co-localize as dynamic structures throughout the membrane (Loose & Mitchison, 2014).

Similar to MreB filament movement, FtsZ protofilaments move dynamically around the cell circumference at the incipient division site in a large ring-like structure called the Z-ring. Movement is generated by filament treadmilling, in which FtsZ filaments are depolymerized into monomers at one end, with incorporation into the filament by polymerization at the other end. Treadmilling is dependent on the rate of GTP hydrolysis, which is required to stimulate polymerization (Bisson-Filho *et al.*, 2017, Mukherjee & Lutkenhaus, 1998, Yang *et al.*, 2017). Independently treadmilling protofilaments, when associated with each other through lateral interactions as well the membrane, drive the net inward constriction of the Z-ring and with it, the cell membrane and PG synthases required for constructing the septal cell wall (Bisson-Filho *et al.*, 2017, Lan *et al.*, 2009, Yang *et al.*, 2017).

In addition to FtsAZ, early division components are recruited to the site of division through direct association with FtsZ, including the broadly conserved ZapA (Gueiros-Filho & Losick, 2002), SepF and EzrA in Gram-positives (Haeusser *et al.*, 2004, Hamoen *et al.*, 2006, Ishikawa *et al.*, 2006, Singh *et al.*, 2007), and ZipA in γ-proteobacteria (Hale & de Boer, 1997). These proteins associate with the cell membrane and function to promote or stabilize lateral interactions between protofilaments, also known as bundling, or to regulate FtsZ polymerization dynamics. Together with FtsA, the early division proteins facilitate assembly of the Z-ring and recruitment of late divisome proteins required for synthesis and separation of the septal cell wall (Aarsman *et al.*, 2005, Errington & Wu, 2017, Gamba *et al.*, 2009).

ZapA is highly conserved across prokaryotes and acts as a positive regulator of Z-ring formation by promoting both polymerization of FtsZ and lateral interaction of protofilaments (Gueiros-Filho & Losick, 2002, Monahan *et al.*, 2009). SepF forms large polymer rings that promote protofilament bundling *in vitro* and is conditionally essential as a membrane anchor for FtsZ filaments in the absence of FtsA (Duman *et al.*, 2013, Gundogdu *et al.*, 2011, Hamoen *et al.*, 2006, Ishikawa *et al.*, 2006). EzrA in Gram-positive bacteria like *B. subtilis*, and ZipA in Gram-negative bacteria such as *E. coli* harbor transmembrane domains and share structural homology with the eukaryotic Spectrin family of cytoskeletal proteins, which join together actin filaments, and the actin cytoskeleton to integral membrane proteins (Cleverley & Lewis, 2015, Cleverley *et al.*, 2014, Errington & Wu, 2017, Hale & de Boer, 1997). ZipA associates with FtsA, and is essential in *E. coli* for septum formation (Hale & de Boer, 1997, Vega & Margolin, 2019), whereas EzrA is only conditionally essential in the absence of ZapA, SepF, or the late-stage division protein, GpsB (Claessen *et al.*, 2008, Gueiros-Filho & Losick, 2002, Hamoen *et al.*, 2006).

EzrA has been characterized as both a negative and a positive regulator of cell division. Mutants lacking *ezrA* exhibit *e*xtra *z*-*r*ings at the poles and at midcell, a phenotype for which it is named (Levin *et al.*, 1999). While EzrA inhibits formation of FtsZ protofilaments, it is unable to depolymerize pre-formed filaments and, as a result, raises the critical concentration of FtsZ polymers needed to assemble a Z-ring (Haeusser *et al.*, 2004). This critical concentration is reduced in the absence of EzrA, permitting Z-rings to assemble at multiple sites within the cell (Haeusser *et al.*, 2004, Levin *et al.*,

1999, Singh *et al.*, 2007). *ezrA* mutants are longer due to the delay in cell division caused by the formation of multiple Z-rings (Kawai & Ogasawara, 2006), but are also thinner due to loss of EzrA's second function in directing PG synthesis to the septal wall (Claessen et al., 2008).

EzrA and GpsB play partially redundant roles in regulating the shuttling of the major transpeptidases/transglycosylase PG sythetase, PBP1, between the elongasome and divisome (Claessen *et al.*, 2008). PBP1 is a late divisome protein required for both lateral and septal cell wall synthesis (Claessen *et al.*, 2008, Scheffers & Errington, 2004) and its efficient and timely localization to both sites during the cell cycle is essential for maintaining the integrity of the rod shape. EzrA recruits PBP1 to the site of division, while GpsB facilitates its removal and subsequent re-localization to the elongasome following septal wall synthesis and maturation of the new cells poles (Claessen *et al.*, 2008).

Recruitment of remaining late division proteins in *B. subtilis*, FtsL, DivIB, DivIC, and Pbp2b to the division site is interdependent (Gamba *et al.*, 2009). In *E. coli*, recruitment of late division proteins FtsK, FtsQ (like *B. subtilis* DivIB), FtsL, FtsB (like *B. subtilis* DivIC), FtsW, FtsI, and FtsN occurs in a hierarchal manner (Aarsman *et al.*, 2005). Finally, accessory proteins not considered part of the core divisome localize to the septum, including those of the Min system (DivIVA, MinJ, MinD, MinC), which inhibits Z-ring and divisome assembly at sites immediately adjacent to the newly formed septum (Figure I.1), as well as proteins required for resolving and segregating chromosome termini during the final stages of replication.

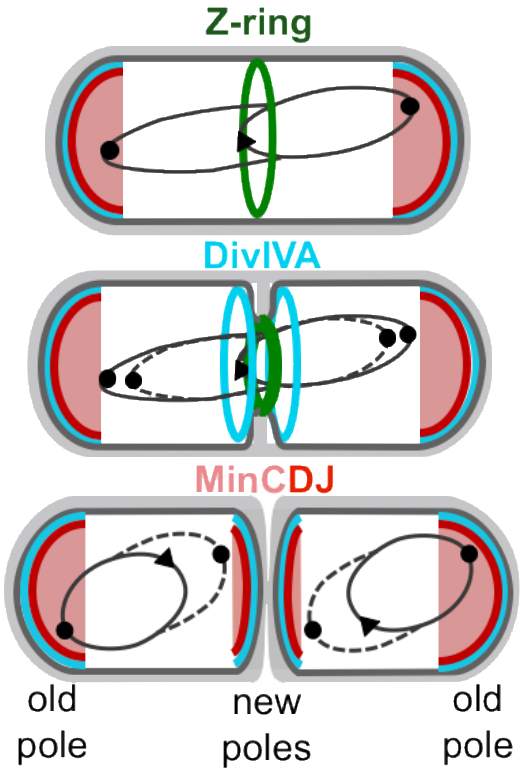

Figure I.1 The Min system prevents cell division in the nucleoid free polar regions in rod-shaped bacteria. The Min system (MinCDJ and DivIVA) are localized on either side of the nascent division septum which become new poles of the resulting cells. The MinC protein (pink) inhibits FtsZ, preventing Z-rings from assembling at the poles.

I.1.2 Nucleoid dynamics during reproduction

The structure of the nucleoid is largely defined by the geometry, or shape, of the cell, and can adopt alternative conformations that reflect the cell's response to changing growth conditions, such as fluctuations in nutrient availability (Dorman, 2014, Kim *et al.*, 2004, Sobetzko *et al.*, 2012). Nucleoids can occupy different volumes within the cell, for instance, in the crescent-shaped bacterium, *Caulobacter crescentus*, the nucleoid occupies a much larger portion of the cytoplasmic volume compared to the rod-shaped

bacteria, *B. subtilis* and *E. coli*, in which the nucleoid occupies a more central portion of the cell and is generally restricted from the cell poles (Surovtsev & Jacobs-Wagner, 2018). Bacterial nucleoids in some rod-shaped species have been observed to adopt a largely helical structure, which may reflect the most energetically favorable conformation for DNA in cells of this particular shape (Berlatzky *et al.*, 2008, Butan *et al.*, 2011, Fisher *et al.*, 2013).

I.1.2.2 Nucleoid structure

The circular bacterial chromosome is composed of double-stranded helical DNA that is maintained in a negatively supercoiled state by the action of enzymes called topoisomerases. Processes that unwind duplex DNA, including transcription, DNA replication, and recombination (Liu & Wang, 1987, Postow *et al.*, 2004, Wu *et al.*, 1988), impart mechanical forces on the chromosome by altering local DNA topology. Progressive movement of the transcription and replication machinery on single, unwound strands introduces positive supercoiling ahead of the complexes while compensatory negative supercoiling occurs behind the complexes.

DNA topoisomerases induce or relieve superhelicity by introducing temporary single or double-stranded breaks in the phosphodiester backbone to counteract the torsional strain generated on under- or over-wound DNA (Bush *et al.*, 2015, Vos *et al.*, 2011). The type IIA topoisomerases, like DNA gyrase, make double-stranded breaks to relieve positive supercoiling, while the type I topoisomerases, like TopA, remove negative supercoils (Cozzarelli, 1980, Khodursky *et al.*, 2000, Levine *et al.*, 1998,

Wang, 1991). Positive supercoils must be removed in order to prevent stalling and dissociation of the transcription and replication complexes, whereas removal of negative supercoils is important for preventing formation precantanes that, left unresolved, result to chromosome dimers.

Physical forces

In the confines of the cell, a combination of physical, electrostatic, and mechanical forces that act on and within the DNA macromolecule facilitate compaction of the chromosome into a highly organized nucleoid structure. The individual contributions of these forces can be best appreciated when considering the supercoiled chromosome as a negatively charged, flexible polymer which readily assumes conformations that maximize the available degrees of freedom within its segments (Surovtsev & Jacobs-Wagner, 2018). Supercoiling induces the formation branched superhelical segments called plectonemes, similar to the way a coiled telephone cord behaves when over-wound (Figure I.2) (Lin *et al.*, 1998, Surovtsev & Jacobs-Wagner, 2018). The cytosol contains large amounts of crowding agents, like globular, non-DNA binding proteins and RNA, that exert repulsive forces on the DNA polymer (Cunha *et al.*, 2001, de Vries, 2010, Murphy & Zimmerman, 1995, Odijk, 1998). Macromolecular crowding collapses loops in the DNA polymer through excluded volume effects, effectively concentrating the DNA and cytosol into separate phases (de Vries, 2001, Odijk, 1998) (Asakura & Oosawa, 1954). Phase separation is enhanced by multivalent cations and abundant non-globular, Nucleoid Associated Proteins, or NAPs, that mitigate

repulsive forces between polymer segments by partially neutralizing the net charge of the DNA (Bloomfield, 1997, de Vries, 2010).

Nucleoid-associated proteins (NAPs)

NAP contribution to nucleoid structure is two-fold: in addition to suppressing negative charges throughout the chromosome, they also generate mechanical forces that impact local DNA topology and superhelicity by bending, bridging, or wrapping segments of the chromosome (Figure I.2) (Badrinarayanan *et al.*, 2015). NAPs are small DNA-binding proteins that bind fairly non-specifically throughout the nucleoid. The abundance of NAPs is dependent on growth phase which accounts for the conformational changes observed in the nucleoid structure from one phase to another (Ali Azam *et al.*, 1999, Dorman, 2014, Hadizadeh Yazdi *et al.*, 2012).

NAPs that bend DNA segments, such as IHF and Fis, drastically alter local chromosome structure and influence DNA replication and recombination (Badrinarayanan *et al.*, 2015). IHF (Integration Host Factor) can bend chromosome segments 160°, into nearly perfect U-shapes that promote loop formation and alter gene expression by bringing transcription machinery in close proximity to otherwise distal regulatory proteins (Figure I.2) (Rice *et al.*, 1996).

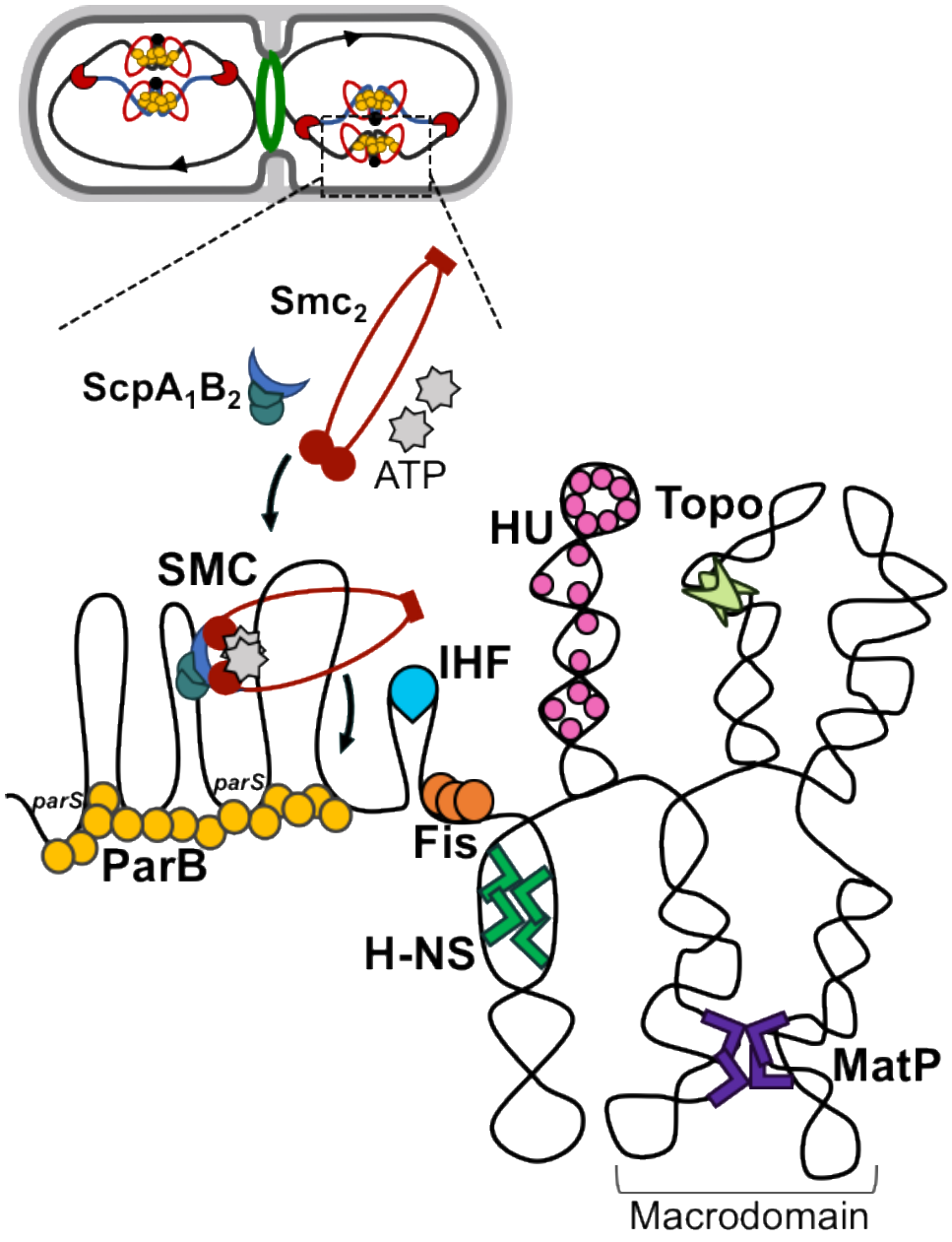

Figure I.2 Chromosome organization by various nucleoid-associated proteins.
NAPs (H-NS, Fis, IHF, HU) that bend, bridge, and wrap the chromosome contribute to chromosome condensation and are responsible for generating topological domains, called macrodomains. In *E. coli*, MatP bridges *matS* sites in the *ter* regions but can also bridge *ter* macrodomains between sister chromosomes. Topo refers to the various topoisomerases that cut single or double strands of duplex DNA to alleviate torsional strain generated by NAPs and cellular processes that constrain or alter the writhe of the duplex. SMC complexes also contribute to chromosome condensation by threading one or two strands of dsDNA through their loops, constraining and condensing chromosomes along their length. SMC dimers are loaded with the ScpAB sub-complex in an ATP-dependent and ParB (Spo0J) dependent manner. ParB also influences chromosome topology by binding and nucleating on DNA at *parS* sites, forming large loops in the DNA required for SMC loading.

Fis (Factor for inversion stimulation) is one of the most abundant proteins in fast-growing *E. coli* cells and forms stable nucleoprotein complexes at AT-rich sequences (Ali Azam *et al.*, 1999, Stella *et al.*, 2010). Fis introduces less dramatic "kinks" of 50°-90°, sufficient enough to displace neighboring supercoils (Figure I.2) (Auner *et al.*, 2003, Stella *et al.*, 2010). The abundance, stability, and genome-wide distribution of Fis nucleoprotein complexes significantly influences global chromosome topology and a variety of DNA-related processes (Badrinarayanan *et al.*, 2015, Kahramanoglou *et al.*, 2011).

The small, ubiquitous HU is also a highly abundant NAP that coats nearly 10% of the *E. coli* chromosome and intercalates into the minor groove, creating sharp kinks in the DNA backbone that promotes negative supercoiling (Bensaid *et al.*, 1996, Kar *et al.*, 2005, Malik *et al.*, 1996). HU generates short-range interactions that potentially stabilize plectonemes (Figure 1.3), by wrapping itself with DNA, analogous to the function of eukaryotic histone proteins (Ali Azam *et al.*, 1999, Guo & Adhya, 2007, Prieto *et al.*, 2012).

NAPs like H-NS (Histone-like Nucleoid Structuring) play a significant role in altering the superhelicity by bridging DNA between distal plectonemic loops (Figure I.2). H-NS mutants tend to harbor chromosomes with reduced levels of negative supercoiling (Hardy & Cozzarelli, 2005). H-NS in *E. coli* can oligomerize and silence or repress gene expression in AT-rich sequences, regions that are often associated with foreign or horizontally acquired DNA sequences (Grainger *et al.*, 2006, Lucchini *et al.*, 2006, Oshima *et al.*, 2006, Singh *et al.*, 2014). In this way, NAPs like H-NS have a

significant impact both on the overall architecture and topology of the nucleoid and, consequently, have a substantial influence gene expression by controlling the accessibility of the transcription machinery to different chromosome segments (Browning *et al.*, 2010, Dillon & Dorman, 2010).

Notably, H-NS bridging activity also aids in the formation of isolated chromosome domains, called macrodomains. The position of macrodomains within the cell has been extensively characterized in *E. coli*, which has four macrodomains each roughly 1 Mb (1 million basepairs) in size: the Ori MD is centered around *oriC*, the Ter MD is centered on the replication terminus region, with the Left and Right MDs between them (Niki *et al.*, 2000, Valens *et al.*, 2004). More recently, the development of advanced chromosome capture techniques (i.e. HiC), fluorescent reporter-operator systems, and in situ hybridization (FISH) has allowed macrodomain scale chromosome organization to be probed for many species (Badrinarayanan *et al.*, 2015, Berlatzky *et al.*, 2008, Dupaigne *et al.*, 2012, Fisher *et al.*, 2013, Gruber & Errington, 2009, Lioy *et al.*, 2018, Montero Llopis *et al.*, 2010, Niki *et al.*, 2000, Ptacin & Shapiro, 2013, Sobetzko *et al.*, 2012, Sullivan *et al.*, 2009, Thiel *et al.*, 2012, Valens *et al.*, 2004, Wang *et al.*, 2017, Wang & Rudner, 2014). The results of these studies indicate that chromosomes remain highly organized within the cell despite the effect of continuous replication/segregation, transcription/translation, and global compaction. In fact, the well-ordered structures of chromosomes positions genes (loci) at distinct positions within the nucleoid such that their linear order is preserved (Ptacin & Shapiro, 2013, Sobetzko *et al.*, 2012).

I.1.2.3 Chromosome organization and segregation

In bacteria, DNA replication and chromosome segregation occur simultaneously, which helps ensures the chromosome remains organized and properly oriented within the cell prior to division. Faithful transmission of the genome requires a combination of proteins that organize, condense, and segregate chromosomes within the bulk of the nucleoid. Most bacteria employ a similar set of proteins to sequentially segregate chromosome segments during replication: bacterial SMC condensin/cohesin complexes, ParABS, and FtsK/SpoIIIE family DNA translocases (Gruber, 2018). The Par system is particularly important in initiating segregation of newly replicated sister origins as they exit the replisome (Figure I.3). Bacterial SMC complexes play a critical role in structuring the nucleoid by condensing large regions of the chromosome, and are particularly important for spatially resolving sister chromosomes as they exit the replisome (Figure I.3)(Wang *et al.*, 2017, Wang *et al.*, 2015). FtsK/SpoIIIE proteins segregate chromosome termini at the end of replication, and are especially critical for maintaining genome integrity when cells divide over un-replicated chromosomes.

Importantly, these systems are not mutually exclusive and typically overlap in function at different phases of segregation. For instance, ParB-*parS* functions to recruit SMC condensin complexes to newly replicated origins and together these systems are responsible for the ordered segregation of the bulk nucleoid and for maintaining chromosome organization within the cell (Gruber & Errington, 2009, Lee & Grossman, 2006, Sullivan *et al.*, 2009, Wang *et al.*, 2014). In fact, many bacteria that employ a Par system to segregate chromosome origins also use ParB-*parS* to localize SMC to *oriC*.

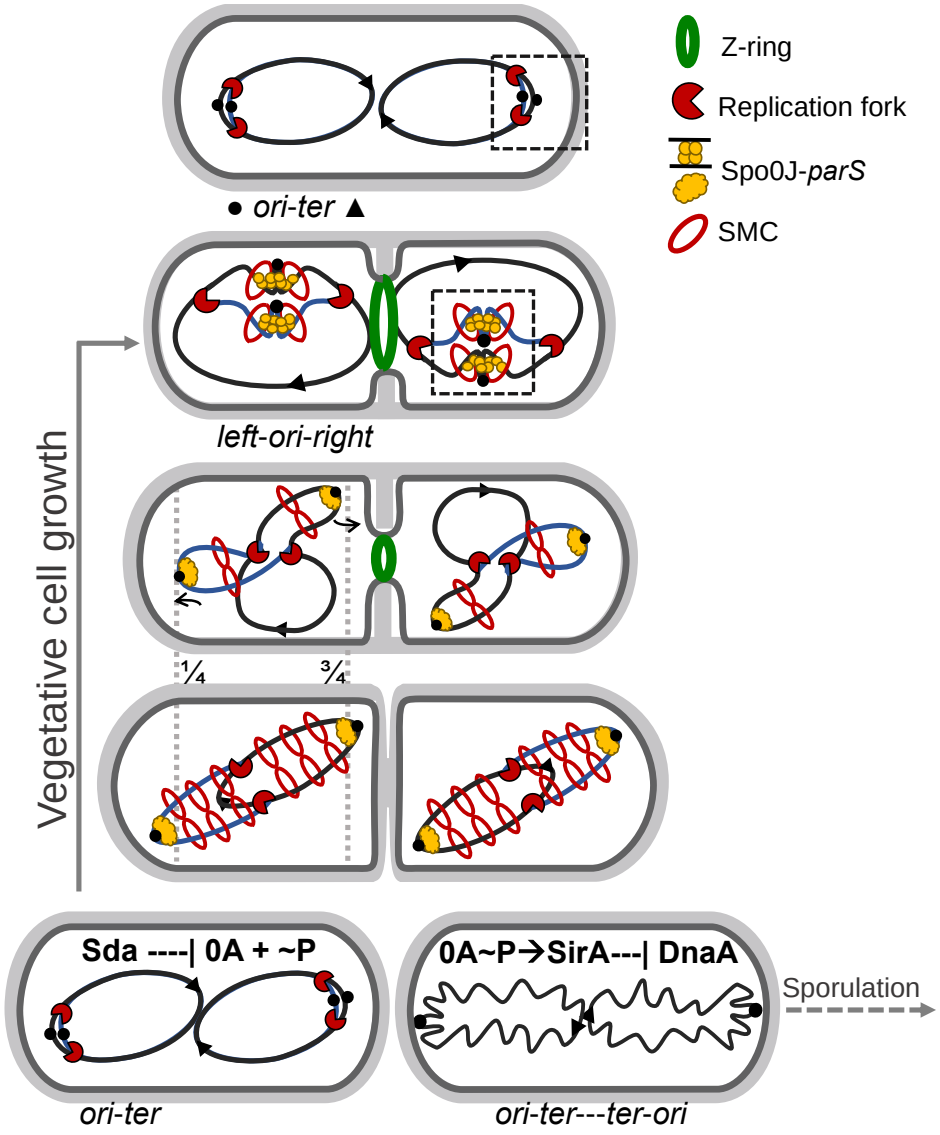

Figure I.3 Chromosome replication and segregation are tightly coordinated within the cell cycle in *Bacillus subtilis*.
During growth, vegetative cells of *B. subtilis* reproduce by binary fission ("Vegetative cell growth"). Chromosome orientation is depicted as observed during slow growth conditions, which oscillates between *ori-ter* and *left-ori-right* states during a replication-segregation cycle. Prior to replication initiation, the origins of replication (*oriC*) are positioned at the quarter cell and the replication termini (*ter*) are near midcell. Upon replication of *oriC*, ParB (Spo0J) nucleates at *parS* sites and organizes individual sister origin regions. The complexes migrate to midcell where ParB loads SMC to constrain and resolve sister origins, generating *left-ori-right* state. SMC remains at mid-nucleoid to condense and individualize chromosome arms as they exit the replisome. Resolved *oriC*s are actively segregated to the quarter cell position in a manner that requires ParA (Soj) (curved arrows) and the *ori-ter* arrangement is re-established. The cell-cycle checkpoint protein, Sda, inhibits sporulation in starving cells that have re-initiated replication. SirA inhibits replication in cells that have initiated sporulation. Boxed regions in the first and second levels correspond to Figure I.3 and Figure I.2, respectively.

In addition, the contribution of each systems depends on the bacterium, growth condition, and on the presence of functionally redundant or accessory systems that would mitigate a need for their use. *E. coli*, for instance, lack Par system homologs and instead employ a distant relative of SMC condensin complexes called MukBEF (Hajduk *et al.*, 2016) to efficiently segregate chromosomes. Accessory proteins are also required that act in conjunction with MukBEF proteins, including the chromosome *ter*-organizing system, MatP-*matS* (Dupaigne *et al.*, 2012, Espeli *et al.*, 2012, Mercier *et al.*, 2008), and the abundant nucleoid structuring protein, HU (Lioy *et al.*, 2018).

Bacterial SMC condensin complexes

Bacterial SMC (Structural Maintenance of Chromosomes) complexes are homologous in architecture to the eukaryotic SMC ring complexes, condensin and cohesin, which are required during mitosis to compact and segregate sister chromatids (Hirano, 2006, Nasmyth & Haering, 2005). During fast growth in *B. subtilis*, the absence of SMC results in interlinked sister chromosomes and gross chromosome loss (Britton *et al.*, 1998, Gruber *et al.*, 2014, Wang *et al.*, 2014). SMC complexes are recruited to the origin region by ParB-*parS* nucleoprotein complexes, as in *B. subtilis* and *C. crescentus*, where they assemble around the DNA duplex (Figure I.2)(Graham *et al.*, 2014, Gruber & Errington, 2009, Minnen *et al.*, 2011, Sullivan *et al.*, 2009, Wang *et al.*, 2017, Wang *et al.*, 2015).

Bacterial and eukaryotic SMC complexes are similar in subunit composition, containing a dimer of the SMC ATPase (Smc in bacteria) and a kleisin family protein,

which together form a tripartite ring. The N and C termini of Smc proteins interact to form the ATPase "head" domain, and are separated from the distal hinge region by a variable length anti-parallel coiled-coil segment (Burmann *et al.*, 2017, Melby *et al.*, 1998). In *B. subtilis*, Smc forms a homodimer via an interaction at the hinge domains, while the kleisin protein, ScpA, closes the ring by interacting with each head domain (Figure I.2)(Burmann *et al.*, 2013, Soppa *et al.*, 2002). The accessory kite protein, ScpB, interacts with ScpA (Palecek & Gruber, 2015, Schleiffer *et al.*, 2003, Soppa *et al.*, 2002).

DNA becomes entrapped within the SMC-ScpA ring upon ATP hydrolysis, which releases of the Smc/ScpAB complex onto flanking DNA where it is free to translocate to distal chromosome regions (Figure I.2 and Figure I.3)(Minnen *et al.*, 2016, Wilhelm *et al.*, 2015). SMC complexes spatially constrict the chromosome during translocation by "zipping up" the chromosome arms through a mechanism termed "loop extrusion" (Tran *et al.*, 2017, Wang *et al.*, 2017, Wang *et al.*, 2015). This movement is driven by ATP hydrolysis, and was recently suggested to be necessary in order to achieve the high degree of juxtaposition between left and right chromosome arms (Figure I.3)(Miermans & Broedersz, 2018).

ParABS chromosome segregation systems

The ParABS system functions to actively segregate newly replicated chromosome origins to opposite cell halves (Gruber & Errington, 2009, Lee & Grossman, 2006, Lindow *et al.*, 2002, Wang *et al.*, 2014). The Par system was

originally identified as a plasmid partitioning system used to segregate plasmids within the volume of the nucleoid (Gerdes *et al.*, 2010). Par modules typically encode two *trans*-acting DNA-binding proteins, ParA and ParB, and one or more *cis*-acting *parS* sites (Gerdes *et al.*, 2010, Livny *et al.*, 2007). ParA proteins are Walker-type ATPases that form ATP-bound dimers that associate with DNA non-specifically. ATP hydrolysis releases ParA monomers from the DNA. ParB proteins form stable complexes at *parS* sites, and stimulate ParA ATPase activity through a direct interaction.

Chromosomally encoded orthologs of ParABS proteins have been identified in over 65% of sequenced bacterial genomes, and are typically encoded near the origin of replication (Livny *et al.*, 2007). Despite this conservation, the mechanism of ParABS-mediated segregation is not ubiquitous. For instance, the Par system is essential for segregation in the crescent-shaped bacterium, *Caulobacter crescentus*, the mechanism of which has been well characterized, and is similar to the DNA-relay mechanism used to partition plasmids. The DNA relay relies on pulling forces generated by iterative interactions between ParB-*parS* and ParA dimers bound non-specifically throughout the nucleoid (Lim *et al.*, 2014, Vecchiarelli *et al.*, 2012). ParB interaction stimulates ParA to hydrolyze its bound ATP, which results in dissociation of ParA monomers from the DNA (Scholefield *et al.*, 2011). In the wake of repeated interactions, a gradient of ParA is generated such that ATP-bound dimers are highest at the distal edge of the nucleoid, potentiating recruitment of ParB-*oriC* complexes toward the poles. Such a mechanism, termed “chemophoresis”, relies on the continued affinity of ParB-*parS* for ParA-ATP to

drive the net movement of the origin toward opposite edges of the nucleoid (Vecchiarelli *et al.*, 2012, Walter *et al.*, 2017).

I.1.2.4 Chromosome replication

During reproduction, bacteria replicate their genetic material prior to cell division in order to transmit a complete copy of the genome to each daughter cell. DNA replication occurs in three major stages: initiation, elongation, and termination. Initiation occurs at a single position on the chromosome called the replication origin (*oriC*) where the double helix is melted into an open conformation to which the DNA synthesis machinery, called the "replisome", is recruited (Figure I.4A). The replication initiator protein, DnaA, is a member of the AAA+ family of ATPases (ATPases Associated with diverse cellular Activities) that binds short repeat sequences called DnaA-boxes clustered at *oriC* (Fuller *et al.*, 1984, Messer *et al.*, 1999, Miller *et al.*, 2009). Chromosome topology plays a critical role in many cell cycle processes, especially replication, and negative supercoiling of the DNA near *oriC* is required for duplex unwinding (Rajewska *et al.*, 2012). Cooperative binding of DnaA-ATP molecules elaborates right-handed helical oligomers around the DNA duplex, generating superhelical tension within an adjacent AT-rich region called DUE (DNA Unwinding Element) (Figure I.4A) (Kowalski & Eddy, 1989, Bramhill & Kornberg, 1988). The resulting instability within the DUE stimulates duplex unwinding (Duderstadt *et al.*, 2011, Erzberger *et al.*, 2006). Following unwinding, DnaA oligomers spread onto ssDNA to stabilize the open complex to which the first replisome components are

recruited (Duderstadt *et al.*, 2011, Duderstadt *et al.*, 2010, Speck & Messer, 2001, Richardson *et al.*, 2016).

The first protein, DNA helicase, is an ATPase motor protein that assembles as hexameric ring on ssDNA and is responsible for mechanically unwinding dsDNA ahead of the replisome during elongation (Figure I.4B) (Jameson & Wilkinson, 2017). A helicase loader protein, which interacts with DNA helicase through its N-terminal domain, is required for DNA helicase assembly and activation (Jameson & Wilkinson, 2017). DNA helicase does not become active until the helicase loader dissociates, which ensures the remaining replisome components are in place before helicase starts translocating (Figure I.4A) (Jameson & Wilkinson, 2017). Activation of an ATPase domain within the C-terminus of the helicase loader facilitates its dissociation. The mechanism of helicase loading and activation can differ significantly across bacterial species including the model Gram-positive bacterium, *Bacillus subtilis* and the model Gram-negative *Escherichia coli*. (Li & Araki, 2013, Beattie & Reyes-Lamothe, 2015).

Helicase loading in *B. subtilis* occurs via a "ring assembly" mechanism (Soultanas, 2012), and requires two additional proteins, DnaD and DnaB, absent from the *E. coli* initiation complex. DnaD and DnaB associate with DnaA at the DUE and recruit the helicase loader (Smits *et al.*, 2010). The loader protein assembles the helicase ring around ssDNA from monomeric subunits. Pre-assembled hexamers are not compatible with loading (Velten *et al.*, 2003). The ATPase activity of the helicase loader is stimulated in the presence of ssDNA, the binding site for which becomes exposed only once helicase is bound at the N-terminus (Ioannou *et al.*, 2006).

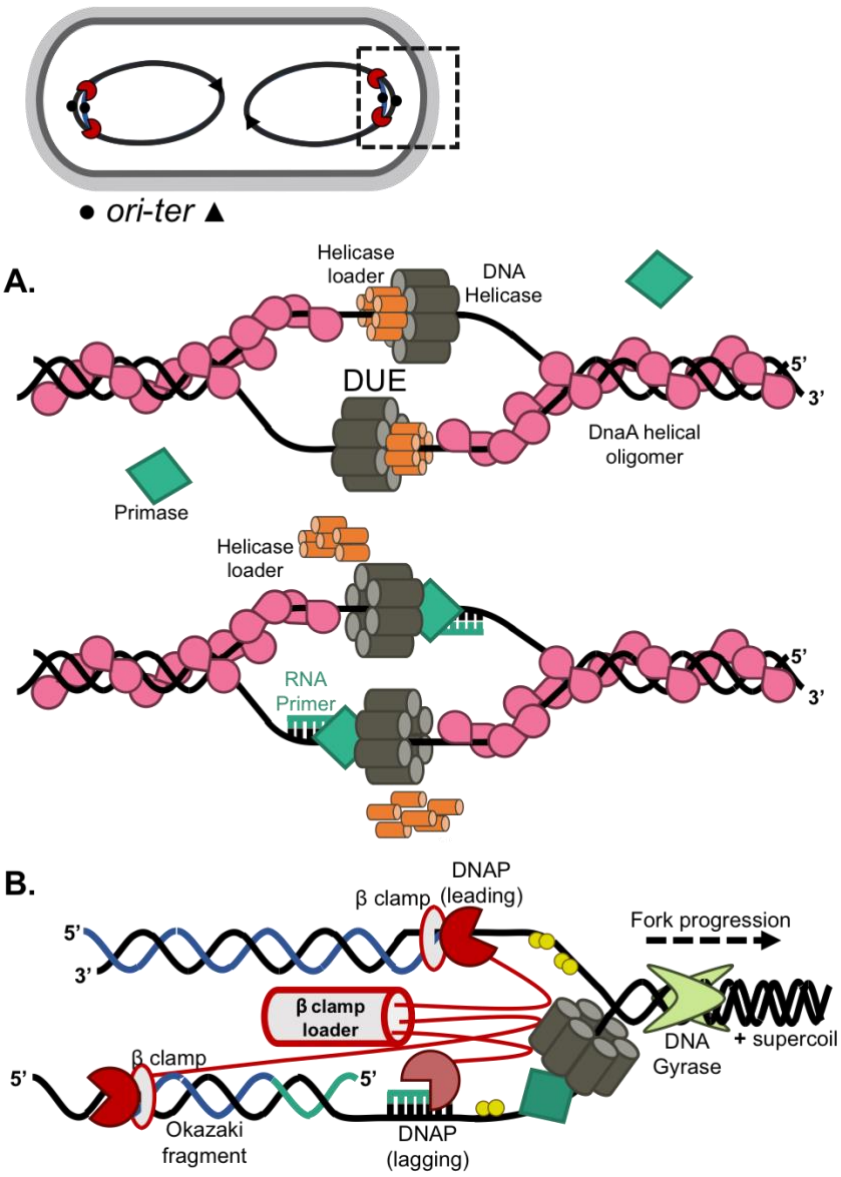

Figure I.4 Initiation of bi-directional DNA replication.
Adapted from Jameson & Wilkinson, 2017. DNA replication initiation complex (A) and the core replisome components at the replication fork during elongation (B). **(A)** Helical oligomerization of the replication initiator protein, DnaA (pink), stimulates duplex unwinding at the DUE. Assembly of the DNA helicase (brown) onto ssDNA is facilitated by the helicase loader protein (orange). Dissociation of the loader protein is required for DNA helicase activity. In *E. coli* dissociation is triggered by formation of an RNA primer by Primase (teal), which is recruited to the initiation complex by DNA helicase. **(B)** DNA helicase unwinds dsDNA ahead of the replisome creating a replication fork. DNA gyrase relieves positive supercoiling ahead of the replication fork. On the leading strand, DNA is synthesized continuously in the 5' to 3' direction by DNA polymerase ("DNAP leading"); in *E. coli* this is performed by Pol III. Lagging strand synthesis is not continuous, and elongation yields short Okazaki fragments that are joined together by ligase (not shown). Lagging strand synthesis requires Primase, which associates with DNA helicase and generates RNA primers that are extended into Okazaki fragments. In *B. subtilis*, PolC is predominantly responsible for both leading and lagging strand synthesis but a second polymerase, DnaE ("DNAP lagging") is required to extend RNA primers with DNA on the lagging strand before PolC can take over.

In contrast, *E. coli* helicase is loaded by a "ring breaking" mechanism (Arias-Palomo *et al.*, 2013). Pre-assembled hexamers undergo a structural deformation upon binding the loader, which opens the ring enough to accommodate the ssDNA. The helicase loader dissociates upon recruitment of the primase protein by DNA helicase and subsequent RNA primer formation (Makowska-Grzyska & Kaguni, 2010).

Primase is a DNA-dependent RNA polymerase that associates with DNA helicase and is responsible for generating short RNA primers, the 3'-OH of which becomes part of the substrate for both leading and lagging strand replication (Figure I.4) (Corn *et al.*, 2008, Corn & Berger, 2006, Rowen & Kornberg, 1978). The replicative DNA polymerase, Pol III in *E. coli* or PolC in *B. subtilis*, and its associated processivity clamps (β-clamps) assemble on both strands at the 3'-OH of the RNA:DNA hybrid (Figure I.4B). Lagging strand synthesis is not continuous, and requires primase to deposit an RNA primer that is elongated by Pol III into short Okazaki fragments (Figure I.4B), which become joined together by ligase. The Pol III subunits are held together by the β-clamp loader, which couples unwinding and synthesis through interactions with the helicase and polymerase subunits (Beattie & Reyes-Lamothe, 2015, Corn & Berger, 2006).

A second distinguishing feature of the *B. subtilis* replisome is the presence of a second polymerase, DnaE (Sanders *et al.*, 2010). Only PolC is required for leading strand synthesis, but both are necessary for synthesis on the lagging strand, due to the inability of PolC to extend DNA from the RNA primers deposited by primase (Dervyn *et*

al., 2001). DnaE likely functions to fulfill this function, providing a DNA-extended template from which PolC can continue synthesis (Rannou *et al.*, 2013).

During strand elongation, DNA synthesis occurs bi-directionally along template DNA strands, as replisomes travel in opposite directions away from *oriC*. Translocation of DNA helicase in the 3' to 5' direction creates so-called replication forks ahead of the replisome (Figure I.4B). The topoisomerase, DNA gyrase, travels ahead of the replication forks and relieves the positive supercoiling created by DNA unwinding. DNA replication terminates when the two replication forks meet in the terminus (*ter*) region and the replisome disassembles (Jameson & Wilkinson, 2017).

Under conditions that support rapid growth, bacteria can initiate subsequent rounds of replication from newly synthesized *oriC*'s even before the previous round has terminated, a phenomenon called "multifork replication." To sustain this rapid growth, cells require equally rapid processing of DNA into RNA then protein by transcription and translation. One of the many features that distinguish prokaryotes from eukaryotes is the coupling of transcription and translation, in which newly synthesized mRNA transcripts become bound by ribosomes and translated into protein as they exit the transcription machinery. As a result, newly synthesized DNA becomes readily decorated by ribosome-bound mRNAs (polysomes) (Surovtsev & Jacobs-Wagner, 2018). Despite the potential for DNA replication, transcription, and translation to interfere with one another due to macromolecular crowding, deleterious conflicts are largely avoided due in part to the ordered structure of the nucleoid. For instance, polysomes have been observed to be largely excluded from the centrally positioned

nucleoid in *B. subtilis* and *E. coli*, accumulating in the nucleoid-free polar regions (Bakshi *et al.*, 2015, Bakshi *et al.*, 2012, Lewis *et al.*, 2000), indicating transcription and translation are subject to partial physical separation in certain bacteria.

Replication control by B. subtilis ParABS

In *B. subtilis*, chromosome orientation during the replication-segregation cycle is dynamic, oscillating between an *ori-ter* arrangement, where origins are partitioned to opposite edges of the nucleoid, and a *left-ori-right* arrangement following replication initiation, in which sister origins are positioned at mid-nucleoid with the chromosome arms flanking either side (Wang *et al.*, 2014). Oscillation between these two states requires the concerted action of both SMC and Spo0J/Soj. The mechanism for Par-mediated segregation in *B. subtilis* is poorly understood, but appears to lack distinct features of characterized systems like *C. crescentus*, such as a ParA localization gradient, have not been observed in *B. subtilis*. While ParABS segregation is not essential in *B. subtilis*, its absence leads to a 100% increase in the number of anucleate or "empty" daughter cells compared to wild-type (Ireton *et al.*, 1994).

The ParB protein, Spo0J, interacts with at least eight *cis*-acting *parS* sites in the *oriC*-proximal 20% of the chromosome and also forms large nucleoprotein complexes (Breier & Grossman, 2007, Lin & Grossman, 1998, Murray *et al.*, 2006). Spo0J facilitates long-range chromosome interactions by bridging nucleoprotein complexes into large loops in the DNA, to which Smc/ScpAB complexes are recruited and loaded (Gruber & Errington, 2009). Spo0J-mediated condensation of the *oriC* region is thought

to be analogous to the association between eukaryotic kinetochores and centromeres, to which spindle fibers attach to facilitate chromosome segregation during mitosis (van Ruiten & Rowland, 2018).

When replication is initiated, chromosomes are in an *ori-ter* configuration (Figure I.3). Following replication of *oriC*, sister origins migrate together to mid-nucleoid, where Spo0J bound at *parS* loads the SMC ring complex onto DNA loops, establishing the *left-ori-right* orientation (Figure I.3). Newly resolved sister origins become segregated to opposite cell quarters establishing the *ori-ter* orientation; this orientation allows a new round of replication to initiate (Figure I.3) (Wang *et al.*, 2014).

For the majority of the cell cycle, *B. subtilis* ParA, or Soj, is maintained in a monomeric state by Spo0J, which induces DNA-bound Soj dimers to hydrolyze their ATP (Scholefield *et al.*, 2011). This is important because ParABS in *B. subtilis* has a second, divergent function in regulating DNA replication initiation. Soj acts like a molecular switch during the replication-segregation cycle, either activating or inhibiting replication initiation via direct interaction with the initiator protein, DnaA (Murray & Errington, 2008). In monomer form, Soj prevents replication initiation by inhibiting DnaA oligomerization, whereas Soj ATP-dimers stimulate initiation, possibly by directly binding to sites near *oriC* and directing DnaA association with DnaA-boxes (Lee & Grossman, 2006, Murray & Errington, 2008, Ogura *et al.*, 2003, Scholefield *et al.*, 2012, Scholefield *et al.*, 2011). The presence of such a switch could signify that chromosomes have resumed the *ori-ter* pattern and is likely employed as a checkpoint for starving

Bacillus, which need to shut down replication prior to development, as described in Chapter I.2 (Wang *et al.*, 2014).

I.1.3 Cell cycle coordination

Division in most rod-shaped bacteria occurs between nucleoids at midcell with remarkable accuracy (Barak & Muchova, 2018, Migocki *et al.*, 2002, Rodrigues & Harry, 2012). During growth, the timing and positioning of Z-ring assembly is mediated, in part, by the coordinated actions of two division-inhibitory systems, Min and nucleoid occlusion (NO), that collectively promote septum formation at midcell between replicated chromosomes. Disrupting both Min and NO systems severely impairs cell division due to unconstrained FtsZ polymerization at multiple sites in the cell, such that any one site is rarely sufficient to produce a mature Z-ring. In the rare event a Z-ring is formed in the double mutants it still does so at midcell with surprising accuracy, a phenomenon that demonstrates bacteria rely on a complex regulatory network to localize and coordinate essential cell cycle processes (Badrinarayanan *et al.*, 2015, Bailey *et al.*, 2014, Barak & Wilkinson, 2007, Bernhardt & de Boer, 2005, Hajduk *et al.*, 2016, Levin *et al.*, 1998, Rodrigues & Harry, 2012, van Teeffelen & Renner, 2018).

The Min system

The Min system functions to inhibit Z-ring assembly in DNA-free regions of the cell and has been well characterized in both *E. coli* and *B. subtilis*. In *B. subtilis*, the Min system is comprised of four components that localize to the division septum through

a hierarchy of protein-protein interactions: DivIVA, MinJ, MinD, and finally MinC, which directly inhibits FtsZ polymerization (Blasios *et al.*, 2013). DivIVA is a multifunctional membrane-curvature sensing protein that localizes in patches at the poles of rod-shaped cells, regions considered to have the highest degree of negative curvature that are generated upon maturation of division septa (Lenarcic *et al.*, 2009, Oliva *et al.*, 2010, Ramamurthi & Losick, 2009). DivIVA localizes to the divisome at a similar time as DivIB, DivIC, FtsL, and Pbp2b, and forms ring structures on either side of constricting Z-rings to which it recruits the topological specificity adaptor protein, MinJ, which in turn targets the membrane-bound ATPase, MinD (Figure I.1) (Bramkamp *et al.*, 2008, Eswaramoorthy *et al.*, 2011, Marston *et al.*, 1998, Patrick & Kearns, 2008, van Baarle *et al.*, 2013). Finally, MinD localizes the FtsZ-inhibitory protein, MinC, to the cytoplasmic membrane (Figure I.1) (Dajkovic *et al.*, 2008, Gregory *et al.*, 2008, van Baarle & Bramkamp, 2010).

Following division, DivIVA rings continues to associate with the septum until pole maturation, which forces them to collapse into membrane patches that maintain a zone of Min inhibition at the cell poles (Figure I.1). DivIVA also plays a critical role during the developmental program of sporulation in *B. subtilis*, acting as a scaffold in the recruitment and assembly of a variety of proteins with pole-associated functions (Chapter I.II) (dos Santos *et al.*, 2012, Kloosterman *et al.*, 2016, Thomaides *et al.*, 2001, van Baarle *et al.*, 2013).

DivIVA is absent in *E. coli*, and is replaced by the functionally analogous protein, MinE (de Boer *et al.*, 1989). Instead of assuming a static localization at the

poles and nascent division septa like DivIVA, MinE undergoes rapid oscillation across the length of the cell stimulating the ATPase activity of membrane-bound MinD-ATP, resulting in release of MinD and MinC into the cytoplasm (de Boer *et al.*, 1989, Lutkenhaus, 2007). In order to rebind ATP and subsequently the membrane and MinC, MinD undergoes diffusion toward the opposite pole where ATP concentrations are highest, resulting in an oscillatory pattern of MinCD localization (Ghosal *et al.*, 2014, Lutkenhaus, 2007, Raskin & de Boer, 1999, Rowlett & Margolin, 2015). The net result of MinCDE oscillation establishes a region of reduced Z-ring inhibition at midcell and regions of high inhibition at the poles.

Nucleoid occlusion

Many bacteria including *E. coli* and *B. subtilis* encode DNA-binding proteins that inhibit cell division when bound at specific sequences on the chromosome. This phenomenon, termed Nucleoid Occlusion (NO), functions to occlude division from the DNA-occupied regions of the cell (Woldringh *et al.*, 1991). The two best characterized NO systems, *E. coli* SlmA and *B. subtilis* Noc, were first identified as mutants that produced a synthetic lethal phenotype in strains lacking a functional Min system (Bernhardt & de Boer, 2005, Wu & Errington, 2004).

SlmA (Synthetic Lethal with Min) is a TetR family DNA-binding protein that orchestrates NO from specific sites on the chromosomal called SBS (SlmA Binding Sequences) by directly inhibiting FtsZ polymerization (Cabre *et al.*, 2015, Cho & Bernhardt, 2013, Cho *et al.*, 2011, Du & Lutkenhaus, 2014, Tonthat *et al.*, 2011). *B.*

subtilis Noc is a ParB family DNA-binding protein that binds the chromosome at its cognate NBSs (Noc Binding Sites) (Figure I.5A)(Sievers *et al.*, 2002, Wu *et al.*, 2009). Unlike SlmA, Noc does not appear to facilitate NO through direct regulation of FtsZ. Instead, Noc localizes to the cell periphery and associates with the membrane via an N-terminal amphipathic helix in a manner that is dependent on Noc-NBS nucleoprotein complexes (Figure I.5A), suggesting that NO in *B. subtilis* operates by physically occluding assembly of divisome at the membrane (Adams *et al.*, 2015).

SBS and NBS exhibit similar non-uniform distributions throughout their respective chromosomes and are largely underrepresented in the terminus (*ter*) regions (Cho *et al.*, 2011, Tonthat *et al.*, 2011, Wu *et al.*, 2009). During replication, sister chromosome origins are segregated toward opposite cell poles, with the SBS and NBS-deficient *ter* regions at midcell. This arrangement ensures Z-ring assembly occurs at midcell at a time when DNA replication is near complete (Elmore *et al.*, 2005, Li *et al.*, 2003, Wang *et al.*, 2014, Youngren *et al.*, 2014). Perturbing DNA replication in either NO single mutant is sufficient to permit division over the nucleoid (Bernhardt & de Boer, 2005, Wu & Errington, 2004), supporting long standing hypotheses that NO primarily functions to prevent nucleoid bisection by coupling the initiation of cell division to the end of DNA replication and chromosome segregation (Mulder & Woldringh, 1989, Woldringh *et al.*, 1990).

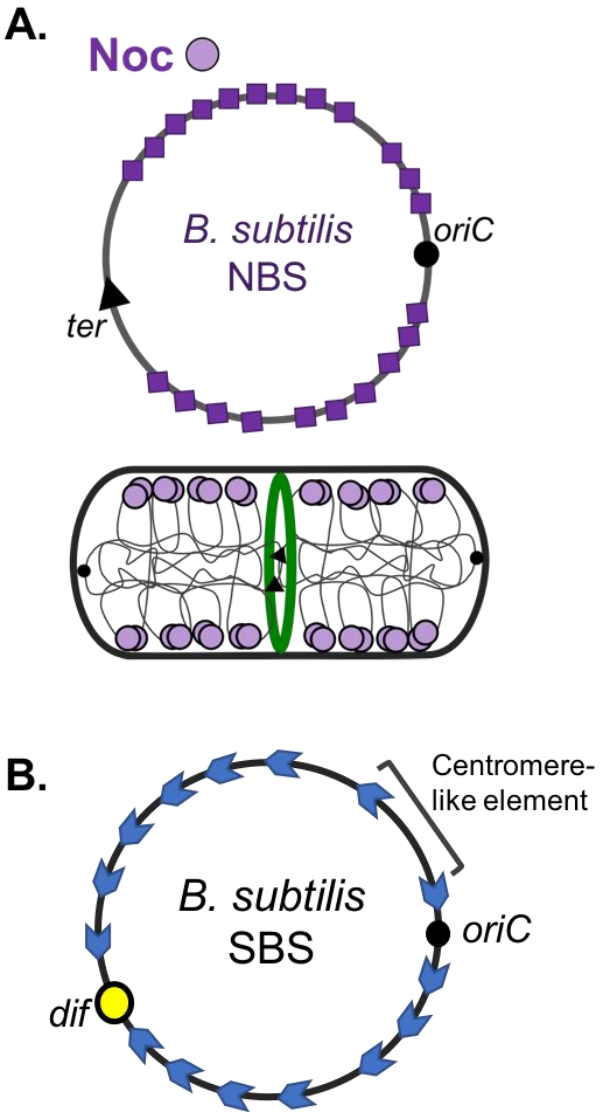

Figure I.5 Cell cycle coordination during reproduction.
(A) The NO system, comprised of Noc-NBS in *B. subtilis* (or SlmA-SBS in *E. coli*) utilizes the nucleoid to localize Noc's division inhibition activity to specific chromosome sequences (NBS, purple boxes on circular chromosome). Unlike SlmA, Noc prevents Z-ring assembly by crowding the membrane in the vicinity of the nucleoid. NBS are largely absent from the chromosome *ter* region, which is segregated last during DNA replication. **(B)** Recognition sites of DNA translocases are highly skewed toward the *dif* site (yellow) within the *ter* region. Shown are SBS (blue) recognized by *B. subtilis* SpoIIIE and SftA. *E. coli* FtsK binds KOPS similarly skewed toward *dif*, but the orientation of KOPs switches direction at the origin rather than to the left of *oriC*, a region containing a centromere-like element that is anchored to the far pole during *Bacillus* sporulation.

Post-septation chromosome segregation

Resolution of chromosome dimers and segregation of the chromosome termini often finishes well into Z-ring constriction. Cells encode proteins called translocases that act late in cell division to clear chromosome termini away from the incipient septum to prevent bisection of the nucleoid and work in conjunction with site-specific recombinases to resolve chromosome dimers generated during replication.

E. coli FtsK and *B. subtilis* SpoIIIE are members of the FtsK/SpoIIIE/Tra family of DNA translocases found across a variety of bacterial species (Wu *et al.*, 1995). Proteins of this family share a highly conserved C-terminal translocase motor domain and a less conserved N-terminal domain comprised of a transmembrane segment responsible for localizing activity to the division septum (Massey *et al.*, 2006). In the conserved motor domain, α-and β-subdomains encode an ATPase motor, which is required for the assembly of monomers into a hexameric ring, while the γ-subdomain mediates interaction with oriented DNA sequences on the chromosome. KOPS (FtsK Orienting Polarized Sequences) and SRS (SpoIIIE Recognition Sequences) are highly skewed toward the *ter*-proximal *dif* sites on the *E. coli* and *B. subtilis* chromosomes (Figure I.5B), respectively (Bigot *et al.*, 2005, Pease *et al.*, 2005, Ptacin *et al.*, 2008, Ptacin *et al.*, 2006).

Initial binding does not require recruitment to SRS, and SpoIIIE is able to being translocating along the chromosome from non-specific DNA sites by simple 1-D diffusion (Cattoni *et al.*, 2014, Chara *et al.*, 2018). However, when SpoIIIE encounters SRS oriented in the same direction as its diffusion, the catalytic activity within the motor

domain is stimulated, and the rate of translocation increases dramatically (Chara *et al.*, 2018). In this way, the SRS bias the direction of translocation by stimulating motor processivity (Burton *et al.*, 2007, Chara *et al.*, 2018).

B. subtilis also encode a second translocase, SftA, that also shares homology to the C-terminus of FtsK and SpoIIIE (Biller & Burkholder, 2009, Kaimer *et al.*, 2011). Unlike SpoIIIE, which freely diffuses within the membrane and localizes to division septa only when DNA is bisected (El Najjar *et al.*, 2018, Kaimer *et al.*, 2009), SftA is a soluble divisome component and, similar to FtsK in *E. coli*, is recruited to all division sites by the membrane anchor, FtsA (El Najjar *et al.*, 2018). At the septum, FtsK recruits the site-specific recombinases, XerCD, responsible for resolving chromosome dimers at *dif* sites (Sciochetti *et al.*, 2001). FtsK mediates recombination by activating XerD and is required for complete resolution of the Holliday junction intermediate (Sherratt *et al.*, 2004, Yates *et al.*, 2006). Neither SpoIIIE or SftA are alone required for dimer resolution but the absence of both severely impairs resolution by *B. subtilis* recombinases RipX and CodV (Kaimer *et al.*, 2011).

Importantly, these DNA "pumps" can actively segregate nucleoids that have been bisected by the division septum, a consequence in cells where division and DNA replication/segregation is not coordinated. For instance, the absence of segregation systems like ParABS and SMC prevents cells from efficiently organizing newly replicated chromosome segments and, as a result, these cells are more susceptible to dividing over their chromosomes. Loss of failsafe post-septation segregation mechanisms permits the septum to break, or "guillotine" the trapped chromosome,

resulting in increased numbers of anucleate progeny and cell lysis (Britton & Grossman, 1999).

In addition to the Min and NO systems, which rely on the cell envelope and nucleoid to influence the timing and position of initiating cell division, respectively, bacteria also incorporate a variety of additional and sometimes more subtle cues into regulatory circuits governing the cell cycle, including cell size, nutrient status, and population density, to ensure both cell growth and division, and DNA replication and chromosome segregation are regulated in a manner that accurately accommodates fluctuations in the extracytoplasmic environment.

I.2 *BACILLUS* SPORULATION

Bacillus subtilis is a Gram-positive model organism used to investigate the cellular, molecular, and genetic mechanisms that govern processes required for reproduction, and is a particularly tractable system for studying specialized cellular processes like horizontal gene transfer, natural competency, and cellular differentiation. *B. subtilis* has two lifestyles depending on the availability of nutrients. As "vegetative cells", *B. subtilis* reproduce by binary fission through cycles of chromosome replication, segregation, and symmetric division between segregated chromosomes at midcell. In response to environmental and nutritional stresses, *Bacillus* species are capable of differentiating into a physiologically dormant cell type called a spore (Figure I.6).

B. subtilis initiates differentiation in response to a variety of physiological and environmental signals, including nutrient deprivation, DNA damage, and high cell

density. Members of the *Bacillus* genus are polar endospore formers, meaning the spore evolves from a smaller "forespore" compartment that is formed following an asymmetric division at one pole of the cell (Figure I.6). The forespore becomes engulfed by the larger compartment, or "mother cell", which functions to nurturing the nascent spore as it matures. Ultimately, the mother cell lyses and the mature spore, containing a complete copy of the genome, is released into the environment.

Unlike vegetative cells, spores are metabolically dormant and can survive without nutrients for extended periods of time, possibly millions of years (Vreeland *et al.*, 2000). Spores are highly resistant to treatments that kill vegetative cells, such as desiccation, UV radiation, extremes in temperature, and chemical assults (Atrih & Foster, 2001, Setlow & Setlow, 1993, Setlow, 2006) and are even capable of surviving harsh extraterrestrial environments (Moeller *et al.*, 2012, Nagler *et al.*, 2016, Nicholson *et al.*, 2000). When the environment becomes favorable for growth, the spore germinates and subsequently resumes vegetative cell growth (Figure I.6).

I.2.1 Entry into sporulation

Sporulation is an irreversible time and energy-consuming process, and is therefore considered as a last resort for survival. Not all cells in a population experiencing stress will initiate sporulation synchronously due, in part, to the stochastic of activation of the master developmental transcriptional regulator, Spo0A (Figure I.7A)(Hilbert & Piggot, 2004, Hoch, 1991). Spo0A becomes active in its phosphorylated state, Spo0A~P, via a multi-protein phosphorelay system initiated by

phosphorylation of three histidine autokinases, KinA, KinB, and KinC (Burbulys *et al.*, 1991). The phosphorylation cascade continues via Spo0F and Spo0B, then terminates with Spo0A (Figure I.7A).

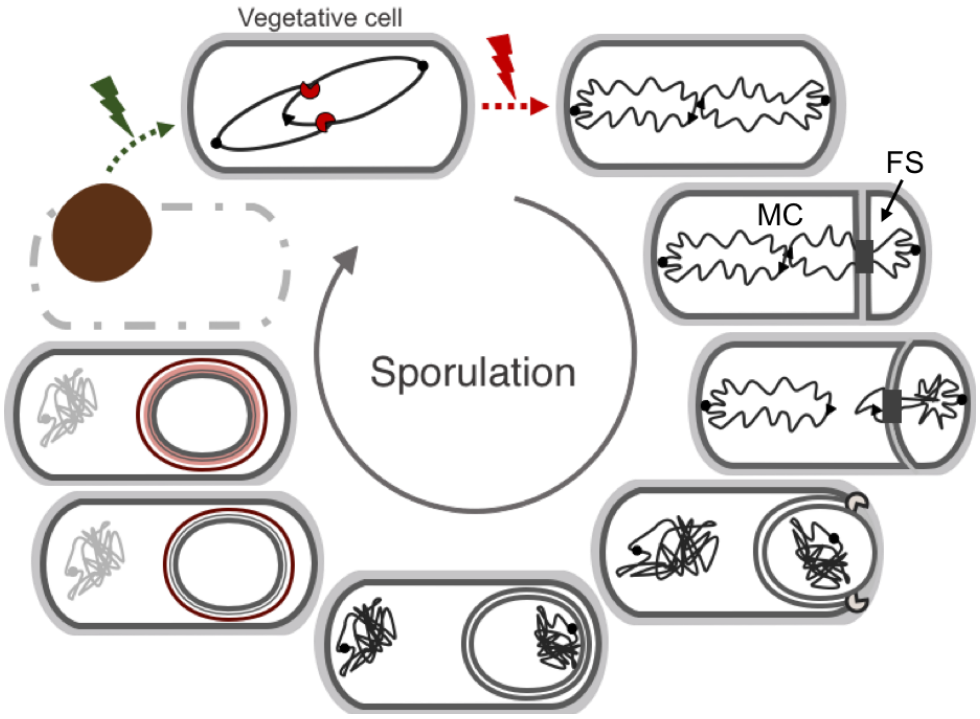

Figure I.6 Developmental cycle of *Bacillus subtilis.*
Numerous environmental cues, including nutrient starvation (red bolt), signal vegetative *Bacillus* cells to seek alternative means for survival such as cellular differentiation during the developmental program of sporulation. Sporulating cells undergo a series of genetic and morphological changes, the earliest of which is the reduction of chromosome copy number to two and anchoring of the origins to the far poles, which creates a nucleoid structure called the axial filament. Next, the site of division is shifted from midcell to an asymmetric position near one pole, where the septum forms over one of the cell's two chromosomes, generating the forespore (FS) and mother cell (MC) compartments. The DNA pump, SpoIIIE (black square) moves the remainder of the trapped chromosome into the forespore compartment. Once the forespore receives a full copy of the chromosome, a hierarchal cascade of intercompartment signaling initiates compartment-specific transcriptional programs that drive additional morphological changes. During engulfment, hydrolases (grey pacmen) thin the septal cell wall separating the two compartments to permit migration of the mother cell membrane around the forespore. At the end of engulfment, membrane fission frees the double membrane-bound forespore within the mother cell, which nurtures the forespore during maturation. During maturation, synthesis and deposition of the spore coat and cortex layers give *Bacillus* spores their remarkably high resistance to heat, desiccation, light, and chemical assaults. Once the spore is fully mature, it is released into the environment following lysis of the mother cell. Spores can lay dormant for extended periods of time until, upon encountering favorable environmental conditions (green bolt), they undergo germination to resume growth as a vegetative cell.

B. subtilis relies on multiple levels of regulation to maintain precise control of Spo0A phosphorylation states. *spo0A* expression is controlled by the housekeeping factor, σ^A, and the stationary-phase factor, σ^H (Hilbert & Piggot, 2004). Levels of Spo0A~P are positively regulated by a feedback loop in which Spo0A~P indirectly stimulates expression of σ^H (Predich *et al.*, 1992) which in turn directs transcription of *spo0A*, *spo0F*, and *kinA* (Figure I.7A)(Hoch, 1991). Negative regulation of Spo0A~P levels occurs via a variety of phosphatases called Rap that target Spo0A~P and the upstream intermediate, Spo0B~P (Ishikawa *et al.*, 2002, Ohlsen *et al.*, 1994).

Stochastic Spo0A activation results from noise within the phosphorelay, and is critical to maintain a gradual increase in the level and regulatory activity of Spo0A~P (Eswaramoorthy *et al.*, 2010, Fujita & Losick, 2005, Levine *et al.*, 2012, Narula *et al.*, 2012). Spo0A phosphorylation is coupled to the cell cycle, with a pulse of Spo0A~P occurring at the end of replication (Narula *et al.*, 2015, Veening *et al.*, 2009). Spo0A~P pulsing results, in part, from an excess of Spo0F, which inhibits KinA autophosphorylation (Narula *et al.*, 2015). This excess results from a transient 2:1 ratio of Spo0F:KinA generated during replication, as *spo0F* is located near the origin and *kinA* is near the terminus. During starvation, the growth rate slows and the time between replication events increases and allows phosphorelay proteins to accumulate; as a result, the amplitude of the Spo0A~P pulse increases each cell cycle until the threshold level required to initiate sporulation is reached (Narula *et al.*, 2015, Narula *et al.*, 2016).

The gradual accumulation of Spo0A~P contributes to cell fate determination by ensuring the decision to sporulate occurs only once a population has exhausted

alternative strategies for survival. Sub-populations of stationary phase cells with below threshold levels of Spo0A~P can defer entry into sporulation as a bet-hedging strategy that affords cells time to seek alternative means to cope with the stress (Levine *et al.*, 2012, Lopez & Kolter, 2010), including becoming genetically competent and scavengers of foreign DNA (Gamba *et al.*, 2015), becoming motile (Kearns & Losick, 2005), forming biofilms (Chai *et al.*, 2010, Hamon & Lazazzera, 2001), and cannibalizing neighboring siblings for temporary nutrients (Gonzalez-Pastor *et al.*, 2003).

Transcription of more than 10% of all genes in *Bacillus* is controlled directly or indirectly by Spo0A~P (Fawcett *et al.*, 2000). Roughly 120 genes are under direct Spo0A control (Molle *et al.*, 2003) and are subject to activation and/or repression depending both on the concentration of Spo0A~P, and the number and strength of operator sites (0A boxes) within the promoter (Fujita *et al.*, 2005). The switch from growth to sporulation is ultrasensitive and occurs when cells accumulate high enough levels of Spo0A~P to activate expression of genes required for the early stages of sporulation (Fujita *et al.*, 2005, Fujita & Losick, 2005).

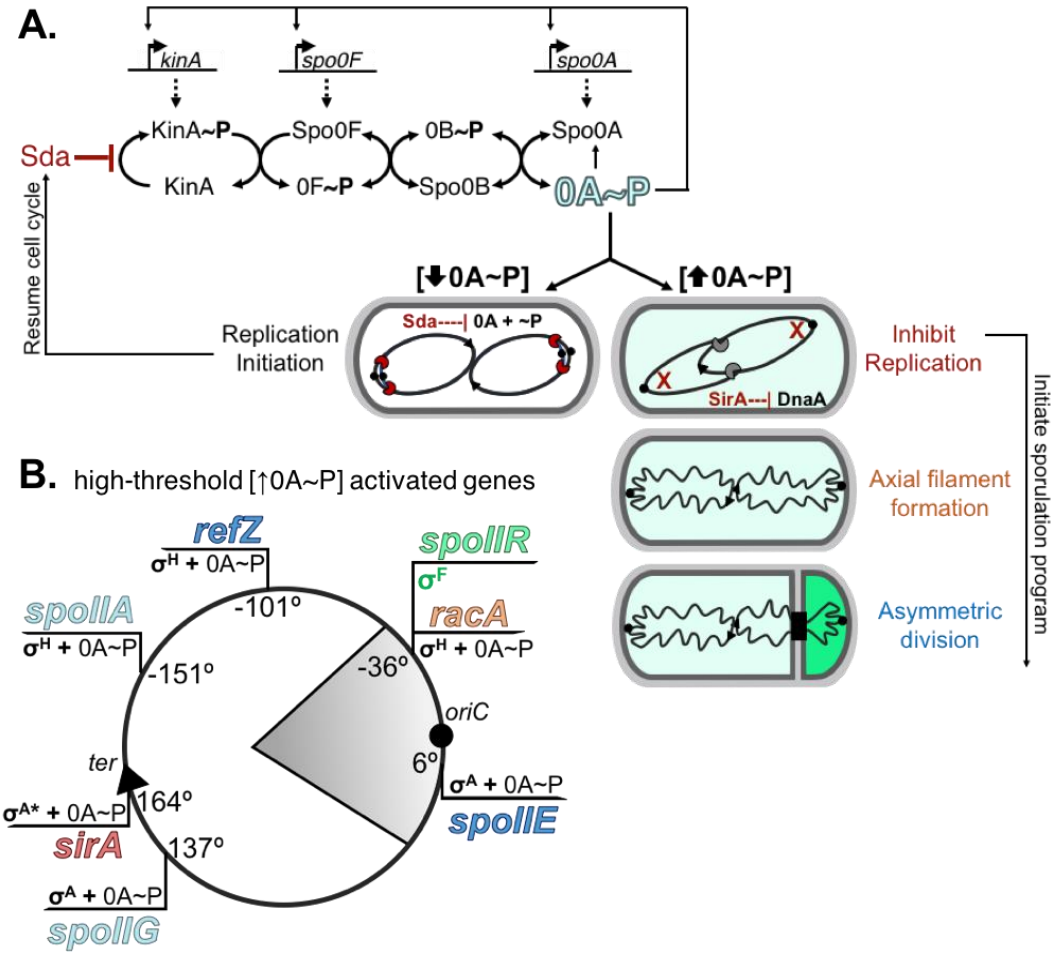

Figure I.7 Cell cycle cues dictate entry into sporulation.
Adapted from Narula *et al*., 2015. **(A)** Spo0A, becomes phosphorylated to the active state (0A~P) in the last step of a signaling cascade initiated by autophosphorylation of KinA (KinA~P). The phosphoryl group is then transferred to Spo0F (0F~P) then to Spo0B (0B~P), and finally to Spo0A. Expression of the phosphorelay proteins is positively regulated by 0A~P, generating a network of positive feed-forward loops that propagate and intensify the signal, resulting in accumulation of activated Spo0A to high levels (↑0A~P). Growing and early stationary cells delay entry into sporulation via a cell cycle checkpoint protein, Sda, which reduces Spo0A activation by inhibition KinA. Sda synthesis strictly occurs during replication initiation. Sda is highly unstable and levels are lowest during termination, leaving a small window of time at the end of replication for a burst of Spo0A activation via the phosphorelay (0A~P, blue). Thus, cells are permitted to initiate sporulation each cell cycle provided the burst of 0A~P reaches the high threshold level (↑0A~P). Until then, cells must re-initiate replication (↓0A~P) and try again during subsequent cycles. As the levels of 0A~P accumulate each cell cycle, the probability of initiating sporulation in the following round increases exponentially. Once the high threshold level is reached, 0A~P activates expression of genes required for entry and commitment to sporulation including those required for inhibiting new rounds of replication (red), for axial filament formation (orange), and for asymmetric division (blue). **(B)** The high-threshold-activated genes corresponding to the early series of genetic and morphological changes shown in (A), their regulation, and their positions with respect to the origin of replication (*oriC*) and terminus (*ter*) are indicated on a 360º circular representation of the chromosome. Genes located within the grey wedge are subject to transient differential expression as this region represent the 30% of one chromosome initially trapped inside the forespore compartment, while the remainder lies within the mother cell. Expression of the σ^F-activated *spoIIR* gene is required for signaling across the forespore membrane to activate σ^E in the mother cell, which occurs almost immediately after asymmetric division/σ^F-activation. During the transient period of genetic asymmetry, the *ori*-proximal location of *spoIIE* and *spoIIR* is a critical element to their function and ensures the timely activation of σ^F and σ^E.

High-threshold Spo0A~P induces proteins required for compartment-specific activation of the first forespore and mother cell-specific sigma factors, σ^F and σ^E, respectively, and proteins that generate a series of required genetic and morphological changes at the onset of sporulation (Figure I.7): 1) synthesis of DNA is inhibited to leave only two chromosomes in the cell (establish diploidy), 2) chromosomes are organized into an elongated structure that spans the cell (formation of the "axial filament"), and 3) division occurs at a polar position on top of elongated chromosomes (asymmetric division) to produce two genetically and cytologically *asymmetric* cell compartments (Hilbert & Piggot, 2004).

High-threshold Spo0A promoters are found upstream of the *spoIIA* and *spoIIG* operons, which encode σ^F and σ^E and their regulators, respectively, and promoters of genes required for their compartmentalization (Figure I.7) (Chung *et al.*, 1994, Fujita *et al.*, 2005, Piggot & Hilbert, 2004). These include: SirA (establish diploidy) (Wagner *et al.*, 2009); RacA (axial filament formation) (Ben-Yehuda *et al.*, 2003); and SpoIIE and RefZ (asymmetric division) (Ben-Yehuda & Losick, 2002, Khvorova *et al.*, 1998, Levin & Losick, 1996, Levin *et al.*, 1997, Miller *et al.*, 2016, Wagner-Herman *et al.*, 2012). With the exception of *spoIIE* and the *spoIIG* operon, the high-threshold genes are also positively regulated by the stationary phase sigma factor, σ^H (Figure I.7B) (Fujita *et al.*, 2005). Finally, many of the proteins involved in cell cycle processes during growth also participate in the early stages of sporulation, and in many cases, perform additional sporulation-specific functions. Consequently, a high degree of coordination between the

DNA replication, chromosome segregation, and cell division machineries is critical for efficient transition between active growth and sporulation

I.2.1.1 Establishing diploidy

A strict requirement for differentiation is that cells enter sporulation in a diploid state. Consequently, vegetative cells maintain partial diploidy regardless of growth rate, medium or temperature (Wang *et al.*, 2014). Chromosome copy number during development is regulated, in part, by the cell cycle checkpoint protein, Sda (Suppressor of DnaA), which transiently delays entry into sporulation in cells that have initiated replication or are responding to DNA damage (Veening *et al.*, 2009) by direct inhibition of the KinA phosphorelay protein (Figure I.3 and Figure I.7A) (Burkholder *et al.*, 2001, Cunningham & Burkholder, 2009, Rowland *et al.*, 2004, Whitten *et al.*, 2007). Copy number is also regulated by the sporulation protein SirA (Sporulation inhibitor of replication A), which directly prevents DnaA from initiating new rounds of replication once diploidy has been established (Figure I.3 and Figure I.7) (Rahn-Lee *et al.*, 2009, Wagner *et al.*, 2009).

The chromosome segregation proteins, Spo0J (ParB) and Soj (ParA), are also important for progression through the cell cycle checkpoint. Early classical genetic studies identified *spo0J* as a mutant that blocked entry into sporulation (Mysliwiec *et al.*, 1991, Piggot & Coote, 1976); however, the blockage was suppressed upon deletion the gene immediately upstream *spo0J*, renamed *soj* (*suppressor of spo0J*), indicating that Soj activity is responsible for inhibiting development whereas Spo0J functions to

antagonize Soj (Ireton & Grossman, 1994, Ireton *et al.*, 1994). Soj dimers cannot hydrolyze their bound ATP in the absence of the Spo0J stimulus, resulting in sustained initiation of DNA replication and, consequently, an Sda-imposed block into sporulation (Veening *et al.*, 2009). Soj acts as a molecular switch by directing DnaA to initiate (ATP-bound dimer) or inhibit new rounds of replication (monomer or ADP-bound dimer), the latter form of which requires Spo0J-stiumulated ATP hydrolysis; in the absence of Spo0J, over-replication triggers Sda to inhibit sporulation (Figure I.3) (Veening *et al.*, 2009).

I.2.2 Compartmentalized gene expression

Compartmentalized gene expression within the two cell types is fundamental to forespore differentiation, and is driven by the hierarchal activation of four cell-specific regulators called sigma factors (Figure I.8) (Hilbert & Piggot, 2004). Limited to the chromosome of the cell in which they become active, the activity of each sigma factor becomes compartmentalized. Compartment-specific activation of early and late acting sigma factors is coupled to two distinct morphological events in the developing cell (Hilbert & Piggot, 2004).

First, immediately following asymmetric septation σ^F becomes active in the forespore, which in turn signals activation of the σ^E in the mother cell. σ^F and σ^E direct expression of proteins required for the mother cell to engulf the forespore (Illing & Errington, 1991) and are responsible for expression of the two late-stage sigma factors, σ^G and σ^K (Kunkel *et al.*, 1990).

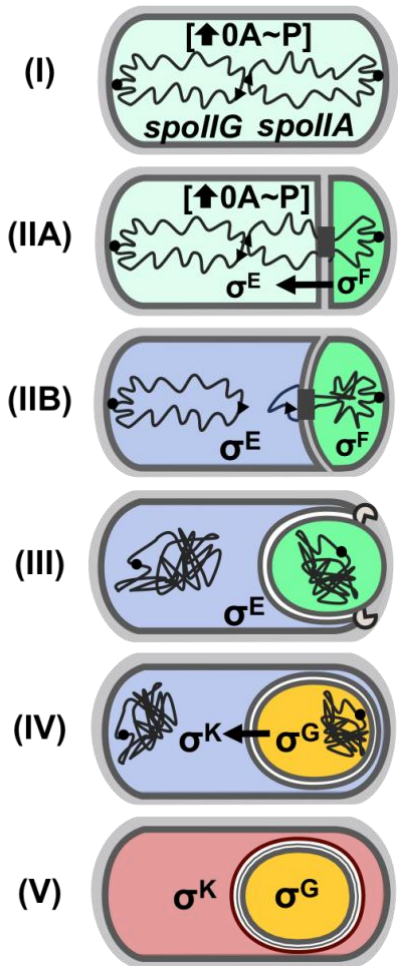

Figure I.8 Compartmentalized gene expression during the progression of sporulation.
In starving populations, concentrations of phosphorylated Spo0A gradually increase until reaching levels sufficient for activating expression of the *spoIIG* and *spoIIA* operons encoding σ^F and pro-σ^E, respectively, and their regulators, and genes required for asymmetric division and axial filament formation. In predivisional cells **(I)**, σ^F is expressed in the active form but held inactive until asymmetric septation, while pro-σ^E must undergo post-translational processing to become active. Asymmetric division **(IIA)** triggers release of σ^F into the forespore where it activates a forespore-specific line of transcription that includes the gene for SpoIIR, which activates the protease SpoIIGA. SpoIIGA acts across the septum to process pro-σ^E to the active form, σ^E, which initiates transcriptional programs specifically in the mother cell **(IIB)**. One-third of the forespore-destined chromosome is trapped by the polar septum promoting a critical period of genetic asymmetry necessary σF activation**.** The translocase, SpoIIIE (black square), localizes to the septum and interacts with the trapped DNA before directionally pumping the remainder of the chromosome into the forespore **(IIB)**. σ^E activates expression of SpoIID, M, and P hydrolases responsible for thinning the septal wall during engulfment **(III)**. σ^E also activates expression the *spoIIIA* operon, whose products act across the forespore membrane signaling forespore regulators to activate the second forespore-specific regulator, σ^G. σ^G is part of the 0A-controlled *spoIIG* operon but expression is controlled post-transcriptionally and requires σ^F-dependent activation as well as the mother cell signal and the completion of engulfment **(IV)** (yellow forespore). σ^G-dependent factors expressed in the forespore signal across both membranes to trigger post-translational activation of σ^K in the mother cell **(IV)**, similar to the activation of σ^E. σ^K expression is also regulated at the transcriptional level; the sequence encoding pro-σ^K only becomes available for transcription after a rearrangement in the chromosome. Activation of σ^K-dependent transcriptional programs in the mother cell (pink) and σ^G activity in the forespore drive formation of the durable spore cortex and coat layers **(V)** that give *Bacillus* spores their characteristic resistance to heat, desiccation, light, and chemicals.

The completion of engulfment is coupled to activation σ^G in the forespore, which in turn signals σ^K activation in the mother cell (Figure I.8). σ^G and σ^K direct expression of proteins that help funnel nutrients from the mother cell to the forespore during maturation and proteins required for assembling the proteinaceous, armor-like coat of the spore (Hilbert & Piggot, 2004).

I.2.2.1. Axial filament formation

When the axial filament forms the cells two chromosomes adopt an *oriC-ter-ter-oriC* arrangement, which positions regions near *oriC* in the vicinity of the incipient polar septum. Genetic asymmetry is generated following polar division, as the sporulation septum initially only captures the *ori*-proximal 30% of one of the cell's two chromosome inside the forespore compartment, leaving the remaining 70% and the second chromosome in the mother cell (Figure I.7B) (Pogliano *et al.*, 2002, Wu & Errington, 1998). A full complement of the genome is eventually restored to the forespore by the DNA translocase, SpoIIIE, which localizes within the forespore membrane at the leading edge of the polar septum (Figure I.6 and Figure I.8) (Fiche *et al.*, 2013, Wu & Errington, 1994, Wu & Errington, 1997) and which uses ATP hydrolysis to directionally pump the rest of the trapped chromosome from the mother cell into the forespore over a period of 10-15 minuntes (Figure I.8) (Bath *et al.*, 2000, Becker & Pogliano, 2007, Khvorova *et al.*, 2000, Pogliano *et al.*, 1999, Wu & Errington, 1994, Wu *et al.*, 1995).

The direction of translocation through the septum is determined by the orientation of SRS, (SpoIIIE Recognition Sequences), short chromosome sequences

highly skewed to the *terminus* region (Figure I.5B) (Ptacin *et al.*, 2008). Unlike KOPS recognized by *E. coli* FtsK, the orientation of SRS on the chromosome do not switch direction exactly at *oriC* but instead switch at a region ~400 kb to the left, comprising the centromere-like element that is tethered to the pole during axial filament formation (Figure I.5B) (Ben-Yehuda *et al.*, 2005, Sharpe & Errington, 1996, Wu & Errington, 2002).

In contrast from the more condensed, bi-lobed nucleoid observed in vegetative cells, the nucleoid of sporulating cells transitions to a less compact, elongated structure called the axial filament (Figure I.9) (Bylund *et al.*, 1993, McGinness & Wake, 1979, Ryter *et al.*, 1966). During axial filament formation, chromosome origins are segregated to and anchored at the distal poles resulting in an *oriC-ter-ter-oriC* arrangement of the cells two chromosomes. The arrangement of the chromosomes within the axial filament ensures that precise regions are positioned within the cell to become efficiently trapped by the polar septum. Chromosome capture is precise and highly reproducible, encompassing the *oriC*-proximal region between the -58° and +38° positions (Figure I.7B)(Sullivan *et al.*, 2009, Wu & Errington, 1994, Wu & Errington, 1998).

Origin anchoring to the poles depends primarily on interactions between the curvature-sensing protein, DivIVA, and the kinetochore-like DNA-binding protein, RacA (Figure I.9) (Ben-Yehuda *et al.*, 2003, Thomaides *et al.*, 2001, van Baarle *et al.*, 2013, Wu & Errington, 2002, Wu & Errington, 2003).

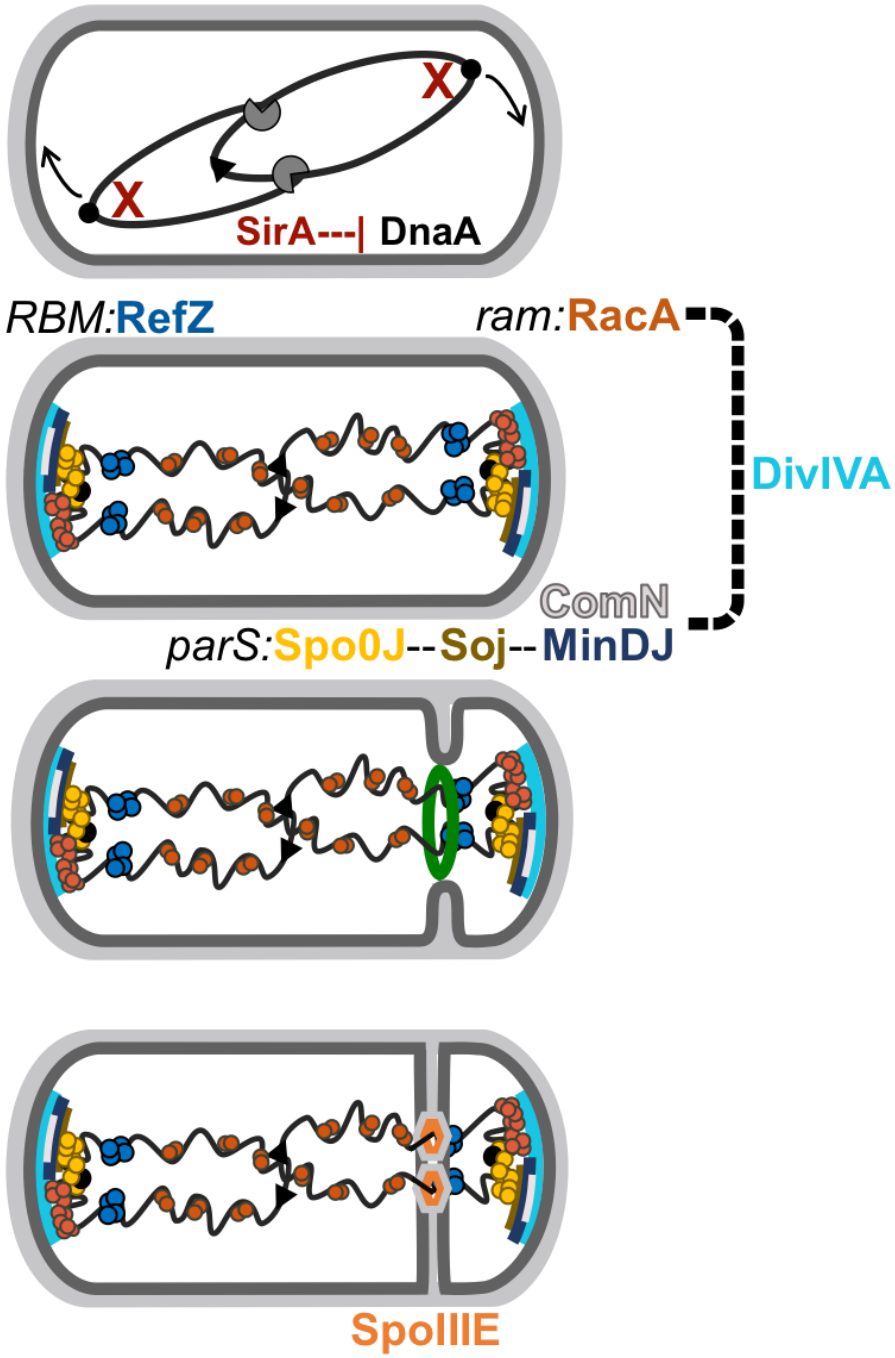

Figure I.9 Axial filament formation and chromosome trapping require multiple DNA binding proteins.
Two systems, RacA-*ram* (burnt orange) and Spo0J-*parS* (yellow), associate directly and indirectly with DivIVA (cyan) at the far poles to anchor the origins. Spo0J-*parS* are recruited to the pole by Soj (brown), which is localized by a hierarchy of interactions: MinD-MinJ (navy), ComN (white), and DivIVA (cyan). RacA also binds non-specifically throughout the chromosome to condense and structure the axial filament. RefZ (blue) interacts at *RBM*s on the left and right arms adjacent to the boundary of the capture region.

RacA (Remodeling and anchoring of chromosomes A) anchors the chromosomal region residing 60-80 kb to the left of *oriC* to the pole via specific interactions at 25 motifs called *ram* (*RacA binding motif*) (Ben-Yehuda *et al.*, 2005). RacA also localizes to the bulk nucleoid via non-specific DNA interactions (Figure I.9) (Ben-Yehuda *et al.*, 2005). RacA is capable of compacting DNA via strong protein-protein interactions (Ben-Yehuda *et al.*, 2005), similar to the ability of ParB-like proteins, Spo0J and Noc, to form nucleoprotein complexes between sites of DNA binding (Figure I.2 and Figure I.5A) (Adams, Wu, & Errington, 2015; Murray, Ferreira, & Errington, 2006).

Condensation of DNA between the *ram*-containing segments into nucleoprotein complexes produces a centromere-like element at the origin (Figure I.5B) that becomes anchored to the pole through the RacA-DivIVA interaction (Figure I.9)(Ben-Yehuda *et al.*, 2005). Moreover, all 25 *ram* segments defining the centromere-like element are present within the capture region, consistent with a critical role for RacA in organizing and stabilizing the *oriC*-proximal chromosome prior to polar septation (Ben-Yehuda *et al.*, 2005). Condensation also occurs at sites where RacA binds the chromosome non-specifically, and is thought to contribute to axial filament structuring (Figure I.9).

The chromosome partitioning function of Spo0J is also important for origin segregation during axial filament formation (Ireton *et al.*, 1994, Lee & Grossman, 2006, Wu & Errington, 2003). Condensed Spo0J-*parS* origin complexes are delivered to the far poles as part of the multi-protein complex anchored by DivIVA (Figure I.9) (Kloosterman *et al.*, 2016, Lin *et al.*, 1997). Repositioning of the Spo0J/*parS* origin region is mediated by Soj, likely via its characterized interaction with MinD (Figure I.9)

(Autret & Errington, 2003). Soj localization to septal sites in non-sporulating cells was previously observed to occur in a MinD- and Spo0J-dependent manner (Autret *et al.*, 2001, Murray & Errington, 2008). During growth and sporulation, MinD localization to DivIVA at the poles and the division septum is mediated by its interaction with MinJ (Figure I.1 and Figure I.9)(Bramkamp *et al.*, 2008, Patrick & Kearns, 2008, van Baarle & Bramkamp, 2010). However, MinD appears to have a discrete function in targeting Soj to the poles during development that additionally requires a second DivIVA adaptor, ComN (Figure I.9)(Kloosterman *et al.*, 2016). ComN post-transcriptionally regulates the expression of late-competence genes by targeting *comE* mRNA to the poles (dos Santos *et al.*, 2012, Ogura & Tanaka, 2009), although its function during sporulation primarily appears to be in stabilizing MinJ-MinD-Soj interactions with DivIVA in the polar complex (Kloosterman *et al.*, 2016).

I.2.2.2 Asymmetric cell division

In growing vegetative cells, FtsZ polymerizes into Z-rings at midcell, resulting in symmetric division between segregated nucleoids (Figure I.1 and Figure I.3). During sporulation however, division must be localized to an asymmetric position near the pole in order to properly capture the *oriC* region of the forespore-destined chromosome and compartmentalize σ^F activity. At the onset of sporulation, FtsZ redistributes through spiral-like intermediate from midcell to each quarter-cell position, resulting in the formation of "bipolar" Z-rings (Figure I.10)(Barak *et al.*, 1998, Ben-Yehuda & Losick, 2002, Levin & Losick, 1996). Eventually, only one Z-ring matures into the asymmetric

septum (Figure I.10) although cells can turn to the second site in the event σ^F is not activated following the first division.

In order to form twice the normal Z-rings, increased expression of FtsAZ and expression of the bifunctional phosphatase, SpoIIE, is required (Ben-Yehuda & Losick, 2002, Khvorova *et al.*, 1998). SpoIIE expression is positively regulated by high-threshold levels of Spo0A~P (Figure I.7B) (Fujita *et al.*, 2005, Levin & Losick, 1996), while increased FtsAZ levels are stimulated by σ^H from a developmental promoter called P2 (Fujita *et al.*, 2005, Gholamhoseinian *et al.*, 1992, Gonzy-Treboul *et al.*, 1992). In this way, Z-ring shifting is only triggered when cells have entered sporulation through the positive feedback loop between σ^H-dependent expression of Spo0A and FtsAZ, and the consequential stimulation of SpoIIE and σ^H expression by Spo0A~P (Figure I.7B).

SpoIIE is a bifunctional seine phosphatase required for asymmetric division and the timing of activation of the first forespore-specific factor, σ^F. SpoIIE redistributes to polar division sites in an FtsZ-dependent manner where it similarly coalesces into ring structures called "E-rings" (Figure I.10) (Arigoni *et al.*, 1995, Barak & Youngman, 1996, Ben-Yehuda & Losick, 2002, Krol *et al.*, 2017, Levin *et al.*, 1997, Lucet *et al.*, 2000), and preferentially localizes to the forespore side of the septum through interactions with the DivIVA (Figure I.10) (Bradshaw & Losick, 2015, Eswaramoorthy *et al.*, 2014, Guberman *et al.*, 2008).

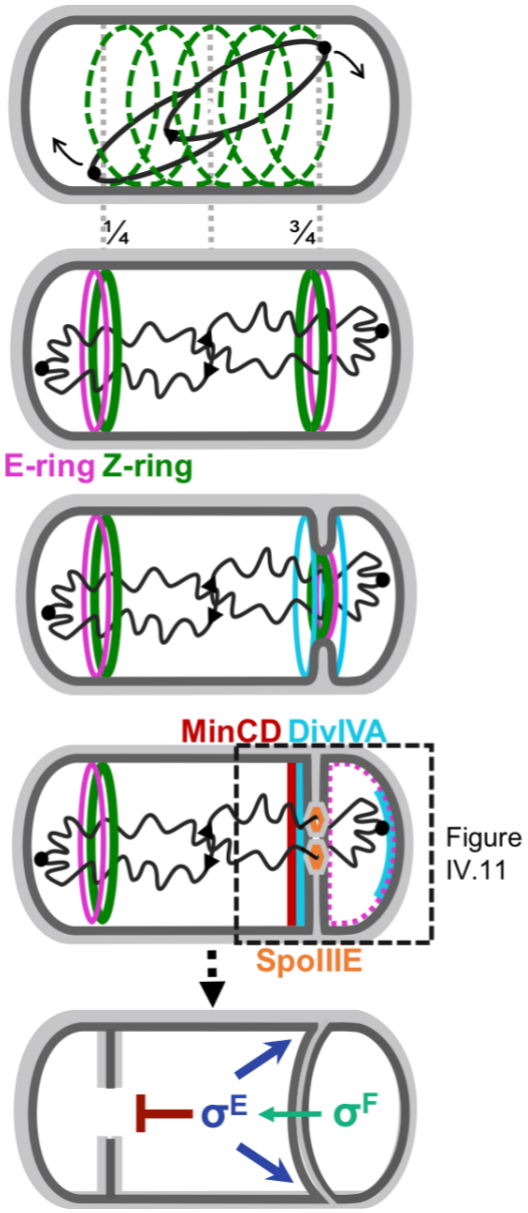

Figure I.10 Bipolar Z-ring assembly and asymmetric division during sporulation.
Midcell FtsZ (green dashed) redistributes to the cell quarters through a spiral like intermediate. Bipolar Z-rings (green) are stabilized by SpoIIE (pink). Only one Z-ring ultimately produces an asymmetric septum, and this recruits Min system proteins, DivIVA (blue) and MinCDJ (red)**.** The DNA translocase, SpoIIIE (orange) assembles in the membrane, forming a protective channel around each arm of the chromosome. When the polar septum is complete, SpoIIE becomes released from the division site and redeploys throughout the forespore membrane (pink dashed). Release triggers SpoIIE's phosphatase activity, which is required for activating σF in the forespore (boxed region, see Figure IV.11). Immediately following σ^F activation, a signal from the forespore triggers σ^E activation in the mother cell. σ^E activates transcription of hydrolases required for thinning the peptidoglycan between the forespore and mother cell membranes during engulfment (dark blue arrows). These hydrolases also dissolve any partial division septa that have formed in the mother cell (red cross).

The phosphatase activity of SpoIIE is stimulated following septation, at which point it redistributes throughout the forespore membrane (Figure I.11) (Bradshaw & Losick, 2015, Campo *et al.*, 2008, Carniol *et al.*, 2005, Eswaramoorthy *et al.*, 2014, Lewis *et al.*, 1998). A second interaction with DivIVA following division is thought to stabilize and enrich SpoIIE in the forespore compartment (Bradshaw & Losick, 2015), which is a critical factor for proper timing of its second function in activating σ^F in the forespore compartment (Figure I.10 and I.11) (Eswaramoorthy *et al.*, 2014, Feucht *et al.*, 1996, Frandsen *et al.*, 1999, King *et al.*, 1999, Lewis *et al.*, 1998).

Temporal activation of σ^F in the forespore

Genes encoding σ^F and σ^E and their respective regulatory proteins are expressed in predivisional cells from two distinct operons, *spoIIA* and *spoIIG*, respectively (Figure I.7B) (Fujita *et al.*, 2005). σ^F is expressed in its active form in predivisional cells but is held inactive by the anti-sigma factor, SpoIIAB, until asymmetric division is complete (Figure I.11)(Duncan & Losick, 1993). The anti-anti-sigma factor, SpoIIAA, triggers release of σ^F from the inactive hold by antagonizing SpoIIAB (Duncan *et al.*, 1994). SpoIIAA activity is controlled by its phosphorylation state: the phosphorylated form, SpoIIAA~P, is inactive whereas dephosphorylation yields the active form, SpoIIAA (Figure I.11). A threshold level of active SpoIIAA must be reached to efficiently attack the SpoIIAB: σ^F complex (Duncan *et al.*, 1996). Following polar division, SpoIIAB:σ^F and SpoIIAA~P molecules are present in both compartments. Levels of active SpoIIAA increase due to the phosphatase activity of SpoIIE, resulting in dephosphorylation of

SpoIIAA~P in the forespore (Figure I.11) (Eswaramoorthy et al., 2014; Carinol, Eichenberger, & Losick, 2004; Arigoni et al., 1996; King et al., 1999; Duncan et al, 1995; Feucht, Abbotts, & Errington, 2002). Thus, activation of σ^F exclusively in the forespore is coupled both to completion of asymmetric division and accumulation of dephosphorylated SpoIIAA in the forespore.

SpoIIAB is a serine kinase, and indirectly prevents premature σ^F activation in predivisional cells by phosphorylating SpoIIAA. SpoIIAB harbors a histidine kinase-like ATPase domain; the ATP-bound form sequesters σ^F in the inactive complex while the ADP-bound form, which is produced after SpoIIAA attack and σ^F release, remains catalytically inactive toward free σ^F until the ADP nucleotide is replaced with ATP (Figure I.11) (Min et al., 1993). The rate of nucleotide exchange is slow, permitting formation of a stable complex with SpoIIAA (SpoIIAB-ADP:SpoIIAA) (Figure I.11) (Lee, Lucet, & Yudkin, 2000; Najafi, Harris, & Yudkin, 1997). In this way, SpoIIAB-ADP serves as a "sink" to sequester any SpoIIAA molecules that have become active outside of the forespore compartment and in predivisional cells (Carinol, Eichenberger, & Losick, 2004; Alper, Duncan, & Losick, 1994). Additionally, free SpoIIAB-ADP is proteolytically unstable and becomes preferentially degraded in the forespore by the ClpCP protease following division, preventing active SpoIIAA from being sequestered in the long-lived complex with SpoIIAA (Figure I.11) (Pan, Garsin, & Losick, 2001).

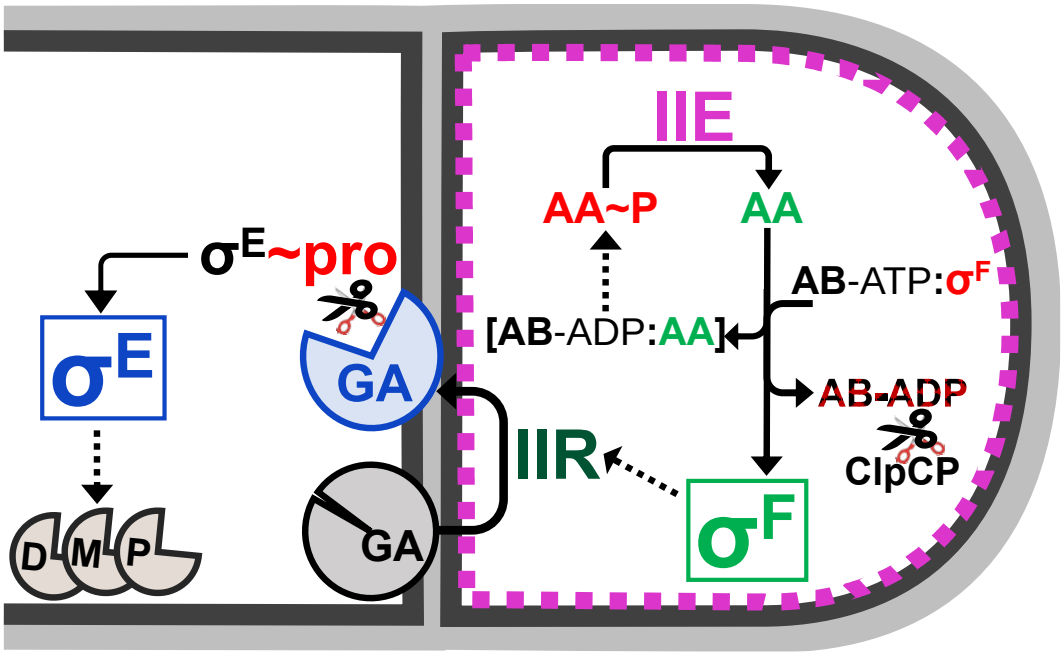

Figure I.11 Asymmetric division is required to establish compartmentalized gene expression in the forespore and mother cell.
Release of SpoIIE into the forespore membrane triggers its phosphatase activity resulting in activation of SpoIIAA (AA, green), which releases σ^F (boxed) from its inactive hold with SpoIIAB. σ^F activates *spoIIR* expression (IIR) which in turn activates the protease, SpoIIGA, in the mother cell membrane (GA, blue pacman). Post-translational cleavage of pro-σ^E generates the active form of σ^E (boxed). σ^E activates expression of SpoIIDMP hydrolases in the mother cell needed for engulfment.

The chromosomal location of the *spoIIA* locus and its position in the cell at the time of polar division are also critical for increasing the ratio of active SpoIIAA to SpoIIAB:σ^F and SpoIIAB-ADP. The *spoIIA* locus lies in the *ter*-proximal chromosome region and is initially excluded from the forespore when the polar septum forms (Figure I.7B). This transient genetic asymmetry allows active SpoIIAA to reach levels in excess of the SpoIIAB-ADP sink by deterring SpoIIAB expression in the forespore until the *spoIIA* locus is transferred (Frandsen et al., 1999; Dworkin & Losick, 2002). The late arrival of *spoIIAB* to the forespore compartment also prevents SpoIIAB from becoming

replenished following proteolysis its proteolysis by ClpCP (Figure I.11) (Pan, Garsin, & Losick, 2001).

Upon release from SpoIIAB, σ^F activity is temporarily restricted to the *ori*-proximal 30% of the chromosome that is initially trapped in the forespore. Genes in the σ^F regulon found within the captured segment of the chromosome include *spoIIR*, the product of which is required for subsequent activation of σ^E in the mother cell (Figure I.7B and Figure I.11) (Karow, Glaser, & Piggot, 1995).

Activation of σ^E in the mother cell

The *spoIIG* operon is expressed prior to asymmetric division (Figure I.7B and Figure I.8) and encodes an inactive form of σ^E, or pro-σ^E, and SpoIIGA, a forespore membrane-bound protease (Imamura et al., 1008; Fujita & Losick, 2002; Satola, Baldus, & Moran, 1992; Patridge & Errington, 1993; Fawcett, Melnikov, & Youngman, 1998). Activation of σ^E occurs in the mother cell following asymmetric division via post-translational cleavage of pro-σ^E by SpoIIGA (Figure I.11) (Jonas et al., 1988; Straiger, Bonamy, & Karmazyn-Campelli, 1988). SpoIIGA activity is stimulated by SpoIIR, the expression of which occurs in the forespore in a σ^F–dependent manner (Figure I.11) (Hofmeister et al., 1995; Londono-Vallejo & Straiger, 1995; Karow, Glaser, & Piggot, 1995). The gene encoding the second forespore-specific factor, σ^G, is also part of the *spoIIG* operon (Karmazyn-Campelli et al., 1989; Masuda et al., 1988), although its expression is dependent on σ^F and requires the completion of engulfment (Figure I.8)

(Gholamhoseinian & Piggot, 1989; Chary *et al*., 2005; Sun, Cabrera-Martinez, & Setlow, 1991). σ^E directs expression of the second mother cell factor, pro-σ^K, that similarly becomes active upon post-translational processing to σ^K in a σ^G-dependent manner (Figure I.8) (Cutting et al., 1991; Wakeley, Hoa, & Cutting, 2000).

I.2.2.3 Commitment to sporulation

σ^F-dependent activation of σ^E is considered the "point of no return" at which the process of sporulation becomes irreversible (Figure I.8 and Figure I.11) (Narula et al., 2012; Hilbert, Chary, & Piggot, 2004). The σ^E regulon is the largest of the four sporulation-specific sigma factors (Feucht, Evans, & Errington, 2003; Eichenberger et al., 2004) and includes genes required for engulfment, during which the mother cell membrane wraps completely around the small compartment by hydrolysis of the septal wall peptidoglycan, to produce a double membrane-bound forespore (Figure I.6 and Figure I.8) (Tocheva et al., 2013; Abanes-De Mello et al., 2002).

σ^E activity also regulates expression of proteins responsible communicating whether gene expression was successfully compartmentalized following polar division (Zhang et al., 1996). The hydrolases SpoIID, SpoIIM, and SpoIIP (DMP complex) are responsible for septal wall thinning during engulfment and are also critical for dissolution of aberrantly formed septa in the mother cell (Figure I.8 and Figure I.10) (Gutierrez, Smith, & Pogliano, 2010; Eichenberger, Fawcett, & Losick, 2001; Pogliano et al., 1999). Premature or artificial activation of σ^E in pre-divisional cells inhibits polar division due in part to SpoIIDMP-mediated septum degradation (Eichenberger *et al.*,

2001, Pogliano *et al.*, 1999). In addition, σ^E positively regulates expression of MciZ, an inhibitor of FtsZ that prevents additional divisions within the mother cell following polar septation and successful capture of *oriC* (Bisson-Filho *et al.*, 2015, Handler *et al.*, 2008).

Mutants deficient in axial filament formation often fail to capture the precise region of the forespore chromosome, specifically *oriC*, resulting in a proportion of cells that lack σ^F activity in the forespore and, subsequently, σ^E activity in the mother cell (Ben-Yehuda, Rudner, & Losick, 2003; Wu & Errington, 2003). Miscapture of *oriC* also occurs in sporulating wild-type cells, albeit in a significantly small proportion of the population (< 3% of the population) (Sullivan *et al.*, 2009). To counter defective axial filament formation and ensure gene expression becomes compartmentalized, *Bacillus* have evolved a failsafe mechanism that permits utility of the second Z-ring and a second septation event to take place at the opposite pole in cells that failed to capture *oriC* in the forespore after the first polar division. For instance, 50% of a *racA* mutant population improperly capture the origin in the mother cell, and these cells undergo a second division at the distal pole, capturing the origin of the second chromosome with similar frequency (Ben-Yehuda *et al.*, 2005, Ben-Yehuda *et al.*, 2003, Wu & Errington, 2003).

A key element of this mechanism is the DNA translocase, SpoIIIE, which ensures that a full copy of the genome is available in the mother cell in the event the origin is properly captured by the second asymmetric septum, and activation of σ^F is successful (Becker & Pogliano, 2007). SpoIIIE assembles co-axial paired channels on both the mother cell and forespore sides of the polar septum (Yen Shin *et al.*, 2015), and

is thought to act as an "exporter" of DNA, translocating trapped chromosomes into the compartment in which the origin was originally captured (Becker & Pogliano, 2007, Ptacin *et al.*, 2008, Sharp & Pogliano, 2002, Wu *et al.*, 1995).

The second division is only permitted due to the absence of SpoIID, M, and P hydrolases from the mother cell, which are not expressed if σ^E has not become activated (Eichenberger *et al.*, 2001, Pogliano *et al.*, 1999). Sporulating cells that do successfully activate σ^F, but fail to activate σ^E in the mother cell exhibit an abortively "disporic" phenotype, in which organisms contain three chambers instead of two, and lack a mother cell chromosome in the middle compartment (Illing & Errington, 1991; Pogliano et al., 1999). Instead, both chromosomes occupy the distal "forespore" compartments as a consequence of SpoIIIE-mediated export following septation at both poles (Figure) (Wu & Errington, 1994; Lewis, Partridge, & Errington, 1994; Sharp & Pogliano, 2002). As abortively disporic organisms are blocked at this stage, and they do not go on to produce viable spores, precise regulation of the early morphological events that lead to σ^F and σ^E activation, including axial filament formation and asymmetric division, is critical to ensure a significant population of cells that initiate sporulation successfully differentiate into mature spores.

A DNA-binding protein involved in chromosome organization and cell division during sporulation

RefZ (formerly YttP) is a member of the TetR/AcrR family of DNA-binding proteins (Marchler-Bauer *et al.*, 2011) and was initially identified in a screen for Spo0A-

controlled genes that contributed to chromosome organization during sporulation (Figure I.7B and Figure I.9) (Wagner-Herman *et al.*, 2012). Mutants were assessed for defects in chromosome organization by fluorescence microscopy using a quantitative, single cell-based "DNA-trapping" assay, which makes use of a translocase deficient variant of SpoIIIE and forespore-specific fluorophore expression to gain a "snapshot" of chromosome morphology at the time of polar division (Sullivan *et al.*, 2009). Fluorophores fused to promoters only activated by σ^F in the forespore can be introduced at ectopic sites along the chromosome to determine the frequency with which that particular region is "trapped" inside the forespore (Sullivan *et al.*, 2009). Sporulating *refZ* mutants were observed to over-capture a reporter positioned at -61°, which was only trapped in the forespore in 20% of otherwise wild-type cells (Wagner-Herman *et al.*, 2012).

RefZ (Regulator of FtsZ) was annotated as such following the observation that its artificial expression in vegetative cells disrupted Z-ring assembly resulting in a block in cell division (Wagner-Herman *et al.*, 2012). Furthermore, RefZ's DNA-binding activity was determined to be required for its ability to inhibit cell division, as variants harboring substitutions in the DNA recognition helix no longer exhibited cell filamentation when artificially expressed during growth cells (Wagner-Herman *et al.*, 2012). RefZ's binding sites were previously identified using ChIP-seq on sporulating cells expressing a single copy of RefZ-GFP from the native P_{refZ} promoter during sporulation (Wagner-Herman *et al.*, 2012). Analysis revealed nine regions of RefZ enrichment on the chromosome, of which six peaks spanning 1-2.5 kb had the highest enrichment (~100-500-fold) and

contained a central, nearly palindromic 20-bp sequence, or *RBM* (RefZ Binding Motif) (Wagner-Herman *et al.*, 2012). Five *RBM*s mapped within the *ori*-proximal ~20% of the chromosome (Figure I.9) and a sixth peak containing a degenerate, or "half site", of the consensus mapped to the *hrcA* locus in the *ter*-proximal region (*RBM*$_T$) (Wagner-Herman *et al.*, 2012). The remaining three regions of lesser enrichment, appearing as broad flat peaks that span 3-4 kb each and lacking a defined *RBM* consensus sequence are also located within the *oriC*-proximal 7% of the chromosome (Wagner-Herman et al, 2012). Intriguingly, these regions contain segments where Spo0J has been shown to nucleate at its cognate *parS* sites and spread along DNA (Breier & Grossman, 2007, Lin & Grossman, 1998, Murray *et al.*, 2006). Spo0J spreading was distinguishable in published ChIP-seq data that revealed similar broad enrichments, which could be consistent with spreading of RefZ along the chromosome (Wagner-Herman *et al.*, 2012).

As discussed in the following chapters, RefZ and its cognate *RBM*s appear to represent one of three conserved systems in *Bacillus* that employ a site-specific DNA-binding protein to maintain the precision of chromosome capture during sporulation. Previously, RacA and Spo0J were characterized for their role in chromosome organization using the single cell-based trapping assay (Ben-Yehuda *et al.*, 2005, Sharpe & Errington, 1996, Lin & Grossman, 1998, Graham *et al.*, 2014, Sullivan *et al.*, 2009). The function of the RefZ-*RBM* system appears distinct from the others, as RefZ does not seem to be a component of the DivIVA-localized polar complex involved in origin capture (Kloosterman *et al.*, 2016), nor does RefZ appear to directly modify the overall organization of the chromosome. We find that while Soj-Spo0J-*parS* and RacA-*ram*

complexes are more important for capturing *oriC* (Ben-Yehuda *et al.*, 2003, Kloosterman *et al.*, 2016, Sullivan *et al.*, 2009, Wu & Errington, 2003), RefZ-*RBM* complexes appear to contribute to precise left and right arm capture (Chapter II)(Miller *et al.*, 2016). In this thesis we also aim to delineate the relationship between RefZ's division modulation activity and its role in capturing the chromosome during sporulation. Our data suggest RefZ exacts its function in chromosome capture by helping to maintain the precision with which the division septum forms over the chromosome (Chapter III)(Brown *et al.*, 2019).

CHAPTER II

A DNA-BINDING PROTEIN DEFINES THE PRECISE REGION OF CHROMOSOME CAPTURE DURING *BACILLUS* SPORULATION*

II.1 INTRODUCTION

A major goal of bacterial cell biology is to identify and characterize the primary determinants underlying the cell's 3D organization and to understand how spatial organization is exploited to regulate physiology. Although not generally thought of as a primary platform from which bacteria organize cellular activities, the nucleoid is well positioned to serve a significant role as a topological marker because it is highly organized and occupies an expansive central space in the cytoplasm (Ptacin & Shapiro, 2013).

The importance of the nucleoid in cellular organization is best understood in the context of division site selection. The signals for divisome assembly are tightly coupled with nucleoid positioning, thus ensuring that each daughter cell inherits at least one copy of the chromosome. In fast-growing *Bacillus subtilis* and *Escherichia coli*, the bulk nucleoid is localized in the middle two-quarters of the cell, with the least amount of DNA present at the cell poles; at the end of replication, there is also less DNA present between replicated chromosomes at midcell. The nucleoid occlusion proteins of *E. coli*

---

* Reproduced with permission under the terms of the licensing agreement from "A DNA-binding protein defines the precise region of chromosome capture during *Bacillus* sporulation" by AK Miller, EE Brown, BT Mercado, and JK Herman, 2016. *Mol Microbiol*, 99(1), 111-22, Copyright [2015] by John Wiley & Sons Ltd.

(SlmA) and *B. subtilis* (Noc) are DNA-binding proteins that inhibit FtsZ polymerization (Bernhardt & de Boer, 2005, Wu & Errington, 2004) when bound to DNA motifs enriched around the nucleoid except near the midcell-localized chromosomal terminus regions (Cho *et al.*, 2011, Tonthat *et al.*, 2011, Wu *et al.*, 2009).

In addition to growing by binary fission, *B. subtilis* is also capable of developing into a resting cell type called a spore. During early stages of sporulation, *B. subtilis* harbors two chromosome copies, stretched across the cell in an *oriC-ter-ter-oriC* arrangement called the axial filament (Piggot & Hilbert, 2004, Bylund *et al.*, 1993). The *oriC*-proximal regions are anchored to the cell poles through interactions between the conserved morphogenic protein DivIVA and the DNA-binding protein RacA (Ben-Yehuda *et al.*, 2003). Shortly thereafter, an asymmetric septation creates two disproportionately sized cell compartments. The smaller compartment, or forespore, eventually becomes the mature spore while the larger "mother" cell nurtures the forespore during development.

To create the two compartments, FtsZ redistributes from midcell toward one or both poles through a spiral-like intermediate (Ben-Yehuda & Losick, 2002). Polar coalescence of FtsZ during sporulation is driven in part by increasing levels of FtsZ, expressed from a developmental promoter called P2 (Gholamhoseinian *et al.*, 1992, Gonzy-Treboul *et al.*, 1992), as well as synthesis of SpoIIE, a bifunctional protein shown to interact with FtsZ (Levin *et al.*, 1997). RefZ (Regulator of FtsZ), a DNA-binding protein upregulated early in sporulation, was also shown to promote the timely redistribution of FtsZ toward the cell pole (Wagner-Herman *et al.*, 2012). Artificial

expression of RefZ during exponential growth inhibits cell division by disrupting Z-rings, a phenotype that can be suppressed by mutant variants of FtsZ or by FtsZ overexpression (Wagner-Herman *et al.*, 2012). The mechanism by which RefZ influences FtsZ dynamics is not currently understood.

In contrast to vegetative growth, during which nucleoid occlusion inhibits FtsZ assembly over the nucleoid, the polar division of sporulation occurs directly over one chromosome, initially capturing approximately 25% of the *oriC*-proximal region in the forespore compartment (Sullivan *et al.*, 2009, Wu & Errington, 1998). This transient genetic asymmetry promotes differential transcriptional programs in the forespore and mother cell that are required for spore development (Dworkin & Losick, 2001). Assembly of the FtsK-like DNA pump, SpoIIIE, prevents the chromosome from being guillotined by the polar division septum (Burton & Dubnau, 2010). Following assembly, SpoIIIE translocates the remainder of the chromosome into the forespore compartment (Wu & Errington, 1994).

Several proteins have been implicated in *oriC* capture in the forespore (Ben-Yehuda *et al.*, 2003, Sullivan *et al.*, 2009, Wagner *et al.*, 2009, Wu, 2003). However, it is less clear how the cell manages to reproducibly define the boundary where cell division takes place around the forespore-destined chromosome (Wu & Errington, 1998, Sullivan *et al.*, 2009). In this work, we show that spatially conserved DNA motifs (*RBM*s) help define the precise location of cell division with respect to the chromosome during sporulation. More specifically, our data support a model in which the FtsZ-

regulating protein, RefZ, associates with *RBM*s localized near the site of polar division to regulate the position of cell division relative to the chromosome during sporulation.

II.2 RESULTS

II.2.1 *refZ* and its DNA-binding sites are conserved across the *Bacillus* genus

During sporulation, RefZ is enriched at several regions on the chromosome harboring a mostly palindromic, 20 bp motif referred to as an *RBM* (RefZ Binding Motif) (Figure II.1B)(Wagner-Herman *et al.*, 2012). The *RBM* is sufficient for interaction with RefZ, as its placement at ectopic sites leads to specific enrichment of the ectopic regions following RefZ immunoprecipitation (Wagner-Herman *et al.*, 2012). Five out of six of the *RBM*s map to the *oriC*-proximal quadrant of the *B. subtilis* circular chromosome, while RBM_T, which is degenerate and lacks the conserved central palindrome, is located near the terminus (Figure II 1A and 1B).

Intriguingly, the boundaries of the *oriC*-proximal sites align closely with regions where polar septation occurs over the forespore-destined chromosome (Figure II.1A and 1D shaded regions)(Sullivan *et al.*, 2009, Wu & Errington, 1998). Since *refZ* is conserved in the *Bacillus* genus (Figure II.1C)(Wagner-Herman *et al.*, 2012), we investigated if the *RBM*s were also conserved by performing a FIMO search (Grant *et al.*, 2011) of bacterial genomes using the *RBM* consensus (see APPENDIX A Methods A.3).

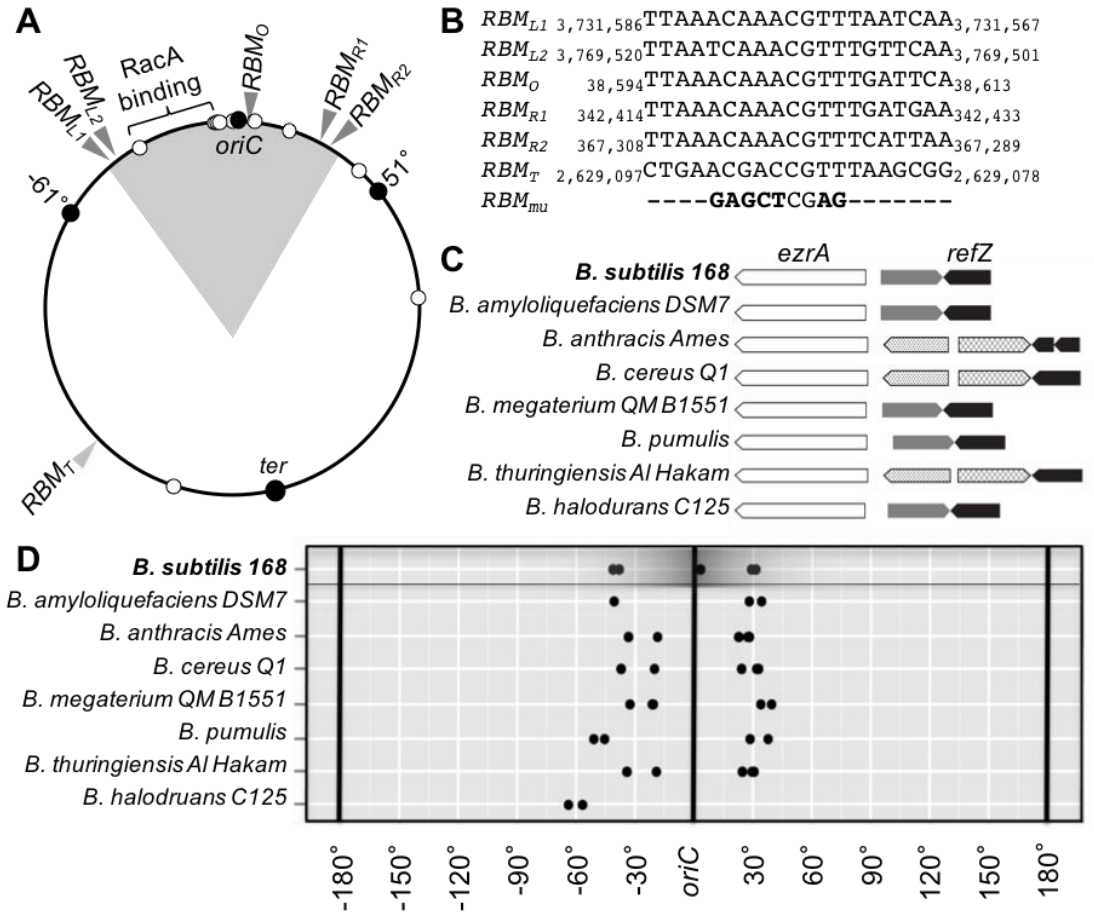

Figure II.1 RefZ and *RBM*s are conserved across the *Bacillus* genus.
Reprinted with permission from Miller *et al*., 2016. **(A)** Location of *RBM*s on the *B. subtilis* chromosome. The shaded region indicates the approximate region of chromosome initially captured in the forespore at the time of polar division. Eighty percent of RacA binding sites are located on the left arm between chromosome coordinates 3,805,000 and 4,211,500 in the labeled region. Spo0J binding sites are shown as white circles. **(B)** Chromosomal coordinates (*B. subtilis* 168) and alignment of the five *oriC*-proximal *RBM*s. RBM_{mu} denotes the point mutations introduced into each *RBM* to create the null strain, RBM_{5mu}. **(C)** Alignment of *refZ* region for multiple members of the *Bacillus* genus. **(D)** *RBM*s identified by FIMO (P<1e-10) mapped to chromosomes of a handful of other *Bacillus* genus members. Since genome sizes differed, all positions were normalized to a 360° circular chromosome linearized at 180° (x-axis). The complete collection of *RBM*s identified by FIMO for all members of the *Bacillus* genus is provided in APPENDIX A Figure A.1. Closely spaced *RBM*s are not resolvable in these figures, so the *RBM* coordinates for each strain are also provided in APPENDIX A Methods A.3.

Our analysis showed that the *RBM* consensus was highly conserved throughout the genus of *Bacillus* polar spore formers. Strikingly, the relative locations of the *RBM*s with respect to *oriC* (0°) are also remarkably similar across the genus; most of the species examined (a subset of species are shown in Figure II.1D; for the entire collection see APPENDIX A Figure A.1) possessed at least four *RBM*s: two on the left arm of the chromosome (approximately -40° in *B. subtilis*) and two on the right arm (approximately 30° in *B. subtilis*) (Figure I.1D and APPENDIX A Figure A.1). Our analysis did not reveal any shared genetic contexts, such as being located in or around specific genes or in promoter regions, which might account for the conserved spatial arrangement of the *RBM*s. These results suggest that there is a strong evolutionary pressure to maintain the motifs at specific chromosomal positions, and is consistent with the idea that the location of the *RBM*s is critical for their function.

II.2.2 RefZ-mediated inhibition of cell division is conserved in *B. megaterium*

RefZ was previously shown to disrupt FtsZ rings when expressed during vegetative growth (Wagner-Herman *et al.*, 2012), and our bioinformatic analyses (Figure II.1D and APPENDIX A Figure A.1) indicate that RefZ and the *RBM*s are conserved across the *Bacillus* genus. To determine if RefZ's FtsZ inhibitory function (Wagner-Herman *et al.*, 2012) is conserved in a distantly related *Bacillus*, we performed a *refZ* swapping experiment between our *B. subtilis* lab strain (*B. subtilis* 168) and *B. megaterium*, another well-characterized and genetically tractable *Bacillus* species (Rossler *et al.*, 1991, Eppinger *et al.*, 2011). We placed *B. megaterium refZ* under the

control of an IPTG-inducible promoter (P_{hy}-*refZ*$_{Bmeg}$) and introduced the construct into the *B. subtilis* chromosome at a non-essential locus. We also performed the reciprocal swap by placing *B. subtilis refZ* under the control of a xylose-inducible promoter (P_{xyl}-*refZ*$_{Bsub}$) and introducing the construct into *B. megaterium*. Prior to induction, *B. subtilis* harboring P_{hy}-*refZ*$_{Bmeg}$ possessed an average cell length of 3.4 ± 0.9 μm and divided at regular intervals (Figure II.2A).

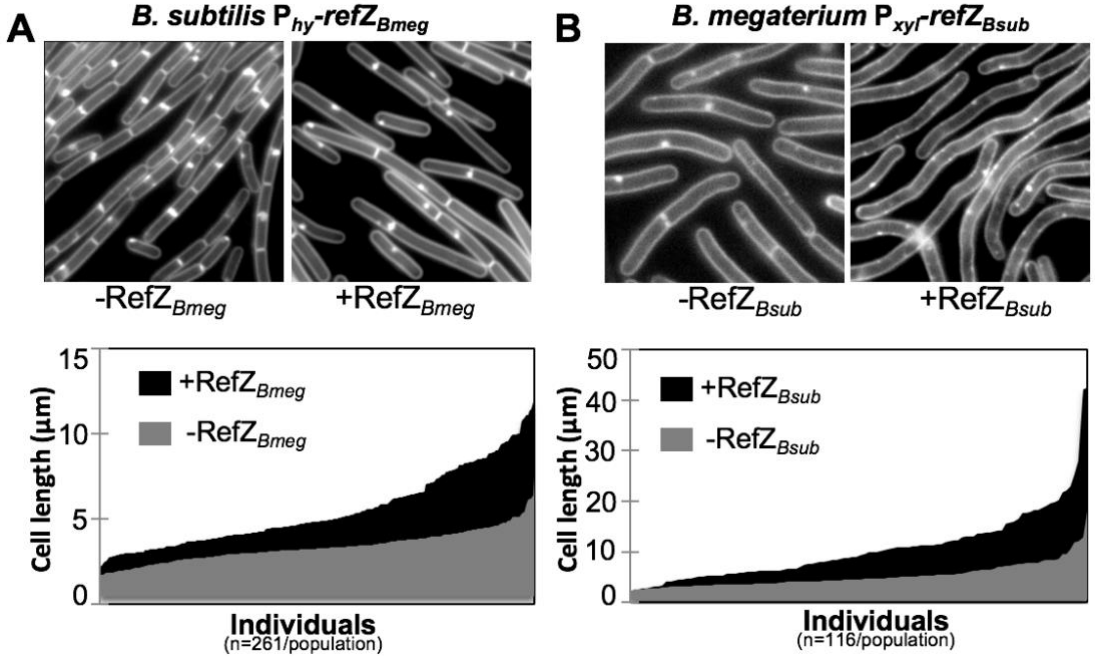

Figure II.2 Induced expression of RefZ homologs results in cell filamentation across *Bacillus* species. Reprinted with permission from Miller *et al*., 2016. **(A)** Expression of *B. megaterium* RefZ (RefZ$_{Bmeg}$) in *B. subtilis* before and after 60 min induction with 1 mM IPTG (top). Quantitation of cell lengths before and after 60 min of RefZ$_{Bmeg}$ induction with 1 mM IPTG (bottom). Cell lengths were rank ordered and plotted without spaces along the x-axis to allow for visualization of the entire population. **(B)** Expression of *B. subtilis* RefZ (RefZ$_{Bsub}$) in *B. megaterium* before and after 60 min induction with 1% xylose (top). Quantitation of cell lengths before and after RefZ$_{Bsub}$ expression (bottom). Cell membranes were stained with TMA.

After 60 min of induction, the cells visibly filamented (Figure II.2A) and averaged 5.5 ± 2.2 μm in length, ~40% longer on average than the uninduced cells ($P<0.0001$). All cell lengths used to calculate the averages are plotted in Figure II.2A. *B. megaterium* harboring P_{xyl}-*refZ*$_{Bsub}$ possessed an average length of 5.4 ± 2.8 μm before induction. After a 60 min induction, *B. megaterium* cells harboring P_{xyl}-*refZ*$_{Bsub}$ also filamented (Figure II.2B) and exhibited an average cell length of 10.6 ± 6.8 μm, ~2-fold longer ($P<0.0001$) on average than the uninduced control (all data points are plotted in Figure II.2B). These results are consistent with the cell filamentation phenotype previously observed following P_{hy}-*refZ*$_{Bsub}$ expression in *B. subtilis* (Wagner-Herman *et al.*, 2012) and suggest that the characterized functions of RefZ are likely to be conserved in other *Bacillus* species.

II.2.3 RefZ binds the five *oriC*-proximal *RBM*s with similar affinity

RefZ, like the *E. coli* nucleoid occlusion and FtsZ inhibitor, SlmA, is a member of the TetR-family of DNA-binding proteins (Cuthbertson & Nodwell, 2013). During sporulation, RefZ is enriched at several sites around the chromosome harboring the consensus *RBM* (Wagner-Herman *et al.*, 2012). Integration of an *RBM* at an ectopic site was sufficient to promote enrichment of RefZ at this non-native site, while a mutated *RBM* is not (Wagner-Herman *et al.*, 2012). To characterize the binding of RefZ to each of the *oriC*-proximal *RBM*s, we PCR amplified DNA fragments from the chromosome centered on each *RBM* and performed electrophoretic mobility shift assays with RefZ-6His. Each of the *oriC*-proximal *RBM*s exhibited two DNA mobility shifts following

incubation with increasing concentrations of RefZ (Figure II.3) and displayed similar apparent affinities for RefZ.

FEME analysis identified three possible degenerate motifs in the *ter* region (Figure II.4). Only one of these motifs, designated as RBM_T (Figure II.1B), showed a visible upshift (Figure II.3 and Figure II.4). The mobility shift pattern differed from the *oriC*-proximal *RBM*s in that the second, higher molecular weight mobility shift was not detectable (Figure II.3). The RBM_T site also required a higher concentration of RefZ to induce a mobility shift, suggesting that RefZ likely has a lower apparent affinity for the RBM_T site.

To determine if the DNA flanking each *RBM*, rather than the motif itself, was sufficient for the mobility shift, we amplified the same *RBM* regions from an *RBM* mutant strain (RBM_{5mu}), which harbors seven point mutations in the central palindrome of each of the five *oriC*-proximal *RBM*s (Figure II.1B). None of the DNA fragments harboring the mutant *RBM*s were visibly shifted in the presence of the highest RefZ concentration tested (Figure II.3, lane 5 for all), corroborating the prior conclusions that the *RBM*s represent RefZ's cognate binding sites (Wagner-Herman *et al.*, 2012). Importantly, these data also demonstrate that the *RBM* mutations we introduced on the *B. subtilis* chromosome are loss-of-function with respect to their ability to be specifically recognized by RefZ.

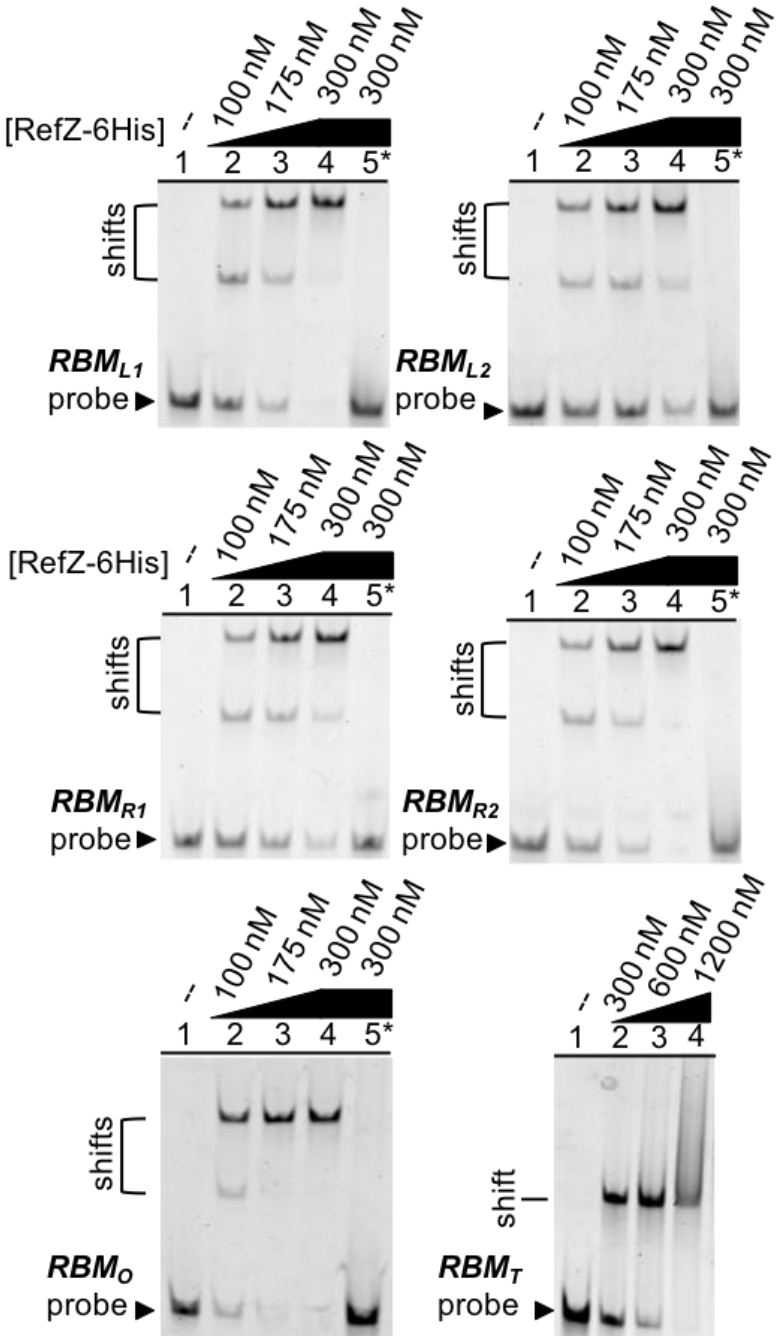

Figure II.3 Characterization of RefZ-*RBM* interactions.
Reprinted with permission from Miller *et al*., 2016. Gel shift analysis of DNA fragments (7 nM) centered on the *RBM* indicated incubated with various concentrations of RefZ-6His. Lane 5 (asterisk) of each gel shows the gel shift results for the mutant version of each *RBM* (see Figure II.1B) incubated with 300 nM RefZ-6His.

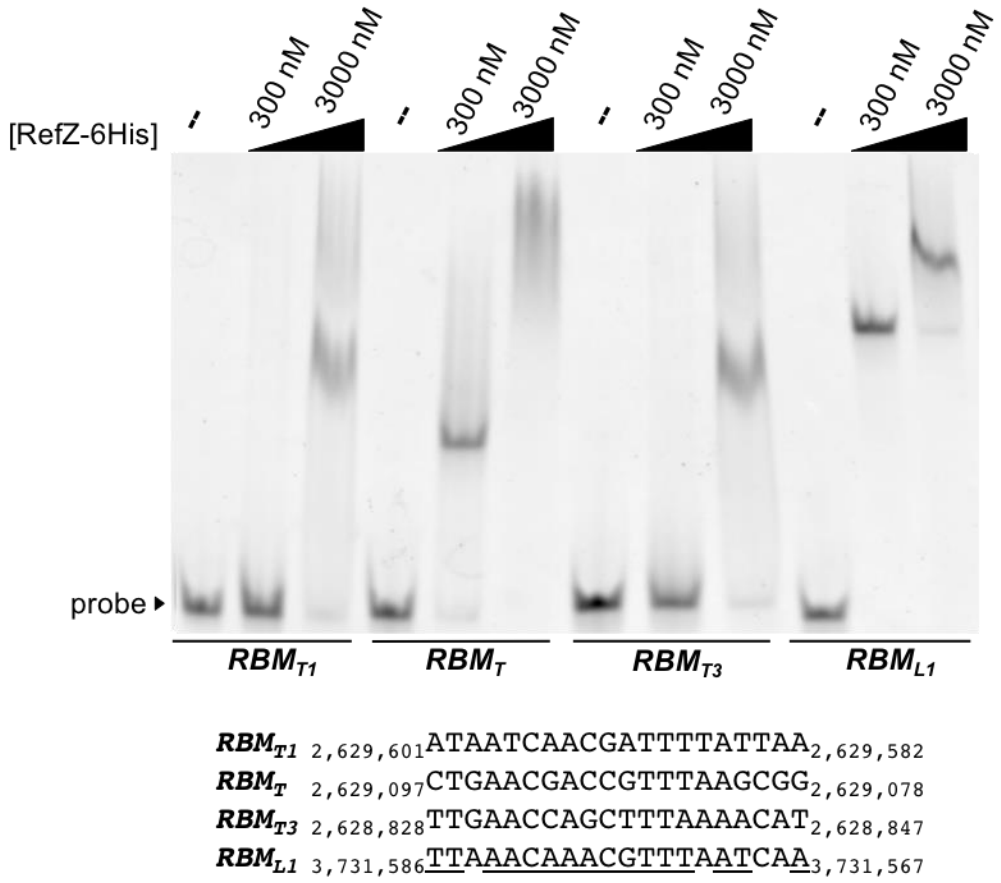

Figure II.4 Characterization of RefZ interaction with degenerate *RBM*s in the terminus region.
Reprinted with permission from Miller *et al*., 2016. Gel shift analysis of DNA fragments (7 nM) centered on the *RBM* indicated and incubated with various concentrations of RefZ-6His. The *RBM* sequences present in the amplified DNA probes are shown at the bottom for reference. The bases that are invariant in the five *oriC*-proximal *RBM*s are underlined on the RBM_{L1} sequence.

II.2.4 RefZ binds to the *oriC*-proximal *RBM*s in units of two and four

The presence of multiple mobility shifts suggests that RefZ is capable of binding to the DNA in several states, each of which may have different functional properties. To determine the number of units of RefZ associated with each mobility shift, we performed a mobility shift assay utilizing RefZ fused to epitope tags of different molecular weights, as shown in Figure II.5A. When the RefZ-6His and SUMO-RefZ were mixed, a mobility pattern indicative of mixed multimers was formed (Figure II.5A and 5B), suggesting that RefZ binds the *RBM*s in units of two and four.

The TetR family members SlmA (an inhibitor of FtsZ) and the multidrug export regulator QacR, have been shown through crystallography studies to bind to their cognate binding motifs as a pair of dimers (Tonthat *et al.*, 2013, Schumacher *et al.*, 2002). Based on these data, and our observation that RefZ binds to the DNA in units of two and four, we propose that RefZ most likely binds as a dimer to RBM_T and as both a dimer and pair of dimers to the five *oriC*-proximal *RBM*s. We did not observe additional, higher molecular weight mobility shifts that might be indicative of RefZ further polymerizing along DNA, but we do not exclude this possibility. We also do not exclude the possibility that RefZ is capable of forming a tetramer when associated with DNA, as such a configuration could also be consistent with the mobility pattern observed.

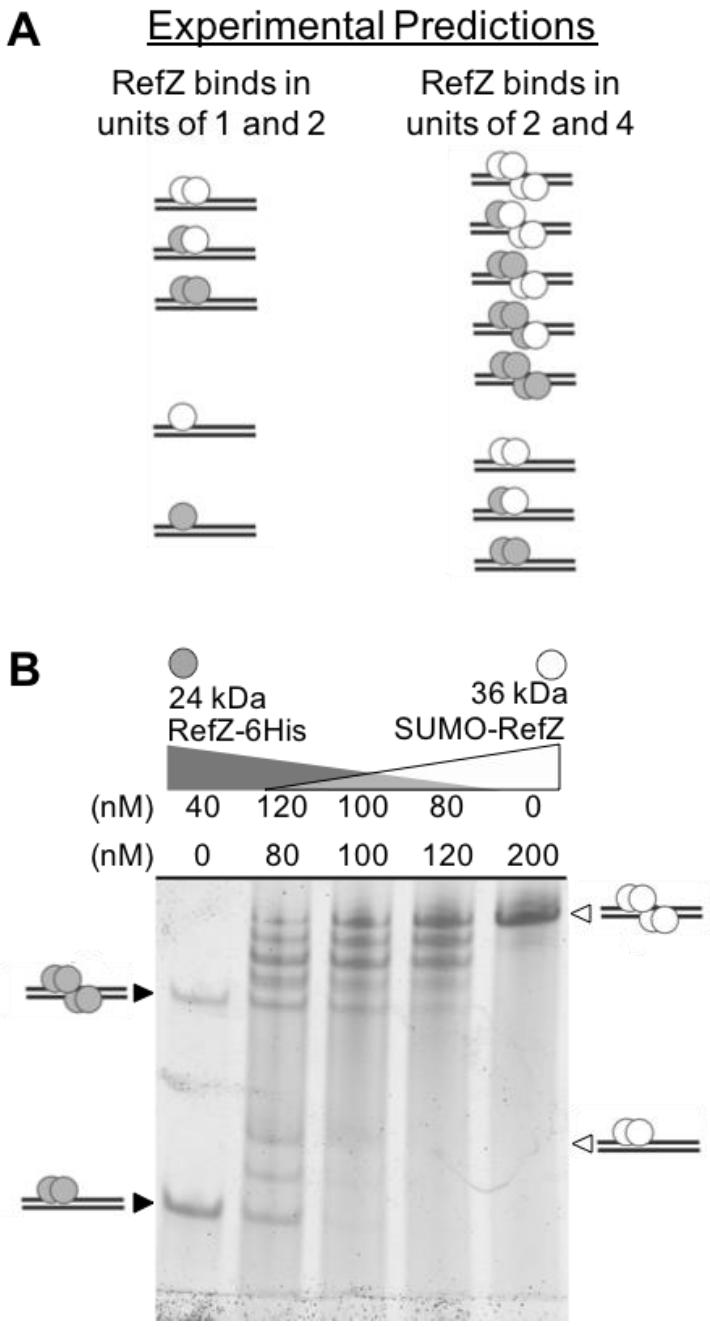

Figure II.5 RefZ binds to *RBM*s in units of two and four.
Reprinted with permission from Miller *et al*., 2016. **(A)** Cartoon showing possible experimental outcomes for RefZ binding to *RBM*-containing DNA. **(B)** Gel shift analysis of DNA fragments (10 nM) centered on RBM_O incubated with the indicated concentrations of RefZ-6His and SUMO-RefZ. Unshifted RBM_O probe was run out of the bottom of the gel. The filled arrowheads indicate the position of RefZ-6His mobility shifts. The unfilled arrowheads indicate the position of SUMO-RefZ mobility shifts. The remaining bands correspond to mixed species.

II.2.5 *RBM* DNA localizes in the vicinity of the polar septum

The *RBM*s flank the region of the chromosome captured by polar division (Figure II.1A and 1D, shaded regions), so we hypothesized that the *RBM*s located on the left and right chromosomal arms would localize in the vicinity of the incipient division plane during sporulation. To examine where the *RBM* DNA localizes during sporulation, we inserted a *tet* operator array immediately adjacent to RBM_{L2} in cells expressing TetR-CFP (Figure II.6A). The reporter was generally localized in the cell quarter regions (near both poles) 60 to 75 min into sporulation, when most cells begin exhibiting the membrane invaginations characteristic of polar division.

The array near RBM_{L2} was localized in the division plane in 91% (n=112) of septating cells (Figure II.6A). Operator arrays inserted on the chromosome near RBM_{R1} and RBM_{R2} exhibited similar localization patterns to the array near RBM_{L2} (Figure II.6B and C, respectively). The localization of the RBM_{L2} array appeared similar in a Δ*refZ* mutant and in an *RBM* mutant harboring loss-of-function mutations in all five *oriC*-proximal *RBM*s (RBM_{5mu}), suggesting that RefZ and the *RBM*s cannot be the sole effectors of organization and/or orientation of this region of the chromosome (Figure II.6D and E, respectively). Given the limited resolution provided by the operator arrays, we do not rule out the possibility that RefZ and/or the *RBM*s mediate smaller, local changes in the positioning of specific regions of chromosome.

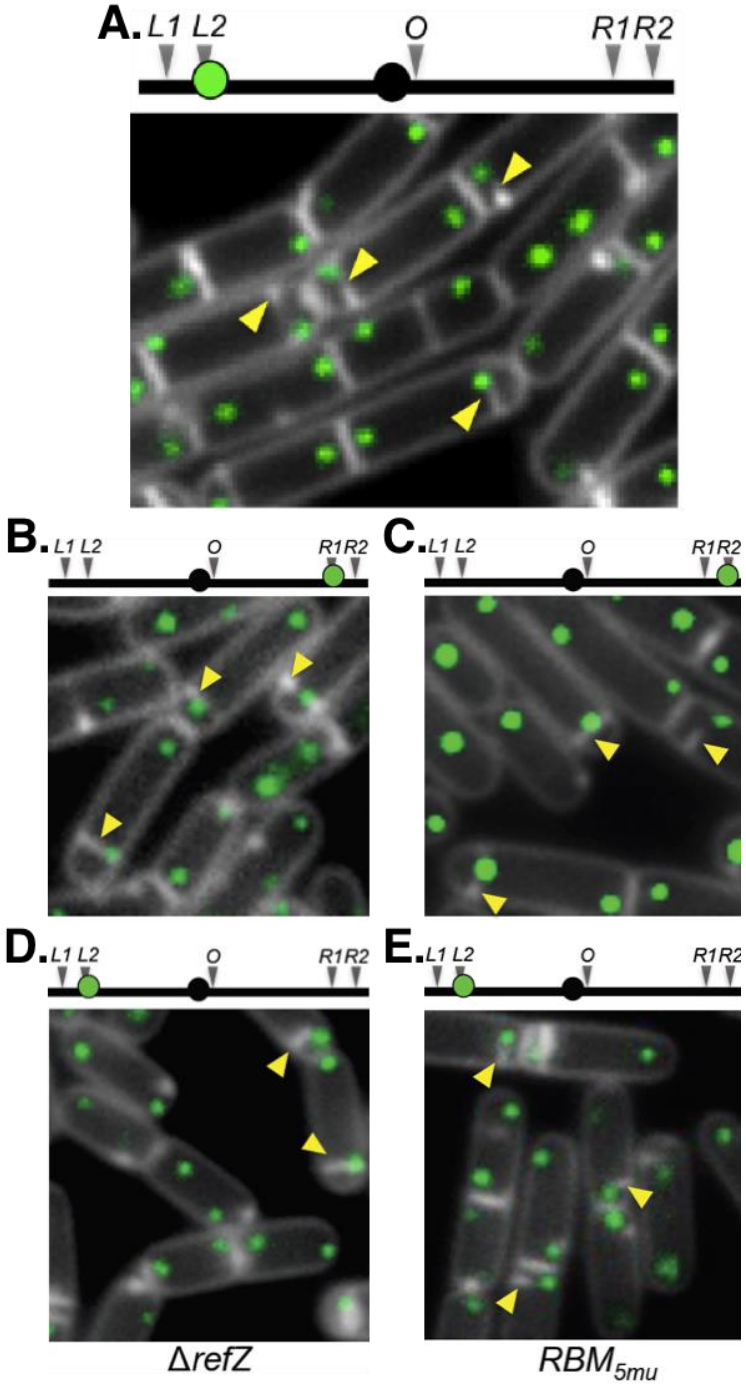

Figure II.6 *RBM* DNA localizes near the site of polar division.
Reprinted with permission from Miller *et al*., 2016. Images of sporulating cells (75 min after resuspension) harboring TetR-CFP and a *tetO48* array integrated into the chromosomes of an otherwise wild-type background strain (A-C) or into the *refZ* (D) or RBM_{5mu} (E) mutant background strains: **(A, D, E)** ~1,100 bp from RBM_{L2}, **(B)** near RBM_{R1}, or **(C)** near RBM_{R2}. The location of array is denoted by green circle in the cartoons. Membranes were stained with TMA (white) and TetR-CFP foci are pseudo-colored green. Yellow arrowheads indicate incipient septa.

The localization of the *RBM*s is consistent with a role in organizing the chromosome and/or regulating FtsZ dynamics at the pole (where polar cell division takes place). However, we do not exclude the possibility that the *in vivo* localization of the *RBM*s near the incipient septum is coincidental. The DNA pump SpoIIIE was recently shown to localize at the leading edge of the sporulation septum (Fiche et al., 2013). Current data favor a model in which SpoIIIE assembles at least two pumps (one for each chromosomal arm) (Burton & Dubnau, 2010, Fiche *et al.*, 2013, Yen Shin *et al.*, 2015) and the observation of a single focus of SpoIIIE *in vivo* suggests that these pumps are in close proximity to each other (Burton *et al.*, 2007, Fiche *et al.*, 2013, Sullivan *et al.*, 2009, Yen Shin *et al.*, 2015).

The juxtaposition of the *RBM*s to the site of polar division (Figure II.6A) and the fact that SpoIIIE localizes to the leading edge of the septum (Fiche *et al.*, 2013) where it must also assemble on DNA in the division plane, prompted us to investigate the possibility that RefZ might interact with SpoIIIE or another divisome component directly. Such a mechanism could be an efficient way to promote pump assembly at precise locations along the chromosome without requiring that SpoIIIE assemble on DNA at specific sequences. It could also ensure that RefZ is precisely positioned in the cell to affect a role in FtsZ activity at the pole (see Chapter II.3 Discussion).

To test these ideas, we performed bacterial two-hybrid analysis with RefZ and several putative interaction partners. We did not detect an interaction between RefZ and the cell division proteins EzrA (conserved by synteny near *refZ*) or FtsZ in the bacterial two-hybrid analysis. In contrast, we detected a positive interaction between full-length

RefZ and full-length SpoIIIE (Figure II.7), but not a full-length version of the vegetative DNA pump SftA, suggesting that the observed interaction between RefZ and SpoIIIE is specific.

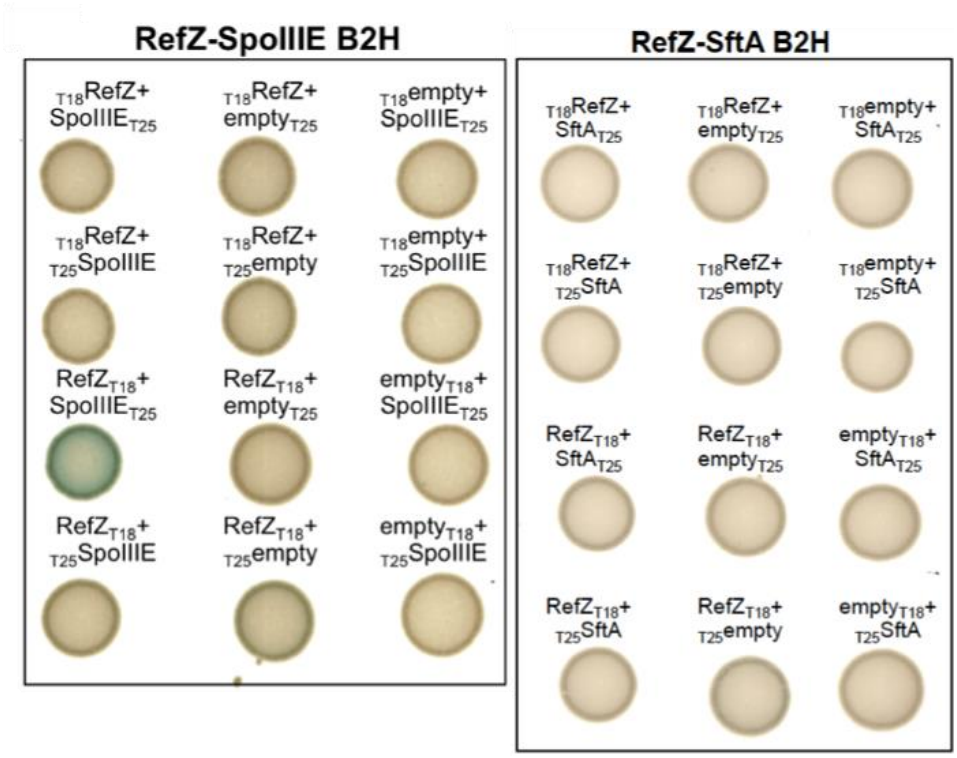

Figure II.7 RefZ interacts with the SpoIIIE DNA pump by bacterial two-hybrid.
Reprinted with permission from Miller *et al*., 2016. Bacterial two-hybrid analysis showing the pairwise interaction between RefZ and SpoIIIE (left) or RefZ and a second DNA translocase, SftA (right).

II.2.6 RefZ promotes precise positioning of the chromosome arms during sporulation

Based on the proximity of the outermost *RBM*s to the region of the chromosome initially captured in the forespore, and RefZ's previously characterized role as a regulator of FtsZ, we hypothesized that by binding to the *RBM*s, RefZ might contribute to defining the region over which cell division takes place on the chromosome. Regions of chromosome initially captured in the forespore can be monitored using a highly sensitive, single-cell assay (Sullivan *et al.*, 2009). The assay works by fusing a forespore-specific promoter to a fluorescent reporter and inserting the fusion into the chromosome at the DNA location of interest. The assay is performed in a SpoIIIE mutant that cannot pump the remainder of the chromosome into the forespore, thus ensuring that only reporters captured or "trapped" on the forespore side of the septum will produce fluorescence (Sullivan *et al.*, 2009). Using the trapping assay, we found that the Δ*refZ* mutant captures a marker located at -61° (Figure II.1A) (approximately 230 kb counter-clockwise from $RBM_{L1)}$, approximately two times more often than wildtype (22% in Δ*refZ* compared to 10% in wildtype) (Figure II.8). Introducing a copy of P_{refZ}-*refZ* at the *amyE* locus (28°**)** fully complemented the left-arm trapping defect (Figure II.8).

To determine if right arm of the chromosome was also affected in the Δ*refZ* mutant, we repeated the assay with a +51° reporter. This location was selected because it is located approximately 230 kb clockwise from RBM_{R2}, the outermost *RBM* on the right arm (Figure II.1B). Similar to the left arm, +51° was trapped in 11% of wildtype

and 21% of Δ*refZ* cells. The +51° trapping defect was largely, but not fully complemented by *amyE*::P$_{refZ}$-*refZ* (Figure II.8). It is not clear why right arm complementation differed from left, however, we speculate that the right arm is more sensitive to perturbations from wildtype (see Chapter II.3 Discussion), including those that might result from shifting P$_{refZ}$-*refZ* from its native locus (-100°) to *amyE* (28°).

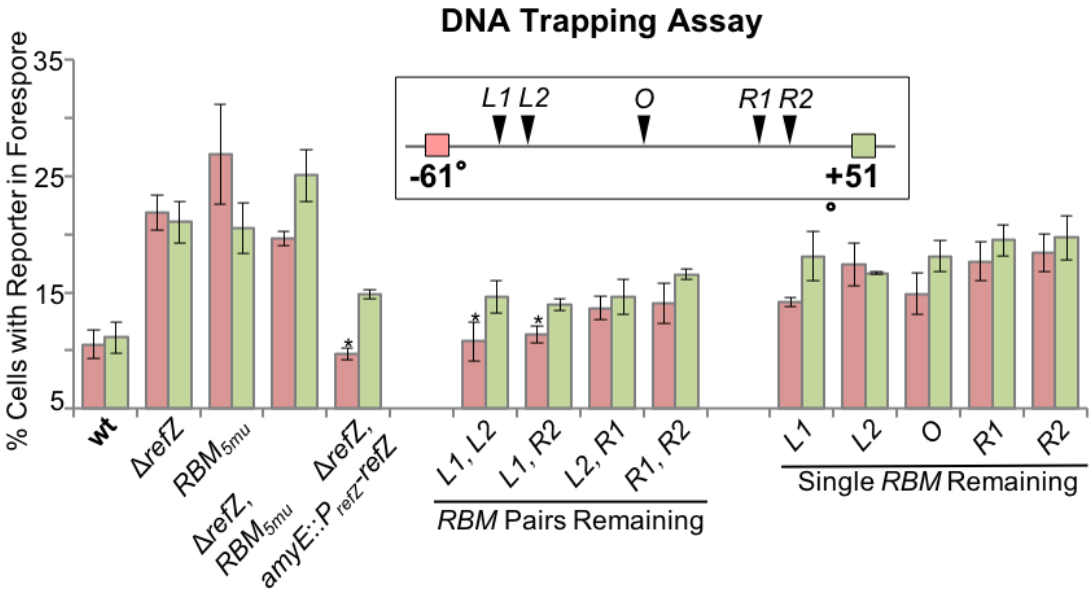

Figure II.8 RefZ and the *oriC*-proximal *RBM*s promote the precise positioning of the left and right chromosome arms during sporulation.
Reprinted with permission from Miller *et al*., 2016. Single cell analysis indicating the average percentage of cells that captured either the left arm (-61°) or right arm (+51°) reporter in the forespore at the time of polar division. Asterisks indicate samples that did not differ significantly from the wild-type controls. All other samples differed significantly from the wild-type controls (P<0.01). A minimum of 1,500 cells from three biological replicates were counted for each strain.

Reporters integrated close to RBM_{L1} and RBM_{R2} (-40° and +30°) were also captured approximately two times more often in the forespore in a Δ*refZ* mutant compared to wildtype, suggesting that shift we observe in chromosome capture is not restricted to the -60° and +51° regions (data not shown). We conclude that RefZ contributes to the proper capture of regions located on both the left and right arms of the chromosome during sporulation.

II.2.7 *RBM*s are required for wild-type chromosome capture during sporulation

Since RefZ binds to the *RBM*s during sporulation (Wagner-Herman *et al.*, 2012), we hypothesized that RefZ would also require one or more of the *RBM*s for wild-type trapping of the chromosome arms. We further hypothesized that a mutant harboring point mutations in all five *oriC*-proximal *RBM*s (RBM_{5mu}), would phenocopy the Δ*refZ* strain. To test these ideas, we performed the chromosome trapping assay on the RBM_{5mu} strain, which harbors point mutations (Figure II.1B) in the five *oriC*-proximal *RBM*s. On average, 27% of RBM_{5mu} cells trapped the -61° reporter, while 20% of cells trapped the +51° reporter, similar to the Δ*refZ* strain (Figure II.8). The RBM_{5mu} strain exhibited a wide standard deviation for left arm trapping (trapping ranged from 20% to 34% in 18 independent experiments) that was not observed in the RBM_{5mu} Δ*refZ* strain (see below), suggesting the emergence of a RefZ-dependent enhancement of variation in chromosome capture in the absence of its cognate *RBM*s.

To test if RefZ and the *RBM*s act in the same genetic pathway to affect chromosome capture, we asked if a double mutant (RBM_{5mu} Δ*refZ*) produced a similar

trapping defect when compared to the single mutants. We found that 20% of the *RBM*$_{5mu}$ Δ*refZ* population trapped the -61° reporter, while 25% trapped the +51° reporter (Figure II.8), consistent with the *RBM*s and RefZ each requiring the other for wild-type function. These results are most consistent with a model in which RefZ binds to one or more of the *RBM*s to achieve its function in chromosome capture.

II.2.8 At least two *RBM*s are required for a wild-type arrangement of the chromosome

When the five *oriC*-proximal *RBM*s are mutated, septation occurs over a different portion of the forespore-destined chromosome, similar to a Δ*refZ strain.* To determine if all five *RBM*s are required to support a wild-type arrangement of the chromosome, we performed the trapping assay on nine additional *RBM* mutant combinations (Figure II.8). The symmetric distribution of the *RBM*s around *oriC* across the *Bacillus* genus (Figure II.1D) supports the idea that *RBM*s positioned on both chromosomal arms are important for RefZ-*RBM* function; however, to test the simplest case in which a single *RBM* is sufficient to maintain wild-type trapping, we first performed the assay on five mutants, each harboring only one remaining functional *RBM*. As shown in Figure II.8, no single *RBM* was sufficient to ensure wild-type trapping of either the left (-61°) or right (+51°) arm reporters. However, the single *RBM* remaining mutants trapped the left arm reporter significantly ($P<0.01$) less often than *RBM*$_{5mu}$. These results suggest that a single *RBM* on either arm can contribute to left

arm trapping. In contrast, right arm was capture was statistically indistinguishable between each of the single *RBM* remaining mutants (P<0.01) and RBM_{5mu}.

We next examined trapping in strains harboring various combinations of two intact *RBM*s. Left arm trapping was statistically indistinguishable from wild-type as long as RBM_{L1} and at least one other *RBM* was intact (Figure II.8). In contrast, right arm trapping was not restored to wild-type levels (P<0.01) for any of the combinations examined, with the RBM_{L1} and RBM_{R2} combination being the combination most similar to wildtype. These results suggest that while the left and right arms both depend on RefZ and the *RBM*s to precisely capture the chromosome, the arms also have different requirements for accomplishing this function. More specifically, the left arm requires RBM_{L1} and at least one other *RBM*, while the right arm appears to require *RBM*s on both the left and right arms.

II.3 DISCUSSION

One of the earliest morphological manifestations of *Bacillus* sporulation is the formation of the axial filament, an elongated, *oriC-ter-ter-oriC* conformation of the cell's two chromosomes (Piggot & Hilbert, 2004, Bylund *et al.*, 1993). RacA, Spo0J, and SMC contribute to axial filament formation by condensing the *oriC* region, creating a centromere-like element favorable for chromosome segregation (Ben-Yehuda *et al.*, 2005, Sharpe & Errington, 1996, Lin & Grossman, 1998, Graham *et al.*, 2014, Sullivan *et al.*, 2009). This element is tethered to the cell pole through interactions between RacA (bound to DNA at *ram* sites) and a membrane protein, DivIVA (Ben-Yehuda *et*

al., 2005, Ben-Yehuda *et al.*, 2003). Another protein, Soj, also contributes to *oriC* capture by permitting segregation of approximately 15-20% of origins that otherwise fail to be captured in the forespore (Sullivan *et al.*, 2009).

Although much is understood about factors that promote *oriC* segregation during sporulation, very little is known about how the cell manages to reproducibly divide over a precise portion of the forespore-destined chromosome. Wu and Errington observed that two regions located approximately 400 kb to the left and right of *oriC* (encompassing the left and right arm *RBM*s) are still captured in the forespore, even in genetic backgrounds where the remainder of the chromosome (including *oriC*) is generally captured in the mother cell compartment (Wu, 2003). This residual capture requires Spo0J, which led them to hypothesize that Spo0J creates an orientation of the chromosome that positions regions +/-400 kb from *oriC* in the vicinity of the division plane (Wu, 2003). Our data indicate that RefZ and the *RBM*s also contribute to determining the relative positioning of the chromosome arms with respect to the division plane. More specifically, we find that both a Δ*refZ* mutant and an *RBM* mutant (RBM_{5mu}) show an increased propensity to capture regions of the chromosome that are normally excluded from the forespore.

II.3.1 RefZ and *RBM*s on both chromosomal arms help define the boundary of chromosome capture

We found that both RefZ, and *RBM*s located on each chromosomal arm are required to support a wild-type chromosome capture, but each arm responds somewhat differently to *RBM* perturbations. In general, for the reporters we tested, the right arm is

more sensitive than the left arm to *RBM* mutations, and no combination of left and right *RBM*s tested was sufficient to support wild-type capture of the right arm (Figure II.8). In contrast, RBM_{L1} in combination with either RBM_{L2} or RBM_{R2} was sufficient to capture the left arm reporter at wild-type levels. The left arm also harbors the majority of the RacA and Spo0J binding sites (Figure II.1A). Therefore, we speculate that the phenotypic consequence of losing *RBM*-dependent organization might be partially dampened on the left arm by RacA-dependent tethering at the cell pole and/or Spo0J-dependent condensation of chromosomal DNA proximal to *oriC*. We found no evidence that deletion of *refZ* in Δ*racA* Δ*soj*, or Δ*racA* Δ*soj* Δ*spo0J* mutant backgrounds lead to enhanced capture of reporters on the left and right arms (Miller and Herman, unpublished). Thus, while RefZ is important for defining the region of chromosome captured at the time of cell division, this role appears to require that the systems that condense, organize, and segregate the DNA proximal to *oriC* are functioning.

II.3.2 *refZ* and *RBM*s across *Bacillus*

The chromosomal position of predicted *RBM*s across the *Bacillus* genus reveals several patterns in *RBM* distribution (Figure II.1D and APPENDIX A Figure A.1). In general, there are multiple *RBM*s on each arm that align fairly closely (especially on the right arm) with the region trapped during polar division in *B. subtilis*. In addition, many of the species, including *B. subtilis*, have one or more additional *RBM*s closer to *oriC* (RBM_O, in *B. subtilis*). The trapping assay data indicates that RBM_O contributes to the overall arrangement of the chromosome during sporulation, although we did not pursue

its specific role further. It is also important to note that the stringent criteria of our bioinformatics analysis likely underrepresent the number of motifs, which might include *RBM*s closer to *oriC* in other species (see APPENDIX A Figure A.1).

We also observe that, compared to the *B. subtilis RBM*s (which were experimentally identified using ChIP-seq), the pathogenic *Bacillus* species (*B. anthracis*, *B. cereus*, and *B. thuringenesis*) have more *RBM*s, some with reduced spacing between them (not resolvable in Figure II.1D and APPENDIX A Figure A.1). For example, we identified seven putative *RBM*s in *B. anthracis Ames*, two sets with less than 100 bp between them (see APPENDIX A Methods A.3 for exact coordinates). The same pathogenic strains also encode a slightly different gene organization in the *refZ* region (Figure II.1C), the implication of which is not yet clear. Curiously, *B. anthracis Ames* RefZ appears to be generated as two distinct polypeptides, the first of which encodes the DNA-binding domain of the protein. The start and stop codons overlap by 1 nucleotide, consistent with the idea that the polypeptides may be translationally-coupled. The separation of RefZ domains was also found in the other *B. anthracis* strains we examined, including *B. anthracis Sterne*, indicating that the genetic arrangement of the domains is unlikely to be a sequencing error.

II.3.3 Models for RefZ's role in chromosome organization and cell division regulation

The conservation of *RBM* chromosomal locations across the *Bacillus* genus argues that their role is position-dependent and critical for fitness in the environment,

and we propose several models for how RefZ-*RBM* complexes might function *in vivo*. RefZ could bind to the *RBM*s and, possibly through interactions with SpoIIIE or another component of the cell division apparatus, fine-tune the positioning of the *RBM* DNA with respect to the division plane. One prediction of this model is that the placement of *RBM*s at ectopic sites should lead to a corresponding shift in the portion of DNA that is captured in the trapping assay. When we introduced RBM_{L1} and RBM_{R2} into the RBM_{5mu} strain at ectopic sites positioned 10° counterclockwise from their original positions, the resultant strain trapped the left and right arm reporters like the RBM_{5mu} parent. These data suggest that the region at which RefZ affects chromosome capture (presumably at the native *RBM* sites) may be secondary to other cellular restrictions. For example, the *B. subtilis RBM*s fall within a region that is noticeably devoid of Noc binding sites, possibly representing a "window" of chromosome that is favorable for FtsZ assembly. Introducing *RBM*s outside of this window could negate their contribution to overall organization because FtsZ assembly is already inhibited in those regions. Moreover, the *RBM*s may be present in specific configurations within the 3D landscape of the axial filament (promoted by proteins like RacA and Spo0J) that act upstream of a RefZ's position-sensitive function.

Multiple lines of evidence (Wagner-Herman *et al.*, 2012), including those in this study, suggest that RefZ acts as a negative regulator of cell division. If RefZ is a negative regulator of FtsZ activity during sporulation, then how might it function at the pole, where the FtsZ-ring assembles to promote division? We can envision several possibilities that are consistent with the known data. First, early in sporulation (before

polar division occurs) RefZ could function as an inhibitor of FtsZ-ring assembly at the cell poles. Then, at the time when FtsZ redistributes from midcell toward the pole, its activity could be localized to another cellular location. Consistent with this model, RefZ-GFP localizes at the poles early in sporulation (60 min) and at midcell around the time of septation (75 min) (Wagner-Herman *et al.*, 2012). A non-exclusive model is that RefZ-mediated inhibition of FtsZ is spatially restricted to the immediate vicinity of the *RBM*s. In such a scenario, RefZ might influence the absolute positioning of the FtsZ-ring with respect to specific regions of the chromosome, but not necessarily inhibit polar cell division itself. Similarly, RefZ could function to inhibit additional FtsZ-rings from forming at the same pole of cells that fail to capture *oriC* after the first polar division. Lastly, it is possible that in its native context, RefZ may act as a positive regulator of polar cell division although data to support this interesting possibility are currently lacking.

The remarkable evolutionary conservation of RefZ and the *RBM*s across the genus argues that the system is critical for fitness in the environment. Excluding the sequences that control DNA replication initiation and termination, a relatively small number of well-characterized, non-coding and non-regulatory DNA motifs are conserved in chromosomal position either across multiple genera or among a given genus. The best characterized of these motifs are involved in regulating chromosome segregation and condensation (Livny *et al.*, 2007) and *ter* resolution following DNA replication (Mercier *et al.*, 2008). Other motifs are position-dependent even if their sequence degeneracy precludes identification in other species bioinformatically (Ben-

Yehuda *et al.*, 2005, Cho *et al.*, 2011, Tonthat *et al.*, 2011, Wu *et al.*, 2009). Excitingly, a growing body of evidence suggests that proteins that bind position-dependent motifs are often multifunctional, regulating cellular functions that are also position-dependent such as FtsZ polymerization (Cho *et al.*, 2011, Bernhardt & de Boer, 2005) and DNA translocase activity (Stouf *et al.*, 2013). It is attractive to speculate that many undiscovered chromosomal placeholders exist, possibly regulating processes like cell elongation and chromosome segregation. We anticipate that bioinformatic approaches will be central to navigating this largely unexplored area of prokaryotic biology.

II.4 MATERIALS AND METHODS

II.4.1 General methods

All *B. subtilis* strains were derived from *B. subtilis* 168. *E. coli* and *Bacillus* strains, plasmids, and oligonucleotides utilized in this study are listed in APPENDIX A, Tables A.1, A.2, and A.3, respectively. Sporulation was induced by resuspension at 37°C according to the Sterlini-Mandelstam method (Harwood, 1990). For microscopy experiments, all samples were grown in volumes of 25 ml in 250 ml baffled flasks in a shaking waterbath set at 280 rpm. For transformation and selection of *B. subtilis*, antibiotics were included at the following concentrations: 100 μg ml^{-1} spectinomycin, 7.5 μg ml^{-1} chloramphenicol, 10 μg ml^{-1} tetracycline, and 1 μg ml^{-1} erythromycin (erm) plus 25 μg ml^{-1} lincomycin (MLS).

II.4.2 Microscopy

Fluorescence microscopy was performed with a Nikon Ti-E microscope equipped with a CFI Plan Apo lambda DM 100X objective, and Prior Scientific Lumen 200 Illumination system, C-FL UV-2E/C DAPI, C-FL GFP HC HISN Zero Shift, C-FL YFP HC HISN Zero Shift, and C-FL Cyan GFP, filter cubes, and a CoolSNAP HQ2 monochrome camera. Membranes were stained with either TMA-DPH (0.02 mM) or FM4-64 (3 μg ml^{-1}) (Life Technologies) and imaged with exposure times of 200-1000 ms. All images were captured with NIS Elements Advanced Research (version 4.10), and processed with Adobe Photoshop (version 12.0) and ImageJ64 (Rasband, 1997-2014). Cells were mounted on glass slides with polylysine-treated coverslips prior to imaging.

II.4.3 *refZ* swapping

For the *refZ* swapping experiment, cultures were grown in LB liquid media to midlog, back-diluted to an OD_{600} of ~0.05 and induced with 0.5% (w/v) xylose (BAM073) or 1.0 mM isopropyl-beta-D-thiogalactopyranoside (BAM071). At 60 min post-inductions, samples were collected, stained with TMA imaged as described in microscopy.

II.4.4 RefZ-6His protein purification

To obtain RefZ-6His, BL21(λDE3) pLysS cells were freshly transformed with pLM025. To obtain SUMO-RefZ, BL21(λDE3) pLysS was freshly transformed with

pAM030. All protein overexpression cultures were grown in Cinnabar high-yield protein expression media (Teknova) supplemented with 25 µg ml^{-1} kanamycin, 25 µg ml^{-1} chloramphenicol, and 0.1% (v/v) glucose. Overnight starter cultures were avoided. A 25 ml culture in a 250 ml baffled flask was grown in a shaking waterbath at 300 rpm, 37°C to an OD_{600} of approximately 5 and expression was induced by the addition of 1 mM final IPTG. Cultures were grown to an OD_{600} of 10 to 15 and cells were harvested by centrifugation. Pellets were stored at -80°C prior to processing. To lyse cells, pellets were resuspended in 25 ml of lysis buffer (50 mM Tris-HCl [pH 9.0], 300 mM KCl, 25 µl of 1 mg ml^{-1} DNase I, and 50 µl of Protease Inhibitor Cocktail (Sigma)). The sample was passaged through a French press cell three times at 10,000 PSI and then spun at 24,000 x *g* for 30 min to pellet cell debris. The supernatant was applied to a 0.5 ml bed volume of pre-equilibrated Ni-NTA (Qiagen) and washed with 5 ml wash buffer (50 mM Tris-HCl [pH 9.0], 300 mM KCl, 20 mM imidazole, and 10% (v/v) glycerol). The protein was eluted with 2 ml elution buffer (50 mM Tris-HCl [pH 9.0], 300 mM KCl, 250 mM imidazole, and 10% (v/v) glycerol) and collected in eight 250 µl fractions. Peak fractions were pooled (typically ~2 ml total) and the imidazole was removed by buffer exchange using a 10,000 kDa molecular weight cutoff spin filter and 50 mM Tris-HCl [pH 9], 300 mM KCl, 10% glycerol. The purified protein was then stored at -80°C in aliquots until use. Each 25 ml culture typically yielded ~1 mg of protein.

II.4.5 Analysis of RefZ-*RBM* interaction using electrophoretic gel mobility shift assays

DNA fragments (~150 bp/each) were generated for the gel-shifts by PCR amplification of DNA centered on the native *RBM*s (using *B. subtilis* 168 as template) or mutant *RBM*s (using RBM_{5mu} as template). Fragments were generated using the following primer pairs: RBM_{L1}, oEB012 and oEB013; RBM_{L2}, oEB009 and oEB010; RBM_{O}, oEB014 and oEB015; RBM_{R1}, oEB016 and oEB017; RBM_{R2}, oEB018 and oEB019; RBM_{T1}, oEB027 and oEB028; RBM_{T}, oEB029 and oEB030; RBM_{T3}, oEB031 and oEB032; DNA binding reactions were prepared according to directions of the SYBR Green EMSA Nucleic Acid Gel Stain kit (Life Technologies) except that instead of binding buffer, the samples were prepared in ddH_2O [pH 6.7]. Incubation of the samples in KCl or NaCl-based DNA-binding buffers significantly reduced the affinity of RefZ for the *RBM*-containing DNA. After 30 min incubation, 10X DNA loading buffer (45% glycerol, 50 mM EDTA [pH 8], and 1 mM Tris-HCl [pH 8]) was added to a final concentration of 1X and samples were resolved on a 5% Mini-PROTEAN TBE polyacrylamide gel (Biorad). After electrophoresis, the gel was stained with SYBR Green EMSA gel stain (Life Technologies) for 20 min. The gel was then washed and DNA was visualized with a Typhoon Trio fluorescence imager (GE Healthcare) at an excitation wavelength of 488 nm.

II.4.6 Quantitative forespore chromosome trapping assay

Assays were carried out as previously described (Sullivan *et al.*, 2009). An *oriC*-proximal reporter (-7° P_{spoIIQ}-*YFP)* was trapped in the forespores in greater than 99.5% for both wildtype and all of the mutants examined, and thus served as a baseline for σ^F activity. The chromosomal arms harbored either the left (-61° P_{spoIIQ}-*CFP*) or the right (+51° P_{spoIIQ}-*CFP*) reporters. Cell membranes were stained with TMA as described in microscopy. YFP, CFP, and TMA (C-FL UV-2E/C DAPI filter) images were captured 2.5 hrs after cells were resuspended in sporulation media (Harwood, 1990). Images for eighteen biological replicates were captured for wild-type and RBM_{5mu}. Images for at least three biological replicates were captured for all other strains. To quantitate the number of cells with the experimental reporters trapped in the forespore, the CFP images were overlaid with the control YFP channel and TMA (membrane stain). Forespores containing YFP, CFP, or both from three independent fields (n>500 cells per trial) were counted manually for each biological replicate. Forespores trapping the -61° or +51° reporters, but not the -7° reporter were also counted, and generally represented less than 0.5% of cells counted. Forespores devoid of any fluorescent signal were rarely observed and were not counted. The percentage of forespores with CFP signal (indicating trapping of the left or right arm reporter) was plotted using Microsoft Excel. The averages and standard deviations are shown in Fig. 6. Statistical significance (P-values) was determined using a student's t-test.

II.4.7 Two-hybrid analysis

Bacterial two hybrids were performed as described (Karimova *et al.*, 1998) with the following modifications: cloning was carried out in the presence of 0.2% glucose. Cells harboring the relevant pairwise interactions were grown to early exponential phase in LB with 0.2% glucose, ampicillin (50 μg/ml), and kanamycin (25 μg/ml). Five μl of equivalent OD_{600} cultures were spotted on M9-glucose minimal media plates containing 40 μg/ml X-Gal, 250 μM isopropyl-β-D-thiogalactopyranoside, ampicillin (50 μg/ml), and and kanamycin (25 μg/ml). Plates were incubated at room temperature in the dark for 50 to 70 hrs for color development prior to image capture. We found that spotting liquid cultures on M9-glucose produced clearer, more reproducible differences in color development that were not detectable on LB media or with 37°C incubation.

CHAPTER III

A DNA-BINDING PROTEIN TUNES SEPTUM PLACEMENT DURING *BACILLUS SUBTILIS* SPORULATION*

III.1 INTRODUCTION

To regulate cellular processes spatially, some macromolecules within the cell must assume a non-uniform distribution. One way that bacteria create heterogeneity along the bacterial envelope is to utilize proteins that induce and/or partition to sites of membrane curvature (Antonny, 2011, Updegrove & Ramamurthi, 2017). From there, membrane curvature proteins can serve as a platform for the localization of additional molecules in the cell. For example, in the rod-shaped bacterium *Bacillus subtilis*, the negative membrane curvature-sensing protein DivIVA coalesces adjacent to past and future cell division sites where it then recruits a cell division inhibitory system called Min to inhibit FtsZ polymerization (Bramkamp *et al.*, 2008, Eswaramoorthy *et al.*, 2011, Gregory *et al.*, 2008, Marston & Errington, 1999, Patrick & Kearns, 2008). Another mechanism to restrict physiological processes to specific cellular regions is to require that molecules assemble into larger, multi-subunit complexes to be active. For example, cell division, which requires the coordinated synthesis and turnover of all layers of the

---

cell envelope, is carried out by a localized multi-subunit complex comprised of over 30 proteins called the "divisome" (Du & Lutkenhaus, 2017).

Like the cell envelope, the highly organized (Badrinarayanan *et al.*, 2015) bacterial nucleoid is also utilized to regulate processes spatially. DNA-binding proteins that recognize specific motifs regulate the initiation of DNA replication (Scholefield *et al.*, 2011), mediate DNA repair and recombination (Grilley *et al.*, 1989, Modrich, 1989), and segregate chromosomes (Lim *et al.*, 2014, Sullivan *et al.*, 2009, Surovtsev *et al.*, 2016, Wang & Rudner, 2014). Moreover, some DNA-binding proteins simultaneously interact with the nucleoid and the cell envelope to perform functions in DNA replication (Hansen & Atlung, 2018, Leonard & Grimwade, 2015), chromosome organization (Ben-Yehuda *et al.*, 2005, Ben-Yehuda *et al.*, 2003, Wang *et al.*, 2017, Wu & Errington, 2003), DNA segregation (Burton & Dubnau, 2010), and regulation of cell division (Adams *et al.*, 2015).

The most extensively studied example of a DNA-binding protein that regulates cell division is SlmA, a TetR family member found in *Escherichia coli* (Bernhardt & de Boer, 2005) as well as several other important Gammaproteobacteria (Schumacher *et al.*, 2016). *E. coli* SlmA binds to dozens of motifs (SBSs) distributed throughout the chromosome except in the terminus (*ter*) region (Cho *et al.*, 2011, Tonthat *et al.*, 2011). In a mechanism termed nucleoid occlusion (NO), SlmA-SBS complexes inhibit cell division by disrupting polymerization of FtsZ (Cho *et al.*, 2011, Tonthat *et al.*, 2011). By restricting SlmA activity to sites of SBS enrichment, *E. coli* effectively inhibits the formation of Z-rings over the bulk nucleoid while at the same time permitting Z-ring

assembly in the midcell-localized *ter* region. In this way, SlmA utilizes the chromosome as a landmark to spatially regulate its FtsZ-inhibitory function.

Like *E. coli*, *B. subtilis* also possesses a NO system to prevent cell division over the bulk nucleoid (Wu & Errington, 2004, Wu *et al.*, 2009). The NO system of *B. subtilis* is comprised of a DNA-binding protein, Noc, and its cognate binding sites (NBSs), which are also distributed throughout the chromosome, but with a notable gap in the *ter* region (Wu *et al.*, 2009). In contrast to SlmA, evidence for a direct interaction between Noc and FtsZ is currently lacking. Instead, Noc-NBS complexes associate with the cell envelope, where they are hypothesized to perturb the association and/or nucleation of FtsZ filaments at the membrane (Adams *et al.*, 2015).

During *B. subtilis* sporulation, several morphological changes occur to facilitate spore formation. The cell's two chromosomes are stretched from pole to pole in an elongated *oriC-ter-oriC* configuration called the axial filament (Webb *et al.*, 1997, Wu & Errington, 1998). In addition, there is a dramatic adjustment in the location of cell division, with FtsZ shifting from midcell toward a cell quarter, directing septation over one chromosome. During sporulation, Z-ring inhibition imposed by both the Min and NO systems must be relieved. Alleviation of Min inhibition may be facilitated by the repositioning of MinD (required to mediate MinC-dependent inhibition of FtsZ) to the distal cell pole (Kloosterman *et al.*, 2016). Regarding NO, it has been proposed that the axial filament may be arranged such that relatively few Noc-binding sites are positioned at the site of incipient septation (Wu *et al.*, 2009).

The shift of FtsZ from midcell toward the pole is promoted by increased levels of FtsZ (Gonzy-Treboul *et al.*, 1992, Levin & Losick, 1996) and expression of a membrane-associated sporulation protein, SpoIIE (Ben-Yehuda & Losick, 2002, Khvorova *et al.*, 1998). Following septation, the larger mother cell possesses an entire chromosome, whereas the forespore initially contains only one-quarter to one-third of the second chromosome (Sullivan *et al.*, 2009, Wu & Errington, 1998). The genetic asymmetry between the mother cell and forespore is critical for differentiation (Frandsen *et al.*, 1999, Wang *et al.*, 2006) and the region captured is reproducible (Sullivan *et al.*, 2009, Wu & Errington, 1998). The chromosome is not bisected during polar division because SpoIIIE, a DNA translocase localized to the edge of the septum (Fiche *et al.*, 2013), assembles around the chromosomal arms (Burton & Dubnau, 2010, Wu & Errington, 1994). Since the chromosome is threaded through the septum, SpoIIIE must directionally pump the remainder from the mother cell into the forespore for development to progress. To avoid chromosome breakage during septation, capture a reproducible region of DNA in the forespore, and pump the forespore-destined chromosome in the correct direction, there must be coordination between cell division proteins, SpoIIIE, and the chromosome. How this coordination is orchestrated at the molecular level largely remains a mystery.

Precise division over and capture of the forespore-destined chromosome requires RefZ, a TetR family DNA-binding protein conserved across the *Bacillus* genus (Miller *et al.*, 2016, Wagner-Herman *et al.*, 2012). RefZ expression is activated early in sporulation, first via the stationary phase sigma factor, σH (Britton *et al.*, 2002) and then

by Spo0A~P, the activated form of the sporulation master response regulator (Ben-Yehuda *et al.*, 2005, Molle *et al.*, 2003). RefZ binds to five nearly palindromic DNA motifs (*RBM*s), two on each chromosomal arm and one near *oriC* (Miller *et al.*, 2016, Wagner-Herman *et al.*, 2012). The *RBM*s on the left and right arms delineate the boundary between chromosomal regions present in the forespore and mother cell at the time of septation. Chromosomal regions immediately adjacent to each *RBM* localize near the incipient site of polar cell division, suggesting a possible role in division or organization of the chromosome near the sporulation septum (Miller *et al.*, 2016). Consistent with this idea, the *RBM*s are required for precise capture of the forespore-destined chromosome (Miller *et al.*, 2016). Strikingly, the relative position of the *RBM*s with respect to *oriC* is conserved across the entire *Bacillus* genus. This evolutionary conservation strongly suggests that the location of the *RBM*s is functionally important and provides a considerable selective advantage to the genus (Miller *et al.*, 2016).

In addition to imprecise chromosome capture, perturbation of RefZ activity is associated with two other phenotypes: first, during sporulation a Δ*refZ* mutant is modestly delayed in assembly of polar Z-rings (Wagner-Herman *et al.*, 2012). Second, artificially induced expression of RefZ during vegetative growth disrupts Z-ring assembly and inhibits cell division. RefZ-DNA complexes are likely required to disrupt Z-rings, as RefZ DNA-binding mutants no longer disrupt cell division (Wagner-Herman *et al.*, 2012). These data, and the fact that RefZ and SlmA are both TetR family proteins led us to hypothesize that *RBM*-bound RefZ complexes might act as a developmentally

regulated NO system that tunes FtsZ dynamics and/or Z-ring positioning relative to the chromosome.

To test this hypothesis, we isolated and characterized 10 RefZ loss-of-function (rLOF) variants unable to inhibit cell division when artificially induced during vegetative growth, yet still capable of binding *RBM*s. None of the rLOF variants were able to support wild-type chromosome capture when expressed from the native promoter during sporulation, and instead phenocopied a Δ*refZ* mutant. These results are consistent with a model in which RefZ mediates precise chromosome capture by modulating FtsZ activity. To better understand the molecular basis of RefZ's activity, wild-type RefZ and the rLOF variants were overexpressed, purified, and structural and biochemical characterizations were carried out. The location of the rLOF substitutions on the RefZ crystal structure suggests that RefZ affects FtsZ through a mechanism that is distinct from that described for SlmA. Characterization of the rLOF variants indicates that specificity for *RBM*-containing DNA and RefZ's propensity to dimerize are critical determinants in governing RefZ's effect on cell division and precise capture of forespore chromosome *in vivo*.

III.2 RESULTS

III.2.1 Identification of RefZ residues important for inhibition of cell division

Artificial expression of RefZ during vegetative growth disrupts Z-ring formation and inhibits cell division, resulting in filamentation (Wagner-Herman *et al.*, 2012). The division inhibition phenotype can be suppressed in strain backgrounds harboring specific

mutations in *ftsZ* or a second copy of the *ftsAZ* operon (Wagner-Herman *et al.*, 2012). Division inhibition appears to require RefZ's DNA binding activity, as RefZ variants harboring substitutions in the DNA recognition helix (Y43A and Y44A) do not filament cells following artificial expression (Wagner-Herman *et al.*, 2012). DNA binding is also likely required for RefZ's role in chromosome capture, as a strain harboring point mutations in the five *oriC*-proximal RefZ binding motifs (RBM_{5mu}) exhibits the same capture defect as a Δ*refZ* mutant (Miller *et al.*, 2016). Based on these data, we hypothesized that RefZ associates with *RBM*s to modulate FtsZ dynamics in the vicinity of the incipient septum and that this modulation would be required for ensuring precise chromosome capture.

To test whether RefZ's ability to inhibit cell division is required to support precise chromosome capture, we designed a two-stage genetic selection-screen to isolate RefZ loss-of-function (rLOF) variants capable of binding to the *RBM*s, but unable to disrupt cell division upon artificial expression (Figure III.1). Gibson assembly (Gibson *et al.*, 2009) was used to generate a library of linear artificial expression constructs comprised of an IPTG-inducible promoter (P_{hy}), randomly mutagenized *refZ* sequences (*refZ**), a selectable marker ($spec^R$) and regions of homology to direct double crossover integration of the linear DNA at a non-essential locus (*amyE*)(Figure III.1A). To select for rLOF mutants, we took advantage of the fact that in a sensitized background (Δ*minD*), expression of wild-type *refZ* from an IPTG-inducible promoter prevents colony formation on solid medium, whereas expression of RefZ variants unable to inhibit cell division survive (Wagner-Herman *et al.*, 2012).

In addition to *minD*, the native *refZ* gene was also deleted to ensure that the only RefZ expressed would be from the inducible promoter. To eliminate variants unable to bind DNA, survivors of the selection were screened for *RBM*-binding activity using a RefZ-repressible, *lacZ* transcriptional fusion (P_{spremo}-*lacZ*) integrated at the non-essential *sacA* locus. P_{spremo} harbors a single *RBM*, (RBM_{L2}) (Miller *et al.*, 2016) inserted between the -35 and -10 elements of a constitutive promoter (Figure III.1A). In this background, rLOF variants that can bind the engineered *RBM* operator repress *lacZ* expression and produce white colonies on media containing X-gal. In contrast, rLOF variants unable to bind the *RBM* due to decreased affinity for the *RBM*, poor expression, truncation, or misfolding produce blue colonies, allowing them to be excluded from further investigation.

To facilitate selection and screening efficiency and avoid cloning steps, transformation conditions were optimized so that the mutant *refZ* artificial expression construct library could be directly introduced into the *B. subtilis* chromosome (see Chapter III.5, Materials and Methods). RefZ loss-of-function and double-crossover integration were selected for simultaneously by plating transformations on a medium containing both spectinomycin and IPTG. Approximately 1,300 viable transformants were obtained, 37 of which were either white or pale blue on medium containing X-gal and IPTG, consistent with rLOF repression of *lacZ* expression from the engineered *RBM* operator.

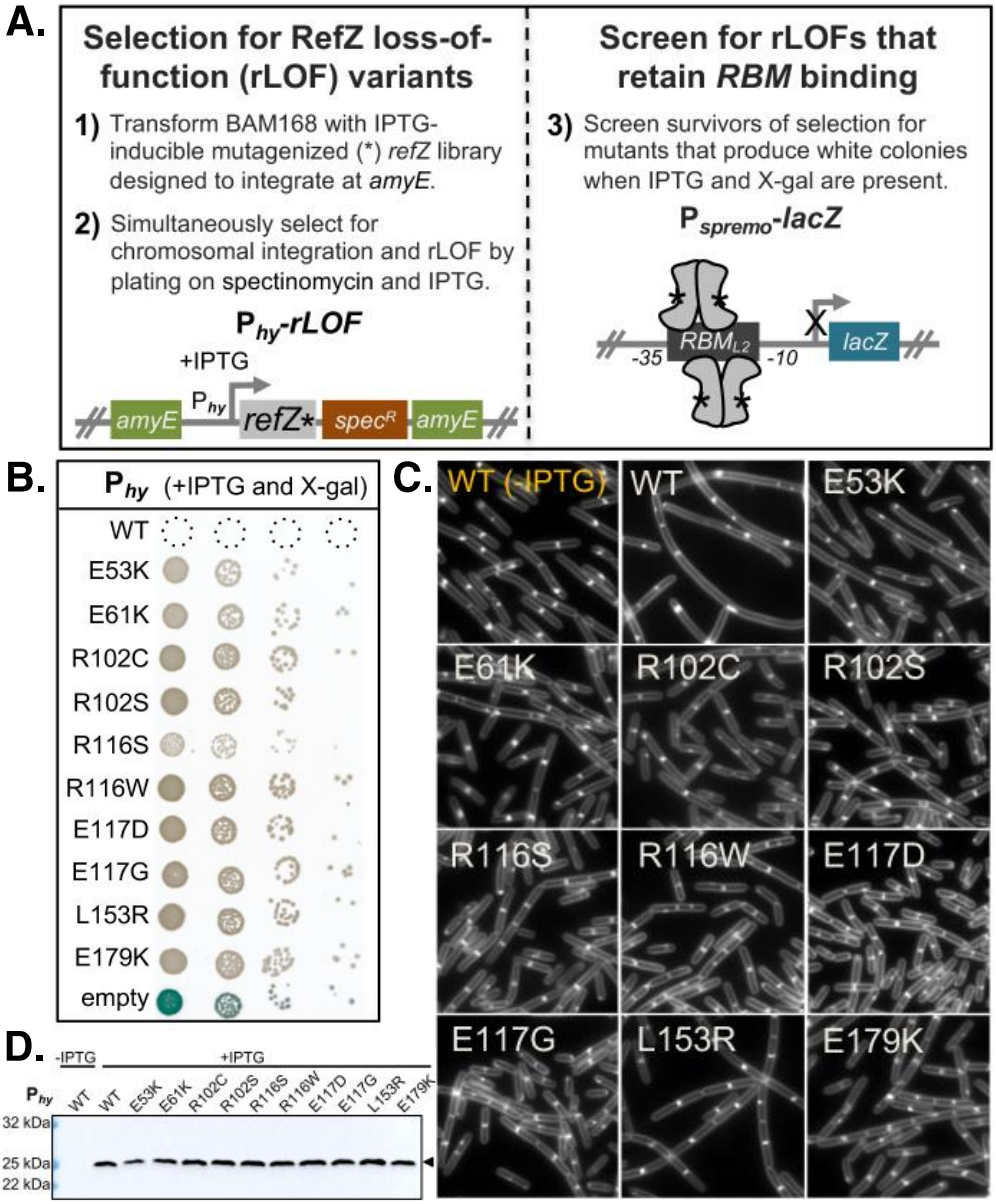

Figure III.1 Isolation of rLOF variants.
Reprinted with permission from Brown *et al*., 2019. **(A)** Schematic of genetic selection (left) and screen (right) used to isolate rLOF variants that retain *RBM*-binding activity. The open-reading frame of *refZ* was mutagenized by error-prone PCR (*refZ**), placed under an IPTG-inducible promoter (P_{hy}), and introduced at the *amyE* locus of competent recipient cells (BAM168). Mutations that interfere with RefZ's division inhibition function (P_{hy}-*rLOF*) permit growth in the presence of IPTG. Survivors were screened for *RBM* binding (P_{spremo}-lacZ) on plates containing X-gal and IPTG. **(B)** Ten unique rLOF variants that do not kill following induction but retain RBM-binding function were identified in the selection-screen. **(C)** The rLOF artificial expression constructs were introduced into a wild-type (*Bs168*) genetic background and the extent of cell filamentation in CH medium following 90 min of induction with 1 mM IPTG was monitored using epifluorescence microscopy. Membranes were stained with TMA (white). The uninduced wild-type (WT) control is labeled in yellow. **(D)** Western blot analysis to monitor the production and stability of wild-type RefZ (WT) and the rLOF variants (black carat) following 45 min of induction with 1 mM IPTG. RefZ is not produced at levels detectable above background with our antibody during vegetative growth (Lane 1, uninduced) or sporulation (data not shown).

Since resistance to RefZ can also be conferred by spontaneous suppressor mutations in *ftsZ* (Wagner-Herman *et al.*, 2012), the 37 artificial expression constructs were transformed into a clean selection-screen background, and survival and *RBM*-binding were reassessed. Four candidates failed to survive on IPTG plates, suggesting the presence of suppressor mutations in the original strains, while an additional eight turned blue on X-gal indicator medium.

To identify rLOF mutations in the remaining 25 candidates, the P_{hy}-*rLOF* region was amplified from the genomic DNA and sequenced (Table III.1). Six candidates had more than one SNP and were not characterized further. Of the 19 remaining candidates, substitutions were identified in only nine residues (Table III.1), indicating our screen was saturating. Two candidates with substitutions at L114 and L123 did not appear as effective as the remaining isolates at repressing *lacZ* expression from the *RBM* operator, and await further characterization. Ultimately, ten unique single-point mutations were identified, corresponding to the 10 rLOF substitutions shown in Figure III.1B. In contrast to wild-type RefZ, artificial expression of the rLOF variants did not result in cell filamentation (Figure III.1C), consistent with a loss of ability to affect FtsZ.

The inability of rLOF variants to inhibit cell division is not anticipated to be attributable to protein misfolding or insufficient expression, as each variant was able to repress *lacZ* expression from the *RBM* operator in the primary screen (Figure III.1B). Consistent with this conclusion, Western blot analysis of the rLOF variants demonstrated that they are stably expressed and present at levels comparable to wild-type RefZ following artificial expression (Figure III.1D). Moreover, we found that the

rLOF variants exhibited co-dominance with wild-type RefZ when co-expressed. We introduced an inducible copy of wild-type *refZ* at the ectopic *yhdG* locus in strains harboring either *refZ (WT)*, an empty vector, or *rLOF* under P_{hy} at the *amyE* locus and assayed for growth on plates containing 1 mM IPTG (Figure III.2A).

BAM	SNP	AA
449	**157 G->A**	**E53K**
462	**181 G->A**	**E61K**
409	**304 C->A**	**R102S**
407	**304 C->T**	**R102C**
410	304 C->T	R102C
412	304 C->T	R102C
442	304 C->T	R102C
405	340 T->A	L114I
402	346 A->T	R116W
440	**346 A->T**	**R116W**
443	**348 G->C**	**R116S**
403	**350 A->G**	**E117G**
441	350 A->G	E117G
444	**351 A->T**	**E117D**
463	351 A->T	E117D
406	368 T->C	L123P
411	**458 T->G**	**L153R**
400	**535 G->A**	**E179K**
459	535 G->A	E179K
537	105 T->C	D35D
404	145 G->C	G49R
538	147 A->G	G49G
401	157 G->A	E53K
460	216 C->T	S72S
447	267 T->A	D89E

SNP	AA
346 A->T	R116W
348 G->C	R116S
193 A->G	K65E
198 G->A	T66T
414 A->T	E138D
347 G->C	R116T

SNP	AA
351 A->T	E117D
444 G->A	L148L
535 G->A	E179K
438 G->A	L146L

Table III.1 Polymorphisms identified in the rLOF selection-screen.
Reprinted with permission from Brown *et al*., 2019.

With the possible exception of the R116S variant, all rLOF variants permitted growth to a similar or greater extent than the single P_{hy}-*refZ* controls when co-expressed with wildtype RefZ, but to a lesser extent than the *rLOF* mutants alone (Figure III.1B). From these data, we conclude that the 10 rLOF variants are perturbed in their ability to affect FtsZ function, either directly or indirectly.

III.2.2 rLOF mutants miscapture the forespore chromosome

A Δ*refZ* mutant and a strain harboring point mutations in all five *oriC*-proximal *RBM*s (*RBM*$_{5mu}$) both exhibit a 2-fold increase in the frequency of left and right arm reporter capture compared to wild-type controls (Miller *et al.*, 2016). We hypothesized that if RefZ's ability to perturb FtsZ assembly is required to mediate precise chromosome capture, then the rLOF mutants would phenocopy the Δ*refZ* mutant with regard to chromosome trapping. To test this hypothesis, chromosome organization was monitored in sporulating cells expressing the rLOF variants from the native locus (native promoter) using a fluorescence-based trapping assay (Miller *et al.*, 2016, Sullivan *et al.*, 2009). For each strain, the native *refZ* gene was replaced with a rLOF mutant sequence in backgrounds harboring reporters for either left (−61°) or right (+51°) arm capture (Figure III.2B). All of the rLOF mutations resulted in significant increases in both left and right arm reporter capture compared to wild-type controls ($P<0.05$)(Figure III.2B).

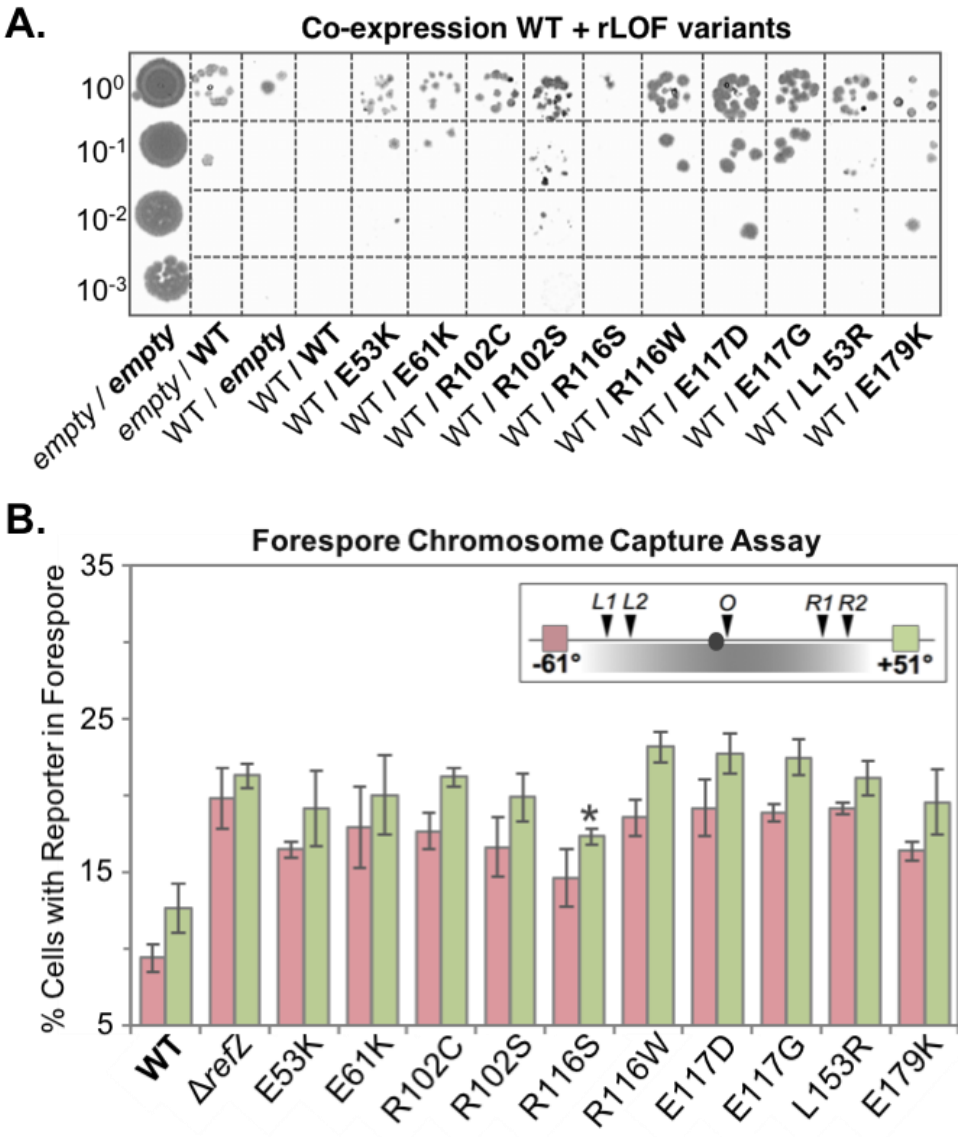

Figure III.2 Functional characterization of rLOF variants.
Reprinted with permission from Brown *et al*., 2019. **(A)** The *yhdG*::P$_{hy}$-*refZ* (WT) construct was introduced into the chromosome of recipient strains (bold text) harboring an inducible copy of wild-type *refZ* (WT/WT), an *rLOF* mutant, or an empty vector (*empty*/WT) at *amyE*. As controls, an empty vector was introduced into the *yhdG* locus of the *amyE*::P$_{hy}$-*empty* (*empty*/*empty*) and *amyE*::P$_{hy}$-*refZ* (WT/*empty*) backgrounds. The resulting strains were grown in lysogeny broth at 30ºC until mid-log. Cultures were normalized to the lowest OD$_{600}$ reading in PBS (10^0) and serially diluted to 10^{-3}. Five µl of the indicated dilution was spotted on LB plates supplemented with phleomycin and 1 mM IPTG, followed by overnight incubation at 37°. **(B)** Quantitative single cell analysis of chromosome capture is represented as the average percentage of cells that captured either the left arm (−61°, pink) or right arm reporter (+51°, green) in the forespore at the time of polar division. The black circle represents oriC (0°). The inset indicates the location of the reporters relative to the *RBM*s, with the region of chromosome typically captured in the forespore shaded grey. All strains encoding rLOF variants miscapture the left and right arm reporters at levels statistically indistinguishable from the Δ*refZ* mutant control (P>0.05) with the exception of the R116S variant (continued on next page). The R116S variant exhibited an intermediate defect for right arm reporter capture that was statistically different from both Δ*refZ* (asterisk, P=3.9x10-3) and wildtype (P=2.3x10-3). Error bars represent standard deviations.

Moreover, with the exception of right arm capture in the R116S mutant, miscapture of both left and right arm reporters in the rLOF mutants was statistically indistinguishable from the Δ*refZ* controls (P>0.05). The right arm reporter in the R116S mutant exhibited an intermediate capture defect that was statistically different from both Δ*refZ* ($P=3.9x10^{-3}$) and wild-type ($P=2.3x10^{-3}$). The intermediate capture defect observed in the R116S mutant suggests this variant retains some functionality, and is consistent with the reduced growth we observed on selection medium in the sensitized Δ*minD* background (Figure III.1B and III.2A). These data demonstrate that the same residues required for RefZ's ability to inhibit division upon artificial expression are also required for precise chromosome capture, and are consistent with a model in which *RBM*-bound RefZ modulates FtsZ activity to position the polar septum relative to the chromosome.

III.2.3 Structural characterization of RefZ

Like the *E. coli* NO protein, SlmA, RefZ belongs to the TetR family of DNA-binding proteins (Wagner-Herman *et al.*, 2012). At the sequence level, RefZ and SlmA share no significant similarity. We reasoned that structural characterization of RefZ and mapping of the rLOF substitutions to the RefZ structure would not only provide insight into how RefZ functions, but also allow for comparison to what is known about SlmA's mechanism of FtsZ inhibition. RefZ-His6 was purified, crystallized, and the structure was solved using single-wavelength anomalous dispersion (SAD) phasing at a resolution of 2.6 Å.

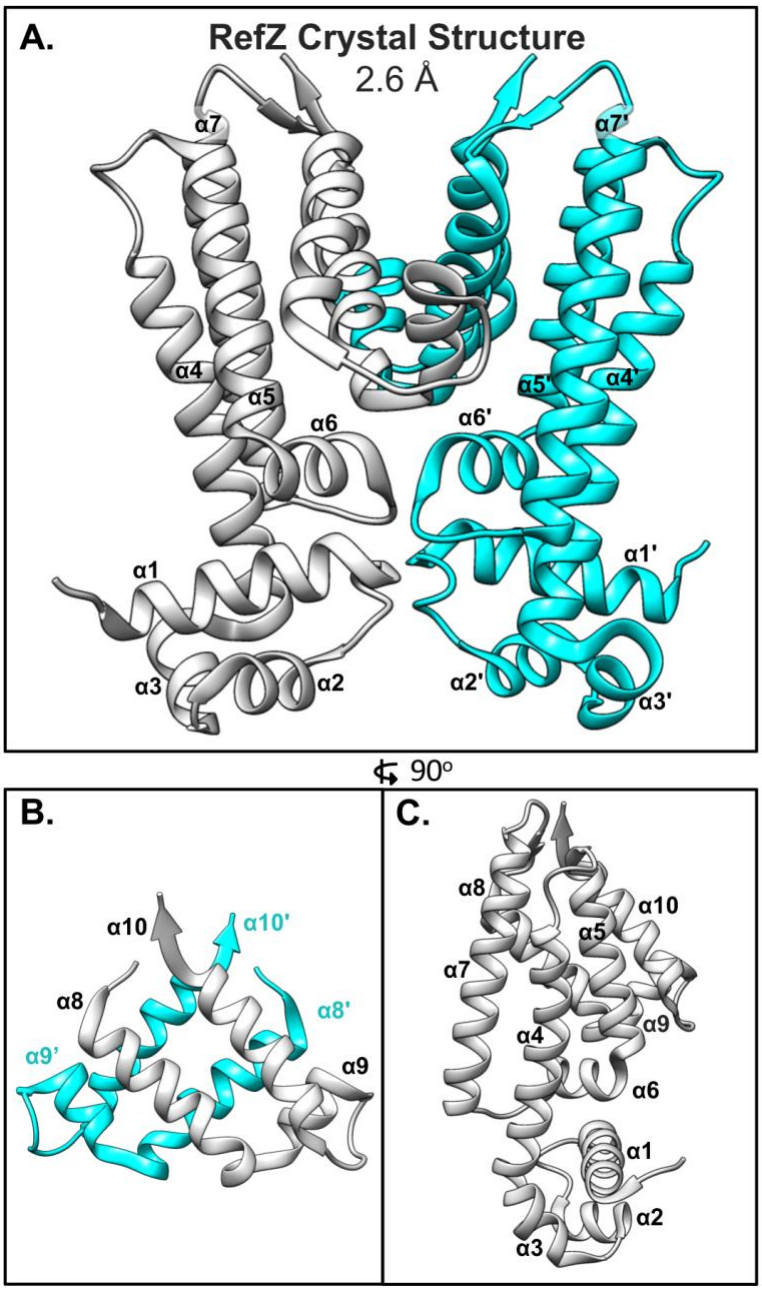

Figure III.3 Crystal structure of the RefZ homodimer at 2.6 Å resolution.
Reprinted with permission from Brown *et al*., 2019. **(A)** Structure of the RefZ homodimer. Subunits are colored grey and cyan. **(B)** Helices α8-α10 of RefZ's regulatory region with antiparallel helices α8, α10, α8', and α10' comprising the four-helix dimerization motif. **(C)** The RefZ monomer, rotated 90° relative to panel (A).

PDB ID	6MJ1
Data collection	
Space group	P 4_1 2_1 2
Cell dimensions	
a, *b*, *c* (Å)	100.021, 100.021, 100.177
α, *β*, *γ* (°)	90, 90, 90
Resolution (Å)	2.6
R_{merge}	0.11 (0.79)
$I / \sigma I$	11.59
Completeness (%)	100 (100)
Redundancy	17.6 (15.6)
Refinement	
Resolution (Å)	44.952-2.6
No. reflections	16,039
R_{work} / R_{free}	22.20 / 25.36
No. atoms	
Protein	1,683
Water	25
B-factors	
Protein	76
R.m.s. deviations	
Bond lengths (Å)	0.009
Bond angles (°)	1.082

Table III.2 Data collection, phasing and refinement statistics for the RefZ structure.
Reprinted with permission from Brown *et al*., 2019.

RefZ crystallized as a homodimer (Figure III.3A) with one molecule in the asymmetric unit of a $P4_12_12$ crystal lattice. The model for residues 1-200 was built and refined with R_{work}= 22% and R_{free}= 25% (Table III.2). Each RefZ subunit is composed of 10 α-helices connected by loops and turns. Similar to other structurally characterized TetR family proteins (Yu *et al.*, 2010), α1, α2, and α3 comprise the DNA binding helix-turn-helix (HTH) domain and α4-α10 comprise the regulatory domain (Figure III.3A). There are two major regions for dimerization contacts. Helices α7, α8, α9, and α10 form regulatory domain contacts with α7', α8', α9', and α10'; α8, α10, α8' and α10' form a four-helix dimerization motif (Figure III.3B). A second interface is formed by α6 and

α6', at the junction between the regulatory and DNA binding domains (Figure III.3A). Although the crystallization condition included *RBM*-containing DNA, we observed no DNA in the crystal structure. In fact, the HTH DNA binding domain is involved in extensive crystal packing interactions, likely precluding DNA binding within the crystal lattice.

According to a structural similarity search using VAST (Gibrat *et al.*, 1996), RefZ shares the highest homology with PfmR from *Thermus thermophilus* (PDB: 3VPR)(Agari *et al.*, 2012), with a VAST similarity score of 15.4, closely followed by KstR2 of *Mycobacterium tuberculosis* (PDB: 4W97)(Crowe *et al.*, 2015), with a score 15.2. The SlmA structure (PDB: 4GCT) (Tonthat *et al.*, 2013) was the tenth closest in similarity with a score of 13.6. Superposition of SlmA and RefZ produced a root-mean-square deviation (rmsd) in Cα of 2.8. RefZ's HTH domain (residues 1-45) has the highest contiguous alignment similarity score with QacR from *Staphylococcus aureus* (PDB: 1JT6) (Schumacher *et al.*, 2001), with a VAST similarity score of 4.0 and a rmsd value of 0.7.Superimposition of the HTH domains demonstrates the structures align closely (Figure III.4A). However, when the RefZ dimer is superimposed with DNA-bound QacR (PDB: 1JT0), it is apparent that the RefZ dimer would need to undergo a conformational change for the α3 and α3' helices to be accommodated in adjacent DNA major grooves (Figure III.4B and III.4C).

DNA binding in TetR family proteins can be allosterically regulated by ligand binding in a pocket formed by α5, α6, and α7. For QacR, ligand binding results in a pendulum motion of α4 that repositions the HTH domains such that the distance between

α3 and α3' becomes incompatible with DNA binding (Grkovic *et al.*, 2001). In the RefZ structure (unbound from DNA), there is no obvious ligand binding pocket in the α5-α7 regulatory region, therefore its affinity to DNA is unlikely to be regulated in this manner. At the same time, we do not exclude this possibility.

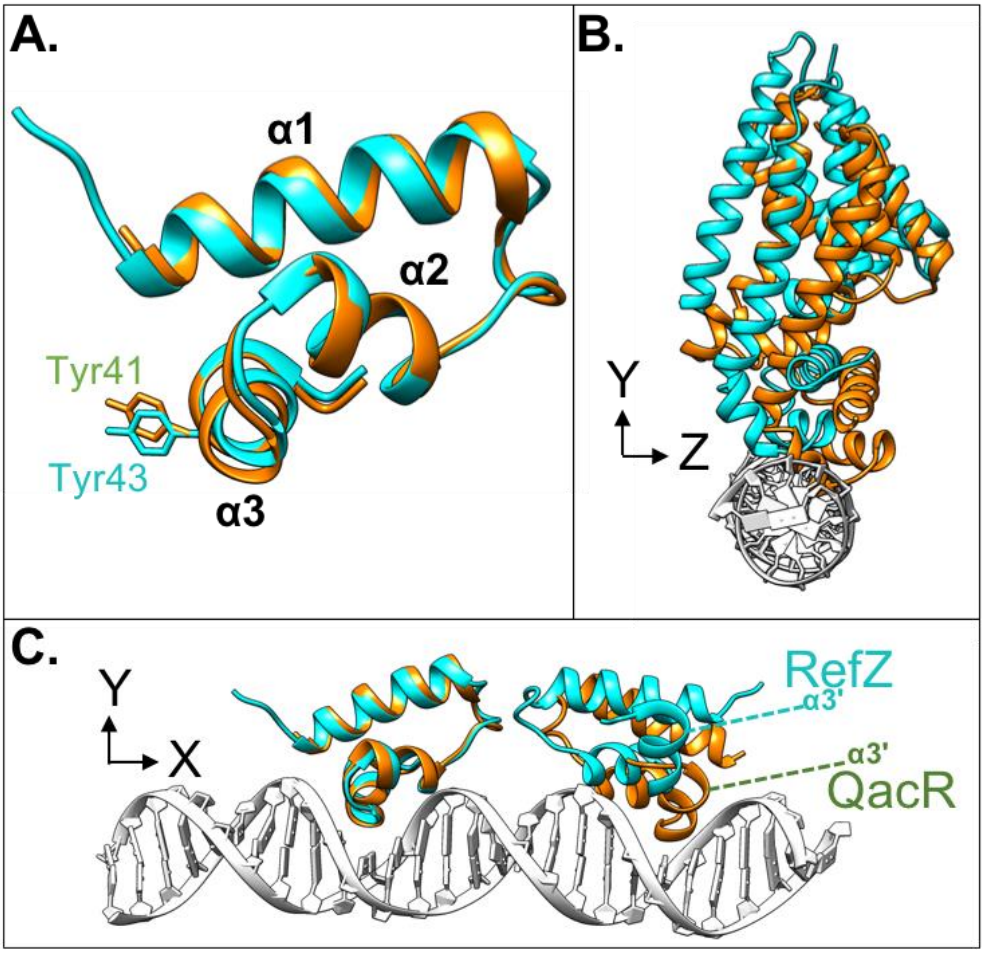

Figure III.4 Superimposition of the N-terminal domains of RefZ and QacR.
Reprinted with permission from Brown *et al*., 2019. **(A)** Superimposition of the HTH domains of RefZ (cyan) and QacR (PDB: 1JT6)(orange). The Y43 residue on α3 of RefZ which is required for DNA binding and the corresponding residue in QacR (Y41) are shown as sticks. **(B)** Superimposition of RefZ (cyan) with QacR (PDB: 1JT0) (orange) in complex with IR1 DNA (white). **(C)** Superimposition of the HTH domains of RefZ (cyan) with QacR (orange) in complex with IR1 DNA (white)(PDB 1JT0).

III.2.4 The regions of RefZ and SlmA important for inhibiting cell division are distinct

To analyze which regions of RefZ are important for its effect on cell division, and compare them to the location of the loss-of-function residues identified for SlmA, the residues with rLOF substitutions were mapped to the RefZ crystal structure (Figure III.5). Nine of the 10 rLOF substitutions (L153R being the exception) occur in charged residues that are surface exposed and map to the same surface of the RefZ homodimer (Figure III.5A and B). L153 maps to the dimerization interface (Figure III.6A) and participates in several hydrophobic interactions between subunits that are likely important for RefZ dimerization. Residue R102 is not only surface exposed, but also hydrogen bonds across the dimer interface to the backbone carbonyl of V108' (NH_2-O = 2.6 Å) (Figure III.6B).

To assess if similar regions of SlmA were implicated in FtsZ regulation, the structures of the RefZ and SlmA homodimers were compared (Figure III.5C-F). In the DNA-bound structure, SlmA binds the C-terminal domain (CTD) tail of FtsZ along a hydrophobic groove located between α4 and α5 (Cho *et al.*, 2011, Schumacher *et al.*, 2016) (Figure III.5E). SlmA loss-of-function substitutions map to this region clustering primarily along α4 (Figure III.5E and F) (Cho & Bernhardt, 2013, Schumacher *et al.*, 2016). In contrast, the surface-exposed residues implicated in RefZ loss of function are positioned both at or on either side of the RefZ dimerization interface and all but L153 are positively or negatively charged (Figure III.5A and B).

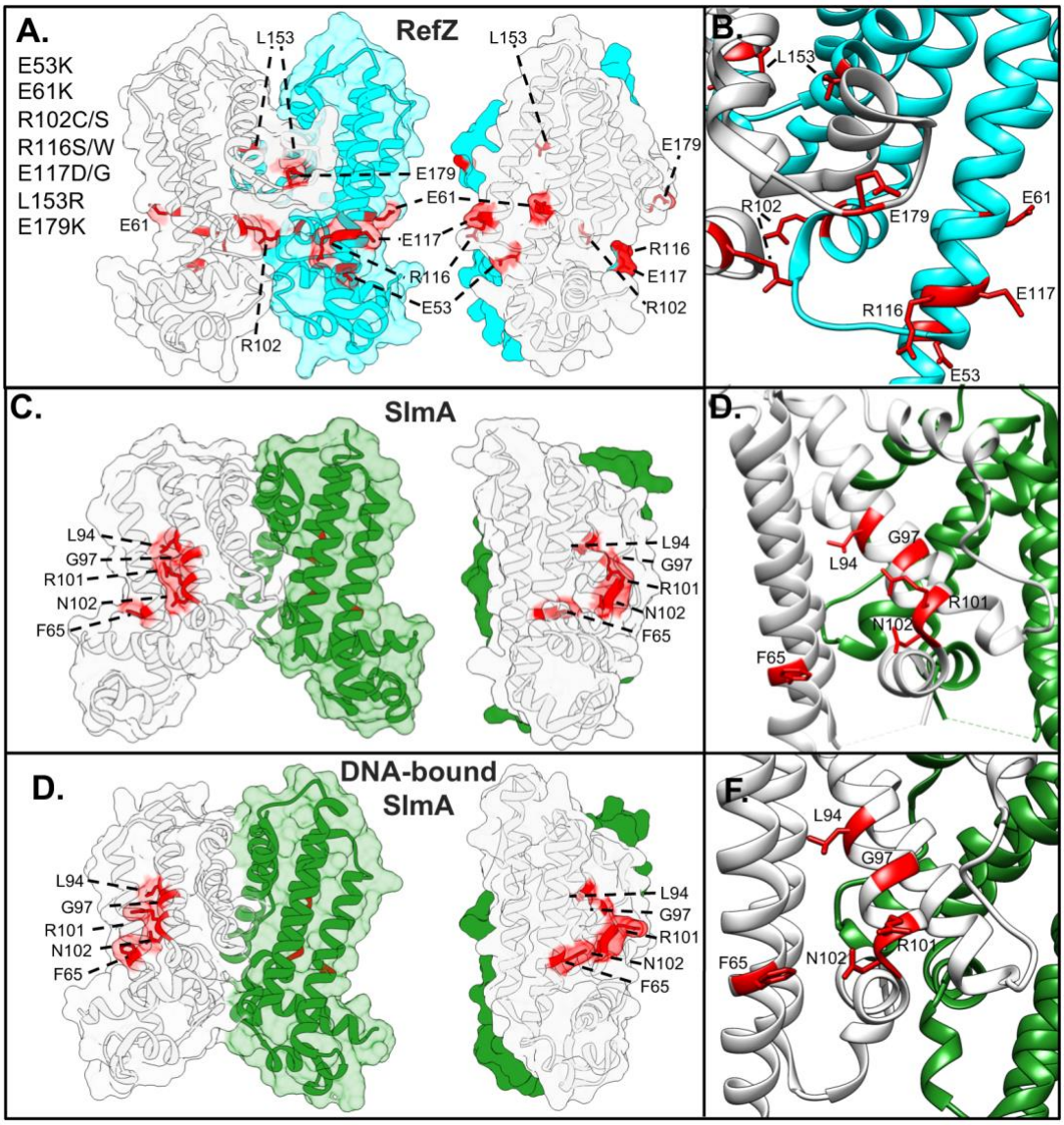

Figure III.5 Position of residues implicated in RefZ's regulation of cell division.
Reprinted with permission from Brown *et al*., 2019. **(A)** Surface/cartoon representation of the RefZ homodimer highlighting residues with substitutions conferring loss-of-function (red, sticks). Subunits are colored white and cyan. **(B)** Ribbon model of RefZ region showing residues conferring loss of function as sticks. Surface/cartoon representations of the **(C)** SlmA homodimer (PDB:3NXC) and **(E)** SlmA homodimer bound to DNA and the C-terminal domain tail of FtsZ (PDB: 5HBU), highlighting residues with substitutions conferring loss of function (red, sticks). Subunits are colored white and green. Ribbon models corresponding to the **(D)** SlmA homodimer (PDB:3NXC) and **(F)** SlmA homodimer bound to DNA and the C-terminal tail of FtsZ (PDB: 5HBU), showing residues conferring loss of function as sticks.

Furthermore, the structure of RefZ and the SlmA homodimer not bound to DNA/FtsZ CTD tail adopt distinct confirmations (compare Figure III.5A and C). From these data we conclude that, if RefZ regulates FtsZ through direct interaction, the precise mechanism is likely to differ significantly from that of SlmA.

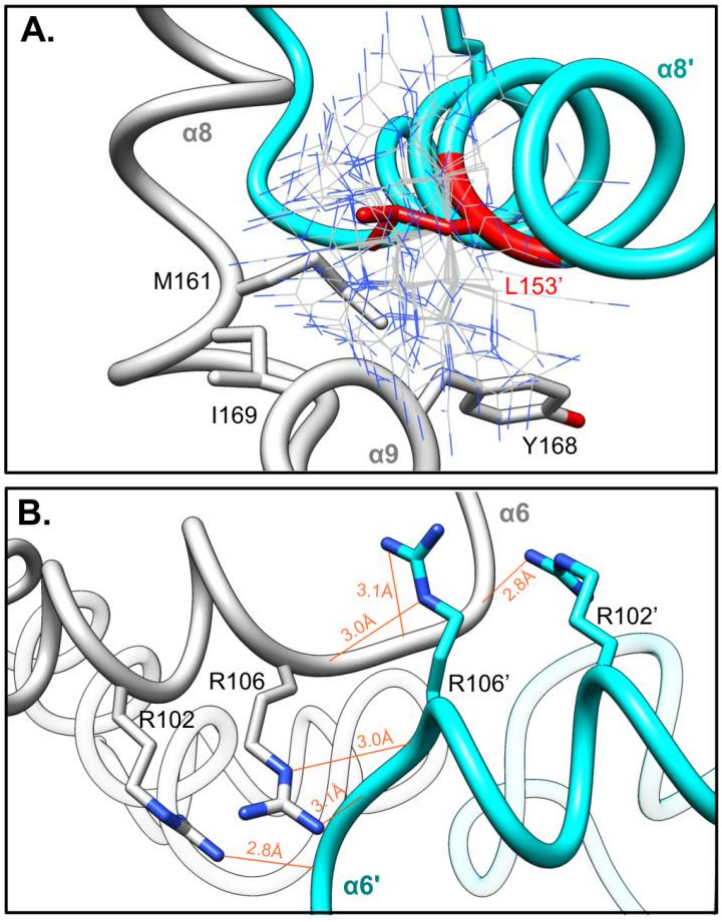

Figure III.6 Dimer interface residues implicated in RefZ function.
Reprinted with permission from Brown *et al*., 2019. RefZ subunits are shown in light gray and cyan. **(A)** Hydrophobic dimerization interface near the L153 residue. Thin blue and gray sticks display possible positions of an R153 side-chain based on a rotamer library. **(B)** Helices α6 and α6' of RefZ with residues implicated in loss of function shown as sticks. The hydrogen bonds formed across the dimer interface by R102 and R106 are displayed as red lines.

III.2.5 Characterization of RefZ and rLOF variant DNA-binding

RefZ's ability to inhibit cell division is dependent upon DNA binding (Wagner-Herman *et al.*, 2012). We predicted that the rLOF variants would be DNA-binding proficient because each was able to repress *lacZ* expression from an *RBM* operator in the *in vivo* screening assay (Figure III.1B); however, *RBM*-binding in this assay was qualitative and not designed to differentiate between specific and non-specific DNA interactions. To directly examine the behavior of the variants with DNA, we overexpressed and purified each of the rLOF variants (Figure III.7) and performed electrophoretic mobility shift assays (EMSAs) with wild-type and mutant *RBM* DNA probes as described previously (Miller *et al.*, 2016).

Incubation of wild-type RefZ with a 150 bp *RBM*-containing probe produced two major mobility shifts (Figure III.8), corresponding to RefZ binding to *RBM*-containing DNA in units of two and four. Consistent with previous observations (Miller *et al.*, 2016), the upshifts were lost when RefZ was incubated with a mutant *RBM* probe (harboring seven point-mutations in the central palindrome) indicating that DNA binding is specific to the *RBM* sequence (Figure III.8). Four of the rLOF variants (R116S, R116W, E117D, and E179K) produced specific upshifts similar to wild-type RefZ, suggesting that their loss-of-function phenotypes are not attributable to altered affinity or non-specific DNA binding.

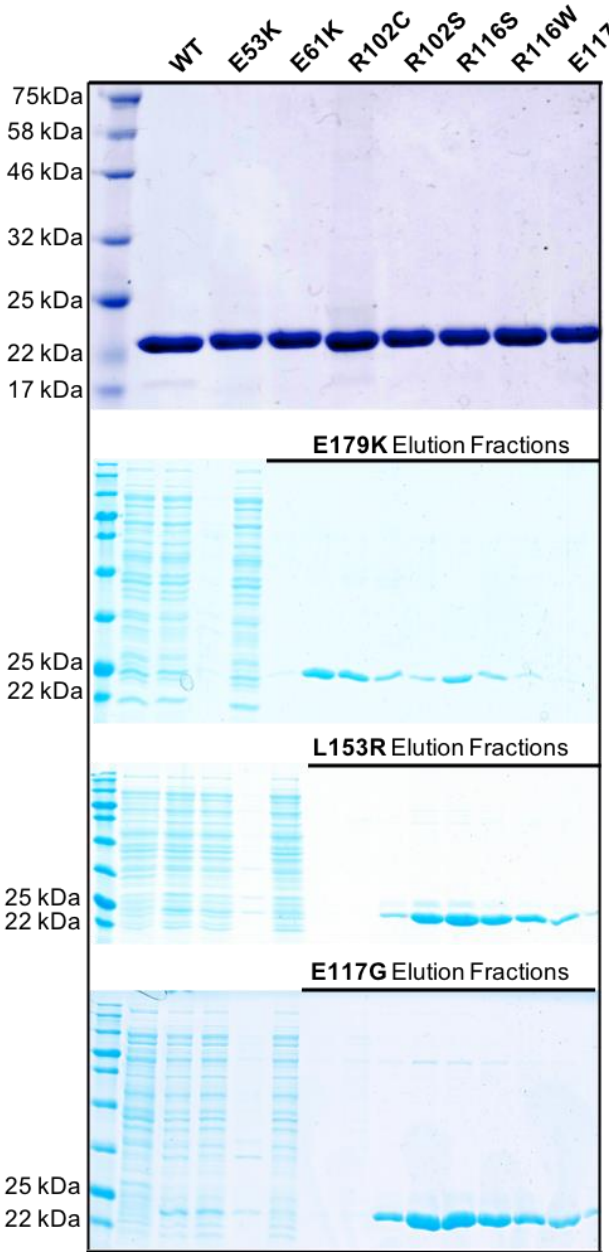

Figure III.7 Example purification of wild-type RefZ and rLOF variants.
Reprinted with permission from Brown *et al*., 2019. The top gel was loaded with 5 ug protein/lane and stained with Coomassie blue dye (R-250). Gels below show example elution profiles from Nickel-NTA agarose beads. The elution gels were stained with Coomassie brilliant blue dye (colloidal Coomassie, G-250). G-250 is approximately 10x more sensitive than R-250, allowing for detection of less abundant proteins.

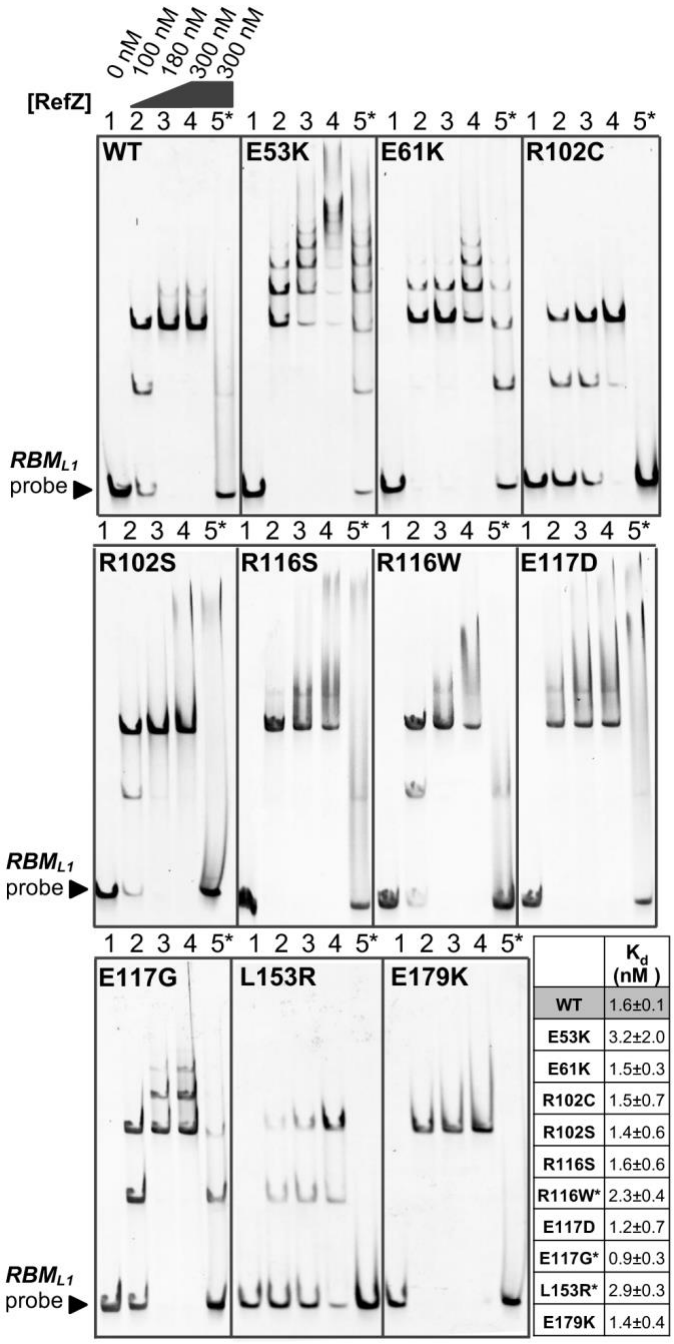

	K_d (nM)
WT	1.6±0.1
E53K	3.2±2.0
E61K	1.5±0.3
R102C	1.5±0.7
R102S	1.4±0.6
R116S	1.6±0.6
R116W*	2.3±0.4
E117D	1.2±0.7
E117G*	0.9±0.3
L153R*	2.9±0.3
E179K	1.4±0.4

Figure III.8 Interaction of the rLOF variants with DNA.
Reprinted with permission from Brown *et al*., 2019. Electrophoretic mobility shift assays were performed with 150 bp DNA probes (10 nM) centered on either the wild-type (lanes 1-4) or the mutant (lane 5*) *RBM*$_{L1}$ sequence. Probes were incubated with the indicated concentrations of purified RefZ-His6 (WT) or rLOF-His6 variants for 30 min. Reactions were run on a 5% TBE gel for 30 min at 150 V. The tabulated K_d values of RefZ for an immobilized 41 bp *RBM*-containing DNA segment were determined using a bio-layer interferometry assay. All the variants possessed K_d values within 2-fold of the wild-type K_d. The differences in K_d between wild-type RefZ and R116W, E117G, and L153R are significant (indicated by asterisks)(P=0.05, P=0.025, and P=0.003, respectively).

The remaining variants exhibited altered DNA interactions with respect to either specificity and/or mobility shift pattern. Two variants (E53K and E61K) exhibited a laddering pattern, possibly due to additional subunits of RefZ binding nonspecifically along the DNA (Figure III.8). These variants also shifted a mutant *RBM*, consistent with enhanced nonspecific binding.E53K and E61K may assume conformations more favorable for nonspecific DNA binding since the substitutions are located on α4, a helix important for modulating DNA interaction in response to ligand binding in other TetR family members (Cuthbertson & Nodwell, 2013).

Although the laddering behavior was most extensive with E53K and E61K mutants, wild-type RefZ is also observed to ladder slightly (Figure III.8). The laddering behavior is more apparent when the EMSA gels are run at a higher voltage (200 V vs. 150 V) (Figure III.9A), likely because EMSAs are non-equilibrium assays and the faster run time reduces RefZ disassociation. E117G also produced laddering, albeit to a lesser extent than either E53K or E61K (Figure III.8). The remaining variants, R102C, R102S, and L153R, each possess substitutions in residues that make dimerization contacts (Figure III.6). R102C, R102S and L153R produced two major upshifts, but were unable to ladder on DNA even under EMSA conditions in which wild-type RefZ displayed some laddering (Figure III.9B).

To determine if there were quantitative differences in DNA binding that might account for the loss-of-function phenotypes, we determined the dissociation constant (K_d) of wild-type RefZ and each of the rLOF mutants for a 41 bp segment of *RBM*-containing DNA using bio-layer interferometry.

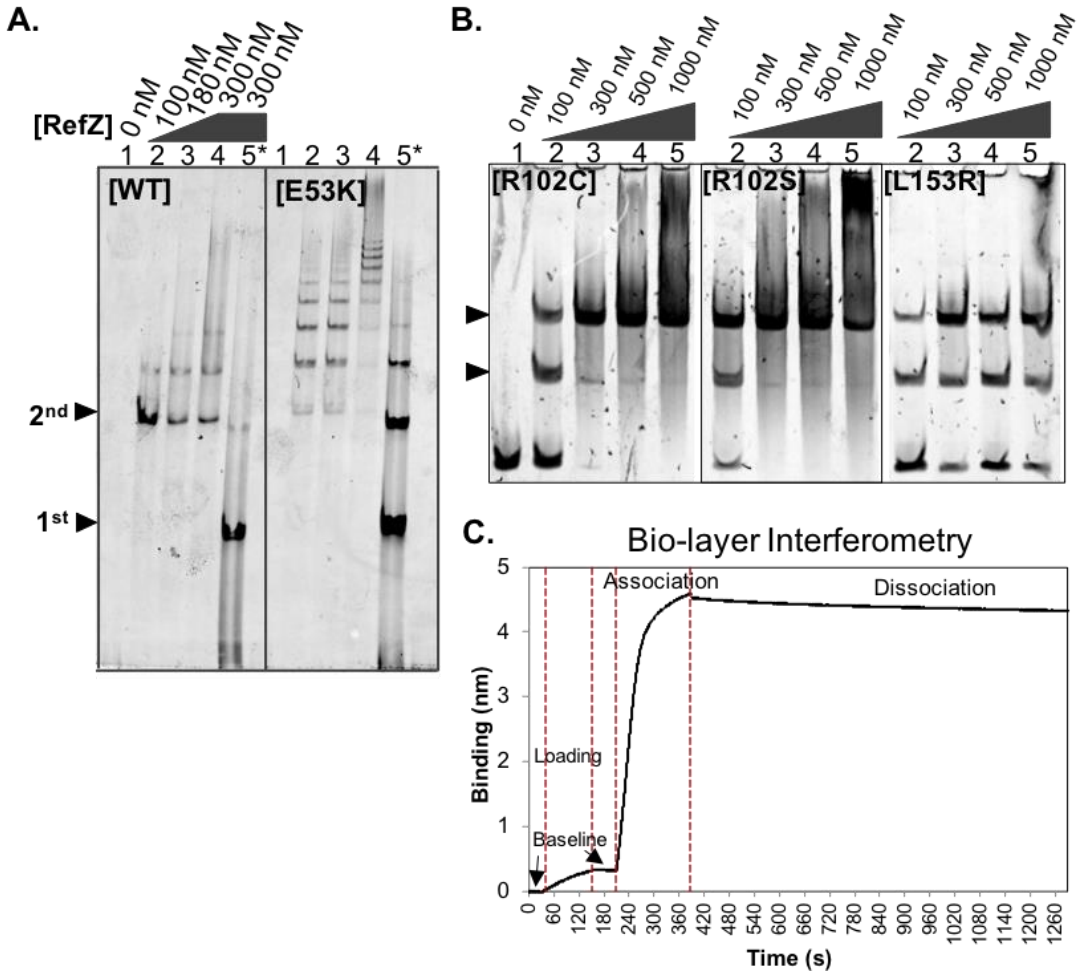

Figure III.9 EMSA laddering behavior of wild-type RefZ and rLOF variants.
Reprinted with permission from Brown *et al*., 2019. **(A)** Laddering of DNA in the EMSAs can be observed wild-type RefZ and to a greater extent E53K when samples are resolved at 200 V on a 7.5% TBE gel. **(B)** The rLOF variants R102C, R102S, and L153R do not produce laddering on EMSAs when samples are resolved at 200 V on a 7.5% TBE gel. **(C)** Typical bio-layer interferometry binding curve for wild-type RefZ with RBM-containing DNA. Sensors are pre-equilibrated for 10 min in DNA binding buffer (150 mM KCl and 10 mM Tris [pH 8]) at room temperature (not shown). The experiment is then initiated and performed at 30˚C (30 sec baseline is established). The streptavidin sensor is dipped into a solution of biotinylated dsDNA (a 41 bp segment centered on RBM_{L1}) for 2 min. After incubation a new baseline is established by returning the biosensor to the DNA binding buffer (30 sec). The biosensor is then moved to a well containing 800 nM protein to monitor association (3 min). The sensor is then transferred to a well containing fresh DNA-binding buffer to monitor dissociation (15 min).

The *RBM*-containing DNA, which was 5' biotinylated, was immobilized on a streptavidin sensor. The association and dissociation of wild-type RefZ (Figure III.9C) and the rLOF variants was then assessed by monitoring the change in thickness of the bio-layer. All of the rLOF variants displayed K_d values within 2-fold of wild type (Figure III.8, inset table). The decreased K_d for the L153R mutant was most significant ($P<0.01$), consistent with the reduced apparent affinity for DNA observed by EMSA (Figure III.8).These results suggest that the *in vivo* chromosome capture defect observed in strains harboring rLOF mutations (Figure III.2B), with the possible exception of L153R, are unlikely attributable to markedly reduced affinity for DNA.

III.2.6 RefZ oligomerization state by size-exclusion chromatography

Three of the rLOF substitutions (R102C, R102S, and L153R) map to residues implicated in RefZ dimerization based on structural analysis (Figure III.6), suggesting dimerization may be important for RefZ's effect on cell division. Purified TetR proteins have been shown to exist as both monomers and dimers in solution and as pairs of dimers on DNA (Cuthbertson & Nodwell, 2013, Engohang-Ndong *et al.*, 2004, Rodikova *et al.*, 2007, Singh *et al.*, 2015, Tonthat *et al.*, 2011). RefZ also binds DNA in units of two and four (Figure II.5B)(Miller *et al.*, 2016), but its oligomerization state in the absence of DNA is unknown. To determine the oligomerization state of purified RefZ and the rLOF variants, we performed size-exclusion chromatography. Wild-type RefZ-His6 eluted from a Superdex 200 column primarily as a single peak corresponding to an apparent molecular weight of 21 kDa, close to the actual monomeric molecular

weight of 25.4 kDa (Figure III.10A and III.11A). A minor peak, corresponding to an aggregate or higher-order oligomer, was also observed (Figure III.11A). All of the rLOF variants tested displayed elution profiles comparable to wild type (Figure III.10A). These data indicate that, if RefZ forms dimers in the absence of DNA under the buffer conditions utilized, then they are not stable enough to be maintained during size-exclusion chromatography.

III.2.7 Bacterial two-hybrid analysis of RefZ self-interaction

Size-exclusion chromatography is known to disassociate weaker oligomers, including dimers of at least one TetR family protein (Grkovic *et al.*, 2001). Therefore, to further investigate if any of the rLOF substitutions altered RefZ's ability to form dimers, we performed bacterial 2-hybrid (B2H) analysis (Karimova *et al.*, 1998). In the B2H assay, wild-type RefZ displayed a self-interaction that was not observed in the negative controls (Figure III.10B). The self-interaction is unlikely to require *RBM* binding, as the B2H assay is performed in an *E. coli* strain that lacks native *RBM* motifs. Consistent with this observation, a DNA-binding deficient variant, Y43A (Wagner-Herman *et al.*, 2012), displayed self-interaction similar to wild type (Figure III.10B and Figure III.11B). Moreover, in addition to Y43A the Y44A mutant, also harboring a substitution within the DNA recognition helix, and two mutants harboring substitutions in residues conserved in RefZ homologs, R106A and E107A (Wagner-Herman *et al.*, 2012), do not efficiently bind the *RBM* operator *in vivo* (Figure III.11C) but exhibit differing degrees of self-interaction (Figure III.10B and Figure III.11B).

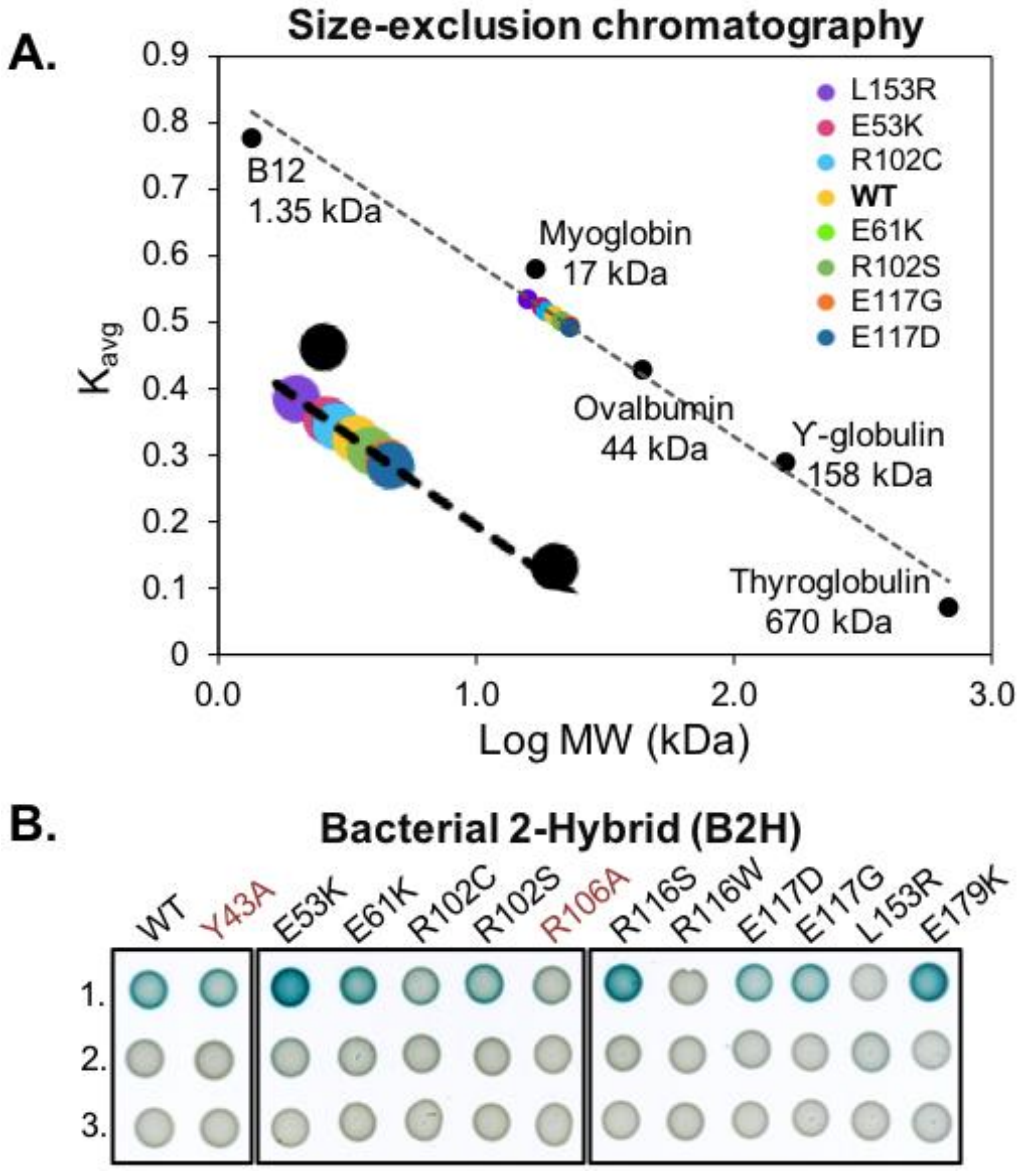

Figure III.10 Oligomeric state and thermostability of wild-type RefZ and the rLOF variants.
Reprinted with permission from Brown *et al*., 2019. **(A)** Size-exclusion chromatography of wild-type RefZ-His6 and a subset of rLOF-His6 variants on a Superdex 200 column. The K_{avg} values for the indicated standards were used to generate a standard curve and to estimate the apparent molecular weights of the experimental samples. The E61K and R102C variants share the same position on the curve and only R102C (cyan) is visible. **(B)** Self-interaction of wild-type RefZ or rLOF variants in a B2H assay. The RefZ variants in red (Y43A and R106A) were generated by site-directed mutagenesis and do not bind *RBM*-containing DNA. Pairwise interactions between wild-type RefZ subunits or the subunits of the indicated variants fused to T25 and T18 tags (row 1), T25 tagged subunits paired with an empty T18 vector (row 2), or T18 tagged subunits paired with an empty T25 vector (row 3). Color development after 41 h of growth at room temperature is shown.

The B2H is most likely reporting on dimerization as the RefZ forms a homodimer in the crystal structure (Figure III.3A). Consistent with this hypothesis, the alanine substitution at R106, which participates in two hydrogen bond contacts across the dimer interface (four bonds total) (Figure III.6B), resulted in reduced self-interaction as expected (Figure III.10B).

B2H analysis of the 10 rLOF variants revealed three classes of reproducible self-interaction phenotypes (Figure III.10B and III.11B): loss-of-interaction, gain-of-interaction, and wild-type interaction. Three rLOF variants, L153R, R102C, and R116W classed as loss-of-interaction. Like R106, R102 and L153 are located on the dimer interface. R102 contributes a total of two hydrogen bonds to RefZ dimer formation (Figure III.6B). Substitution of a cysteine at R102 would therefore be expected to reduce dimerization and this is consistent with the reduced self-interaction observed (Figure III.10B). The L153R substitution introduces a longer, positively charged side chain into a hydrophobic region of the RefZ dimer interface, and thus is also predicted to reduce dimerization (Figure III.6A). No self-interaction was observed for the L153R variant, consistent with the structural prediction. These data suggest that the loss-of-function phenotypes of R102C and L153R may be related to a reduced ability to dimerize.

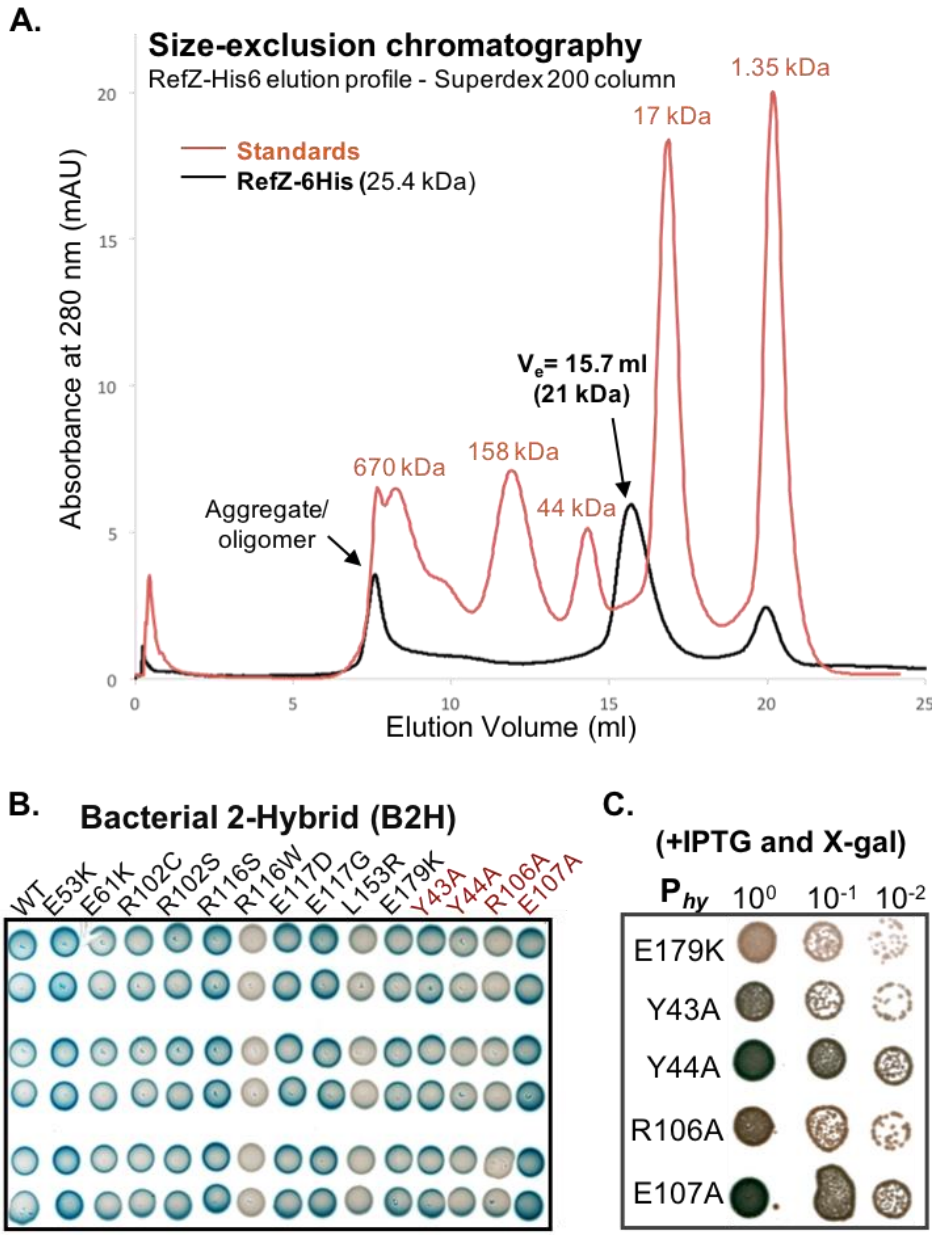

Figure III.11 *In vivo* and *in vitro* analysis of RefZ oligomer state.
Reprinted with permission from Brown *et al*., 2019. **(A)** An example Supradex 200 elution profile for 200 µl of 1 µg/ml RefZ-His6 (7.7 nmol) ran with 50 mM Tris-HCl [pH 9], 300 mM KCl and 10% (v/v) glycerol. Absorbance at 280 nm is shown on the Y-axis (mAU – milli-absorbance). Aggregated RefZ elutes near the column void volume (V_e =7.6 mL). **(B)** RefZ and rLOF self-interaction is highly reproducible. *E. coli* DHP1 (*cya*-) co-transformants containing plasmids harboring N-terminal or C-terminal fusions of wild-type RefZ and rLOF to T25 and T18 tags were grown as described in Chapter III.4, Materials and Methods. Cultures were normalized to the lowest OD_{600} reading and 5 µl were spotted on M9 glucose minimal plates supplemented with 25 µg ml^{-1} kanamycin, 50 µg ml^{-1} ampicillin, and 40 µg ml^{-1} X-gal and grown for 44 h at room temperature. **(C)** In the sensitized selection-screen background, RefZ variants harboring substitutions within the DNA recognition helix (Y43A and Y44A) or in residues conserved in RefZ across the *Bacillus* genus (R106A and E107A) survive on plates containing IPTG and X-gal, but do not efficiently repress l*acZ* expression from the *RBM* operator compared to rLOF variants (E179K). Strains were grown and spotted as described for Figure III.1B.

Three variants, E53K, R116S, and E179K displayed enhanced self-interaction compared to wild type (Figure III.11B). E53K is positioned on α4, the helix connecting the regulatory domain (α4-α10) to the DNA-binding domain (α1-α3). In TetR and QacR, conformational changes caused by ligand binding to the regulatory domain are transmitted through α4 to the HTH, leading to DNA release (Cuthbertson & Nodwell, 2013). Since the E53K mutant also shows higher affinity for non-specific DNA (Figure III.8), we hypothesize that E53K facilitates a conformation that both dimerizes and binds DNA more readily.

Given that the R116S and R116W variants display opposite phenotypes (enhanced and weakened self-interaction, respectively), R116 clearly has an important role in determining RefZ's dimerization state. The E179K substitution is located just proximal to α8, a helix that participates in hydrophobic interactions between RefZ subunits (Figure III.3B). The E179K substitution may cause a change in RefZ's overall conformation that enhances hydrophobic interactions between helices α8 and α8' of the RefZ subunits.

Four variants, R102S, E61K, E117D, and E117G, exhibited self-interaction comparable to wild type (Figure III.10B). Notably, even though the R102S and E117D substitutions support wild-type self-interaction and *RBM* binding (Figure III.8), they are not functional *in vivo* (Figure III.1C and Figure III.2B). These results suggest that R102 and E117 are perturbed in functions not revealed by the *ex vivo* assays. At the same time, since six of the 10 rLOF variants display either reduced or increased self-

interaction, these data suggest that the ability of RefZ to switch between monomer and dimer forms is likely important for the mechanism leading to FtsZ inhibition.

III.2.8 Thermostability of RefZ and the rLOF variants

To examine the effect of the rLOF substitutions on RefZ's thermostability, we performed differential scanning fluorimetry (DSF). Wild-type RefZ displayed a single transition melting curve (Figure III.12A, WT), with a melting temperature (T_m) of 39°C (Figure III.12B). With the exception of R116W, all of the variants displayed single transition melting curves (Figure III.13A). Most of the variants exhibited a lower T_m compared to wild type (L153R<R102C<R116S<R102S<WT) (Figure III.12B). Notably, L153R and R102C were the most destabilized (-5°C and -4°C, respectively) and also showed the weakest self-interaction in the B2H (Figure III.10B). Conversely, E53K was more thermostable than wild type and also displayed the most self-interaction by B2H (Figure III.10B). R116W also displayed reduced thermostability and self-interaction; however, unlike L153R and R102C, the R116W melting curve displayed two transitions (Figure III.12B, arrow), suggesting that the R116W variant assumes more than one conformation in solution. These results suggest that RefZ and the rLOF variants may assume multiple conformations in solution, and that RefZ's oligomerization state may be partly reflected in the thermostability measurements.

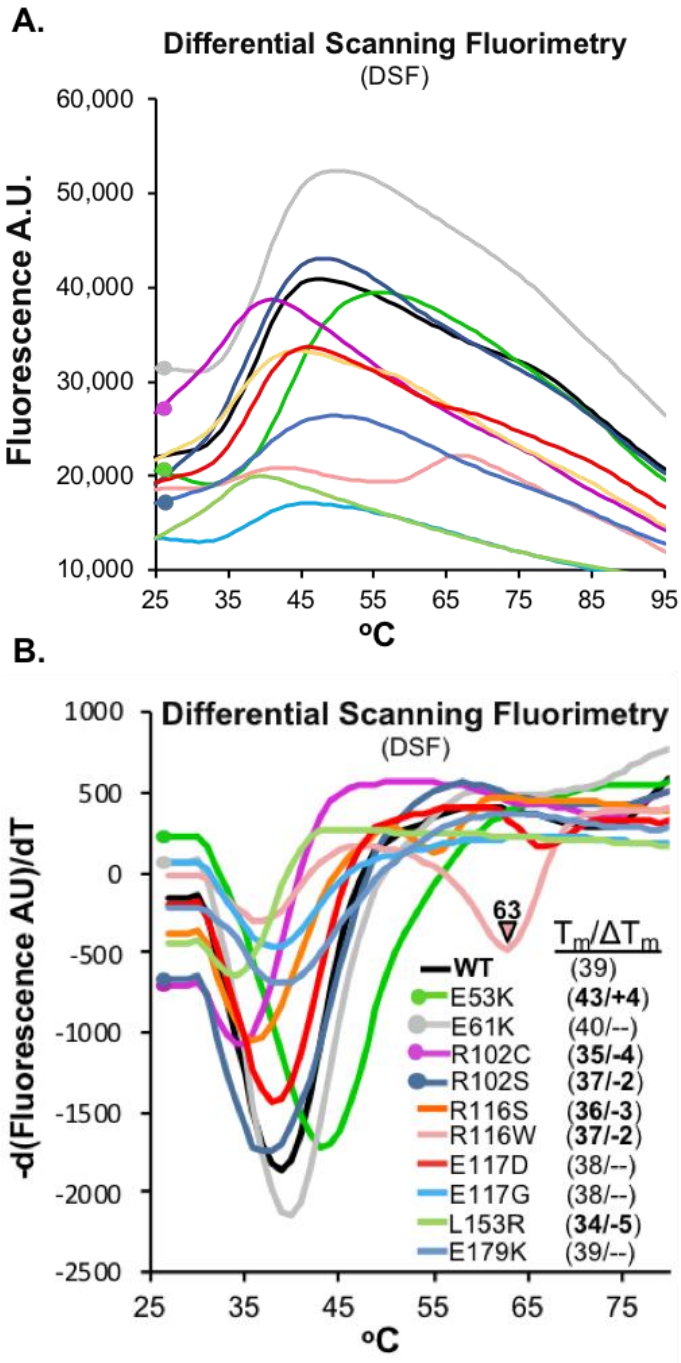

Figure III.12 Thermostability of RefZ and the rLOF variants.
Reprinted with permission from Brown *et al*., 2019. DSF estimates of wild-type RefZ-His6 and rLOF-His6 variant stability reported by fluorescence of SYPRO orange as a function of increasing temperature. **(A)** Representative sigmoidal melting curves. **(B)** DSF of wild-type RefZ-His6 and the rLOF-His6 variants. T_m values were calculated by determining the temperature at which the first derivative, d(Fluorescence AU)/dT, is at a minimum. ΔT_m (inset) is the difference in T_m values between wild-type RefZ and each rLOF variant. ΔT_m values of 1.5°C or less were not considered to be significant, and are shown as dashes.

III.3 DISCUSSION

RefZ is required for the timely redistribution of FtsZ from midcell to the pole (Wagner-Herman *et al.*, 2012). RefZ can also inhibit Z-ring assembly and filament cells when it is artificially induced during vegetative growth, an activity that requires DNA binding (Wagner-Herman *et al.*, 2012). Under its native regulation, RefZ is expressed early in sporulation and requires the *RBM*s to facilitate precise capture of the chromosome in the forespore (Miller *et al.*, 2016). Together, these results suggest that RefZ's effect on FtsZ, whether direct or indirect, is regulated by interactions with the nucleoid. Strikingly, the *RBM*s and their relative positions on the chromosome with respect to *oriC* are conserved across the entire *Bacillus* genus, indicating there is strong selective pressure to maintain the location of the *RBM*s. In *B. subtilis*, the *RBM*s are positioned in the cell near the site of polar septation. These observations, and the fact that RefZ, like SlmA (the NO protein of *E. coli*) belongs to the TetR family of DNA-binding proteins led us to hypothesize that RefZ binds to the *RBM*s to tune Z-ring positioning relative to the chromosome during sporulation.

To determine if RefZ's FtsZ-inhibitory activity was important for chromosome capture, we took advantage of RefZ's vegetative artificial expression phenotype (filamentation and cell killing in a sensitized background) to isolate 10 rLOF variants capable of binding DNA, but unable to inhibit FtsZ. All 10 of the rLOF variants were unable to support correct chromosome capture (Figure III.2B), consistent with a model in which RefZ-*RBM* complexes act through FtsZ to facilitate precise septum placement with respect to the chromosome during polar division. This model is also supported by

recent evidence showing that on average, Δ*refZ* mutants position Z-rings approximately 15% further away from the cell pole compared to wildtype (Barak & Muchova, 2018).

III.3.1 RefZ and SlmA do not inhibit FtsZ through a common mechanism

To better understand RefZ's mechanism of action at the molecular level, wild-type RefZ and the rLOF variants were overexpressed, purified, and analyzed using structural and biochemical approaches (summarized in Table III.3). The RefZ crystal structure revealed that RefZ is capable of forming a homodimer (Figure III.3), similar to other TetR proteins, including SlmA. The relative locations and nature of the loss-of-function substitutions in RefZ and SlmA are different (Figure III.5) suggesting that, if RefZ interacts with FtsZ directly, then RefZ's mechanism of action is distinct from that of SlmA. At least some mechanistic differences would be expected, as the C-terminal tails of FtsZ from *B. subtilis* and *E. coli* are distinct. More specifically, while the portion of *E. coli* FtsZ observed to interact with SlmA in the co-crystal is relatively conserved (DIPAFLR in *E. coli* and DIPTFLR in *B. subtilis*), the remainder of the C-termini differ significantly (KQAD in *E. coli* and NRNKRG in *B. subtilis*).

III.3.2 The role of self-interaction and *RBM*-binding in RefZ function

An important finding of this study is that both enhanced and reduced RefZ dimerization are correlated with loss-of-function phenotypes *in vivo*. B2H analysis indicates that the majority of rLOF variants (6/10) exhibited either stronger or weaker self-interaction (Figure III.10B), suggesting that RefZ's propensity to switch between a

monomer and dimer states is integral to affecting FtsZ function. Two rLOF variants (R102C and L153R) possess substitutions predicted to disrupt dimerization (Figure III.6), a result corroborated by B2H analysis (Figure III.10B). L153R also causes a 2-fold reduction in affinity for *RBM*-containing DNA, which could affect its ability to appropriately localize to *RBM*s *in vivo*.

Two rLOF variants (E53K and E61K) are located on α4. Based on the observation that E53K and E61K exhibit enhanced laddering and an increased apparent affinity for nonspecific DNA by EMSA (Figure III.8 and Figure III.9A), we propose that these variants assume a conformation that is more favorable for nonspecific DNA-binding than the conformation assumed by wild type. *In vivo*, enhanced nonspecific binding would reduce the formation of RefZ-*RBM* complexes, which prior data suggest is the functional form of RefZ (Miller *et al.*, 2016, Wagner-Herman *et al.*, 2012).

The ability of RefZ to generate DNA laddering in EMSAs (Figure III.8 and Figure III.9A) is presumably due to the association of additional RefZ subunits to adjacent DNA after the initial pair of dimers binds the *RBM* (Miller *et al.*, 2016). Other TetR proteins, including SlmA, have also been observed to "spread" on DNA *in vitro* (Engohang-Ndong *et al.*, 2004, Shiu-Hin Chan *et al.*, 2017, Tonthat *et al.*, 2013). In the case of SlmA, spreading on DNA is hypothesized to facilitate interaction with the exposed C-terminal tails of FtsZ to promote filament breakage (Tonthat *et al.*, 2013). Although genetic and cell biological data suggest RefZ and FtsZ interact (Barak & Muchova, 2018, Miller *et al.*, 2016, Wagner-Herman *et al.*, 2012), evidence for direct interaction between RefZ and FtsZ is lacking. We were unable to detect a positive

interaction between FtsZ and RefZ *in vivo* by bacterial 2-hybrid analysis (Figure III.13), and our attempts to test for RefZ-FtsZ interaction *in vitro* have been impeded by RefZ's limited solubility outside of the specific conditions identified in this study. Therefore, the precise mechanism by which RefZ affects FtsZ remains to be determined.

One of the most interesting observations obtained from characterizing the rLOF variants is that the R116S and R116W substitutions on the first turn of α7 result in opposite self-interaction phenotypes (Figure III.10B). Both variants behave comparably with regard to affinity and specificity for the *RBM*-containing DNA (Figure III.8), suggesting the loss-of-function phenotypes are not attributable to differences in DNA interaction or protein misfolding. Instead, these results suggest that R116 is a key residue in determining the stability of the RefZ dimer.

We hypothesize that R116 participates in intramolecular bonds with residues within a flexible loop region (between α6 and α7, residues 109-114) (Figure III.3A), possibly contributing to the formation of a more stable homodimer. R116 could participate in formation of either ionic or hydrogen bonds with an invariant aspartate residue (D111) located in the flexible loop. Our ability to assess R116's role in intramolecular bond formation is limited in the current crystal structure, as the electron density for the R116 side-chain is not well defined. Moreover, the electron density for the main chain of the flexible loop is moderately disordered, showing peaks of positive Fo-Fc electron density next to the I110 and D111 side-chains.

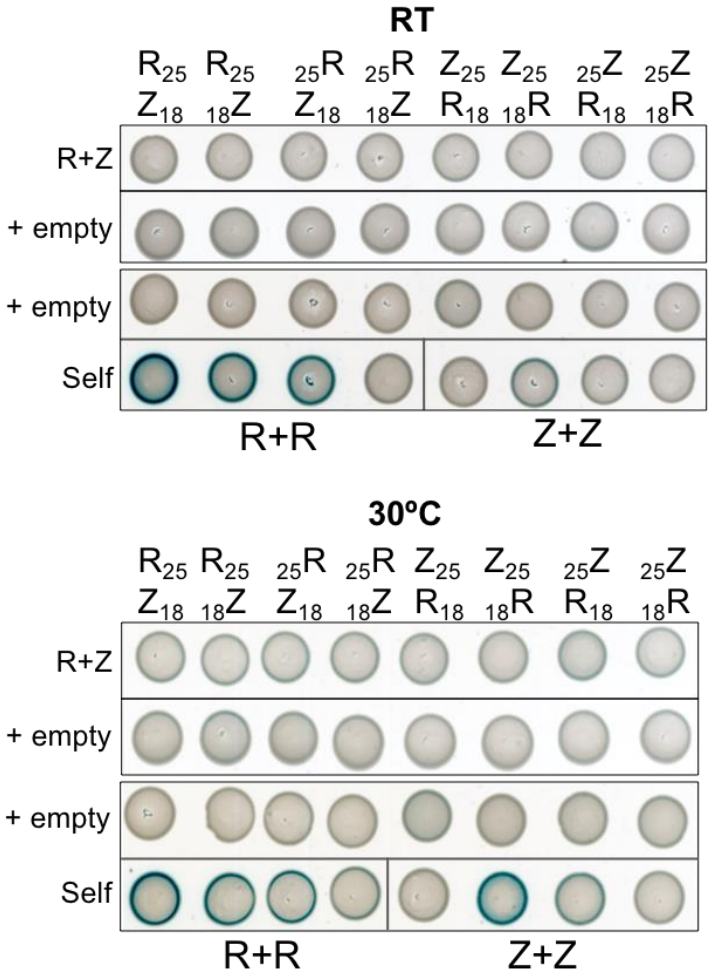

Figure III.13 Bacterial two-hybrid assay for pairwise interaction between RefZ and FtsZ.
Reprinted with permission from Brown *et al.*, 2019. *E. coli* DHP1 (*cya*-) co-transformants containing plasmids harboring N-terminal or C-terminal fusions of RefZ and FtsZ to T25 and T18 tags were grown in Lysogeny broth at 37°C in the presence of 25 µg ml^{-1} kanamycin, 50 µg ml^{-1} ampicillin, and 0.1% glucose as described in Experimental methods. Cultures were normalized to the lowest OD_{600} reading and 8 µl were spotted on M9 glucose minimal plates supplemented with 25 µg ml^{-1} kanamycin, 50 µg ml^{-1} ampicillin, and 40 µg ml^{-1} X-gal and grown for 40-50 h at room temperature (top) or at 30°C (bottom) until a similar degree of color change was observed for the RefZ self and FtsZ self-interaction controls.

R116 is also immediately adjacent to E117, another critical residue identified in this study. E117D is the only rLOF variant that is loss of function with regard to inhibiting cell division and capturing the forespore chromosome, yet is not detectably altered in the other RefZ properties implicated in function (Table III.3). If RefZ targets FtsZ directly, then these data point toward E117 as a likely candidate residue for mediating interaction. The E117D substitution is intriguing because the glutamate to aspartate change is highly conservative; however, if the interaction is direct, the shorter sidechain of the aspartate could compromise RefZ's ability to target FtsZ.

	EMSA laddering	*RBM* specificity	K_d	Self-interaction	ΔT_m (°C)
WT	++	+++	++	++	--
E53K	++++	+	++	++++	+4
E61K	++++	+	++	++	--
R102C	+	+++	++	+	-4
R102S	+	+++	++	++	-2
R116S	++	+++	++	+++	-3
R116W	++	+++	+	-	-2
E117D	++	+++	++	++	--
E117G	+++	++	+++	++	--
L153R	-	+++	+	-	-5
E179K	++	+++	++	+++	--

Table III.3 Summary of rLOF phenotypes.
Reprinted with permission from Brown *et al*., 2019.

III.3.3 Working model for RefZ-mediated septum positioning

Based on the data available, we propose a model in which RefZ mediates chromosome capture by fine-tuning the position of FtsZ assembly over the forespore-destined chromosome. In our model, RefZ is primed to inhibit FtsZ polymerization near the pole by binding specifically to the polarly-localized *RBM*s. Based on structural studies of other TetR family proteins and the observation that RefZ binds to *RBM*s in units of two and four *in vitro* (Miller *et al.*, 2016, Wagner-Herman *et al.*, 2012), RefZ likely binds each *RBM* as a pair of dimers. We were not able to report RefZ copy number as native RefZ levels are too close to the detection limit of our antibodies; however, our preliminary data suggest that RefZ is likely a relatively low copy number protein.

Current data suggest the activity of RefZ inhibits rather than promotes FtsZ assembly (Barak & Muchova, 2018, Miller *et al.*, 2016, Wagner-Herman *et al.*, 2012). This raises the question as to how an inhibitor of FtsZ could act near the pole to promote precise placement of a polar division apparatus. In our model, RefZ is a locally-acting inhibitor of FtsZ and its primary function is not to inhibit the formation of polar Z-rings altogether, but rather to tune the location of Z-ring assembly away from the immediate vicinity of the *RBM*s. Based on comparative analysis of the rLOF mutants, both decreased and increased ability to dimerize appears to be detrimental to the inhibitory function of RefZ. This implies that a dynamic process of monomer-dimer exchange, not maintaining a specific oligomeric state, is what is important for RefZ function. One

possibility is that *RBM*-bound dimers disassociate from DNA as monomers after engaging with FtsZ.

We present no evidence that RefZ's DNA association or monomer-dimer exchange is influenced by a ligand, and no obvious ligand binding pocket is observed in the regulatory domain of the solved crystal structure. At the same time, we do not exclude the possibility that RefZ activity could be regulated through interaction with FtsZ or ligand binding. Recently EthR, an important TetR family protein from *Mycobacterium tuberculosis* that regulates drug resistance, was shown to bind the nucleotide cyclic-di-GMP (Zhang *et al.*, 2017). Interestingly, EthR's proposed nucleotide binding region (based on mutagenesis and docking studies) is at the dimer interface, outside the canonical ligand binding pocket (Zhang *et al.*, 2017) (near R102 in RefZ).

Another paradox raised is why a Δ*refZ* mutant exhibits a slight delay in shifting Z-rings from midcell to the pole during sporulation (Wagner-Herman *et al.*, 2012). If RefZ acts as an inhibitor at the pole, then assembly of the polar Z-ring would be expected to accelerate in a Δ*refZ* mutant. This seeming contradiction may be explained by considering RefZ's localization during sporulation. At early timepoints, just before polar division occurs, RefZ-GFP localizes as foci near the poles. These foci likely represent RefZ-*RBM* complexes, as they are lost in a RefZ mutant that cannot bind DNA (Y43A) (Wagner-Herman *et al.*, 2012). Around the time polar division initiates, the polar RefZ foci become less apparent and RefZ is observed to coalesce near midcell at or near the membrane (Wagner-Herman *et al.*, 2012). The redistribution of RefZ's

inhibitory activity from the pole to midcell as sporulation progresses could facilitate disassembly of the midcell Z-ring and its reassembly at the pole (Ben-Yehuda & Losick, 2002, Khvorova *et al.*, 1998). Preliminary data also suggest that RefZ has a second role, to prevent additional midcell divisions as sporulation progresses (Miller and Herman, unpublished), and current investigations are aimed at exploring this possibility.

III.4 MATERIALS AND METHODS

III.4.1 General methods

Strains, plasmids, and oligonucleotides are listed in APPENDIX B, Tables B.1, B.2, and B.3, respectively. All *Bacillus subtilis* strains were derived from *B. subtilis* 168 or PY79. Strain and plasmid construction is detailed in the Supplementary text. Transformations in *B. subtilis* were carried out using a standard protocol as previously described (Harwood & Cutting, 1990) unless otherwise stated. For selection in *B. subtilis*, antibiotics were included at the following concentrations: 100 μg ml^{-1} spectinomycin, 7.5 μg ml^{-1} chloramphenicol, 10 μg ml^{-1} kanamycin, 10 μg ml^{-1} tetracycline, 0.8 μg ml^{-1} phleomycin, and 1 μg ml^{-1} erythromycin (erm) plus 25 μg ml^{-1} lincomycin (MLS). For transformation and selection in *E. coli*, antibiotics were included at the following concentrations: 100 μg ml^{-1} ampicillin, 25 μg ml^{-1} kanamycin, and 25 μg ml^{-1} chloramphenicol (for protein overexpression). Co-transformations for B2H assays were selected for on LB plates supplemented with 50 μg ml^{-1} ampicillin, 25 μg ml^{-1} kanamycin, and 0.2% (v/v) glucose.

III.4.2 Two-step genetic selection-screen to isolate *rLOF* mutants

Comprehensive details on construction of the Gibson assemblies and strains below are available in the supplemental text. The *refZ* gene was mutagenized by error-prone PCR and the mutant fragment library was introduced into an IPTG-inducible artificial expression construct using Gibson assembly (Gibson *et al.*, 2009). Multiple assembly reactions were pooled on ice and directly transformed into super-competent BAM168 cells (selection-screen background). For transformations, competent cell aliquots were thawed at room temperature and 0.2 ml were incubated in a 13 mm glass test tube with 20 µl assembly reactions for 90 min in a rollerdrum at 37°C before selecting on LB plates supplemented 100 µg ml^{-1} spectinomycin and 1 mM IPTG. After overnight growth at 37°C, surviving transformants were patched on LB plates supplemented with 1% (w/v) starch to screen for integration at *amyE*, and on LB plates supplemented with the following antibiotics to assess the presence of the expected parental background resistances: 7.5 µg ml-1 chloramphenicol, 10 µg ml-1 kanamycin, 10 µg ml-1 tetracycline, and 1 µg ml-1 erythromycin (erm) plus 25 µg ml-1 lincomycin (MLS). Transformants were also patched on LB plates supplemented with 100 µg ml^{-1} spectinomycin and 1 mM IPTG and 40 µg ml^{-1} X-gal to screen for *lacZ* expression from the P_{spremo} promoter. Replica plates were grown overnight at 37°C. Surviving *rLOF* mutants that did not turn blue on patch plates were cultured from replica plate in liquid LB and stored at -80°C. Genomic DNA prepared from these strains was PCR amplified with OJH001 and OJH002 to test for the presence of the expected integration product. PCR products of the expected size were sequenced to identify mutations.

III.4.3 Generation of super-competent cells

Super-competency was achieved using two-fold approach to maximize transformation efficiency. First, BAM168 (selection-screen background) harbors a xylose-inducible copy of *comK* at the non-essential *lacA* locus (Zhang & Zhang, 2011). The presence of 1% (w/v) xylose in standard transformation cultures improved efficiency ~2.5-fold compared to cultures grown without xylose. Second, competent cells were prepared by modifying an established (Harwood & Cutting, 1990) two-step *B. subtilis* competent cell protocol as described below. The modifications improved transformation efficiency an additional 7-fold over xylose induction alone. A single colony of freshly streaked recipient cells (BAM168) was used to inoculate a 250 ml baffled flask containing 25 ml of 1X MC medium (10.7 g L^{-1} K_2HPO_4, 5.2 g L^{-1} KH_2PO_4, 20 g L^{-1} glucose, 0.88 g L^{-1} tri-sodium citrate dihydrate, 0.022 g L^{-1} ferric ammonium citrate, 1 g L^{-1} casein hydrolysate (Neogen), 2.2 g L^{-1} potassium glutamate monohydrate, 3 mM $MgSO_4$, and 0.02 g L^{-1} L-Tryptophan) (Harwood & Cutting, 1990). The culture was grown overnight (20-22 h) in a 37°C shaking waterbath set at 250 rpm. The overnight culture (OD_{600} 1.5-2.5) was diluted to an OD_{600} of 0.1 in a 250 ml baffled flask containing 40 ml of 1X MC supplemented with 1% (w/v) xylose. The culture was incubated at 37°C in a shaking waterbath set at 200 rpm. After 5-6 h of growth, the OD_{600} was monitored every 30 min until readings remained unchanged between two timepoints, at which point the culture was diluted 1:10 with pre-warmed 1X MC supplemented with 1% (w/v) xylose to a final volume of 250 ml in a 2 L flask. After 90 min of growth at 37°C and 280 rpm, cells were harvested at

room temperature at 1,260 x *g* for 10 min in six 50 ml conical tubes. Twenty ml of the culture supernatant was retained and mixed with 5 ml 50% (v/v) glycerol. The diluted supernatant was used to gently resuspend the pellets, and the cell suspensions were immediately frozen at -80°C in aliquots.

III.4.4 Blue-white screen to assess RBM-binding by rLOF mutants

Artificial expression constructs harboring either wild-type *refZ* (BAM374), *rLOF* mutants (BAM400, 403, 407, 409, 411, 440, 443, 444, 449, 462), or an empty P_{hy} vector (BAM390) in clean selection-screen backgrounds Chapter III.5.1, Strain Construction were streaked from frozen glycerol stocks on LB plates supplemented with 100 µg ml^{-1} spectinomycin and 0.2% (v/v) glucose and grown overnight at 37°C. Single colonies were used to inoculate 3 ml of Lysogeny Broth (LB-Lennox) and cultures were grown in a rollerdrum at 30°C until early to mid-log (3-5 h). Cultures were normalized to the lowest OD_{600} with PBS (10^0) and serially diluted (10^{-1}, 10^{-2},10^{-3}). Five µl of each dilution was spotted on LB plates supplemented with 100 µg ml^{-1} spectinomycin and 1 mM IPTG and 40 µg ml^{-1} X-gal followed by overnight incubation at 37°C to visually screen for *lacZ* expression from the P_{spremo} promoter. Plates were scanned with a ScanJet G4050 flatbed scanner (Hewlett Packard) using VueScan software and medium format mode. Images were processed using Adobe Photoshop (version 12.0).

III.4.5 rLOF dominance growth assay

A wild-type copy of *refZ* under an IPTG-inducible P_{hy} promoter was introduced at the ectopic *yhdG* locus of each of the IPTG-inducible variant strains listed in *Blue-white screen to assess RBM-binding by rLOF mutants* as described in Chapter III.5.1, Strain Construction. As controls, an empty P_{hy} vector was introduced at the *yhdG* locus of the wild-type *amyE::*P_{hy}*-refZ* (BAM374) and the *amyE::*P_{hy}-empty vector (BAM390) strains. The resulting strains, BAM1662-1676, were streaked from frozen glycerol stocks on LB plates supplemented with 0.8 µg ml^{-1} phleomycin and 0.2% (v/v) glucose and grown overnight at 30°C. Single colonies were used to inoculate 3 ml of Lysogeny Broth (LB-Lennox) and cultures were grown in a rollerdrum at 30°C until early to mid-log (3-5 h). Cultures were normalized to the lowest OD_{600} with PBS (10^0) and serially diluted (10^{-1}, 10^{-2}, 10^{-3}). Five µl of each dilution was spotted on LB plates supplemented with 0.8 µg ml^{-1} phleomycin and 1 mM IPTG, followed by overnight incubation at 37°C to visually screen for wild-type RefZ toxicity in the presence of absence of the rLOF variants. Plates were scanned with a ScanJet G4050 flatbed scanner (Hewlett Packard) using VueScan software and medium format mode. Images were processed using Adobe Photoshop (version 12.0).

III.4.6 Artificial expression of wild-type refZ and rLOF variants

Artificial expression constructs harboring either wild-type *refZ* (BJH228) or the *rLOF* mutants (BAM428, 431, 434, 436, 450, 451, 454, 455, 457, 490) in a wild-type background (Chapter III.5.1, Strain Construction) were streaked from frozen glycerol

stocks on 100 µg ml^{-1} spectinomycin plates and grown overnight at 37°C. CH cultures (25 ml) were prepared as described under *Fluorescence microscopy*. Expression was induced with 1 mM IPTG following 1.5-2 h of growth at 37°C (approx. OD_{600} 0.10). For the uninduced controls in Figure III.1C and III.1D, an independent culture of the control strain, BJH228 (P_{hy}-*refZ*), was grown in parallel but was not induced. Growth was resumed at 37°C with shaking for 45 min (see *Western blotting*) or 90 min (see *Fluorescence microscopy*) before 1 ml samples were harvested.

III.4.7 Fluorescence microscopy

For microscopy experiments, isolated colonies were used to inoculate 5 ml CH and cultures were grown overnight at room temperature in a rollerdrum. Cultures below an OD_{600} of 0.7 were used to inoculate 25 ml CH medium in 250 ml baffled flasks to a calculated OD_{600} of 0.006 (for artificial expression) or 0.018 (for chromosome capture assays) and cultures were grown for the indicated time at 37°C in a shaking waterbath set at 280 rpm. Samples were collected at 6,010 x *g* for 1 min in a tabletop microcentrifuge. Following aspiration of supernatants, pellets were resuspended in 3-5 µL of 1X PBS containing 0.02 mM 1-(4-(trimethylamino)phenyl)-6-phenylhexa-1,3,5-triene (TMA-DPH)(Life Technologies) and cells were mounted on glass slides with polylysine-treated coverslips. Images were captured and analyzed with NIS Elements Advanced Research (version 4.10) software, using 600 ms (CFP), 900 ms (YFP), or 1 s (TMA) exposure times on a Nikon Ti-E microscope equipped with a CFI Plan Apo lambda DM 100X objective, a Prior Scientific Lumen 200 Illumination system, C-FL

UV-2E/C DAPI, C-FL YFP HC HISN Zero Shift, and C-FL Cyan GFP filter cubes, and a CoolSNAP HQ2 monochrome camera.

III.4.8 Western blotting

Samples were harvested at 21,130 x *g* for 1 min in a tabletop centrifuge. Pellets were washed with 50 µl of 1X PBS and the remaining supernatant was carefully removed using a P20 pipet. Pellets were frozen at -80°C until processing. Frozen pellets were thawed on ice before resuspension in 25 µl of lysis buffer (20 mM Tris [pH 7.5], 10 mM EDTA, 1 mg ml^{-1} lysozyme, 10 µg ml^{-1} DNase I, 100 µg ml^{-1} RNase A, and 1 mM phenylmethylsulfonyl fluoride). Samples were normalized by OD_{600} values obtained at the time of harvest by diluting resuspensions in additional lysis buffer before incubating at 37ºC for 15 min. Samples were diluted 1:1 with 2X sample buffer (250 mM Tris [pH 6.8], 10 mM EDTA, 4% (v/v) SDS, 20% (v/v) glycerol, and 10% (v/v) 2-mercaptoethanol) and boiled for 10 min. Five µl of each lysate was loaded on a 4-20% gradient polyacrylamide gel (Lonza) and proteins were separated by electrophoresis prior to transfer to a nitrocellulose membrane (Pall)(1 h at 60 V). Membranes were blocked for 1 h at room temperature in 5% (w/v) nonfat milk in PBS [pH 7.4] with 0.05% (v/v) Tween-20. Membranes were incubated overnight at 4ºC with polyclonal rabbit anti-RefZ antibody (Covance) diluted 1:1,000 in 5% (w/v) nonfat milk in PBS [pH 7.4] with 0.05% (v/v) Tween-20. Membranes were washed prior to a 1 h room temperature incubation with horseradish peroxidase-conjugated goat anti-rabbit Immunoglobulin G secondary antibody (Bio-Rad) diluted 1:10,000 in 5% (w/v) nonfat

milk in PBS [pH 7.4] with 0.05% (v/v) Tween-20. Washed membranes were incubated with SuperSignal West Femto Maximum Sensitivity substrate (Thermo Scientific) according to the manufacturer's instructions. Chemiluminescence was detected and imaged using an Amersham Imager 600 (GE Healthcare). Images were processed using ImageJ64(Schneider *et al.*, 2012).

III.4.9 Chromosome capture assay with the *rLOF* mutants

Strains used in the chromosome capture assay in Figure III.2B harboring the left arm (-61° P_{spoIIQ}-*cfp*) or right arm (+51° P_{spoIIQ}-*cfp*) reporter in the wild type, *refZ* mutant, or *rLOF* mutant trapping backgrounds (Chapter III.5.1, Strain Construction) were streaked from frozen stocks on LB agar plates and grown overnight at 37°C. Chromosome capture assays were carried out as previously described (Miller *et al.*, 2016, Sullivan *et al.*, 2009). CH cultures (25 ml) were prepared as described in *Fluorescence microscopy* and grown for 2.5-3 h (OD_{600} 0.6-0.8) before sporulation was induced by resuspension according to the Sterlini-Mandelstam method (Harwood & Cutting, 1990). Growth was resumed at 37°C in a shaking waterbath for 2.5 h prior to TMA-DPH, YFP, and CFP image acquisition (see *Fluorescence microscopy*).
Each strain harbors a σ^F-dependent *oriC*-proximal reporter (-7° P_{spoIIQ}-*yfp*) that is captured in the forespore in 99.5% of sporulating cells. Cells expressing YFP serve as the baseline for total sporulating cells counted in the field. To visualize cells in a given field that expressed the left or right arm reporters in the forespore, captured YFP and CFP images were individually merged with the TMA (membrane) image. The total

number of forespores with YFP signal (total YFP) or CFP signal (total CFP) were manually marked and counted as described previously (Miller *et al.*, 2016).
For quantitation and statistical analysis, a minimum of 1,500 cells per strain were counted from three independent biological and experimental replicates, with the exception of wildtype (left and right arms, n=7) and the E53K (right arm, n=4). The average proportion of cells expressing both reporters for each strain is given in Figure 2, with error bars representing one standard deviation above and below the average. Two-tailed Student's t-tests were performed to determine the P-values indicated in the pairwise comparisons.

III.4.10 Protein Purification

E. coli BL21(DE3) pLysS competent cells were transformed with either pLM025a (RefZ-His6) or pEB013-pEB022 (rLOF-His6) and grown overnight at 37°C on LB plates supplemented with 25 µg ml^{-1} kanamycin, 25 µg ml^{-1} chloramphenicol and 0.1% (v/v) glucose. Transformants were scraped from plates and resuspended in 2 ml of ProGroCinnabar High-Yield protein expression media (Expression Technologies) containing 25 µg ml^{-1} kanamycin, 25 µg ml^{-1} chloramphenicol and 0.1% (v/v) glucose. The OD_{600} was measured and used to inoculate 4 x 25 ml of the same medium in 250 ml baffled flasks to an OD_{600} of 0.1. Cultures were grown at 37°C in a shaking waterbath at 280 rpm for 6-7 h until the culture density reached OD_{600} = 5.0. Protein expression was induced with 1 mM IPTG and growth was resumed for an additional 3 h before cultures were harvested by centrifugation at 9,639 x *g* for 5 min at 4°C. Pellets were stored at -

80°C until processing. Four pellets (25 ml culture each) were resuspended in 40 ml of lysis Buffer (50 mM Tris-HCl [pH 9.0], 300 mM KCl, 10% (v/v) glycerol, and 10 mM imidazole). 1 µl protease inhibitor (Sigma-Aldrich, Cat No. P8465) (215 mg powder dissolved in 1 ml of DMSO and 4 ml ddH_20) was added per 35 OD_{600} units. DNase I was added to a final concentration of 1 µg ml^{-1} of cell suspension. Suspensions were passed through a Microfluidizer LM20-30 five times at 10,000 psi. Cell debris was cleared by centrifugation at 22,662 x *g* for 30 min at 4°C. Supernatants were passed over a 1 ml bed volume of Nickel-NTA agarose beads (Qiagen, Cat No. 30210) pre-equilibrated with lysis buffer. Bound protein was washed with 10 ml of wash buffer (50 mM Tris-HCl [pH 9.0], 300 mM KCl, 10% (v/v) glycerol, and 20 mM imidazole). Protein was eluted with 7 ml of elution buffer (50 mM Tris-HCl [pH 9.0], 300 mM KCl, 10% (v/v) glycerol, and 250 mM imidazole) and collected as ~250 µl fractions. 2 µl was removed from each fraction for SDS-PAGE analysis, and elutions were immediately stored at -80°C. Peak elution fractions were thawed and pooled before dialyzing at 4°C with stirring into either elution buffer (50 mM Tris-HCl [pH 9.0], 300 mM KCl, 10% (v/v) glycerol, and 250 mM imidazole) or ddH_2O using Slide-A-Lyzer® 7.0 kDa MWCO dialysis cassettes (Thermofisher) Scientific). Final protein concentrations were determined using Bradford reagent (Bio-Rad) and a BSA standard.

III.4.11 Protein crystallization, data collection, and data analysis

RefZ-His6 was overexpressed and purified as described above. Before dialysis the RefZ concentration was determined and dsDNA (generated by annealing

OEB025/OEB026) was added to a 4:1 molar ratio of RefZ:$RBM_{L2\text{-}24bp}$. The protein was dialyzed into 50 mM Tris-HCl [pH 8.5] and 300 mM KCl. After dialysis, RefZ was concentrated in a 10 kDa Vivaspin Turbo MWCO filter (Sartorius) to ~5 mg ml^{-1}, and 0.5-1.0 µl of the concentrated protein was used to set crystallization plates. RefZ crystals formed within 48 h by hanging drop vapor diffusion at 16ºC after mixing the protein in a 1:1 volume ratio with 10% ethanol (v/v), 0.1 M imidazole [pH 8.0], and 0.2 M $MgCl_2$. The crystals were cryoprotected in 20% (v/v) glycerol in mother liquor before flash freezing in liquid nitrogen. For anomalous signal, RefZ crystals were soaked with 1 mM lead acetate for 5 h and the data were collected at the Argonne National Lab APS synchrotron, beamlines 23-ID, at 0.9496 Å. Diffraction data were indexed, integrated, and scaled in HKL2000 (Otwinowski & Minor, 1997) and the single heavy atom site was identified by phasing using single anomalous dispersion (SAD) in the SHELX program (Sheldrick, 2008). The resultant phases were extended to a native crystal data set collected at the same beamline at 0.98 Å. The native set was indexed, integrated, and scaled using PROTEUM3 software (Version 2016.2, Bruker AXS Inc). The native crystal data were truncated in Ctruncate (Zwart, 2005) from CCP4 suite (Winn *et al.*, 2011) and subjected to iterative building and phase improvement by PHENIX (Adams *et al.*, 2010). The partial model produced by PHENIX was rebuilt in BUCCANEER (Cowtan, 2006) relying on improved phases. BUCCANEER was able to build the whole model in one continuous chain, docked in sequence and covering residues 1-200. The model was improved through iterative runs of inspection and manual modification in COOT (Emsley *et al.*, 2010) and refinement in PHENIX (Adams

et al., 2010) with simulated annealing on initial runs. The data collection and refinement statistics can be found in Table III.2. The coordinates and structure factors for RefZ have been deposited in the Protein Data Bank (PDB: 6MJ1).

III.4.12 Annealing of oligos to generate dsDNA

Oligonucleotides were resuspended in annealing buffer (10 mM Tris-HCl [pH 7.5], 50 mM NaCl, and 1 mM EDTA) to a concentration of 1 mM. Equal volumes were mixed and annealed in a thermocycler by heating to 95°C for 2 min followed by ramp cooling for 45 min to 25°C. The annealing buffer was removed by dialysis into ddH_2O with Slide-A-Lyzer® 7.0 kDa MWCO Dialysis Cassettes (Thermo Scientific).

III.4.13 Electrophoretic gel mobility shift assays

DNA fragments centered on either the native (using *B. subtilis* 168 as template) or the mutant (using BJH205 as template) RBM_{L1} sequence (Miller *et al.*, 2016) were generated by PCR using primer pair OEB009 and OEB010. Purified RefZ-His6 or rLOF-His6 protein (final concentrations indicated in Figure III.8) were incubated with 10 nM RBM_{L1} or RBM_{L1mu} DNA probes in binding buffer (150 mM KCl and 10 mM Tris-HCl [pH 8.0]) for 30 min. After 30 min incubation, 10X loading buffer (50 mM EDTA [pH 8.0], 1 mM Tris-HCl [pH 8.0] and 45% (v/v) glycerol) was added to a final concentration of 1X and binding reactions were resolved at room temperature on a 5% TBE polyacrylamide gel run for 45 min at 150 V (Figure 6) or a 7.5% TBE polyacrylamide gel for 17 min at 200 V (Figure III.9A and B). After electrophoresis,

gels were incubated with agitation in 1X SYBR Green EMSA gel stain (Life Technologies) (diluted from 10,000X stock in TBE buffer) for 5 min then rinsed with dH_2O. Stained DNA was imaged with a Typhoon FLA 9500 scanner using the setting for Fluorescence and LPB (510LP) filter for SYBR Green. The data presented in Figure III.8 is representative of a minimum of three independent experimental replicates for wild type and each variant.

III.4.14 Bio-layer Interferometry Assay

The Octet system (Pall Forte Bio) was used to monitor the kinetic interactions between wild-type RefZ or the rLOF variants and *RBM*-containing DNA. Streptavidin biosensors (Part NO 18-5019) were purchased from Pall Forte Bio. A 41 bp *RBM*-containing (RBM_{L1}) segment of dsDNA was generated by annealing 5' biotinylated OEB091 with OEB092 as described (see *Annealing of oligos to generate dsDNA*) except that the annealing buffer was not removed by dialysis. All subsequent assays were performed in DNA binding buffer (150 mM KCl and 10 mM Tris-HCl [pH 8.0]). Sensors were pre-equilibrated for 10 min at room temperature in DNA-binding buffer to establish a baseline reading. Sensors were then dipped into a well containing 50 nM RBM_{L1} dsDNA and incubated for 2 min with shaking at 1,000 rpm to immobilize DNA on the biosensor. The sensor was washed for 30 s to establish a new baseline before transfer to a solution containing 800 nM of wild-type RefZ or rLOF variants. Following a 3 min monitored association, the complex was placed into fresh buffer and dissociation was monitored continuously for 15 min. The K_d was calculated using the global fit in

Pall Forte Bio's analysis software. Three experimental replicates of each assay were performed except for variant R102C (n=4). The mean values and standard deviations are given in Figure III.8. P-values were determined using a two-tailed unpaired Student's t-test.

III.4.15 Size-exclusion chromatography

A Superdex 200 PC 3.2/30 3.2 × 300 mm column was equilibrated with 50 mM Tris-HCl [pH 9.0], 300 mM KCl, and 10% (v/v) Glycerol. Wild-type RefZ and rLOF proteins from frozen stocks (ddH_2O) were diluted to a final concentration of 1 mg ml^{-1} in 200 µl of buffer (50 mM Tris-HCl [pH 9.0], 300 mM KCl, 10% (v/v) Glycerol). Samples were pre-spun at 21,130 x *g* for 10 min at 4°C in a tabletop centrifuge prior to injection. The absorbance at 280 nm was continuously measured and the V_e, peak maximum, was taken from the resulting elution profile and used to calculate K_{av} using the formula $(V_e - V_o)/(V_t - V_o)$. The void volume, V_o was experimentally determined to be 7 ml. The total volume, V_t, of the column was 24 ml. The apparent molecular mass was estimated using a curve generated from an identical run with a molecular mass standard (Bio-Rad Gel filtration chromatography standard, cat. no. 151-1901).

III.4.16 Bacterial 2-hybrid analysis

Assays were carried out essentially as previously described (Karimova *et al.*, 1998). Plasmids harboring wild-type *refZ* and the rLOF sequences fused with C-terminal T18 and T25 tags (Chapter III.5.1, Plasmid Construction) were co-transformed

into competent *E.coli* DHP1 (*cya*-) cells with selection on LB plates supplemented with 50 µg ml^{-1} ampicillin, 25 µg ml^{-1} kanamycin, and 0.2% (v/v) glucose. Co-transformed *E.coli* strains were streaked from frozen stocks and single colonies were cultured in 4 ml of LB supplemented with 50 µg ml^{-1} ampicillin, 25 µg ml^{-1} kanamycin, and 0.1% (v/v) glucose in a 37ºC roller drum to mid-log growth phase. Culture samples were normalized to the lowest OD culture with fresh LB supplemented with 50 µg ml^{-1} ampicillin and 25 µg ml^{-1} kanamycin, and 5 µl were spotted on M9-glucose minimal plates supplemented with 50 µg ml^{-1} ampicillin, 25 µg ml^{-1} kanamycin, 250 µM IPTG, and 40 µg ml^{-1} X-gal. Pairwise interactions between the T18 and T25 fusions were assessed by monitoring the development of blue color (corresponding to *lacZ* expression) following 40-50 h of growth at room temperature.

Interaction between FtsZ and RefZ was assayed for as described above (Figure III.13). Spot plates were grown at both room temperature as described as well as 30ºC until positive RefZ and FtsZ self-interaction controls exhibited a color change distinct from the corresponding negative controls. Growth at either temperature did not produce a detectable positive interaction between RefZ and FtsZ.

III.4.17 Differential Scanning Fluorimetry (DSF)

Purified RefZ or rLOF variants from frozen stocks (50 mM Tris-HCl [pH 9.0], 300 mM KCl, 10% (v/v) glycerol, and 250 mM imidazole) were thawed and diluted in 20 mM Tris-HCl [pH 7.5] to a final concentration of 10 µM. To ensure an identical final concentration of storage buffer for all rLOF variants, reactions were normalized to the

maximum required concentration of storage buffer determined by the lowest rLOF variant concentration; the final buffer concentration was 0.16X. All reactions contained 5X SYPRO™ Orange Protein Gel Stain (Thermofisher) diluted to a working concentration in DMSO. The DSF assays were performed in a 96-well hardshell PCR plate (Bio-Rad, HSP9601) using a CFX96 Touch™ Real-Time PCR Detection System (Bio-Rad). The reactions were ramped from 25°C to 95°C at a rate of 1°C min^{-1}.

CHAPTER IV

REFZ-*RBM* COMPLEXES ACT IN CONJUNCTION WITH THE NUCLEOID OCCLUSION PROTEIN NOC TO PREVENT ABERRANT SEPTATION DURING *BACILLUS SUBTILIS* SPORULATION

IV.1 INTRODUCTION

In order to survive during periods of starvation, the rod-shaped bacterium *Bacillus subtilis* can differentiate into a metabolically dormant and highly resistant cell type called an endospore (Hilbert & Piggot, 2004). *B. subtilis* are considered polar spore formers, meaning they shift the site of cell division from midcell to an asymmetric position near one pole at the onset of sporulation (Khvorova *et al.*, 1998, Levin & Losick, 1996). In vegetative (non-sporulating) cells, division occurs at midcell, between replicated chromosomes, and produces two genetically and morphologically identical daughter cells that initially share a cell wall, which becomes degraded during cell separation.

In contrast, the asymmetric division that occurs during sporulation produces two unequal sized compartments, a smaller forespore and larger mother cell, that do not become separated (Piggot & Coote, 1976). Instead, following division a thin layer of peptidoglycan (PG) is present in the septal wall which must be partially degraded by sporulation-specific hydrolases during the process of engulfment (Gutierrez *et al.*, 2010, Ojkic *et al.*, 2016, Perez *et al.*, 2000, Tocheva *et al.*, 2013), when the mother cell

membrane migrates around the forespore to produce a double membrane-bound precursor that eventually develops into the mature spore (Hilbert & Piggot, 2004).

During growth and sporulation, division is initiated by the polymerization of tubulin-like protein, FtsZ, into protofilaments (Beall & Lutkenhaus, 1991, Mukherjee & Lutkenhaus, 1998) that are tethered to the membrane by the actin-like protein, FtsA (Pichoff & Lutkenhaus, 2005, Pichoff & Lutkenhaus, 2007). Additional membrane proteins that regulate FtsZ polymerization or polymer stability, including ZapA (Gueiros-Filho & Losick, 2002, Monahan *et al.*, 2009), SepF (Gundogdu *et al.*, 2011, Hamoen *et al.*, 2006, Ishikawa *et al.*, 2006), and EzrA (Haeusser *et al.*, 2004, Levin *et al.*, 1999, Singh *et al.*, 2007), are recruited to the division site through direct interaction with FtsZ (Gamba *et al.*, 2009). Together, these proteins are responsible for assembling the Z-ring, composed of multiple dynamic FtsZ filaments that move in a circumferential motion at midcell to trigger membrane constriction (Dominguez-Escobar *et al.*, 2011, Garner *et al.*, 2011, Haeusser & Margolin, 2016, Stricker *et al.*, 2002).

Once the Z-ring is formed, it functions as a scaffold to recruit late division proteins, including cell wall remodeling enzymes required for inward septal growth (Bisson-Filho *et al.*, 2017, Lan *et al.*, 2009, Monahan *et al.*, 2009, Yang *et al.*, 2017), and regulatory proteins of the Min system responsible for inhibiting Z-ring assembly at the cell poles. In *B. subtilis*, the FtsZ-inhibitory MinCD complex is localized at growing division septa by the topological specific factor, DivIVA, through interactions with the adaptor protein, MinJ (Bramkamp *et al.*, 2008, Eswaramoorthy *et al.*, 2011, Patrick & Kearns, 2008), where it prevents Z-ring assembly in the immediate vicinity of nascent

division septa (van Baarle & Bramkamp, 2010). Following septum completion, Min inhibition persists at mature poles through continued association with DivIVA (Ramamurthi & Losick, 2009). Since Min functions predominantly in DNA-free polar regions, many bacteria also employ a nucleoid occlusion system (NO) to circumvent cell division in the central, DNA-occupied regions of the cell. Together, Min and NO promote efficient utilization of the midcell division site between replicated chromosomes (Rodrigues & Harry, 2012).

NO in *B. subtilis* is mediated by the ParB-like DNA-binding protein, Noc, which localizes to cognate NBSs (Noc Binding Sequence) distributed throughout the chromosome except in the midcell-positioned chromosome terminus (*ter*) regions (Wu et al., 2009). Prior to cell division, the chromosome is replicated and sister origins are segregated to opposite regions of the cell (Webb *et al.*, 1997). As regions of the chromosome occupied by Noc (or SlmA) become segregated toward the poles, NO inhibition is relieved at midcell where Z-ring assembly is permitted in the NO-free *ter* regions (Cho et al, 2011; Tonthat et al, 2011; Wu et al, 2009).

The division inhibition generated by Min and NO must be countermanded during sporulation. Early in sporulation, midcell FtsZ is redeployed to both cell poles through a helical intermediate (Ben-Yehuda & Losick, 2002, Levin & Losick, 1996). Initially, Z-rings assemble at both sites (bipolar Z-rings), although only one ring matures to produce the sporulation septum (Piggot & Coote, 1976). The formation of bipolar Z-rings is dependent on the increased expression of *ftsAZ* from a developmental promoter activated during stationary phase (Gholamhoseinian *et al.*, 1992, Gonzy-Treboul *et al.*, 1992), and

on expression of the bi-functional serine phosphatase, SpoIIE (Barak & Youngman, 1996, Bradshaw & Losick, 2015, Carniol *et al.*, 2005, Frandsen *et al.*, 1999) activated by the master developmental regulator of sporulation, Spo0A (Fujita *et al.*, 2005, Khvorova *et al.*, 1998, Levin & Losick, 1996). Furthermore, the sporulation septum forms over a precise *oriC*-proximal region of one of the cell's two chromosomes leaving roughly 70% inside the mother cell compartment; thus, the bulk of the forespore-destined chromosome is not segregated until after asymmetric division (Wu & Errington, 1994, Wu & Errington, 1998). The captured chromosome is segregated into the forespore post-septation by the DNA pump, SpoIIIE, which assembles a protective DNA-conducting channel across the septum (Bath *et al.*, 2000, Burton *et al.*, 2007, Wu & Errington, 1994, Wu & Errington, 1997).

The TetR family DNA-binding protein, RefZ, was previously shown to be required for precise forespore chromosome capture (Miller *et al.*, 2016). The *refZ* gene is conserved across the *Bacillus* genus by synteny with the division regulator *ezrA*, and is expressed at the onset of sporulation under the control of both the stationary phase sigma factor, σ^{H} (Britton *et al.*, 2002), and Spo0A~P (Fujita, Gonzalez-Pastor, & Losick, 2005, Molle et al, 2003). RefZ's five binding sites, the *RBM*s (RefZ Binding Motifs), are also conserved with respect to their symmetric position about *oriC*, with two sites in close proximity on both the left (RBM_{L1} and RBM_{L2}) and right arms (RBM_{R1} and RBM_{R2}), as well as a single site near the origin (RBM_{O}) (Chapter II, Figure I.1) (Miller *et al.*, 2016, Wagner-Herman *et al.*, 2012). The outermost *RBM*s on the left and right arms lie at the boundary of the region captured in the forespore, and the absence of *refZ* or the *RBM*s

results in a higher frequency of sporulating cells that over-capture regions normally excluded from the forespore (Chapter II, Figure II.8) (Miller *et al* 2016).

Artificial RefZ expression in vegetative cells disrupts Z-ring formation and inhibits cell division in a DNA-binding dependent manner (Wagner-Herman et al 2012). We recently demonstrated that RefZ's function in precise chromosome capture is dependent on its ability to affect division, as variants loss-of-function for perturbing cell division (rLOF) phenocopy the trapping defect of the *refZ* and *RBM* null mutants (Chapter III, Figure III.2B). The rLOF still retain DNA-binding activity, indicating that RefZ-*RBM* complexes act through FtsZ, directly or indirectly, to direct polar septation over a precise chromosome region (Chapter III). RefZ is also hypothesized to regulate division at midcell during sporulation, as deletion of *refZ* delays Z-ring shifting to the poles (Wagner-Herman *et al.*, 2012).

RefZ-GFP exhibits dynamic localization during sporulation, first appearing in predivisional cells (60-70 min) as diffuse cytoplasmic signal and as discrete foci at the far poles (Wagner-Herman *et al.*, 2012). A qualitatively brighter RefZ-GFP focus appears at midcell, predominantly in cells that have initiated polar septation (75-80 min), and a short time later a sub-polar focus is observed at the polar septum, where it remains throughout the engulfment stage (Herman *et al*, 2012). Herman-Wagner *et al* previously proposed two non-mutually exclusive models to reconcile the RefZ's dynamic localization with its functions promoting the switch from medial to polar division and capturing the chromosome during sporulation. In model one, RefZ becomes localized at the poles through interactions with the *oriC*-proximal *RBM*s, and functions as a positive

regulator of Z-ring assembly over the forespore chromosome. In model two, RefZ accumulates at midcell, possibly after saturating available *RBM* sites, and it acts as a negative regulator of medial Z-ring assembly (Herman-Wagner *et al*, 2012). The prolonged appearance of medial and shifting FtsZ in the *refZ* mutant is most consistent with the second model.

The polar foci that appear very early in sporulation likely represent RefZ-GFP bound at the *oriC*-proximal *RBM*s, as only a diffuse cytoplasmic signal was observed when GFP was fused to a DNA binding-deficient variant, Y43A (Wagner-Herman *et al.*, 2012). These observations are further supported by evidence that *RBM*s on the left and right arms adopt both extreme and sub-polar localization, the latter of which is also often found coincident with a division septum (Figure II.6, yellow carats) (Miller *et al.*, 2016).

However, midcell localization does not appear to depend on an interaction between RefZ and DNA, as foci were still observed both when GFP was fused to a second DNA binding-deficient variant, E107A, and in mutants deleted for the *hrcA* locus, which harbors the degenerate *ter*-proximal *RBM* (*RBM*$_T$) (Wagner-Herman *et al.*, 2012). These observations suggest that localization to the far poles reflects RefZ's interaction with *oriC*-proximal *RBM*s and that polar foci, but not midcell foci, represent RefZ in a "DNA bound" state. We cannot exclude the possibility that the RefZ localized at midcell cannot interact with DNA at all, but the data suggests that if RefZ also regulates division when localized at midcell, then it likely does so by a mechanism that differs from its activity at the poles.

As the midcell RefZ-GFP focus is a prime candidate for affecting cell division events during sporulation, we sought to delineate the functional requirements for RefZ's dynamic localization. Here we show that formation of dynamic foci is not dependent on RefZ's ability to inhibit cell division or bind *RBM*s near the origin, suggesting that its subcellular localization may reflect spatio-temporal regulation and/or attenuation of RefZ's division regulation function (Herman-Wagner *et al*, 2012). We used a candidate-based approach to identify additional factors required for the function of midcell RefZ. We find that during sporulation, RefZ's division regulation at the *RBM*s, but not its midcell localization, is required in the absence of the NO protein, Noc. Specifically, a high frequency of cells lacking both *refZ* and *noc* experience aberrant midcell divisions that block development at or before asymmetric division.

To our knowledge, this is the first instance that a sporulation-specific role has been defined for Noc. The absence of a sporulation phenotype or terminal defect in *noc* single mutants likely excluded its inclusion in comprehensive, high-throughput genetic screens (Meeske *et al*, 2017). However, the ability of sporulating cells to divide over the chromosome suggests that inhibition by Noc must be at least temporarily attenuated when the polar Z-ring forms. Our evidence suggests RefZ functions as a temporal regulator of the switch to polar division during the cell cycle checkpoint that governs entry into sporulation, and that Noc activity is critical for tight coordination between replication, segregation, and division events during this transition.

IV.2 RESULTS

IV.2.1 RefZ loss-of-function substitutions do not interfere with dynamic localization during sporulation

Two lines of evidence suggest that RefZ's function during the early stages of sporulation may differentiate based on its sub-cellular localization. First, loss-of-function variants Y43A, harboring a substitution in a helix-turn-helix (HTH) residue required for DNA-recognition, and E107A, harboring a substitution at an invariant residue among RefZ homologs, altered localization during sporulation in distinct manners (Wagner-Herman *et al.*, 2012). Cells expressing the E107A-GFP fusion did not produce polar foci but almost exclusively localized as a bright midcell focus whereas localization was abolished in cells expressing the Y43A-GFP variant (Wagner-Herman *et al.*, 2012). Both variants were recently confirmed to be impaired in binding *RBM* DNA *in vivo* (Figure III.11C), supporting the idea that DNA-binding is not strictly required for midcell localization during sporulation. Since DNA binding activity is required for division inhibition (Wagner-Herman *et al.*, 2012) these observations also suggest that midcell localization does not depend on RefZ's ability to regulate cell division.

To further test this, we took advantage of the rLOF variants that no longer disrupted cell division when artificially expressed during vegetative growth or during chromosome capture (Chapter III, Figure III.1 and III.2B). The ten rLOFs isolated in the selection-screen still retain DNA-binding function (Figure III.1B and Figure III.8), allowing us to test if these activities were required for RefZ's dynamic localization. The

localization data previously published was in the PY79 background (Wagner-Herman *et al.*, 2012), while our strains, including the strain with the five unmarked *RBM* point mutations and the those referenced herein, were constructed in the *Bacillus subtilis* 168 laboratory strain. In *B. subtilis* 168, the signal intensity of RefZ-GFP foci is slightly reduced, even in the wild-type control, making the foci more difficult to distinguish from cytoplasmic signal. The exact reason for this difference was not investigated further, though PY79 is known to sporulate more synchronously and there are genetic differences between the two backgrounds that could account for the differences (Ziegler *et al*, 2008, Youngman *et al*, 1984, Bower *et al*, 1995).

To better distinguish possible differences in localization between the rLOF variants, plasmids harboring translational *gfp* fusions to each of the *rLOF* mutants were introduced into the chromosome at the native *refZ* locus in the PY79 background, as previously described (Wagner-Herman *et al.*, 2012). The resulting strains were induced to sporulate by resuspension and GFP fluorescence was evaluated by scoring cells for the presence or absence of polar and midcell foci (Figure IV.1, blue and yellow carats, respectively; Table IV.1). We hypothesized that localization to the far poles early in sporulation, likely reflecting RefZ binding at the *RBM*s, would not significantly differ in cells expressing the rLOF-GFP variants as they were all capable of binding *RBM* DNA with similar affinity (Figure III.8). Moreover, if RefZ is recruited to or stabilized at midcell through interaction with DNA in the *ter* region, the rLOF would be expected to maintain binding.

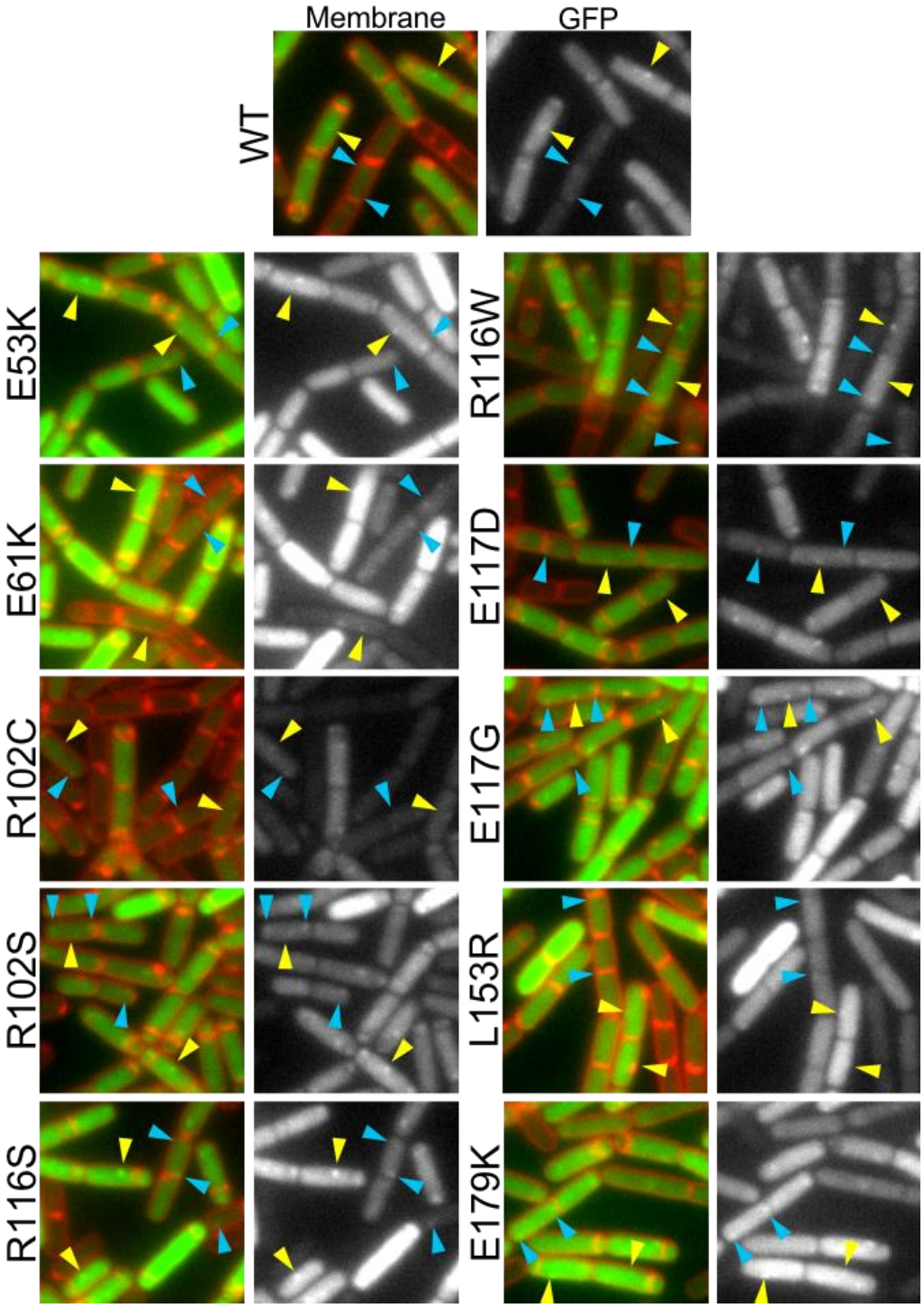

Figure IV.1 rLOF variants exhibit dynamic localization similar to wild-type during sporulation.
Strains harboring single copies of *rLOF-gfp* expressed from the native P_{refZ} promoter were imaged 80 min following induction of sporulation by resuspension. (Left) Membranes were stained with TMA (pseudo-colored red), GFP (pseudo-colored green). (Right) GFP signal alone in grey scale. Cells were assessed for the presence of foci at the far poles (blue carats) and a midcell focus (yellow carats).

As predicted, all rLOF variants formed polar foci (Figure IV.1, blue carats), consistent with the hypothesis that an *RBM* interaction directs RefZ to the poles. All of the variants formed midcell foci (Figure IV.1, yellow carats) consistent with our hypothesis that the ability to moderate cell division does not appreciably interfere with midcell localization. Notably, we did observe qualitative differences in signal intensity of the diffuse cytoplasmic signal between the variants (Table IV.1 and Figure IV.1). Signal from R102S, R116W, and E117D was most similar to wild-type RefZ-GFP. Both classes of foci were easily distinguished against the cytoplasmic signal and corresponded to morphological changes expected of cells during the early stages of development (Figure IV.1).

Signal intensity both at foci and in the cytoplasm of R102C-GFP was considerably reduced compared to wild-type, however since the majority of this population appeared to enter sporulation later than the rest of the variants it's likely that *refZ-gfp* expression was also lower. In contrast, the remainder of the variants exhibited a diffuse cytoplasmic signal greater than or equal to the intensity of the midcell focus. For E53K, R116S, E117G, and E179K fusions, the increased signal was predominantly associated with cells that had progressed further into development, and were similar to what we observe for a majority of wild-type cells at a later time point (90 min). These differences might be explained, in part, by the stochasticity with which cells in the population enter sporulation, during which RefZ expression increases due, in part, to increased levels of Spo0A~P (Fujita *et al.*, 2005, Nicolas *et al.*, 2012).

	Polar[a]	Medial[a]	Cyto[b]	B2H[c]	EMSA[c]
WT	++	++	++	++	++
R102S	++	++	++	++	+
R116W	++	++	++	-	++
E117D	++	++	++	++	++
R116S	++	++	+++	+++	++
E117G	++	++	+++	++	+++
E53K	++	++	++++	++++	++++
E179K	++	+	+++	+++	++
E61K	++	+	++++	++	++++
L153R	+	+	+++	-	-
R102C	+	+	+	+	+

Table IV.1 RefZ-GFP and rLOF-GFP foci observed during sporulation.
[a] rLOF-GFP fusions (represented by images in Figure IV.1) were classed on their ability to form wild-type foci at the poles (and sub-polar regions), and at midcell ("Polar" and "Medial", respectively).
[b] Diffuse cytoplasmic signal ("Cyto") was scored for intensity. The highest Cyto score (++++) denotes fluorescence that overwhelms signal from polar and/or medial foci in a large number of cells that have yet to reach a stage in sporulation (i.e. asymmetric division) that correlates with increased *refZ* expression. Cyto score (+++) denotes modest increased signal that does not interfere with the ability to distinguish between individual foci.
[c] Columns reproduced from Table III.3. "B2H" and "EMSA" correspond to "Self-interaction" and "EMSA laddering" in Table III.3, respectively. B2H, propensity for RefZ dimerization as assayed by bacterial 2-hybrid; EMSA, extent of laddering on a 120-bp DNA probe centered on an *RBM* (multimerization).

However, this explanation alone cannot account for the intensity of the signal in the remaining variants, L153R and E61K. Differences in signal intensity between the variants may reflect distinctions in variant self-interaction or *RBM*-binding affinity (Table IV.1, B2H and EMSA, respectively) or DNA-binding specificity (Figure III.8), properties that might be expected to alter the stability and/or dynamics of RefZ-GFP foci. For example, L153R is the least functional of the variants (Chapter III, Table II.3), and foci from both classes were generally smaller and weaker with a concomitant

increase in diffuse GFP signal (Figure IV.2). In addition, the hyper-functional variants E61K and E53K exhibited similar cytoplasmic intensity; however, E61K-GFP scored less on foci robustness, which was most obvious in predivisional cells where no foci were detected (Figure IV.1).

IV.2.2 RefZ-GFP assembles midcell foci in the absence of the *ori*- and *ter*-proximal *RBM*s

The observation that each of the ten rLOF-GFP fusions were able to assemble polar, sub-polar, and midcell foci indicates RefZ's dynamic localization is not strictly dependent on its ability to inhibit cell division. This is consistent with the second line of evidence indicating that the midcell and polar RefZ-GFP foci represent distinct functional species: deletion of *hrcA,* and consequently the degenerate *ter*-proximal *RBM*s, did not abolish midcell focus formation, although foci were noted to be less robust and appear less frequently compared to wild-type cells (Wagner-Herman *et al.*, 2012). These observations could not be directly attributed to the loss of RefZ's *ter*-proximal binding sites, as *hrcA* mutant cells appeared delayed in entering sporulation (Wagner-Herman *et al.*, 2012). To eliminate the potential off-target effects of deleting *hrcA* and determine conclusively the requirement for *ter*- and *ori*-proximal *RBM*s in formation of midcell and polar foci, we monitored RefZ-GFP localization in strains harboring loss-of-function point mutations in the RBM_T site (RBM_{Tmu}), the five *ori*-proximal sites (RBM_{5mu}), or in all six sites (RBM_{6mu})(Figure IV.2).

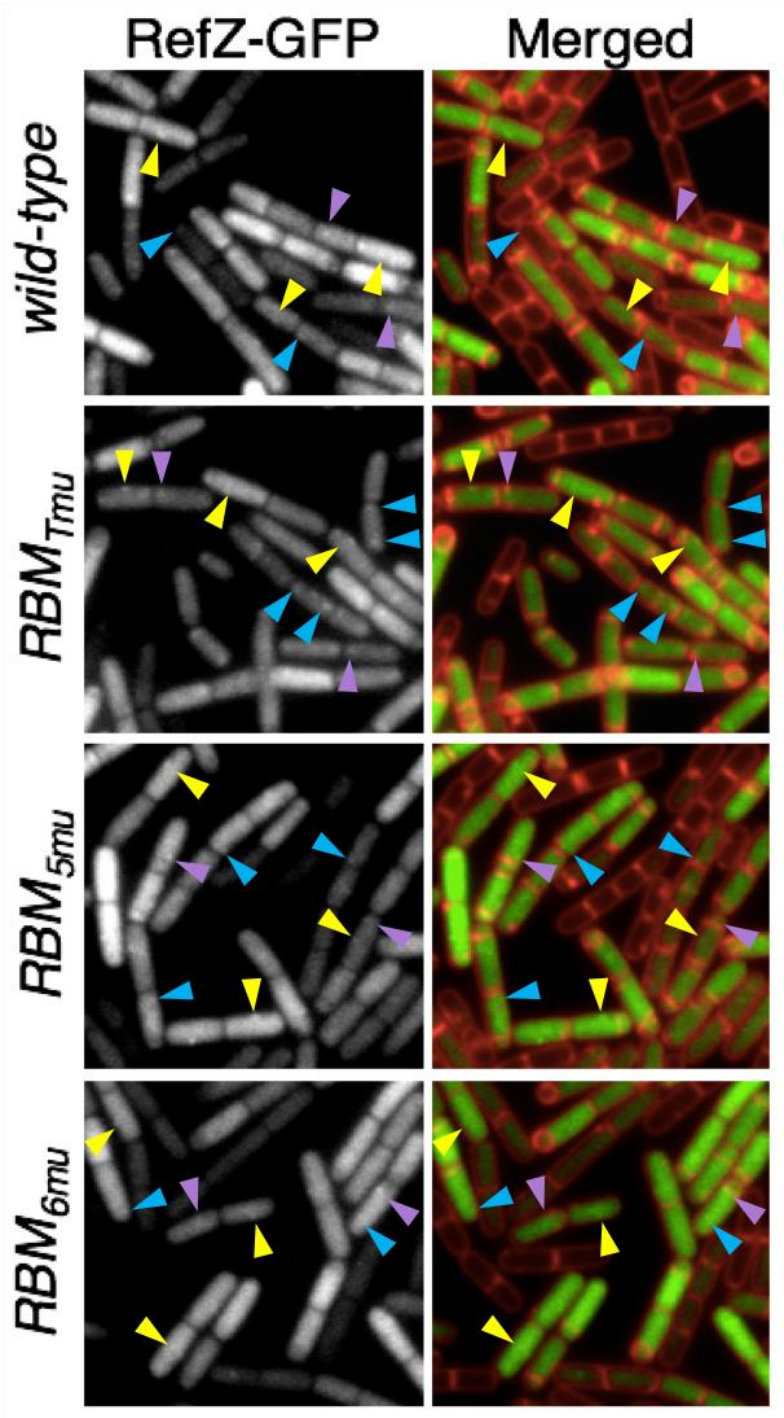

Figure IV.2 RefZ-GFP localization to midcell does not require *oriC*- or *ter*-proximal *RBM*s.
RefZ-GFP localization was monitored 75 min following resuspension in wild-type or strains harboring single point mutations in the consensus sequence of either the five *ori*-proximal or a *ter RBM* sequence, or all six sites. GFP fluorescence is shown alone (left) or overlaid with the membrane (red) pseudo-colored green (right panels). Indicated are examples of RefZ-GFP foci at the far poles in predivisional cells (blue carats), at midcell (yellow carats), or at the sub-polar position (purple carats).

Midcell foci, similar to the wild-type control, were observed in *RBM*$_{Tmu}$ cells (Figure IV.2, yellow carats), in line with the prior conclusion that the *RBM*$_T$ is not required for RefZ localization midcell. Midcell foci were also detected in both *RBM*$_{5mu}$ and *RBM*$_{6mu}$ cells (Figure IV.2, yellow carats), indicating that RefZ is not maintained at midcell through interactions with *RBM*s present at the terminus or origin of the chromosome. Mutation of the *RBM*$_T$ site also had no effect on the formation of polar foci and sub-polar foci, which were generally observed in cells at the pre-divisional and post-division stage, respectively (Figure IV.2, blue and purple carats, respectively).

In contrast, polar foci were largely absent in both *RBM*$_{5mu}$ and *RBM*$_{6mu}$ cells, although in some cases more polar-positioned foci were observed (Figure IV.2, blue carats). These foci were distinguishable from sub-polar foci in that they appeared in pre-divisional cells. Moreover, for all strains tested sub-polar foci at nascent division septa (Figure IV.2, purple carats) were observed in cells with and without polar foci, suggesting that RefZ may not remain associated with the *RBM*s during polar septum formation, perhaps independently associating with a component of the divisome. Consistent with this idea, RefZ-GFP foci are observed at some of the polar junctions between chained cells (>2) and at partial septa at midcell (Figure IV.2, blue carats). Thus, if RefZ also regulates division at midcell during sporulation, then it likely does so by a mechanism distinct from that employed at the poles and may depend on other sporulation-specific cues such as chromosome copy number or axial filament formation, bi-polar Z-ring assembly, or a stabilizing interaction with a membrane-associated protein.

IV.2.3 Noc is required for spore development in the absence of *refZ* and *RBM*s

The conservation of *refZ* across *Bacillus* polar spore formers likely reflects a fitness advantage associated with its function in regulating polar division over the chromosome during development. The arrangement of RefZ's binding sites, the *RBM*s, on the left and right chromosome arms with respect to *oriC* is also highly conserved across *Bacillus*, indicating that an immense selective pressure exists to maintain these sites (Miller *et al.*, 2016). While the RefZ-*RBM* system is likely critical for survival in the environment, we suspect functionally redundant systems exist that would preclude detection of terminal sporulation phenotypes in laboratory strains lacking *refZ* or the *RBM*s.

RefZ's function in moderating division, when bound at the *RBMs* and/or when localized at midcell, is expected to be redundant with other systems that engage the nucleoid to regulate cell cycle processes. The major nucleoid-associated systems that function during sporulation have been well characterized, including Spo0J-*parS* and Soj (replication initiation control and origin condensation) and RacA-*ram* (origin anchoring and axial filament formation) and perturbing these systems results in distinct defects in chromosome capture (Miller *et al.*, 2016, Sullivan *et al.*, 2009). We previously evaluated these systems as candidates for redundancy by assessing whether the arm capture defect of cells lacking the RefZ-*RBM* system was enhanced in their absence (Chapter II.3, Discussion) (Miller *et al.*, 2016). However, our results indicated that these systems function in a more dominant role, and we suspect are not likely the driving force behind *refZ* and *RBM* conservation.

One system that both associates with the nucleoid and plays a regulatory role in cell division is NO. During growth, Noc is localized throughout the chromosome at its cognate binding sites, NBS, where it forms large nucleoprotein complexes that associate with the cell membrane (Adams *et al*, 2015). These large complexes are thought to inhibit division over the nucleoid by physically occluding assembly of the divisome at the membrane (Adams *et al*, 2015). Noc expression is constitutive during growth and was shown to decrease substantially in cells transitioning into sporulation (Sievers *et al.*, 2002). A terminal sporulation phenotype has not been reported for a Δ*noc* mutant; however, it is well poised to perform a redundant function with RefZ, as Noc levels only gradually decline over the first few hours of sporulation (Sievers *et al.*, 2002) when *refZ* expression is maximal (Fujita *et al.*, 2005, Nicolas *et al.*, 2012).

In order to test if *refZ* and *noc* act redundantly, we constructed Δ*refZ* Δ*noc* and *RBM*$_{5mu}$ Δ*noc* double mutants and assessed spore development compared to wild-type and single mutant controls using a plate-based sporulation assay (Figure IV.3A). A *lacZ* transcriptional fusion to a late-stage sporulation promoter (P$_{cotD}$-*lacZ*) was introduced into the wild-type, single, and double mutant backgrounds to permit visual assessment of defects. The resulting strains were grown in sporulation medium to mid-log and spotted on DSM plates supplemented with X-gal and incubated at 37°C to induce sporulation. Strains blocked or delayed in sporulation appear white or light blue, respectively, while strains able to progress through sporulation appear blue. Deleting *noc* in backgrounds mutant for *refZ* or the *RBM*s resulted in obvious sporulation defects compared to the

wild-type and the single mutant controls (Figure IV.3A), indicating that Noc is required for normal sporulation in the absence of RefZ and/or RefZ-*RBM* complexes.

For comparison, we also evaluated the relationship between RefZ or the *RBM*s and well characterized division regulators EzrA, SepF, and MinD, as well as Soj (ParA). None of these regulators appear to be required for sporulation in a RefZ and/or *RBM*-dependent manner (Figure IV.3A), suggesting that the defect is specific to the loss of Noc rather than division regulation or chromosome organization in general.

To determine whether the defect in sporulation observed for the Δ*refZ* Δ*noc* and RBM_{5mu} Δ*noc* double mutants resulted in a terminal sporulation phenotype, we assessed the efficiency of mutant spore production compared to wild-type following heat treatment (Figure IV.3B). In contrast to the Δ*refZ* and RBM_{5mu} single mutants, spore production in the Δ*noc* mutant was considerably reduced (2-fold) compared to wildtype. An additional 2-fold reduction in efficiency was observed both for the Δ*refZ* Δ*noc* and the RBM_{5mu} Δ*noc* double mutants, suggesting that the two systems promote spore formation through distinct mechanisms.

IV.2.4 Δ*refZ* Δ*noc* double mutants divide symmetrically during sporulation

Previously, a severe block in sporulation at the stage of asymmetric division was reported for cells engineered to overexpress Noc (Sievers *et al.*, 2002). In these cells, multiple and aberrant division septa were frequently observed. Based on the sporulation defect observed in strains lacking *noc* (Figure IV.3B), we wondered if division might also be impaired in these strains.

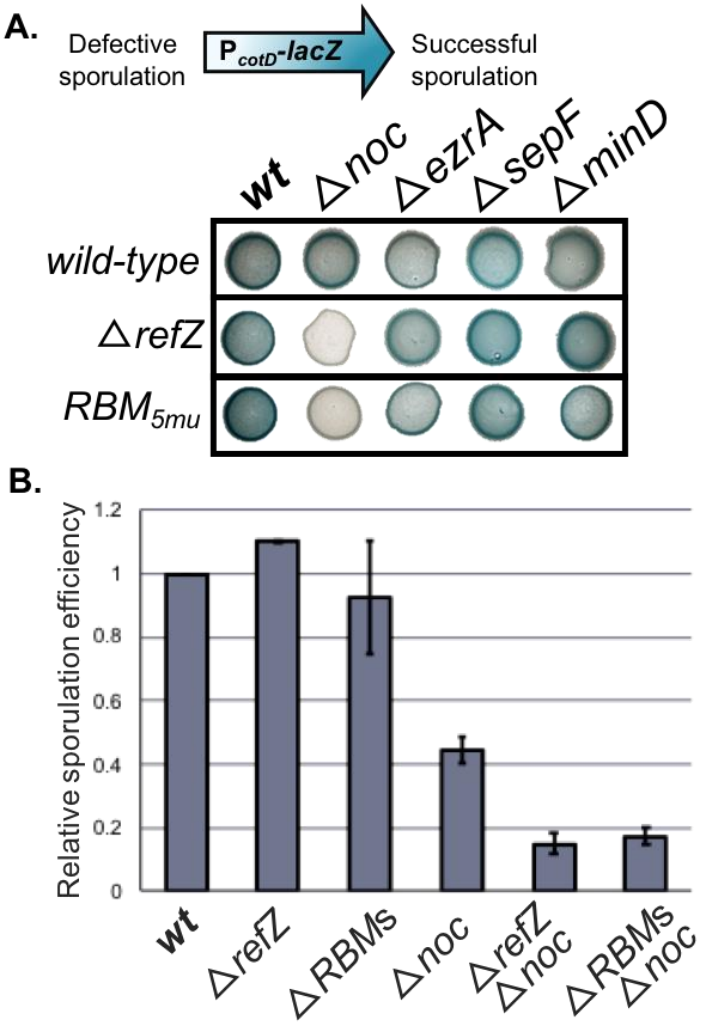

Figure IV.3 Noc is required for sporulation in the absence of *refZ* or *RBM*s.
(A) Plate-based assay for sporulation by activation of P_{cotD}-*lacZ* . Deletions of *noc, ezrA, sepF, and minD* were assayed on sporulation media with X-gal in a wild-type, Δ*refZ, or* RBM_{6mu} background. **(B)** Relative sporulation efficiencies of the indicated mutant strains compared to the wild-type control following heat treatment at 80°C for 20 min. Relative efficiencies were determined as the number of mutant heat-resistant spores/CFU compared to those of the wild-type control (*wt* is 1). Vertical bars indicate standard deviation from average of two trials (n=2).

In order to test this, we monitored cell morphology in wild-type, single mutants, and the Δ*refZ* Δ*noc* and RBM_{5mu} Δ*noc* double mutants 2 h after resuspension in sporulation medium (Figure IV.4). The backgrounds also contained a fluorescent fusion to the *spoIIG* promoter which allowed us to monitor Spo0A~P activity and differentiate between vegetative cells and cells which have initiated sporulation. Transcription from P_{spoIIG} occurs early in sporulation in predivisional cells and is activated by high-threshold levels of Spo0A~P (Fujita *et al.*, 2005). Two hours after resuspension, roughly the time when Spo0A is known to reach peak levels (Fujita, Gonzalez-Pastor, & Losick, 2005)(Fujita *et al.*, 2005), the single and double mutant populations displayed CFP fluorescence (initiated sporulation) at qualitatively similar intensities to the wild-type control, suggesting that the defect in sporulation occurs downstream of Spo0A activation (Figure IV.4).

Wild-type cells and the majority of single mutant cells that had initiated sporulation (CFP) had divided asymmetrically and progressed into the early engulfment stage, when the forespores become rounded (Figure IV.4). In contrast, many double mutant cells harboring an asymmetric septum at one or both poles also had a midcell division septum (Figure IV.4). We also observed many predivisional cells (no asymmetric septum) with a flat, midcell septum in which one or both "daughter" cells contained a partial septum that appeared to form at a more medial position, rather than at the poles (Figure IV.4, white carats).

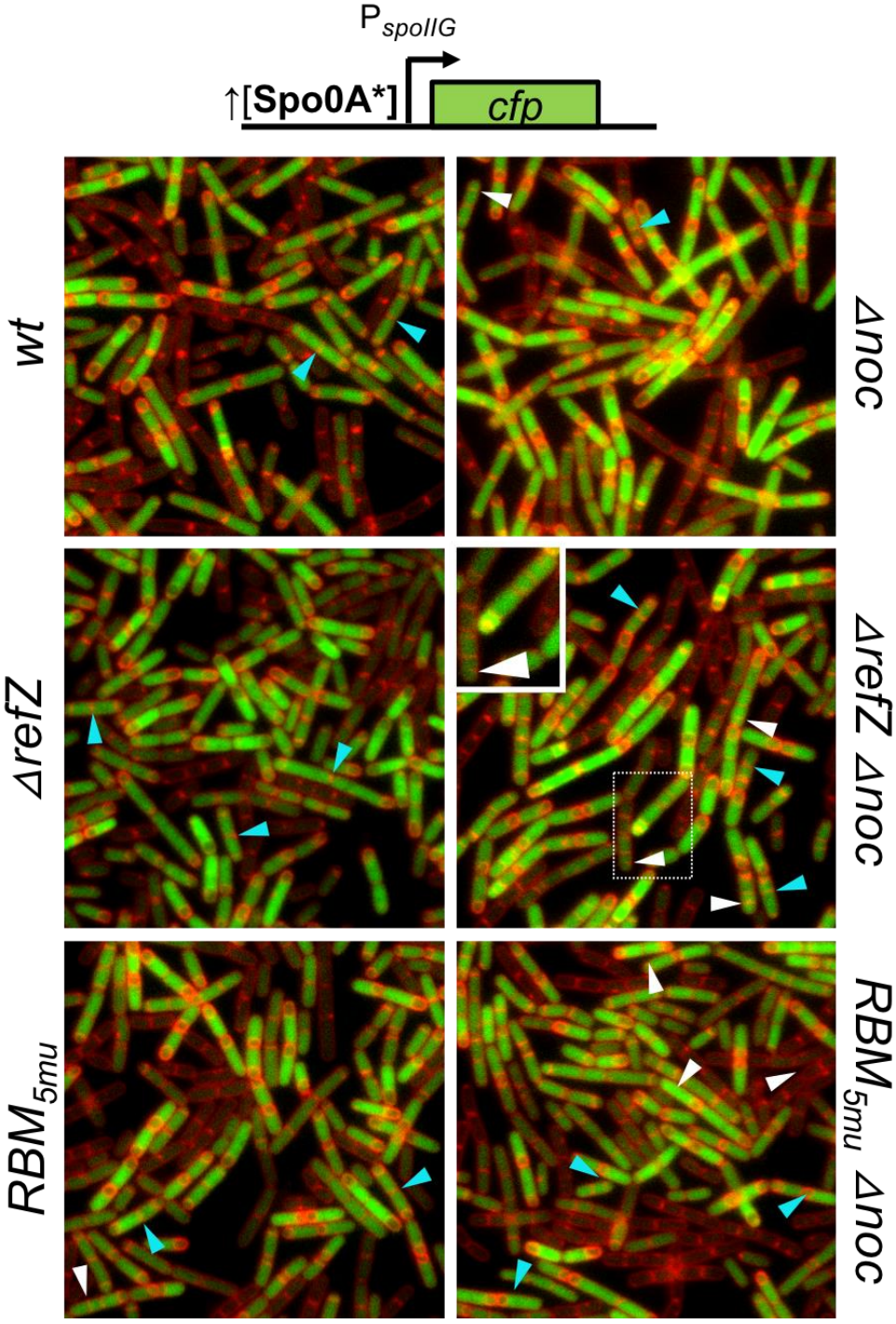

Figure IV.4 Sporulation is initiated in noc refZ double mutants.
GFP expression from the Spo0A~P dependent P_{spoIIG} promoter was monitored 2 h after sporulation was induced by resuspension in the indicated mutants. CFP signal (green) was normalized between images and is shown overlaid with membrane signal (red, FM4-64). Indicated are sporulating cells (CFP) with midcell septa accompanied either by polar septa (blue carats) or partial or complete septa in a central, sub-polar position (white carats). Inset image corresponding to boxed section indicates shorter cells dividing near midcell.

The same phenotype was also observed in a smaller portion of single mutant and wild-type cells; however, these daughters were likely undergoing the last round of symmetric division as they were substantially longer than those found in the double mutants. This suggests that a portion of double mutant cells fail to properly mitigate symmetric division at the onset of sporulation (Figure IV, inset).

In a similar experiment images were captured later, 3 h after resuspension, to permit better distinction between cells undergoing a final symmetric division and those aberrantly dividing at midcell (Figure IV.5A). Division septa were classed and quantified in wild-type, Δ*refZ*, Δ*noc*, and the Δ*refZ* Δ*noc* double mutant cells that had initiated sporulation (Figure IV.5A, inset table). At this time, wild-type, Δ*refZ* mutant, and Δ*noc* mutant cells displayed a low frequency (1, 2, and 5%, respectively) of medial divisions within mother cell compartments. By contrast, 22% of the mother cells in the Δ*refZ* Δ*noc* double mutant contained non-polar septa. This indicates that, in the absence of Noc, RefZ is important for preventing additional midcell division events. In RBM_{5mu} Δ*noc* double mutant populations we observed qualitatively similar proportions of each class (not shown and Figure IV.4), in support of a RefZ-dependent role for the *oriC*-proximal binding sites in preventing extra midcell divisions.

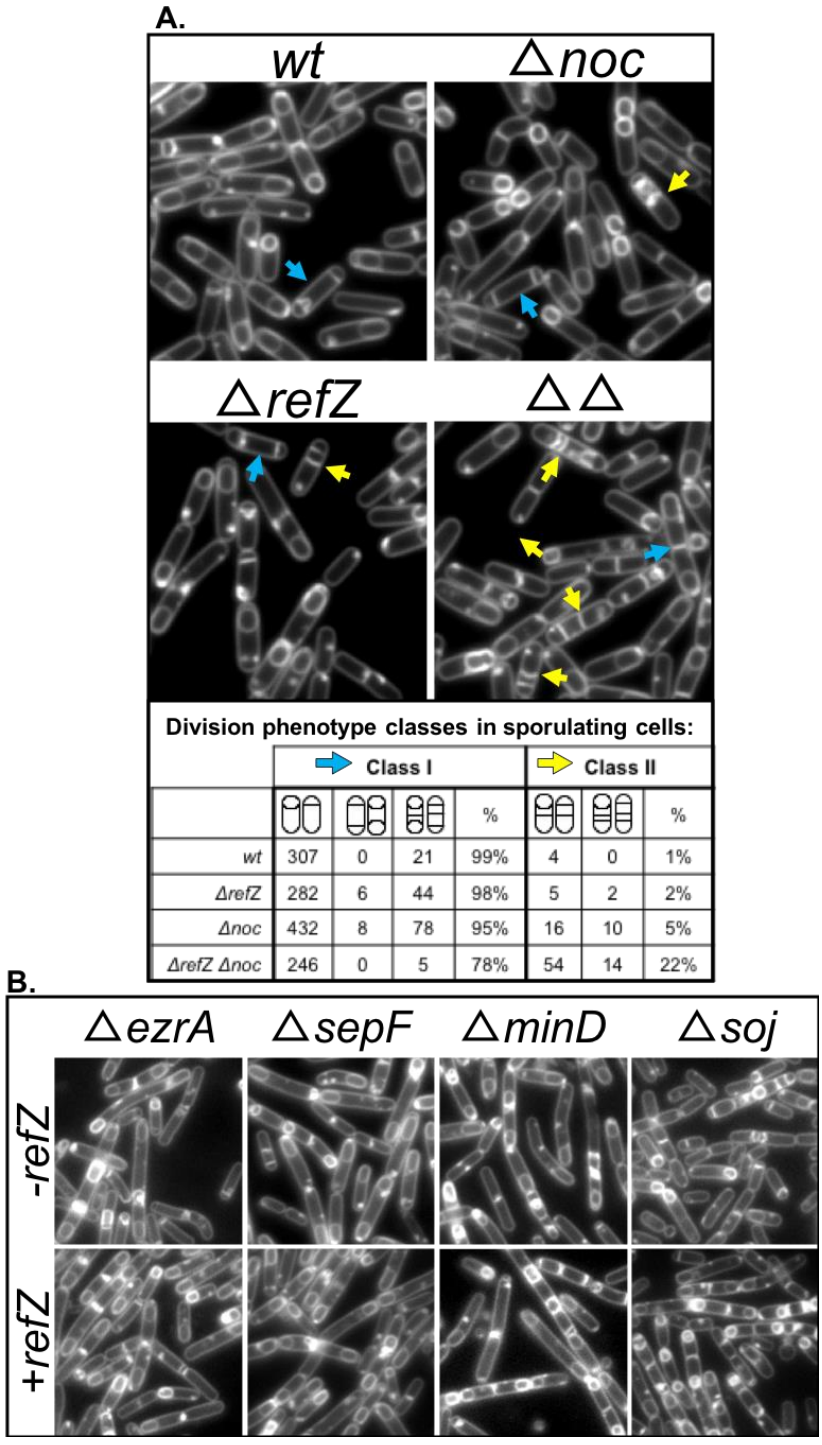

Figure IV.5 Noc and RefZ are required to prevent extra divisions at midcell during sporulation.
(A) Indicated strains harboring a fluorescent reporter for Spo0A~P activity were induced to sporulate and images were captured after 3 h. Individual cells expressing GFP were classed according to septum morphology (inset table), indicated in representative images above. **(B)** Significant division defects observed in single *ezrA*, *sepF*, *minD*, and *soj* mutants ("+*refZ*") are not substantially worsened by the absence of RefZ ("-*refZ*").

For comparison, we also monitored division in Δ*ezrA*, Δ*sepF*, and Δ*minD* mutants in the presence or absence of *refZ* (Figure IV.5B). Cell morphology was severely perturbed in cells of the double mutants. In all cases, however, the defects appeared to be dependent on the loss of the candidate genes, rather than *refZ*, as we observed similar phenotypes in the single mutant controls (Figure IV.5B). These results are consistent with the hypothesis that the aberrant cell divisions are specific to the activities of both RefZ and Noc. Deletion of these factors in the RBM_{5mu} background produced very similar phenotypes as those observed upon their deletion in the Δ*refZ* background (not shown), consistent with the results of our plate-based sporulation assay (Figure IV.3A).

In the case Soj, these results are also consistent with previous data indicating that RefZ-*RBM* function in chromosome capture relies on more dominant factors that organize the chromosome (Chapter II, Discussion). EzrA, SepF, and MinD contribute significantly to Z-ring stability and division site selection during growth (Haeusser & Margolin, 2016, Hajduk *et al*., 2016). While the RefZ-*RBM* system might also be a source of division regulation during sporulation, its contribution only appears to have a moderate influence in cells lacking *ezrA* and/or *sepF*. Like Soj, we reason that these factors play a dominant role in relation to RefZ rather than a redundant one.

IV.2.5 RefZ's division regulation activity is required for preventing aberrant septum formation in the absence of Noc

The division inhibition functions of both RefZ and Noc are dependent on interactions with their cognate binding sites, *RBM*s and *NBS*, respectively. The *RBM*s and RefZ's DNA-binding activity are required both for RefZ localization to the poles and chromosome capture during asymmetric division (Chapter II)(Miller *et al*, 2016), while neither appear to be required for RefZ's localization to midcell (Figure IV.1)(Herman-Wagner *et al*, 2012). Deletion of *noc* in the RBM_{5mu} background produced multiple sporulation phenotypes similar to what we observe in the Δ*refZ* Δ*noc* double mutant: a defect in sporulation on plates and following heat treatment (Figure IV.3), and an increased proportion of sporulating cells with aberrant midcell septa (Figure IV.4 and IV.5). These data strongly suggest that RefZ's redundant role with Noc is dependent on its interaction with the *RBM*s. We wondered whether the same substitutions in RefZ conferring loss of division regulation and chromosome capture function, but not DNA-binding activity, would result in extra midcell divisions in the absence of Noc, similar to the a Δ*refZ* mutant.

To test this, we replaced the native *refZ* gene in wild-type or Δ*noc* backgrounds with the 10 *rLOF* sequences that code for DNA binding-proficient variants, and four that encode the DNA binding-deficient variants (Y43A, Y44A, R106A, and E107A). We first evaluated sporulation defects using the plate-based assay by introducing into these strains the late-stage sporulation reporter, P_{cotD}-*lacZ*. The resulting strains were cultured in liquid sporulation media and spotted at equivalent cell densities on DSM plates

supplemented with X-gal to monitor LacZ expression (Figure IV.6A). None of the rLOF variants supported wild-type LacZ expression in the a Δ*noc* background (Figure IV.6A, "-*noc*"), whereas sporulation defects were not observed in strains where *noc* was present (Figure IV.6A, "+*noc*"), similar to the Δ*refZ* Δ*noc* double mutant (Figure IV.3A). These results indicate that RefZ's division regulation activity is required for sporulation in the absence of Noc.

To determine whether the sporulation defect observed in the *rLOF* Δ*noc* double mutants was also the result of increased aberrant midcell divisions, we monitored division events in sporulating cultures by fluorescence microscopy (Figure IV.6B). Consistent with the preliminary results from the plate-based assay, the rLOF variants behaved similar to Δ*refZ* and did not prevent medial divisions when expressed in the Δ*noc* background. We did not detect any remarkable differences in septum morphology or in the abundance of midcell septa between the variants, regardless of DNA-binding capability, indicating that residues of RefZ required to coordinate polar division over the forespore chromosome are also required to mitigate symmetric divisions in conjunction with Noc.

IV.2.6 Noc is not required for dynamic RefZ localization

Replication becomes inhibited in cells that have initiated sporulation at which point a final vegetative division at must occur to generate cells with exactly two chromosome copies, one destined for the forespore and the other for the mother cell.

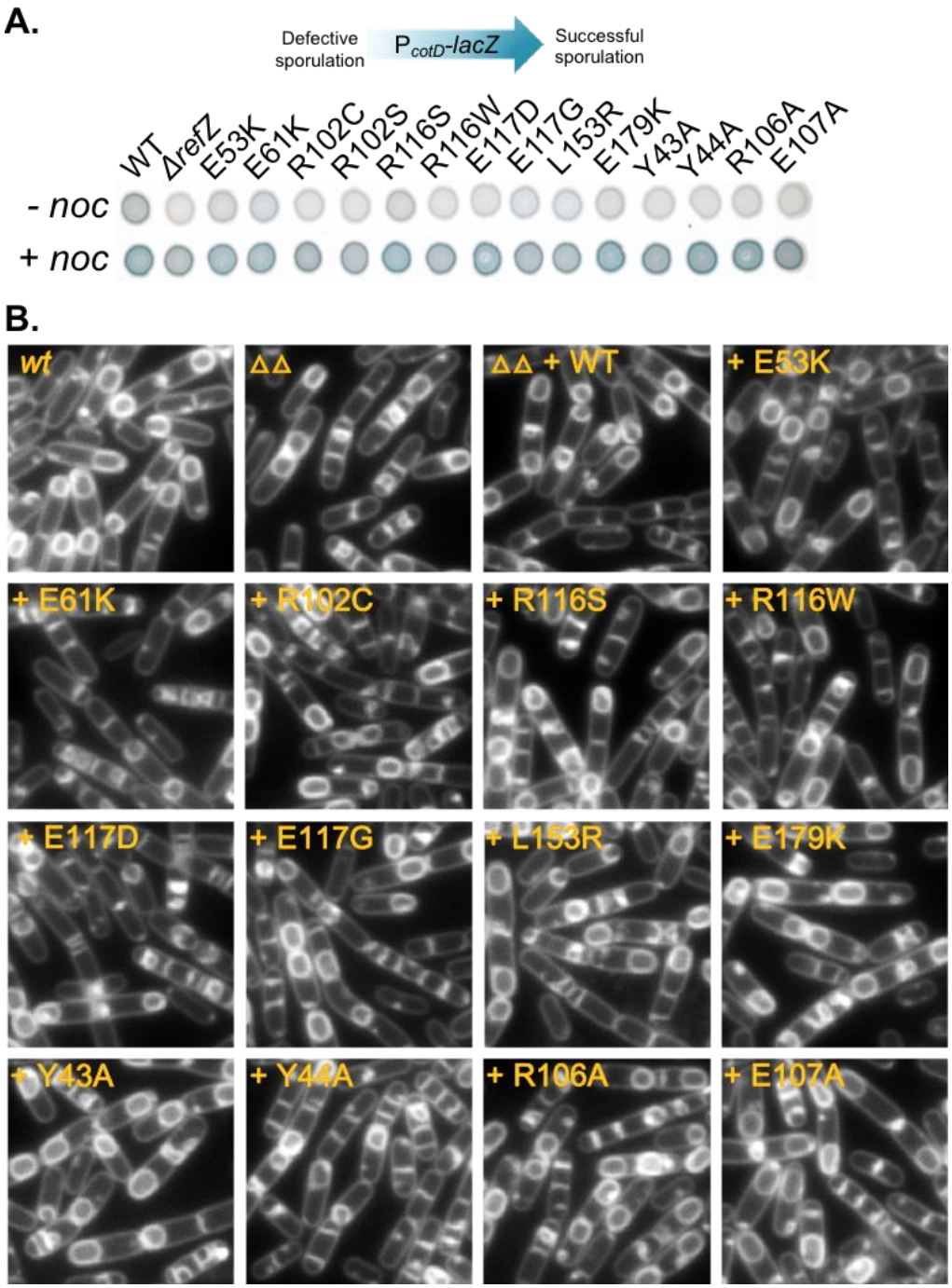

Figure IV.6 RefZ's division regulation activity is required to prevent aberrant midcell septa in the absence of *noc*.

(A) Plate-based assay for sporulation based on P_{cotD}-dependent LacZ expression. △*refZ* and *rLOF* mutants were assayed for defects in a wild-type (+*noc*) or △*noc* (*-noc)* backgrounds on sporulation media with X-gal. **(B)** Aberrant division defects observed in the △*refZ* △*noc* mutant (△△) are lost when wildtype *refZ* is introduced (△△+WT), but are phenocopied when *rLOF* are introduced (+rLOF).

The origins of these two chromosomes become anchored at the far poles by DivIVA interactions with the aforementioned RacA/Soj-Spo0J nucleoprotein complexes, while the termini remain at midcell until the forespore chromosome undergoes translocation. Since Noc inhibition would be largely absent from midcell after the axial filament forms, we wondered if RefZ might prevent symmetric division from its midcell position in cells that have initiated sporulation. This hypothesis is in line with our model in which RefZ might regulate division during different stages of sporulation and/or from multiple subcellular locations. Prior to polar division, RefZ may disrupt or destabilize midcell FtsZ and promote redistribution to the poles, while a short time later, RefZ may either promote or inhibit septum formation over the chromosome during polar division.

In order to test this, we examined RefZ-GFP fluorescence in the Δ*noc* and *RBM*$_{5mu}$ Δ*noc* double mutant compared to wild-type and *RBM*$_{5mu}$ controls (Figure IV.7). One expectation is that RefZ-*RBM* complexes at the poles moderate polar division over the chromosome independent of Noc, but are subject to stabilizing or destabilizing interactions (nucleoid, protein-protein, membrane, etc.) in the presence of Noc. However, the absence of Noc did not result in detectable differences in polar, medial, or sub-polar RefZ-GFP localization compared to wild-type (Figure IV.7). Consistent with our earlier results, only polar foci were significantly reduced in the *RBM*$_{5mu}$, while midcell and sub-polar foci, usually associated with an incipient polar septum, appeared as normal. Further loss of *noc* did not appreciably change focus formation at midcell or the sub-polar position compared to either single mutant, and polar foci were not observed, indicating that Noc is not required for dynamic RefZ-GFP localization.

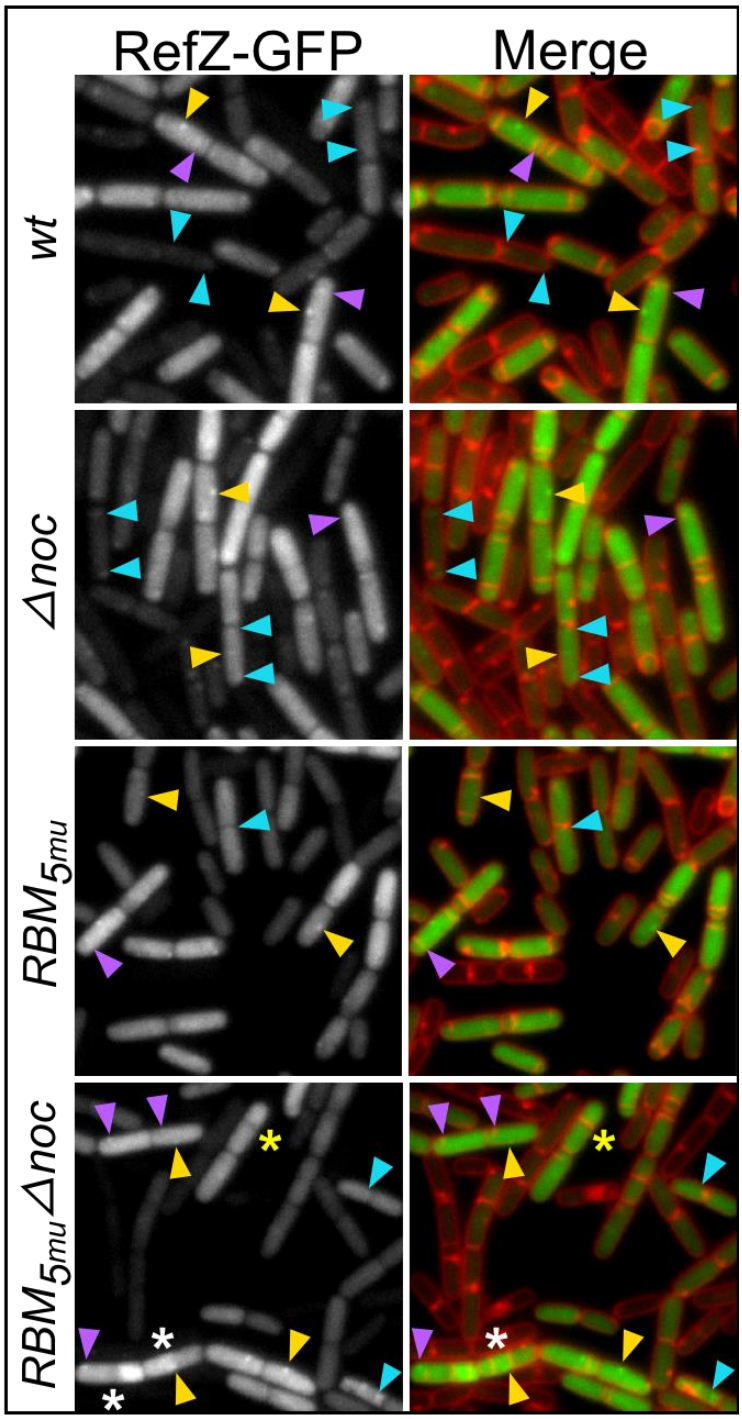

Figure IV.7 Noc is not required for RefZ's dynamic localization.
RefZ-GFP localization was monitored during sporulation 75 min following resuspension in wild-type, Δ*noc*, *RBM*$_{5mu}$, or double *RBM*$_{5mu}$ Δ*noc* strains. GFP fluorescence is shown alone (left) or overlaid with the membrane (red) pseudo-colored green (right). Indicated are examples of RefZ-GFP foci at the far poles (blue carats), at midcell (yellow carats), or at the sub-polar position (purple carats). Yellow and white asterisks indicate compartments with variable RefZ-GFP signal.

We note that for some *RBM*$_{5mu}$ Δ*noc* cells where an aberrant medial division had occurred, the intensity of cytoplasmic GFP signal was more intense than the signal in the compartment immediately adjacent. For two such instances indicated in Figure IV.7 (white asterisks), the brighter of the two compartments contained a polar septum. In the third instance, septa were not observed in either compartment and the difference in signal intensity was substantially less than those with polar septa (Figure IV.7, yellow asterisk). Considering RefZ expression increases in a Spo0A-dependent manner in the early stages of sporulation, we suspect these compartments might contain higher concentrations of Spo0A~P and, consequently, higher levels of RefZ-GFP.

IV.2.7 Aberrant midcell divisions in Δ*refZ* Δ*noc* double mutants generate nucleoid-free mother cell compartments

We next sought to identify the stage of development at which the Δ*refZ* Δ*noc* and the *RBM*$_{5mu}$ Δ*noc* double mutants become arrested. Progression through sporulation is driven by the hierarchal activation of compartment-specific sigma factors and is initiated by σ^F activation in the forespore followed by σ^E activation in the mother cell. Activation of σ^F is dependent on the formation of the asymmetric septum. σ^F and σ^E are responsible for directing expression and activation of the late-stage factors, σ^G in the forespore, then σ^K in the mother cell. In our plate-based sporulation assay, expression of *lacZ* from P$_{cotD}$ is dependent σ^K (Steil *et al.*, 2005), indicating that the block in development observed in Δ*refZ* Δ*noc* and the *RBM*$_{5mu}$ Δ*noc* double mutants occurs upstream of σ^K activation (Figure IV.3A).

The midcell divisions observed in the double mutants often accompanied a polar division septum at one or both poles of the same cell, indicating that Spo0A had activated SpoIIE expression and was not strictly limited to the P_{spoIIG} promoter (Figure IV.4). To determine whether the asymmetric divisions appropriately activated σ^F in the, we monitored forespore fluorescence in wild-type, single mutant, and double mutant strains harboring a σ^F–activated reporter in the *oriC* region of the chromosome (*amyE::*P_{spoIIQ}*-cfp*). Cultures of the resulting strains were induced to sporulate by resuspension and examined by fluorescence microscopy after 3 h. Cells were considered to have successfully activated σ^F if forespores expressed CFP, false-colored blue in representative images of the Δ*refZ* Δ*noc* double mutant and a wild-type control strain Figure IV.8 in overlays of membrane (FM4-64, red) and DNA (DAPI, green).

Nearly all wild-type and single mutant cells, and a substantial proportion of double mutant cells, contained a condensed mother cell chromosome distal to a forespore expressing CFP, the majority of which had progressed well into the engulfment stage, as indicated by the loss of FM4-64 signal in the forespore membrane (Figure IV.8, blue carats). In contrast, double mutant cells with an asymmetric septum at one or both poles frequently possessed an extra septum at midcell, either between the cell's two chromosomes, creating a physical barrier between them, or on top of the forespore-distal chromosome in the mother cell (Figure IV.8, white carats). In the latter scenario, these trapped chromosomes would likely be pumped into the forespore-distal compartment following SpoIIIE-mediated translocation, resulting in cells with one or two empty middle compartments (Figure IV.8, white carats).

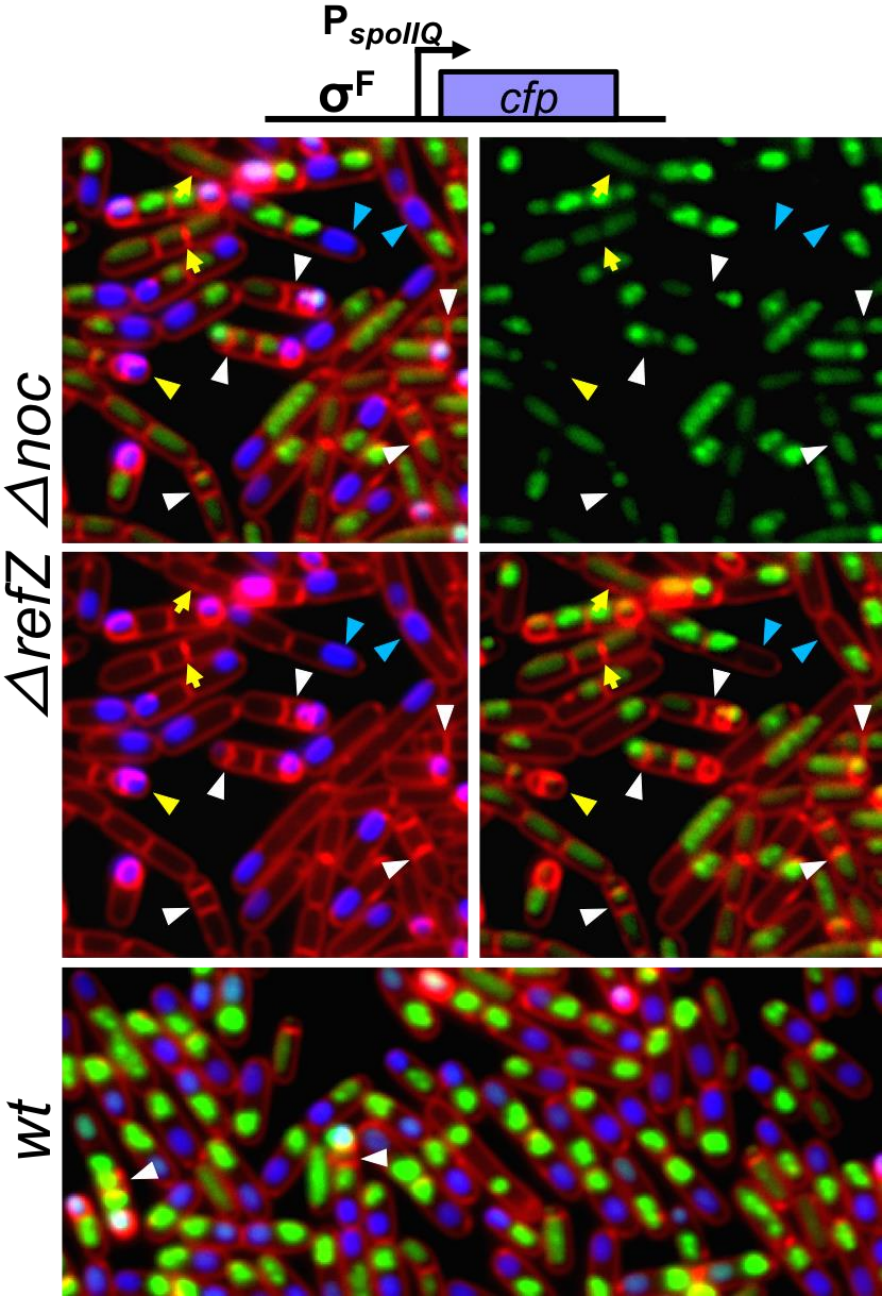

Figure IV.8 Extra midcell divisions in the Δ*noc* Δ*refZ* double mutant frequently guillotine the mother cell chromosome.

The indicated strains carrying a fluorescent reporter for σ^F activation (P_{spoIIQ}-*cfp*) were induced to sporulate by resuspension and examined by fluorescence microscopy after 3 h. Representative images are overlaid and false-colored: green, DAPI (DNA) channel; red, FM4-64 (membrane) channel; and blue, CFP (P_{spoIIQ}) channel. Cells are considered to have successfully activated both σ^F and σ^E if forespores express CFP show signs of engulfment (rounded up forespores and forespores without membrane or DNA signal) (blue carats). Indicated are aberrant septa resulting in an empty middle compartment (white carats), cells with reduced DNA content and partial or complete septa (yellow arrow), and short cells resulting from aberrant divisions that matured to produce daughter cells (yellow carat).

Both scenarios would produce nucleoid-free "mothers" unable to engage in intercompartmental signaling and would therefore be arrested in sporulation. We speculate this class represents a substantial portion of the sporulation deficient population we observe in the double mutant (Figure IV.3B).

Moreover, the DNA content within each membrane-bound compartment appeared to vary considerably across the population, such that a portion of cells did not have readily detectable or significantly diminished DAPI signal. In a portion of cells with apparent reduced DNA content we observed partial or flat medial septa (Figure IV.8, yellow carats), suggesting that symmetric division may continue unabated despite chromosome loss. Consistent with this observation, the cell length and compartment size also varied considerably across the population, suggesting that at least a proportion of the medial septa mature to produce physically separated daughter cells (Figure IV.8, yellow arrows and carat).

IV.2.8 Aberrant cell division in Δ*refZ* Δ*noc* mutants result in heterogeneous sigma factor activities

Extra divisions in both the Δ*refZ* Δ*noc* and *RBM*$_{5mu}$ Δ*noc* double mutants were found in cells with one or two distal forespore compartments, the majority of which had successfully activated σ^F. In the mother cell, σ^E activation occurs very shortly after asymmetric division and is dependent on timely σ^F-dependent expression of SpoIIR in the forespore (Xenopoulos and Piggot, 2011). SpoIIR initiates the intercompartmental signal that leads to σ^E activation (Hofmeister et al., 1995; Londono-Vallejo & Straiger,

1995; Karow, Glaser, & Piggot, 1995). Forespore engulfment and dissolution of aberrant septa in the mother cell requires hydrolases transcribed by σ^E in the mother cell (SpoIID-M-P complex)(Eichenberger *et al.*, 2001, Pogliano *et al.*, 1999). Since many cells with aberrant septa exhibited the characteristic rounding up of the forespore membrane associated with engulfment, we hypothesized that σ^E must become activated in one or both of the larger mother cell compartments created by the midcell septum.

In order to test this, we introduced a second fluorescent reporter fused to a σ^E activated promoter, P_{spoIID}-*yfp*, into the strains harboring the σ^F reporter and assessed CFP and YFP fluorescence 3 h following resuspension (Figure IV.9A). At this time, the majority of wild-type cells exhibited both forespore and mother cell fluorescence (not shown), consistent with the previously established timing of σ^F and σ^E activation (Hilbert & Piggot, 2004).

In the Δ*refZ* Δ*noc* double mutant, the largest class of cells exhibited wild-type morphology and reporter activation, consistent with the early to late stages of engulfment. Similar to observations in Figure IV.8, the majority of these cells contained a condensed mother cell chromosome distal to the forespore compartment, which contained either a complete or near complete copy of the second chromosome and an actively engulfing or completely engulfed forespore membrane (Figure IV.9A, white arrows). The remainder of the double mutant population displayed a range of reporter activities associated with aberrant cell division. A large proportion of cells had not activated either reporter, despite the presence of one or more forespore compartments.

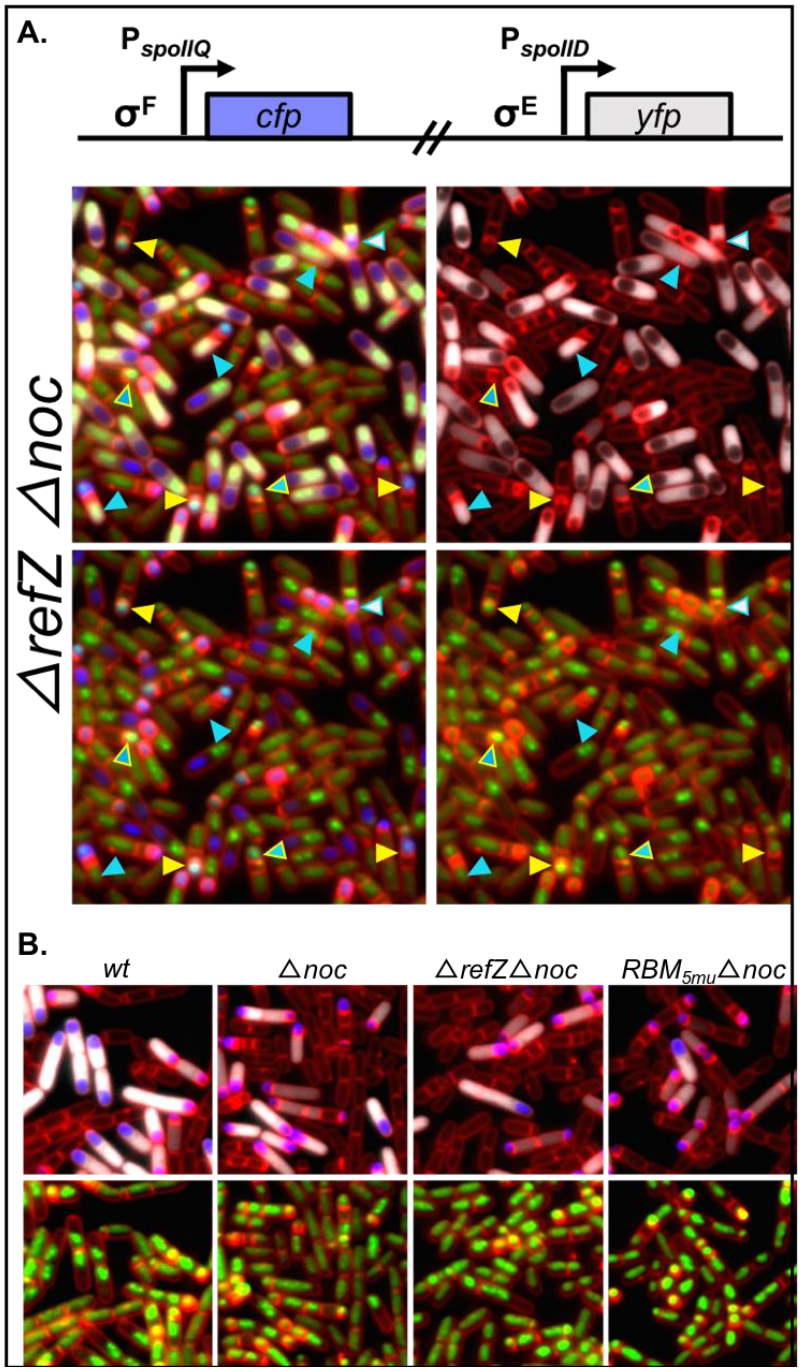

Figure IV.9 Aberrant cell division in Δ*refZ* Δ*noc* mutants result in heterogeneous sigma factor activities.
Sporulating strains carrying fluorescent reporters for σ^F activity (P_{spoIIQ}-*cfp*) and σ^E activity (P_{spoIID}-*yfp*) were examined by fluorescence microscopy (A) 3 h after induction or (B) 1.5 h after induction. Images are overlaid and pseudo-colored: green, DAPI (DNA); red, FM4-64 (membrane); and blue, CFP (P_{spoIIQ}). Indicated are cells with aberrant midcell septa separated by a nucleoid-free compartment from forespores showing σ^F activity either with σ^E activity in a distal compartment (blue carats), in the intervening compartment (blue/white carat), or without (yellow carats). Blue/yellow carats indicate daughter cells that are expected to result from maturation of these aberrant septa.

The majority of cells lacking fluorescence and an asymmetric septum contained a flat septum at midcell, similar to those observed in Figure IV.4 (white carats). In general, the length of cells in these classes were qualitatively shorter than those that had undergone asymmetric division, consistent with the idea that these cells were either severely delayed in polar division or had inappropriately divided at midcell and were blocked in progression to the stage of polar division. For the remaining population lacking both CFP and YFP fluorescence, cells were observed with asymmetric septa at one or both poles generally accompanied by a medial septum. A morphologically similar class in which one or both forespores had activated σ^F were more highly represented in the population (Figure IV.9A, yellow carats). In both classes of cells, the forespore(s) contained DNA while the compartment(s) separating the mother cell and forespore(s) generally did not, or appeared to be in the process of chromosome translocation.

A rare cell type exhibiting otherwise wild-type forespore morphology, with a single rounded polar septum, contained DNA in the forespore but not in the mother cell compartment (Figure IV.9A, blue/yellow carat). CFP fluorescence was not detected in this particular forespore, but on closer examination of the double mutant population, we did observe similar numbers of these rare cells in which σ^F activation had occurred in the forespore. The most likely explanation for this class is that they were generated from the aberrant cell types described above, in which the septation event at midcell is followed by complete separation of daughter cell walls. This reasoning is in line with

our initial hypothesis that cell division events are not appropriately regulated in the absence of NO and the RefZ-*RBM* systems.

The majority of cells with an aberrant midcell septum and one or both asymmetric septa expressed CFP in at least one of the forespores. YFP expression was almost never detected in mother cell compartments in cells with forespores at both poles, regardless if one or both had successfully activated σ^F, likely due to the absence of DNA from these compartments. In contrast, cells with a medial septum and one forespore expressing CFP displayed YFP expression in various compartments (Figure IV.79, yellow and blue carats). We were surprised to find that only a sub-class of these cells had successfully activated σ^E in the compartment sharing a membrane with the forespore expressing CFP (Figure IV.9A, white/blue carat). Instead, the majority of these cells displayed YFP fluorescence exclusively in the forespore-distal compartment (Figure IV.79, blue carats). Although rare, we did observe a sub-class in which YFP expression was detected in the forespore even though no CFP fluorescence was detected in any compartment (Figure IV.79, blue/yellow carat).

These observations are striking considering that the time-scale between σ^F activation in the forespore and σ^E activation in the mother would be too short for a midcell septum to form and generate the broad distribution of phenotype classes reported here. Moreover, σ^E activity is responsible for the expression of proteins that inhibit division (MciZ)(Bisson-Filho *et al.*, 2015, Handler *et al.*, 2008) and degrade any partial septa in the mother cell (SpoIID-M-P complex)(Eichenberger *et al.*, 2001, Pogliano *et al.*, 1999). Thus, it is unlikely the block in sporulation caused by the aberrant midcell

divisions is a direct result of impaired activation or compartmentalization of σ^E in the mother cell.

IV.2.9 Midcell divisions occur early in sporulation and produce daughter cells blocked in development

As reasoned above, our observations are most consistent with a block occurring prior to or simultaneous with asymmetric division, such that an aberrant septum is permitted at the non-polar position, and in certain instances matures to produce daughter cells exhibiting a range of morphologies, compartments, and sigma factor activities. In line with this hypothesis, Δ*refZ* Δ*noc* double mutant populations examined earlier in sporulation (1.5 h) also exhibited a range of division-related phenotypes that would be expected to produce the cell type sub-classes we observe later in sporulation (Figure IV.9B). At these earlier times, the irregular DAPI staining and non-uniform cell length was more pronounced, and a portion of cells appeared to contain multiple nucleoids (chromosomes) and were generally longer than those with faint DAPI staining (Figure IV.9B). Aberrant medial septa were also readily observed overlapping the DAPI signal, irrespective of nucleoid content, consistent with the idea that Noc and RefZ are required to mitigate symmetric divisions in sporulating cells.

The non-uniform nucleoid staining we observed in the Δ*refZ* Δ*noc* double mutants might indicate cells contain more or less than the two chromosome copies strictly required for entry into sporulation. Depending on where a cell is in the cycle when Spo0A~P triggers sporulation, additional vegetative cell divisions may be required

to achieve the necessary chromosome copy number. Therefore, we wondered if the division related phenotype of the double mutants stemmed from a failure to coordinate the last rounds of DNA replication initiation and symmetric division when cells initiate sporulation.

To test this, we examined the number and localization of chromosome origins by introducing a short *tetO* operator array close to *oriC* (*-7°*) and a second construct for constitutive TetR-CFP expression into the wild-type and Δ*refZ* and Δ*noc* single mutant backgrounds (Figure IV.10). The majority of wild-type cells harbored two discrete foci overlapping the periphery of a decondensed nucleoid (inferred from DAPI staining), close to or at opposite cell poles, consistent with axial filament formation. In some cells, a partial or complete asymmetric septum was observed in this class (Figure IV.10, yellow carats). Cells exhibiting this phenotype were found at lower frequencies in both single mutant populations, which were qualitatively more heterogeneous with respect to origin copy number and/or foci intensity.

For a large portion of the Δ*refZ* population, origins appeared most like wild-type, with a decondensed nucleoid spanning the cell capped by two foci at or near the pole (Figure IV.10, yellow carats). However, in contrast to wild-type, these, and equivalent foci observed in the Δ*noc* mutant were visibly brighter and/or larger, which typically indicates there are two overlapping foci produced by replication of the origin, and suggests that DNA replication initiation is not being inhibited (Wang *et al.*, 2014, Webb *et al.*, 1997).

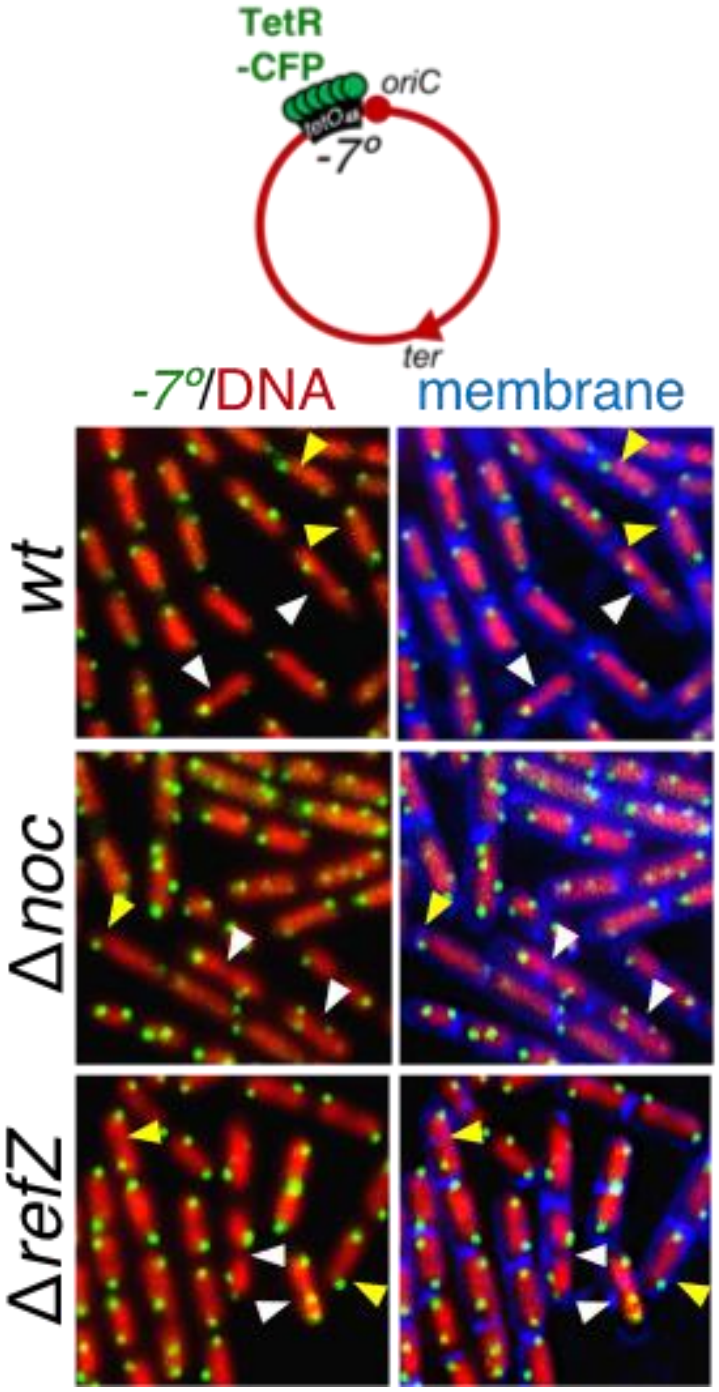

Figure IV.10 Heterogeneous replication activity in sporulating Δ*refZ* and Δ*noc* single mutants.
Chromosome origins (green foci) representing TetR-CFP localized to an array of *tetO* operator sequences inserted at the *-7º* position (cartoon) were examined in the indicated strains 1 h following resuspension in sporulation media. Membranes (FM4-64) and DNA (DAPI) are pseudo-colored blue and red, respectively. Indicated are replicating cells with one bright focus or two foci in close proximity at the center of the nucleoid sometimes seen with with a partial symmetric septum (white carats), and non-replicating cells with dim origin foci at the nucleoid periphery juxtaposed with opposite cell poles sometimes with a partial asymmetric division septum (yellow carats).

Origin firing occurs at the nucleoid periphery but sister origins together with both replication forks relocate to mid-nucleoid and are resolved by SMC condensin complexes before re-segregation back to the edge of the nucleoid (Wang *et al.*, 2014). Consistent with this pattern, a substantial number of the Δ*noc* cells and to a lesser extent the Δ*refZ* mutant cells, contained multiple origin foci and a partial midcell septum (Figure IV.10, white carats), suggesting the final rounds of replication are still ongoing in these cells. In many of these cells, four origins could be resolved at relatively uniform intervals spanning the nucleoid, with two at the distal edges close to the poles and two closely spaced foci near midcell, indicating that the axial filament had formed, but the last symmetric division had not yet occurred (Figure IV.10, blue carats).

A brighter focus was observed at mid-nucleoid in the Δ*noc* mutant, often in shorter cells in which the nucleoid was highly condensed and occupied a central region, in agreement with the idea that replication initiation is not appropriately attenuated in the absence of *noc*. Although similar instances were found in Δ*refZ* mutant cells, the proportion was intermediate between the wild-type and Δ*noc* mutant, suggesting if the large bright polar foci described above are in fact two newly replicated origins, then they are not migrating to mid-nucleoid with the normal timing or to the same degree as is expected in actively replicating cells.

In some Δ*noc* mutant cells with only two origins resolved, we found that they were not uniformly spaced within the confines of the nucleoid, nor were nucleoids sufficiently localized at the far cell poles (Figure IV.10, white arrows), suggesting that origin and/or bulk chromosome segregation may be affected in the absence of *noc*. In

contrast, wild-type and Δ*refZ* mutant cells with poorly segregated origins were associated with nucleoids that were de-condensed and occupied a larger volume of the cell. Intriguingly, throughout the course of experiments described in the text we consistently observed DAPI staining to be more intense in Δ*refZ* mutant (and RBM_{5mu}) cells compared to wild-type cells, whereas the opposite was true for Δ*noc* mutant cells, in which DAPI staining was noticeably reduced compared to wild-type. While possible, these differences are not likely caused by variations in sample preparation, as they were regularly encountered when attempting to normalize fluorescence across images for different strains taken during the same trial.

These results indicate that the loss of either *refZ* or *noc* imposes moderately negative consequences on origin segregation. Standing alone, these consequences would not be expected to significantly interfere with the progression of sporulation. However, in the case of Noc, the chromosome segregation defect could reasonably account for much of the >50% reduction in sporulation efficiency of the Δ*noc* mutant (Figure IV.3B). That we observed origin segregation defects in each single mutant, but inverse nucleoid condensation phenotypes, raises the possibility that Noc and RefZ have opposing effects on chromosome organization. This hypothesis is consistent with the inverse expression levels for *noc* and *refZ* in cells initiating development (Nicolas *et al.*, 2012).

IV.3 MATERIALS AND METHODS

IV.3.1 General methods

Strains, plasmids, and oligonucleotides are listed in APPENDIX C, Tables C.1, C.2, and C.3, respectively. Strain and plasmid construction is detailed in APPENDIX C. *Bacillus subtilis* strains were derived from *B. subtilis* 168 or PY79 (Youngman *et al.*, 1983). Transformations in *Bacillus* were carried out using a standard protocol as previously described (Harwood, 1990) unless otherwise stated. For selection in *B. subtilis*, antibiotics were included at the following concentrations: 100 µg ml-1 spectinomycin, 7.5 µg ml-1 chloramphenicol, 10 µg ml-1 kanamycin, 10 µg ml-1 tetracycline, 0.8 µg ml-1 phleomycin, and 1 µg ml-1 erythromycin (erm) plus 25 µg ml-1 lincomycin (MLS). All *B. subtilis* transformations and strains were grown on plates at 30°C overnight, unless otherwise stated. *B. subtilis* strains were propagated for cryostorage in Lysogeny broth (LB-Lennox) in a room temperature rollerdrum overnight. For transformation and selection in *E. coli*, antibiotics were included at the following concentrations: 100 µg ml-1 ampicillin and 25 µg ml-1 kanamycin. Co-transformations for bacterial 2-hybrid assays were selected for on LB plates supplemented with 50 µg ml-1 ampicillin, 25 µg ml-1 kanamycin, and 0.2% (v/v) glucose. For FROS experiments anhydrotetracycline (aTC) was added to 1X concentration final on plates and in all cultures prior to resuspension to prevent loss of the *tetO* array.

IV.3.2 Plate-based LacZ sporulation assay

For the spot plate sporulation assay with *rLOF noc* double mutants, isolated colonies were used to inoculate 4 ml of DSM broth and cultures were grown at 37°C in a roller drum to mid-log phase, at which point samples from each were normalized to the lowest recorded culture OD_{600} in 1X dilution media and 5 µl from each were spotted on DSM agar plates supplemented with 40 µg ml^{-1} X-gal. Spot plates were grown overnight at 37°C prior to imaging with a ScanJet G4050 flatbed scanner (Hewlett Packard) using VueScan software and medium format mode. Images were processed using Adobe Photoshop (version 12.0) and ImageJ64 (Rasband, 1997-2014).

IV.3.3 Heat kill assay

Strains BAM325, 1295, BJH205, and BJH255 were streaked from frozen glycerol stocks on LB agar plates and grown overnight at 37°C. A single colony was used to inoculate 2 ml of Difco sporulation medium (DSM) (Schaeffer *et al.*, 1965) and cultures were placed in a roller drum (60 rpm) at 37°C for 40 h. Prior to heat treatment, cultures were vortexed vigorously and 100 µL (10^0) of each was serially diluted (10^{-1}, 10^{-2}, $10^{-3,}$ 10^{-4}, 10^{-5}, 10^{-6}) in 900 µL of 1X dilution media and 100 µL was plated on freshly poured DSM agar plates. Serial dilutions were then subjected to heat treatment at 80°C for 20 min, allowed to cool, and 100 µL were plated on DSM agar plates. All plates were incubated at 37°C overnight, and the next day individual colonies were counted to determine the number of CFU per milliliter and the number of heat-resistant spores per milliliter. Relative sporulation efficiencies of the mutant strains compared to

the wild-type control were determined by dividing the number of spores per CFU for each strain by the number of wildtype spores per CFU. The average sporulation efficiency of each mutant compared to wildtype is represented in Figure IV.1C as an average of two independent biological replicates.

IV.3.4 Fluorescence microscopy

For microscopy experiments, isolated colonies were used to inoculate 5 ml CH complete media and cultures were grown overnight at room temperature in a rollerdrum. Exponentially growing overnight cultures were used to inoculate 25 ml CH medium in 250 ml baffled flasks to a calculated OD_{600} of 0.018 and cultures were grown at 37°C in a shaking waterbath at 280 rpm for the indicated times before samples were collected. Three-hundred to 500 µL samples were harvested at 6,010 x *g* for 1 min in a tabletop microcentrifuge. Supernatants were aspirated and pellets were resuspended in 3-5 µL of 1X PBS containing either 0.02 mM 1-(4-(trimethylamino) phenyl)-6-phenylhexa-1,3,5-triene (TMA-DPH) (Life Technologies), or FM4-64 membrane stain (3 µg ml-1) (Life Technologies) plus DAPI DNA stain (2 µg ml-1) (Life Technologies). Cells were mounted on glass slides with polylysine-treated coverslips. Images were captured with NIS Elements Advanced Research (version 4.10) software, using 1 s (CFP, GFP and TMA), 900 ms (YFP), 300 ms (DAPI), and 700 ms (FM4-64) exposure times on a Nikon Ti-E microscope equipped with a CFI Plan Apo lambda DM 100X objective, a Prior Scientific Lumen 200 Illumination system, C-FL UV-2E/C DAPI, C-FL YFP HC HISN

Zero Shift, and C-FL Cyan GFP filter cubes, and a CoolSNAP HQ2 monochrome camera. Images were analyzed with ImageJ64 (Rasband, 1997-2014).

IV.3.5 Quantitation of sporulation septa

Fluorescence microscopy was performed on wild-type and mutant cells as described previously (Doan *et al.*, 2005) using a Nikon Eclipse Ti inverted microscope and NIS Elements software. Membranes were stained with TMA-DPH (0.02mM) and imaged with 500 ms exposure time. GFP images were captured with 500 ms exposure. Images were analyzed using Metamorph v6.1 software (Molecular Devices). Only cells expressing P_{spoIIE}-*gfp* and possessing at least one polar flat or curved polar septa were counted. Cells possessing one polar septum (flat or curved), two polar septa (flat or curved), and two polar septa (flat or curved) with a mid-cell septum were considered Class I. The Class II cells were considered if they possessed at least one polar septum (flat or curved) and one or more mid-cell septa.

IV.3.6 rLOF-GFP localization during sporulation

Plasmids harboring C-terminal translational fusions of either wild-type *refZ* or *rLOF* mutants to *gfp* were introduced into a markerless *refZ* deletion strains (BAM15 by single crossover fused to Cultures were sampled 60 min, 80 min, and 120 min following resuspension and LOF-GFP localization was examined by fluorescence microscopy. Membranes were stained with TMA and are false-colored red in overlaid

images with the GFP channel, false-colored green ("Membrane"). GFP signal was normalized in images obtained from a single experiment.

CHAPTER V

CONCLUSIONS

In the early stages of spore formation, intersecting activities of vegetative and sporulation-specific proteins, with seemingly redundant and/or overlapping functions, coordinate a series of necessary changes that impact DNA replication, chromosome segregation, and cell division. In addition, the activities of certain proteins switches between growth and sporulation. For instance, DivIVA targets the FtsZ-inhibitory activity of the Min system both to nascent division septa and to the far poles (old septa) in vegetative cells (Eswaramoorthy *et al.*, 2011, Gregory *et al.*, 2008, van Baarle & Bramkamp, 2010). During sporulation, DivIVA's critical role is to provide the membrane anchor for the two dominant chromosome organization systems, RacA-*ram* and Soj-Spo0J-*parS* (Thomaides *et al.*, 2001, Ben-Yehuda *et al.*, 2003, Wu & Errington, 2003, Kloosterman *et al.*, 2016). DivIVA is also required for activation of the first forespore-specific sigma factor though its activity maintaining SpoIIE at the polar septum during polar septation (Eswaramoorthy *et al.*, 2014, Bradshaw & Losick, 2015).

During spore formation, *B. subtilis* divides at the pole instead of medially, when the midcell Z-ring is repositioned to both cell quarters through a helical intermediate composed of spiral-like arcs and foci which spreads along the cell circumference (Ben-Yehuda & Losick, 2002). Z-ring shifting requires Spo0A-dependent expression of SpoIIE, and increased expression of FtsAZ (Ben-Yehuda & Losick, 2002). The TetR family DNA binding protein, RefZ (Regulator of FtsZ), also functions to promote the

shift from midcell to polar division (Wagner-Herman *et al.*, 2012). A role for RefZ in moderating cell division was hypothesized following the observation that a *refZ* mutant caused a delay Z-ring shifting (Wagner-Herman *et al.*, 2012). Consistent with this hypothesis, artificially expressing RefZ in vegetative cells disrupts midcell Z-ring formation and FtsZ-GFP localizes as similar spiral, arcs, and foci (Wagner-Herman *et al.*, 2012).

In this thesis, we show that RefZ and its five cognate binding sites, the *RBM*s, are conserved across *Bacillus* and are required for precise capture of DNA in the forespore at the time of asymmetric septation. The *RBM*s are symmetrically arranged on the chromosome with respect to *oriC* and their positions correlate with the boundaries of the region captured by the polar septum (Figure II.1A)(Miller *et al.*, 2016), which is reproducibly captured with a high degree of specificity (Sullivan *et al.*, 2009, Wu & Errington, 1998). The polar localization of the *RBM*s and RefZ-GFP early in sporulation, when the axial filament forms, is consistent with their location near *oriC* (Chapter II, Figure II.6)(Wagner-Herman *et al.*, 2012). Operator arrays inserted near the left and right arm *RBM*s are localized in the polar division plane in 91% septating cells and localization of these arrays to the division plane is not significantly affected in the absence of *refZ* or the five *RBM*s (Figure II.6D and E, respectively)(Miller *et al.*, 2016), consistent with our observations that origin anchoring and structuring of the axial filament by Soj and RacA systems are likely dominant factors determining the overall organization of the chromosome and, subsequently, the position of the *RBM*s.

Furthermore, we find that RefZ's role in capturing the chromosome requires its ability to inhibit cell division following misexpressing during growth (Chapter III), indicating that the mechanism by which RefZ controls left and right arm capture may be to tune the placement of the sporulation septum rather than modify chromosome organization. In support of this idea, we identify a novel sporulation-specific role for the nucleoid occlusion protein, Noc, in preventing aberrant midcell division events in conjunction with RefZ. We further demonstrate that RefZ's role in chromosome capture and its redundant function with Noc depend both on the *oriC*-proximal *RBM*s and on RefZ's ability to affect cell division.

V.1 REFZ-*RBM* COMPLEXES PROMOTE PRECISE CAPTURE THROUGH MODULATION OF CELL DIVISION

V.1.1 Sub-cellular positioning of the *RBM*s and dynamic RefZ localization

In *RBM* co-localization experiments using FROS (Fluorescent Repressor Operator System) to monitor the position of RBM_{L2} and either right arm *RBM*s, we often observe a single *RBM* localized near the far pole, on the forespore side of the developing septum, and the second *RBM* in the plane of the septum (Figure V.1C, pink carats). While we do not yet know whether this "in-on" arrangement of *RBM*s is significant, it is observed qualitatively at a higher frequency than arrangements where both sites are localized exclusively in the forespore or in the mother cell. The "in-on" arrangement of the arm *RBM*s is consistent with RefZ-GFP localization to distinct polar and sub-polar positions in predivisional and septating cells early in sporulation (Figure IV.2 and IV.7,

blue and purple carats, respectively) (Wagner-Herman *et al.*, 2012). RefZ-GFP also becomes localized to midcell, as a bright focus, a short time later. Neither of the DNA-binding deficient variants, Y43A or E107A, exhibit polar foci; however, only E107A is capable of producing the midcell focus (Wagner-Herman *et al.*, 2012), suggesting that DNA-binding activity is not a strict requirement in RefZ's redistribution to midcell. Moreover, mutations in either the degenerate *ter*-proximal *RBM* site, the five *oriC*-proximal sites, or all six sites were not sufficient to abolish midcell foci (Figure IV.2), indicating that the requirements for polar and midcell RefZ-GFP focus formation are not the same.

In contrast to Y43A and E107A, we find that the ten rLOF variants that still bind the *RBM*s support both polar localization and midcell focus formation, consistent with a hypothesis that the polar foci represent RefZ in its *RBM*-bound state (Figure IV.1). In line with this idea, polar foci were not detectable in the majority of *RBM* mutant cells when we assessed RefZ-GFP localization in the RBM_{5mu} background; however, extreme polar foci were not completely abolished, and sub-polar foci were sometimes observed (Figure IV.2 and IV.7, blue and purple carats, respectively).

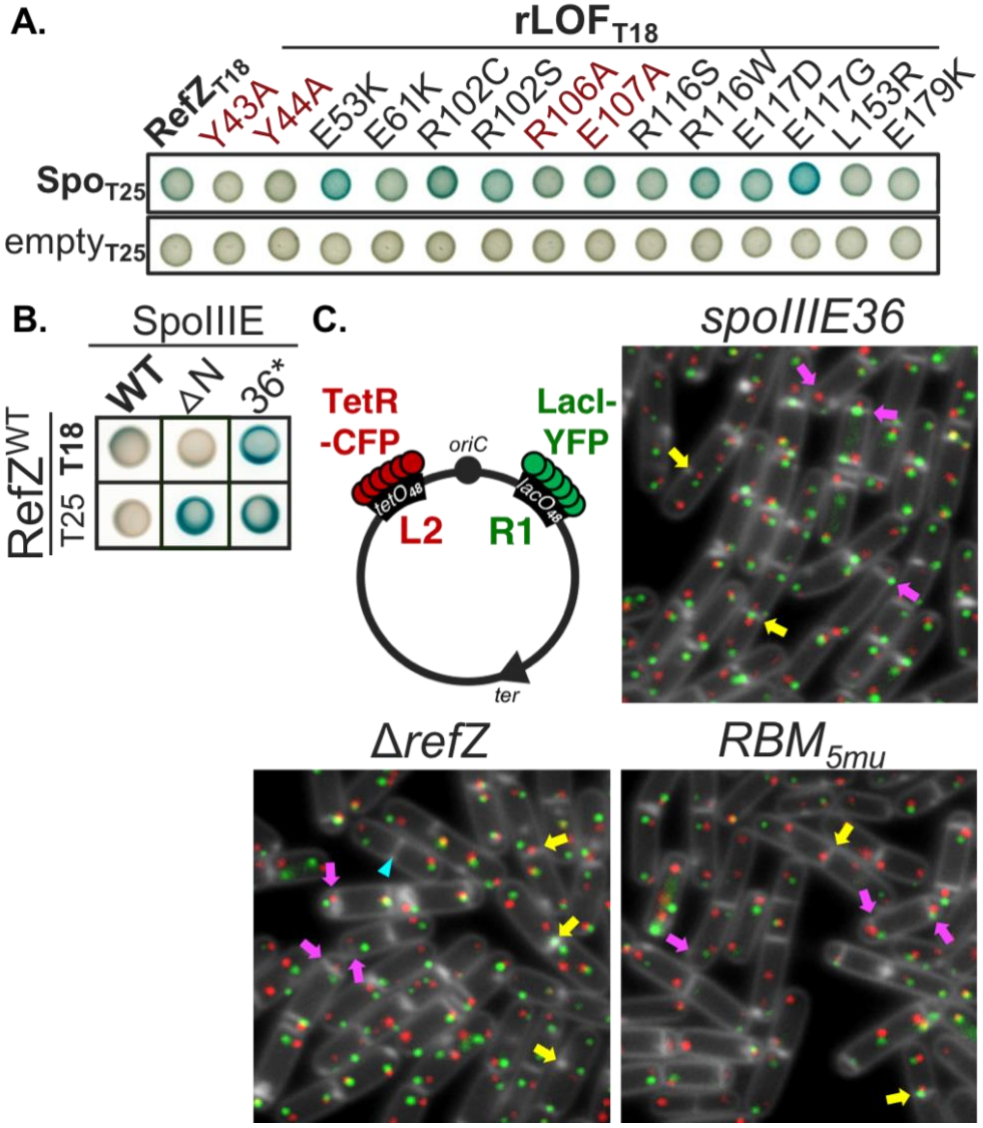

Figure V.1 Evidence for a physiological function for the RefZ-SpoIIIE interaction.
(A) Bacterial 2-hybrid (B2H) assay testing for interactions between rLOF variants and SpoIIIE. *E. coli* (*cya*-) cells were co-transformed with equal amounts of plasmids harboring the indicated variants fused to the T18 portion of adenylate cyclase and either an empty T25 vector control or the SpoIIIE-T25 fusion. Cultures for spot plates were prepared as described in Chapter III.4, Methods). M9 minimal plates supplemented with glucose, antibiotics, IPTG (250 μM) and X-gal (40 μg ml^{-1}). Plates were growth for 41 h at room temperature before imaging. **(B)** B2H assay to test for interactions between wild-type RefZ with C-terminal T18 or T25 tags and SpoIIIE variants, ΔN (truncation of the transmembrane domain) and 36* (translocase dead mutant). RefZ does not show a reproducible interaction with SpoIIE (WT) when fused to T25, but exhibits gain-of-interaction if WT is replaced with either variant. **(C)** Co-localization of the *L2* and *R1 RBM* regions in the *spoIIIE36* mutant in the presence or absence of *refZ* and the *RBM*s. Strains carry *tetO* and *lacO* operator arrays inserted close to the *L2* and *R1* sites, respectively, and constitutively expressed TetR-CFP (false-colored red) and LacI-YFP (false-colored green). Samples were taken from sporulating cells 75 min after resuspension. Membranes were stained with TMA-DPH (white). Indicated are midcell septa that form on top or immediately adjacent to an *RBM* (yellow arrows) and partial or complete asymmetric septa with one *RBM* captured in the forespore and the second in the plane of the incipient division septum (pink arrows). The blue carat indicates a midcell septum in a cell with only two chromosomes; based on the intensity of the foci, this cell does not appear to have initiated replication and would be considered aberrant.

Distinct polar and sub-polar foci are also observed when RefZ-GFP is artificially expressed in vegetative cells, both mutant and wild-type for the *RBM*s, at levels that do not inhibit cell division (Figure V.2, yellow and white carats, respectively). In a wild-type background, RefZ-GFP co-localizes with the nucleoid, predominantly as patches, and a proportion of cells exhibit a distinctly brighter focus at the nucleoid periphery (Figure V.1, white carats). Extreme polar foci are also observed at the junctions in between chained cells and are readily distinguished from the nucleoid-associated sub-polar foci (Figure V.1, yellow and white carats, respectively). As in sporulation, both classes of polar foci were found in an RBM_{5mu} background, albeit less frequently, raising the possibility that additional *RBM*-independent interactions might play a role in or be sufficient for localization of RefZ to the poles.

V.1.2 Evidence of an *RBM*-independent target for RefZ localization

The ChIP-seq experiments were performed using an anti-GFP antibody against a RefZ-GFP fusion that is only partially functional in its ability to inhibit cell division when artificially expressed during growth (Wagner-Herman *et al.*, 2012). While evidence presented throughout this thesis agree with prior conclusions that RefZ binds the five *oriC*-proximal *RBM*s specifically (Wagner-Herman *et al.*, 2012), we cannot eliminate the possibility that RefZ binds at additional sites during sporulation. It's also possible that the absence of *RBM*s, combined with the reduced functionality of the fusion, promotes an associate between RefZ and such alternative sites.

One possible explanation for why we detect polar foci in a number of *RBM* mutant cells is that RefZ-GFP fusions still bind the mutant sites, perhaps with decreased specificity or affinity (Figure IV.2 and V.2). In line with this hypothesis, we observe a degree of non-specific binding *in vitro* (laddering and smearing in EMSAs) when purified RefZ-His6 is incubated with a DNA probe centered on a mutant *RBM* sequence (Figure III.8), and this phenotype was accentuated when gels were run at higher voltages (Figure III.9A).

To test this, ChIP-seq using an anti-GFP antibody could be performed against sporulating cultures expressing RefZ-GFP, both in an RBM_{5mu} and a wild-type *B. subtilis* 168 background (original ChIP was done in strains of the PY79 background). To determine where RefZ is bound on the chromosome during vegetative growth, ChIP-seq could additionally be performed on cells artificially inducing RefZ-GFP at levels similar to those detected in cells harvested early in sporulation (Wagner-Herman *et al.*, 2012). Intriguingly, and for unknown reasons, RefZ-GFP does not produce a midcell focus under these conditions (Figure V.2), nor when induced with maximal concentrations of IPTG (Wagner-Herman *et al.*, 2012).

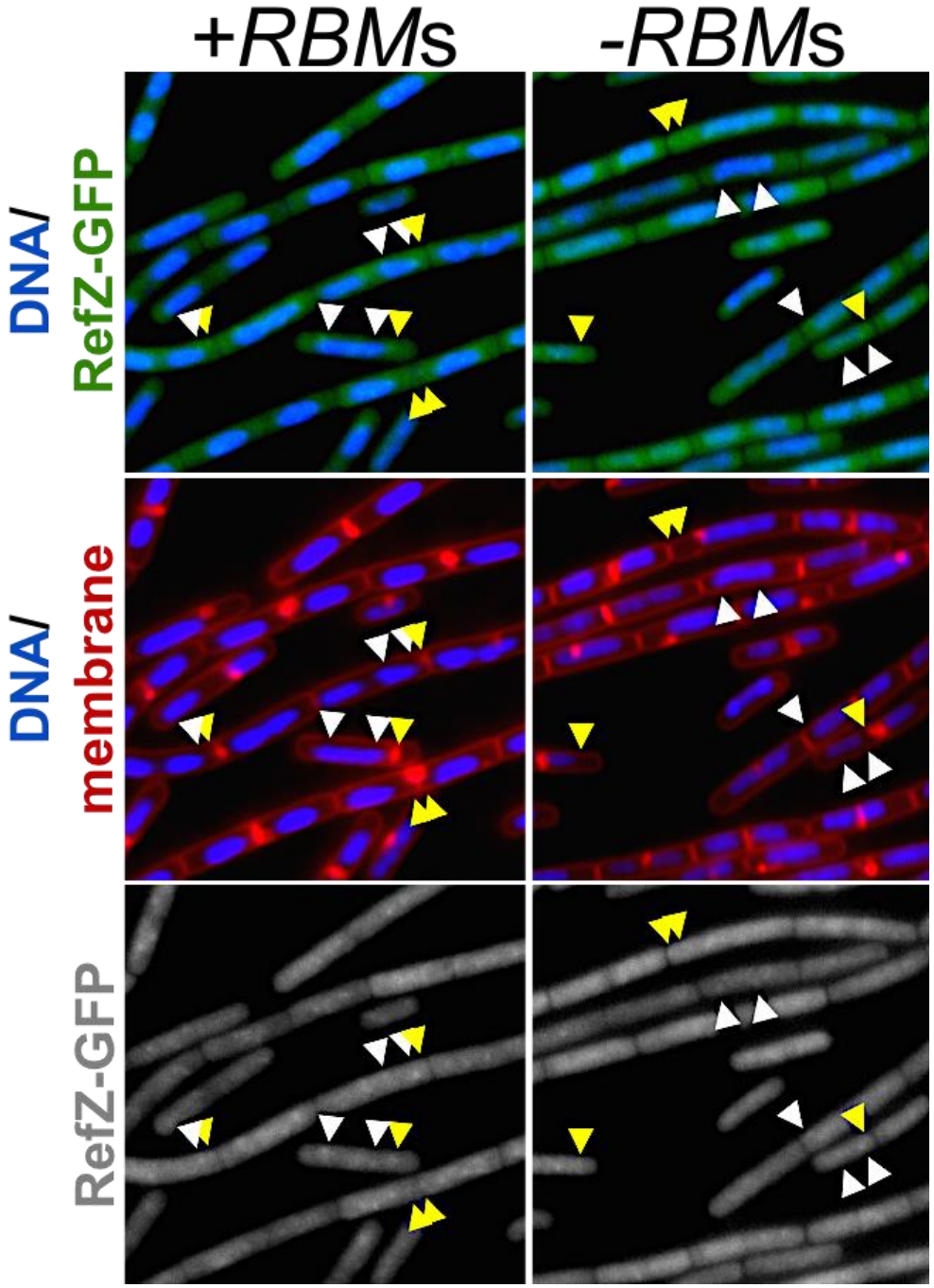

Figure V.2 Sub-inhibitory levels of RefZ in vegetative cells perturbs nucleoid condensation in an *RBM*-dependent manner.
Wild-type or RBM_{5mu} cells harboring an inducible copy of *refZ-gfp* at an ectopic locus (*amyE*) were grown in CH medium to mid-log before induction with 10 µM IPTG. Cultures were growth for 1 h before samples were imaged for GFP (green or B&W), DAPI (DNA, blue), and FM4-64 (membrane, red). GFP and DAPI fluorescence is normalized between all images. Indicated are polar foci that associate with division septa and do not overlap DNA signal (yellow carats) or sub-polar foci that overlap with or associate at the distal edges of the nucleoid (white carats). Nucleoid as appear less condensed in the absence of *RBM*s, as inferred from DAPI staining.

In the ChIP-seq experiments RefZ-GFP was observed to be enriched at additional regions near the origin, overlapping with some of Spo0J's binding sites. These broad flat peaks were reduced in enrichment compared to those corresponding to the five, short *RBM*s (Wagner-Herman *et al.*, 2012). One interpretation for RefZ's enrichment in these regions is that it's capable of spreading along the DNA. Alternatively, or additionally, RefZ could be interacting with a protein like Spo0J, which itself spreads along DNA from its cognate *parS* sites (Murray *et al.*, 2006, Breier & Grossman, 2007). It would be interesting to see whether RefZ is similarly enriched in these regions when artificially expressed in vegetative cells, particularly since Spo0J functions during growth.

Future experiments examining co-localization of RefZ and divisome or septum-associated proteins, or assessing RefZ's localization in their absence are also of interest, and could provide valuable insight into how RefZ's dynamic positioning correlates with the well characterized timing of divisome assembly (Gamba *et al.*, 2009). To our knowledge, neither the early or late arriving divisome proteins have been reported to adopt a midcell localization during sporulation, though it is not clear whether this has been extensively studied. Such protein(s) could potentially interact with RefZ, in which case they would be prime candidates for localizing and/or stabilizing RefZ at midcell as sporulation progresses (Wagner-Herman *et al.*, 2012).

V.1.3 Potential targets of RefZ's division regulation activity

The observation of regularly spaced membrane-associated FtsZ-GFP foci in shifting intermediates and when RefZ is artificially expressed (Wagner-Herman *et al.*,

2012), suggests that RefZ does not interfere with the ability of FtsZ (or FtsA) to localize at potential division sites. FtsZ-GFP localizes as filament-like arcs and spirals during artificial RefZ expression, suggesting that Z-ring assembly may be disrupted downstream of protofilament formation. In this way, RefZ may inhibit further polymerization of existing FtsZ protofilaments, or possibly interfere with their stability or bundling. For instance, RefZ might act as a negative regulator of cell division by altering the critical concentration of FtsZ required to assemble a Z-ring at any one location, similar to EzrA (Haeusser *et al.*, 2004, Levin *et al.*, 1999).

Using multiple methods, including bacterial 2-hybrid assays, we find no evidence for a direct interaction between RefZ and FtsZ (Chapter III, Figure III.13)(Brown *et al.*, 2019). Due to RefZ's decreased solubility in a number of buffers, we have not been unable to identify suitable conditions to assess interaction using *in vitro* assays, similar to those used for characterized FtsZ regulators like SlmA (Cho *et al.*, 2011), EzrA (Haeusser *et al.*, 2004, Levin *et al.*, 1999, Singh *et al.*, 2007), MinC (Blasios *et al.*, 2013), and MciZ (Bisson-Filho *et al.*, 2015, Handler *et al.*, 2008). This might suggest RefZ regulates Z-ring assembly indirectly, possibly through interaction(s) with other septum or divisome-associated proteins. So far, bacterial 2-hybrid assays have not shown positive interactions between RefZ and the divisome proteins EzrA and MinD, or the nucleoid occlusion protein, Noc (data not shown)(Chapter II.5, Discussion).

V.1.3.1 A role for RefZ-RBM complexes in forespore-specific SpoIIIE assembly during septation

We did detect a positive interaction between RefZ and the DNA translocase, SpoIIIE, by bacterial 2-hybrid (Figure II.7). Only one combination of adenylate cyclase fusions, RefZ-T18 and SpoIIIE-T25, produced a detectable and reproducible positive interaction. In contrast, no combination of RefZ and a second FtsK/SpoIIIE ATPase family protein from *B. subtilis*, SftA (El Najjar *et al.*, 2018, Kaimer *et al.*, 2009), produced a positive interaction suggesting that the RefZ-SpoIIIE interaction is specific (Figure II.7). This is supported by observation that the SpoIIIE36 "translocase dead" variant (36*)(Besprozvannaya *et al.*, 2014), exhibits a gain-of-interaction (GOI) with RefZ (Figure V.1B) both in the permissive combination and in a second combination where tags were swapped. Moreover, we found that removing the first 185 aa encoding the transmembrane segment (ΔN) also supported GOI with RefZ in the reverse tag combination. For unknown reasons, the ΔN variant is loss-of-interaction in the permissive combination (Figure V.1B).

We also find that all ten of the DNA-binding proficient rLOF variants exhibit a positive interaction with SpoIIIE similar to or greater than what is observed for wild-type RefZ (Figure V.1A). We also observe a positive interaction similar to wildtype for two of the four DNA-binding deficient variants, R106A and E107A, which harbor alanine substitutions at two charged residues highly conserved in *Bacillus* RefZ homologs (Wagner-Herman *et al*., 2012). In contrast, neither Y43A or Y44A support

interaction with SpoIIIE, suggesting that the DNA recognition domain might be critical for interaction with SpoIIIE *in vivo*.

Considering RefZ and the *oriC*-proximal *RBM*s localize in the plane of division in a large proportion of sporulating cells (Figure II.6, Figure V.1C) and that SpoIIIE localizes at the leading edge of the septum, assembling as two hexameric channels around each DNA duplex at or in close proximity to the region trapped (Sharp & Pogliano, 1999, Wu & Errington, 1997), RefZ-*RBM* complexes are in a prime position to interact with SpoIIIE *in vivo*. The B2H results provide substantial evidence for an *in vivo* RefZ-SpoIIIE interaction, and invoke the interesting possibility that the RefZ-SpoIIIE interaction may be relevant to creating or sensing the state of chromosome organization at the time of polar septation.

One speculation is that RefZ-*RBM* complexes on either side of the division plane could help direct SpoIIIE assembly into "coaxial-paired channels" (Yen Shin *et al.*, 2015) (Figure V.3). SpoIIIE was shown to assemble as two complexes, one in the forespore membrane and one in the mother cell membrane. These complexes create a pore large enough to accommodate a single duplex of DNA and function as seals between the two membranes until fission. SpoIIIE has also been described an exporter of DNA, directionally translocating the chromosome into the compartment (or cell) that initially contains the origin (Becker & Pogliano, 2007, Ptacin *et al.*, 2008, Sharp & Pogliano, 2002). The ability of SpoIIIE to translocate aberrantly trapped chromosomes out of the forespore would be important in situations where chromosome organization and/or origin segregation is perturbed, such as in Δ*racA* Δ*soj* or *divIVA* mutants that fail

to capture *oriC* (but not the arm regions)(Kloosterman *et al*., 2016, Wu & Errington, 2003). Here, the second division site at the distal pole is utilized (within a span of 10 min (Pogliano *et al.*, 1999)); consequently, any portion of the chromosome initially trapped needs to be segregated out of the forespore and back into the mother cell (Becker & Pogliano, 2007, Ptacin *et al.*, 2008, Sharp & Pogliano, 2002, Yen Shin *et al.*, 2015).

While RefZ does not appear to be required for pumping or normal SpoIIIE activity, only the mother cell SpoIIIE assemblies are required for translocation in the forespore (Yen Shin *et al.*, 2015). As such, RefZ could contribute to forespore-specific assembly of SpoIIIE in rare cases where wild-type cells do not capture the origin. We further speculate that this impaired chromosome orientation could be communicated to the septum by the presence of a RefZ-RBM_O complex in the mother cell. One way to test this would be to use a FROS specific to the region near the RBM_O site in mutants that are defective in *oriC* capture and monitor co-localization of the origin site and SpoIIIE-GFP over short intervals or using time-lapse microscopy, in both the presence and absence of RefZ; however, much higher resolution microscopy techniques (Fiche *et al.*, 2013, Yen Shin *et al.*, 2015) are likely necessary to accurately distinguish the fine localization of these foci.

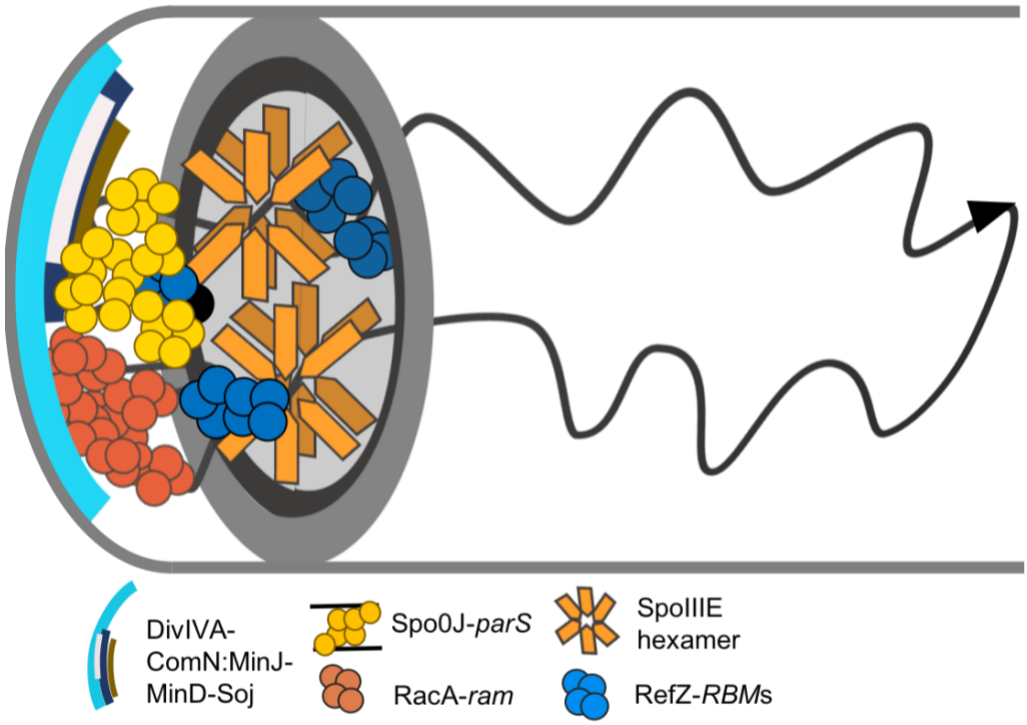

Figure V.3 A model for RefZ-*RBM* complex-mediated positioning of forespore and mother cell SpoIIIE assembly.

V.2.1 RefZ and Noc act redundantly to prevent aberrant midcell divisions

SpoIIIE expression is constitutive, but it is only required under conditions in which the nucleoid becomes bisected by the division septum (Sharpe & Errington, 1995). The nucleoid occlusion protein of *B. subtilis*, Noc, is present during vegetative growth and sporulation (Sievers *et al.*, 2002), and is the cell's primary means of protection from nucleoid bisection. Thus, the function of SpoIIIE outside of sporulation generally occurs when Noc fails to prevent division over the chromosome. Noc becomes required under conditions that interfere with cell cycle coordination, such as when DNA

replication is inhibited (Wu & Errington, 2004), when cell division or elongation is blocked (Wu & Errington, 2004, Biller & Burkholder, 2009), or when chromosome organization (Britton & Grossman, 1999) or segregation is impaired (Biller & Burkholder, 2009). Without Noc, cells experiencing these stresses divide more frequently over their DNA.

The same series of genetic and morphological changes that occur within the cell cycle when cells initiate sporulation are strikingly similar to cell cycle perturbations that make Noc conditionally essential. Intriguingly, we find that Noc function is still required in some respect during the initial stages of sporulation, as deletion of *noc* impairs spore production over 50% (Figure IV.3B). When *refZ* or the *RBM*s were deleted or mutated, respectively, in addition to *noc*, spore production decreased an additional 2-fold, indicating that RefZ-*RBM* complexes are required for efficient sporulation in cells lacking Noc (Figure IV.3B). These findings indicate that loss of both proteins impairs sporulation through in distinct pathways.

The primary reason for the sporulation defect of the double mutants appears to result from a collective failure to moderate division site selection. We show that a substantial proportion of the Δ*refZ* Δ*noc* and RBM_{5mu} Δ*noc* double mutants contain aberrant midcell septa (Figure IV.5A). In contrast, aberrant divisions are significantly less frequent in cells of the single mutants, indicating that RefZ-*RBM* complexes and Noc act redundantly to prevent divisions at midcell during sporulation. Consistent with this, qualitatively similar proportions of aberrant midcell septa were observed in *rLOF* mutants lacking *noc* (Figure IV.6B), and these double mutants were also defective in

sporulation progression (Figure IV.6A). In contrast, deletion of *ezrA*, *sepF*, and *minD*, division regulators conditionally essential in absence of Noc, did not result in comparable division phenotypes in a *refZ* or *RBM* mutant background (Figure IV.5B). In addition, the division phenotypes we did observe appeared to depend predominantly on the regulator rather than on RefZ. Together, these observations define a specific role for Noc in regulating midcell division events during sporulation.

V.2 MODELS FOR DYNAMIC LOCALIZATION OF REFZ FUNCTION DURING SPORULATION

Collectively, experiments described in this thesis were aimed at delineating between RefZ's putative functions during sporulation and our data underscore previous models that incorporate RefZ's dynamic localization early in development. When sporulation is initiated, RefZ binds to the five *RBM* sites in the *oriC*-proximal region of chromosome, which becomes positioned near the cell poles following origin anchoring by Soj-Spo0J-*parS* and RacA-*ram* (Figure IV.4 and Figure V.5). Specific binding at the five 20-bp sites may lead to formation of even higher-order oligomers as a result of cooperative subunit interactions and in response to increasing levels of *refZ* expression (Fujita *et al.*, 2005). At this point, RefZ may also spread along adjacent DNA, consistent with the broad enrichment peaks identified by ChIP-seq (Wagner-Herman *et al*., 2012). RefZ may also form *RBM*-independent interactions with divisome- and septum-associated proteins, such as SpoIIIE, that contribute to stabilizing RefZ in the division plane and/or at the extreme poles.

From its position at the *RBM*s, RefZ modulates division to exact precise capture of the forespore chromosome, either through direct interaction with FtsZ or indirectly through interaction with a divisome-associated protein. In the first model, RefZ functions as an activator of asymmetric division, promoting septum formation, and possibly SpoIIIE assembly (Figure V.3), over the precise chromosome region. In the second model, RefZ acts as an inhibitor of polar division, possibly acting as a checkpoint to coordinate the timing of division with chromosome segregation and/or axial filament formation. As sporulation progresses, RefZ becomes positioned at midcell in a DNA binding- and *RBM*-independent manner (Figure IV.1 and IV.2)(Wagner-Herman *et al*., 2012). We propose that upon saturation of the *RBM*s or, alternatively, upon organization of the chromosome origin, structuring of the axial filament, or upon association with an accessory divisome protein, such as SpoIIIE (all possible mechanisms for driving RefZ from the poles), RefZ may be released from its polar position and redistribute to the midcell site (Figure V.5). Midcell RefZ may also modulate cell division, through a mechanism distinct from the mode of regulation at the *RBM*s. Alternatively, the midcell site could act as a sink for un-bound RefZ that accumulates in the mother cell due to continued *refZ* expression (Figure V.5).

To evaluate whether saturation of the *RBM*s is responsible for driving RefZ to midcell, arrays of *RBM* sequences of varying length could be inserted into the chromosome outside the capture region in backgrounds mutant and wild-type for the five *oriC*-proximal *RBM*s.

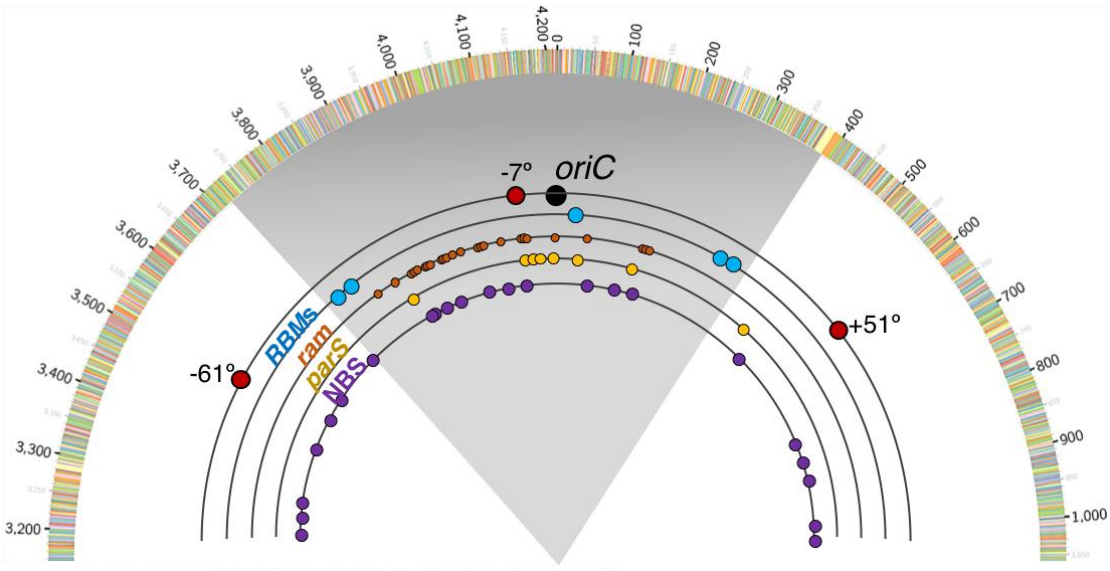

Figure V.4 Binding sites of nucleoid-associated proteins that function during sporulation.
Half of one circular chromosome is shown. Outer ring, individual genes are colored and numbers correspond to genomic position in kb (made with Circos (Krzywinski *et al.*, 2009)). Inner ring shows the origin or replication and positions of the origin and left and right arm reporters used in the trapping assay. Followed are rings showing binding sites for RefZ, RacA, Spo0J, and Noc, respectively: *RBM*s (blue), *ram* (burnt orange), *parS* (yellow), and NBS (purple). Grey wedge corresponds to the ~30% of chromosome reproducibly captured in the forespore during polar division. NBS at capture site are underrepresented in regions spanning the capture boundaries.

We previously followed this line of thought to determine if ectopic *RBM*s, inserted ~10° counterclockwise from the L1 and R1 sites, could rescue the chromosome trapping defect of the RBM_{5mu} (not shown, see Chapter II.4, Discussion). However, the ectopic position was still within the trapping boundary and only single *RBM* sequences were introduced, possibly explaining why we did not see a change in trapping levels. By using an array of *RBM*s and introducing them closer to the terminus, we hypothesize that RefZ may become titrated away from the five native sites at the origin and no longer be able to exact its chromosome capture function, phenocopying the RBM_{5mu} and *refZ*

mutants. Introducing these arrays into a strain mutant for the five *RBM*s should at least phenocopy chromosome capture levels an otherwise isogenic +*RBM* control.

V.2.1 Regulation of asymmetric division by RefZ and Noc

Whether RefZ affects division positively or negatively at the *RBM*s, our data suggest that RefZ's activity is restricted to the regions near the capture boundary. The position of the asymmetric septum was recently found to occur at the 1/5th position in *refZ* mutant cells, whereas wildtype reproducibly divided at the 1/6th position (Muchova *et al*., 2018). If RefZ inhibits division from the *RBM*s, then the fact that the septum is formed further, rather than nearer to the poles, is counter-intuitive and supports the idea that inhibition likely only affects target(s) in RefZ's immediate vicinity.

As noted by others (Adams *et al.*, 2014), conspicuous gaps in NBS occurrence on the chromosome overlap the boundaries of the region trapped in the forespore and thus the *RBM*s on the left and right arms. The intuitive interpretation is that NBS are not likely enriched here since a polar division is necessary for sporulation. Both the increased distance between the pole and the septum, and the presumed absence of Noc inhibition in the vicinity of the *RBM*s are most consistent with Model 1, in which RefZ activates asymmetric division near the poles (Figure V.5). However, if RefZ functions to inhibit Z-ring assembly in the vicinity of the *RBM*s, one question raised is *why Bacillus* would encode, let alone *conserve*, a functionally redundant inhibitor of division that acts in a region of the cell presumably already inhibited by Noc. Considering additional factors like reduced *noc* expression and chromosome remodeling by RacA might also

play a role in attenuating Noc activity at the capture region during sporulation (Adams *et al.*, 2014), Consequently, it is not yet clear what effect, if any, Noc activity in regions outside of these gaps would have on inhibiting polar divisome assembly.

One way to evaluate this would be to determine whether a *noc* mutant is defective in capture of the left and right arm reporters using the trapping assay. If Noc contributes to tuning septum placement over the region occupied by RefZ-*RBM* complexes, we would expect to observe a defect similar to the single *refZ* mutant. In this case, assaying for trapping in a *refZ noc* double mutant would be necessary to determine whether RefZ and Noc act in the same pathway to effect chromosome capture.

V.2.2 Midcell division regulation by RefZ and Noc

One outstanding question is whether RefZ effects cell division from its position at midcell, in addition to when it is bound at the *RBM*s. If RefZ regulated division from the midcell position, this would help explain its role both in preventing aberrant midcell divisions in conjunction with Noc, and in promoting Z-ring shifting to the poles early in sporulation. While the mechanism by which RefZ effects division remains unknown, i.e. whether RefZ acts as an activator or an inhibitor of division, our data suggest that if RefZ controls division when localized at midcell, then it does so by a mechanism distinct from that enacted from the *RBM*s. Neither loss of DNA-binding activity nor mutation of the *ter*- and *oriC*-proximal binding sites are sufficient to eliminate RefZ's midcell focus (Figure IV.1 and IV.2). In contrast, both the *RBM*s and RefZ's ability to effect cell division are required for its redundant function with Noc (Figure IV.6 and IV.9);

however, it remains to be determined whether its role in Z-ring shifting shares similar requirements.

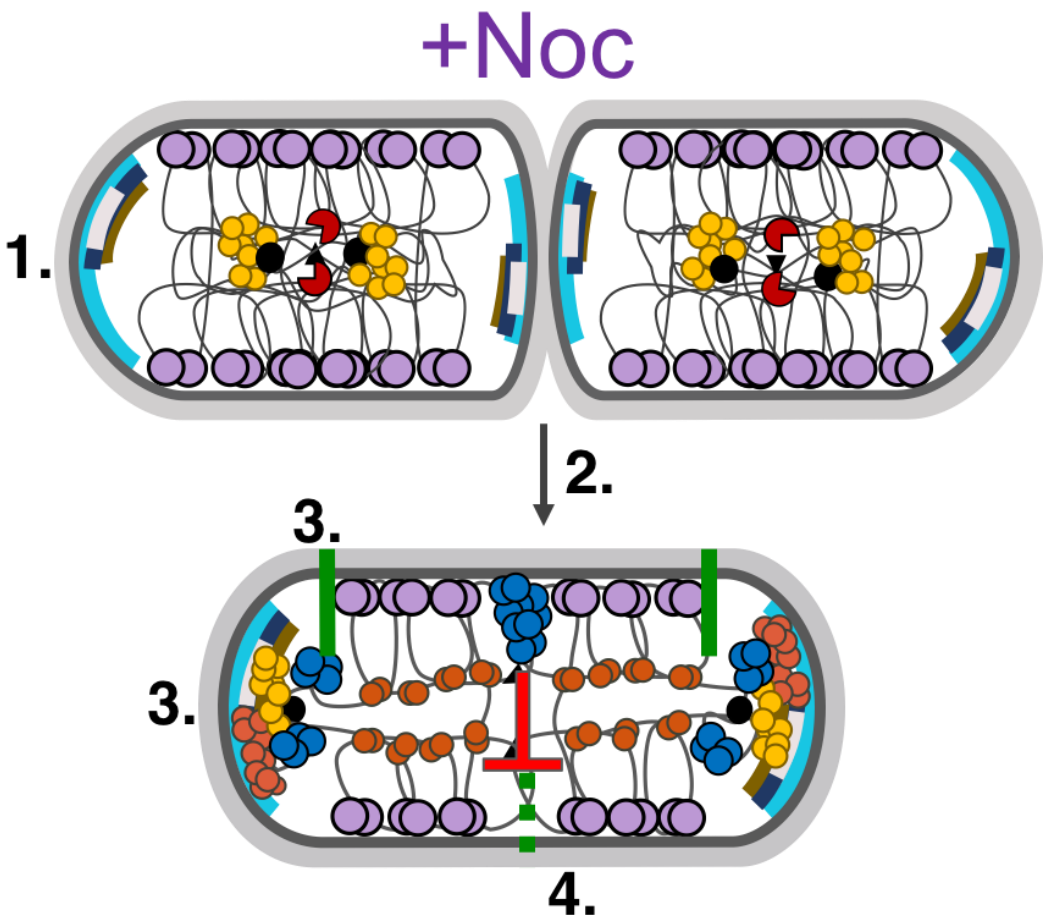

Figure V.5 RefZ promotes polar division in sporulating wild-type cells.

To test this, the FtsZ-GFP localization experiment should be reproduced, both in the *RBM* mutant background and in *rLOF* mutant strains. The expectation is that shifting in cells lacking *RBM*s will be delayed and phenocopy the *refZ* mutant. A similar expectation is raised for the ten DNA-binding proficient *rLOF* mutants, which would together provide strong evidence that the division-related phenotypes observed in the absence of *refZ*, its binding activity and binding sites, and its inhibitory activity, are all likely the result of eliminating one single function of RefZ. On the other hand, if the *rLOF* mutants exhibit a range of shifting phenotypes, this would lend support to the idea that RefZ may influence division by two distinct mechanisms and/or from two sub-cellular positions.

Both artificial expression of RefZ and over expression of Noc in vegetative cells perturbs cell division and results in cell filaments lacking in division septa (Wu & Errington, 2004, Wagner-Herman *et al*., 2012). In addition, deletion of *noc* in vegetative cells blocked at the later stages of division (which causes filamentation) resulted in FtsZ-GFP spirals, arcs, and foci, similar to phenotype produced in cells artificially expressing RefZ, and reminiscent of the helical intermediate that forms during sporulation (Wagner-Herman *et al*., 2012, Ben-Yehuda *et al*., 2002, Wu & Errington, 2004). The ability of the Min system (DivIVA, MinJ, MinD, MinC) to regulate division from the poles breaks down in these filamentous cells, resulting in a portion of nucleoids that are bisected by the division septum (Wu & Errington, 2004, Wagner-Herman *et al*., 2012).

Given the similarities in FtsZ foci between *noc* mutant cells and those artificially expressing RefZ, we wonder whether Z-ring shifting might also be delayed or impaired

when Noc is absent from sporulating cells. Furthermore, the modest cell filamentation generated in the absence of *noc*, combined with the additional stress of starvation, could potentially interferes with normal cell cycle processes and, possibly, the signaling that triggers entry into sporulation. This would be expected to reduce the overall fitness of the mutant upon entering sporulation, which is consistent with the reproducible reduction in total CFU in the *noc* mutant population prior to heat treatment (Figure IV.3B, inset table).

To determine if *noc* mutants effect Z-ring shifting (and division in general) early in sporulation, FtsZ-GFP localization could be monitored similar to experiments described above and previously (Wagner-Herman *et al*., 2012). If, as we speculate, *noc* mutants are already impaired in division prior to sporulation, CRISPR interference could be used to target *noc* expression just prior to resuspension, which should eliminate any additional effects specifically caused by fitness loss. A well characterized CRISPRi system has been developed for *B. subtilis* in which guide RNA (gRNA) specific to the target gene (in this case, *noc*) is constitutively expressed from the chromosome. At the desired time, expression of a nuclease-deficient *cas9* mutant, *dCas9*, can be induced from an ectopic locus, the product of which is targeted to the gRNA where it represses transcription.

V.2.3 Sporulation initiation in *noc* mutant cells with ongoing replication

We observe that a large number of the aberrant midcell septa formed in *refZ* Δ*noc* and RBM_{5mu} Δ*noc* double mutant cells result in nucleoid-free mother cell

compartments, suggesting that at least some cells had established diploidy prior to forming the medial septum (Figure IV.8 and IV.9). For a proportion of the double mutant population, the additional divisions occur in cells that are longer and appear to have a higher content of DNA, whereas another proportion exhibit midcell septa over one of the two nucleoids, or guillotining. In line with this, double mutant cells were also higly heterogeneous in their nucleoid structure and DNA content (DAPI staining, Figure IV.8 and IV.9), consistent with a failure to coordinate symmetric division during the last replication cycle following initiation of sporulation. Depending on where a cell is in the cycle when Spo0A~P triggers sporulation, additional vegetative cell divisions may be necessary to reduce the cell's chromosome copy number to two. If RefZ and/or Noc were responsible for regulating midcell divisions upon initiation of sporulation, a proportion of polyploid cells might be permitted to initiate sporulation.

To test this, we used FROS to monitor the number of origins in wild-type and *refZ* and *noc* single mutant cells 1 h after resuspension (Figure IV.10). We find that wild-type cells display bi-polar origin foci that associate with elongated nucleoids, whereas number of *noc* mutant cells possess additional and/or brighter origin foci. These origin foci were frequently associated with nucleoids that had not adopted an elongated structure characteristic of the axial filament, suggesting that threshold levels of Spo0A-P (needed to activate *racA* transcription) may not be present in these cells (Figure IV.10). However, we did not detect significant differences in Spo0A~P activity in the *noc* mutant at 1.5 h (not shown) and 2 h following resuspension (Figure IV.4) that would indicate genes like *racA, refZ,* and *sirA* are not being expressed. Although, to exclude

the possibility that the absence of Noc perturbs the timing of axial filament formation and/or the ability of RacA to remodel the chromosome, additional experiments are required, for instance, monitoring RacA localization in *noc* mutant and wild-type cells under similar sporulation conditions.

Our observations are more consistent with a portion of *noc* mutant cells enter development actively engaged in DNA replication. Consistent with this, multiple foci or a brighter focus were often observed at the nucleoid periphery, a phenotype reported to result from unresolved sister origins (Lee & Grossman, 2006, Gruber & Errington, 2009, Sullivan *et al.*, 2009, Wang *et al.*, 2014). Brighter and larger foci were also observed at mid-nucleoid, which is consistent with the localization pattern of newly replicated sister origins in cells engaged in the elongation phase of replication (Wang *et al*., 2014). In contrast, cells lacking *refZ* did not appear to be undergoing active replication and segregation, as the majority of cells contained two origin foci that were segregated to the far poles and were predominantly associated with elongated nucleoid structures (Figure IV.10). Of note, however, *refZ* mutant origin foci appeared brighter and often larger compared to those found in the wild-type cells, more closely resembling those found in the *noc* mutant.

Vegetative cells lacking *soj* or *minD*, the latter of which is required for Soj localization to polar/sub-polar cell regions, exhibit fragmented and dispersed Spo0J-GFP foci (Marston & Errington, 1999, Autret & Errington, 2003). Given that foci in the *noc* mutant and the polar foci in the *refZ* mutant are notably brighter and larger compared to wild-type, we suspect that formation of Spo0J-*parS* nucleoprotein complexes is not

likely to be perturbed in these mutants. Although, we do not exclude this possibility since the *tetO*/TetR complexes formed here do not directly report on Spo0J localization. One alternative explanation for the presence of large, bright origin foci at mid-nucleoid in *noc* mutant cells could be the result of impaired origin resolution and/or segregation, which requires SMC in addition to Soj and Spo0J-*parS* (Lee & Grossman, 2006, Gruber & Errington, 2009, Sullivan *et al.*, 2009, Wang *et al.*, 2014). During sporulation, MinD and Soj act in the same pathway and in parallel to RacA to anchor the chromosome origins to the poles (Wu & Errington, 2003, Kloosterman *et al.*, 2016).

Noc was originally studied as a candidate for regulating chromosome segregation, due to its extensive homology to Spo0J (36% identity) (Sievers *et al.*, 2002). The *noc* gene is considered a recent acquisition in *Bacillus* and other members of the Firmicutes, as the result of a gene duplication of the downstream *spo0J* gene (Ogasawara & Yoshikawa, 1992). Unlike Spo0J, Noc does not appear to play a role in chromosome segregation in vegetative cell; however, to our knowledge, evidence eliminating a role for Noc in chromosome segregation at the onset of sporulation is lacking. Both by candidate-based approaches, using the single cell fluorescence trapping assay (Sullivan *et al.*, 2009), and high-throughput genetic screens, using a population-based plate assays (Kloosterman *et al.*, 2016, Wu & Errington, 1998) have been used to identify novel sporulation genes involved in chromosome capture. We speculate that Noc only moderately impacts chromosome segregation, if at all, during sporulation. However, given that the state of nucleoid condensation is tightly controlled and undergoes significant remodeling during sporulation, and that Noc interacts with over 70

sites on the chromosome (Wu *et al.*, 2009), it is poised to have a strong influence on the overall 3D structure of the nucleoid. Further single cell-based assay should be done to fully characterize the impact of Noc during the transition and early stages of sporulation.

V.2.3.1 A role for RefZ in mitigating the consequences of polyploidy during sporulating in the absence of Noc

Our observation that replication appears to be ongoing in *noc* mutants during sporulation suggests that these cells may have bypassed the normal cell cycle checkpoint mediated by Sda (Figure IV.10). Pulses of Spo0A~P occur at the end of replication during each cell cycle and are modulated, in part, by the inhibitory action of Sda on KinA (Cunningham & Burkholder, 2009, Rowland *et al.*, 2004). Sda pulses opposite of Spo0A~P, rapidly increasing upon replication initiation then slowly decreasing, such that levels are lowest when replication terminates, at which sporulation can be initiated in cells that have accumulated threshold levels of Spo0A~P (Veening *et al.*, 2009). In this way, Sda deters entry into sporulation in cells that have initiated new rounds of DNA replication or are experiencing DNA damage (Burkholder *et al.*, 2001). Bypassing this checkpoint would allow polyploid cells with threshold Spo0A~P to initiate sporulation and, consequently, activate expression of *sirA*, *racA*, *refZ*, and *spoIIE*. SirA might be sufficient to prevent new rounds of replication, provided Noc itself is not responsible for triggering over-initiation. Indeed, we do observe that a portion of the *noc* mutant cells show wild-type positioning and number of origin foci

(Figure IV.10), suggesting that a sub-population of cells establish and maintain diploidy and the origins are efficiently segregated.

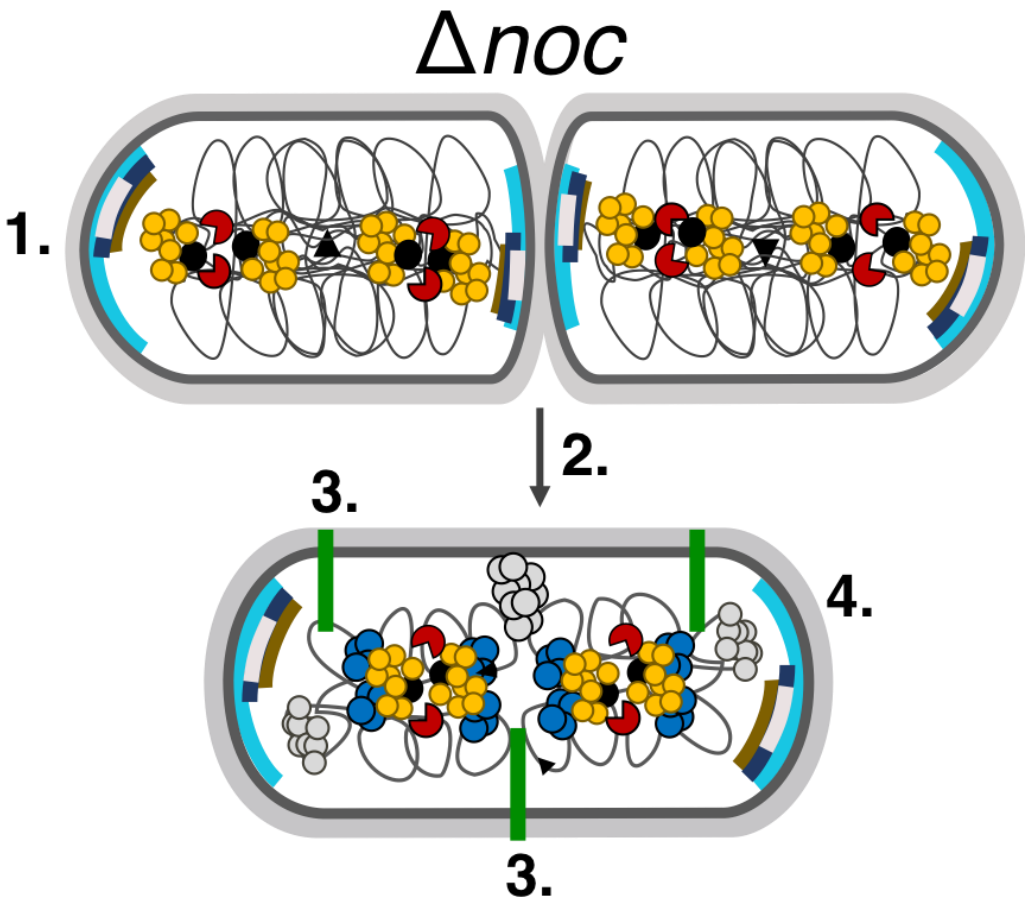

Figure V.6 RefZ promotes medial divisions in replicating *noc* mutants.

Since formation of the axial filament requires exactly two chromosome copies, these chromosomes might be expected to be organized and segregated by SMC and Soj-Spo0J-*parS*, respectively, until a diploid state is reached. Reaching diploidy would also require additional midcell divisions. A direct result of polyploidy in the *noc* mutant cells would be an increase in the number of *RBM*s available for RefZ binding. In these conditions, RefZ may localize to the nucleoid periphery (also corresponding to the quarter cell positions) similar to what is observed in vegetative cells expressing sporulation levels of RefZ-GFP (Figure V.2 and V.6). If RefZ activates division from the *RBM*s, we speculate that polyploidy might increase the potency of RefZ's division modulation activity.

As an activator, RefZ activity should result in increased divisions near the pole or quarter cell position (Figure V.6). Consistent with this, bright origin foci at the periphery of more condensed nucleoids are found in both short and normal length cells in the *noc* mutant (Figure IV.10). In cells with normal length, a more asymmetrically positioned partial septum can be observed immediately adjacent or overlapping the nucleoid periphery. This is similar to what we observe in vegetative cells under inducing conditions (Figure V.2) and is in line with the hypothesis that RefZ might direct division to these locations in the absence of Noc. We speculate that this particular phenotype would not be expected if RefZ was inhibiting division at these sites, although we do not exclude the possibility.

A model for RefZ as an activator in the absence of *noc* is outlined in Figure V.6. Once cells divide following the last round of replication, sporulation would be expected

to resume similar to cells that entered sporulation with the appropriate number of chromosomes (Figure V.6). An intriguing aspect of the model is that deployment of RefZ to midcell might only occur once ploidy has been reduced to two, or a number that sees saturation of the *RBM* sites. Importantly, whether RefZ regulates division from midcell or is merely sequestered here to prevent further activity, our model highlights a scenario that would benefit greatly from an uninhibited midcell division site. Although polyploid wildtype cells essentially never initiate sporulation under laboratory conditions, it is easy to imagine that the existence of such failsafe mechanisms, perhaps mediated by the RefZ-*RBM* system, could provide a significant fitness advantage to staving cells in nature.

Additional considerations regarding Noc-dependent phenotypes

The *noc* gene is the last in an operon encoding upstream tRNA-uridine and 16S ribosomal RNA subunit modification enzymes, and is positively controlled by the master competence regulator, ComK (Figure IV.1B)(Ogura & Tanaka, 2009). Unlike *noc*, homologs of the upstream genes *trmE*, *trmF* (*gidA*), and *rsmG* (*gidB*) are found widely conserved across bacteria at the origin of replication (Ogasawara & Yoshikawa, 1992). Intriguingly, Meeske *et al* recently identified both *trmE* and *gidA* in a screen for new sporulation genes using Tn-seq (Meeske *et al.*, 2016). Deletion of either gene resulted in a significant reduction in sporulation efficiency compared to wild-type, similar to the *noc* mutant (Figure IV.3B). A proportion of cells in either mutant exhibited aberrant septa and longer mother cells (Meeske *et al.*, 2016), raising the possibility that a polar

effect on *noc* transcription may in fact be responsible for these division phenotypes, although the counter agreement could also be true. With the data provided, the *trmE* and *gidA* mutants appear to exhibit similar aberrant midcell divisions, possibly at intermediate frequencies between what we observe for the single *noc* mutant and the *refZ noc* double mutant. Although the authors used markerless gene knockouts, further experiments are necessary to exclude the possibility that *noc* transcription is not attenuated in these strains, and vice versa.

A simple way to test this would be to delete *refZ* in the *trmE* and *gidA* strains. If we observe an increase in aberrant division septa that phenocopies the *refZ noc* double mutant, this would indicate that the sporulation phenotype reported by Meeske and colleagues likely reflects disruption of downstream *noc* expression. On the other hand, if the double mutant strains phenocopy the *trmE*/*gidA* single mutants, then further experiments will be required to determine epistatic interactions between the three genes.

REFERENCES

Aarsman, M.E., A. Piette, C. Fraipont, T.M. Vinkenvleugel, M. Nguyen-Disteche & T. den Blaauwen, (2005) Maturation of the *Escherichia coli* divisome occurs in two steps. *Mol Microbiol* **55**: 1631-1645.

Adams, D.W., L.J. Wu & J. Errington, (2014) Cell cycle regulation by the bacterial nucleoid. *Curr Opin Microbiol* **22**: 94-101.

Adams, D.W., L.J. Wu & J. Errington, (2015) Nucleoid occlusion protein Noc recruits DNA to the bacterial cell membrane. *EMBO J* **34**: 491-501.

Adams, P.D., P.V. Afonine, G. Bunkoczi, V.B. Chen, I.W. Davis, N. Echols, J.J. Headd, L.W. Hung, G.J. Kapral, R.W. Grosse-Kunstleve, A.J. McCoy, N.W. Moriarty, R. Oeffner, R.J. Read, D.C. Richardson, J.S. Richardson, T.C. Terwilliger & P.H. Zwart, (2010) PHENIX: a comprehensive Python-based system for macromolecular structure solution. *Acta Crystallogr D Biol Crystallogr* **66**: 213-221.

Agari, Y., K. Sakamoto, S. Kuramitsu & A. Shinkai, (2012) Transcriptional repression mediated by a TetR family protein, PfmR, from *Thermus thermophilus* HB8. *J Bacteriol* **194**: 4630-4641.

Ali Azam, T., A. Iwata, A. Nishimura, S. Ueda & A. Ishihama, (1999) Growth phase-dependent variation in protein composition of the *Escherichia coli* nucleoid. *J Bacteriol* **181**: 6361-6370.

Antonny, B., (2011) Mechanisms of membrane curvature sensing. *Annu Rev Biochem* **80**: 101-123.

Arias-Palomo, E., V.L. O'Shea, I.V. Hood & J.M. Berger, (2013) The bacterial DnaC helicase loader is a DnaB ring breaker. *Cell* **153**: 438-448.

Arigoni, F., K. Pogliano, C.D. Webb, P. Stragier & R. Losick, (1995) Localization of protein implicated in establishment of cell type to sites of asymmetric division. *Science* **270**: 637-640.

Atrih, A. & S.J. Foster, (2001) Analysis of the role of bacterial endospore cortex structure in resistance properties and demonstration of its conservation amongst species. *J Appl Microbiol* **91**: 364-372.

Auner, H., M. Buckle, A. Deufel, T. Kutateladze, L. Lazarus, R. Mavathur, G. Muskhelishvili, I. Pemberton, R. Schneider & A. Travers, (2003) Mechanism of transcriptional activation by FIS: role of core promoter structure and DNA topology. *J Mol Biol* **331**: 331-344.

Autret, S. & J. Errington, (2003) A role for division-site-selection protein MinD in regulation of internucleoid jumping of Soj (ParA) protein in *Bacillus subtilis*. *Mol Microbiol* **47**: 159-169.

Autret, S., R. Nair & J. Errington, (2001) Genetic analysis of the chromosome segregation protein Spo0J of *Bacillus subtilis*: evidence for separate domains involved in DNA binding and interactions with Soj protein. *Mol Microbiol* **41**: 743-755.

Badrinarayanan, A., T.B. Le & M.T. Laub, (2015) Bacterial chromosome organization and segregation. *Annu Rev Cell Dev Biol* **31**: 171-199.

Bailey, M.W., P. Bisicchia, B.T. Warren, D.J. Sherratt & J. Mannik, (2014) Evidence for divisome localization mechanisms independent of the Min system and SlmA in *Escherichia coli*. *PLoS Genet* **10**: e1004504.

Bakshi, S., H. Choi & J.C. Weisshaar, (2015) The spatial biology of transcription and translation in rapidly growing *Escherichia coli*. *Front Microbiol* **6**: 636.

Bakshi, S., A. Siryaporn, M. Goulian & J.C. Weisshaar, (2012) Superresolution imaging of ribosomes and RNA polymerase in live *Escherichia coli* cells. *Mol Microbiol* **85**: 21-38.

Barak, I. & K. Muchova, (2018) The positioning of the asymmetric septum during sporulation in *Bacillus subtilis*. *PLoS One* **13**: e0201979.

Barak, I., P. Prepiak & F. Schmeisser, (1998) MinCD proteins control the septation process during sporulation of *Bacillus subtilis*. *J Bacteriol* **180**: 5327-5333.

Barak, I. & A.J. Wilkinson, (2007) Division site recognition in *Escherichia coli* and *Bacillus subtilis*. *FEMS Microbiol Rev* **31**: 311-326.

Barak, I. & P. Youngman, (1996) SpoIIE mutants of *Bacillus subtilis* comprise two distinct phenotypic classes consistent with a dual functional role for the SpoIIE protein. *J Bacteriol* **178**: 4984-4989.

Bath, J., L.J. Wu, J. Errington & J.C. Wang, (2000) Role of *Bacillus subtilis* SpoIIIE in DNA transport across the mother cell-prespore division septum. *Science* **290**: 995-997.

Beall, B. & J. Lutkenhaus, (1991) FtsZ in *Bacillus subtilis* is required for vegetative septation and for asymmetric septation during sporulation. *Genes Dev* **5**: 447-455.

Beattie, T.R. & R. Reyes-Lamothe, (2015) A Replisome's journey through the bacterial chromosome. *Front Microbiol* **6**: 562.

Becker, E.C. & K. Pogliano, (2007) Cell-specific SpoIIIE assembly and DNA translocation polarity are dictated by chromosome orientation. *Mol Microbiol* **66**: 1066-1079.

Ben-Yehuda, S., M. Fujita, X.S. Liu, B. Gorbatyuk, D. Skoko, J. Yan, J.F. Marko, J.S. Liu, P. Eichenberger, D.Z. Rudner & R. Losick, (2005) Defining a centromere-like element in *Bacillus subtilis* by Identifying the binding sites for the chromosome-anchoring protein RacA. *Mol Cell* **17**: 773-782.

Ben-Yehuda, S. & R. Losick, (2002) Asymmetric cell division in *B. subtilis* involves a spiral-like intermediate of the cytokinetic protein FtsZ. *Cell* **109**: 257-266.

Ben-Yehuda, S., D.Z. Rudner & R. Losick, (2003) RacA, a bacterial protein that anchors chromosomes to the cell poles. *Science* **299**: 532-536.

Bensaid, A., A. Almeida, K. Drlica & J. Rouviere-Yaniv, (1996) Cross-talk between topoisomerase I and HU in *Escherichia coli*. *J Mol Biol* **256**: 292-300.

Berlatzky, I.A., A. Rouvinski & S. Ben-Yehuda, (2008) Spatial organization of a replicating bacterial chromosome. *Proc Natl Acad Sci U S A* **105**: 14136-14140.

Bernhardt, T.G. & P.A. de Boer, (2005) SlmA, a nucleoid-associated, FtsZ binding protein required for blocking septal ring assembly over chromosomes in *E. coli*. *Mol Cell* **18**: 555-564.

Besprozvannaya, M., V.L. Pivorunas & B.M. Burton, (2014) Mechanistic study of classical translocation-dead SpoIIIE36 reveals the functional importance of the hinge within the SpoIIIE motor. *J Bacteriol* **196**: 2481-2490.

Bigot, S., O.A. Saleh, C. Lesterlin, C. Pages, M. El Karoui, C. Dennis, M. Grigoriev, J.F. Allemand, F.X. Barre & F. Cornet, (2005) KOPS: DNA motifs that control *E. coli* chromosome segregation by orienting the FtsK translocase. *EMBO J* **24**: 3770-3780.

Biller, S.J. & W.F. Burkholder, (2009) The *Bacillus subtilis* SftA (YtpS) and SpoIIIE DNA translocases play distinct roles in growing cells to ensure faithful chromosome partitioning. *Mol Microbiol* **74**: 790-809.

Bisson-Filho, A.W., K.F. Discola, P. Castellen, V. Blasios, A. Martins, M.L. Sforca, W. Garcia, A.C. Zeri, H.P. Erickson, A. Dessen & F.J. Gueiros-Filho, (2015) FtsZ filament capping by MciZ, a developmental regulator of bacterial division. *Proc Natl Acad Sci U S A* **112**: E2130-2138.

Bisson-Filho, A.W., Y.P. Hsu, G.R. Squyres, E. Kuru, F. Wu, C. Jukes, Y. Sun, C. Dekker, S. Holden, M.S. VanNieuwenhze, Y.V. Brun & E.C. Garner, (2017) Treadmilling by FtsZ filaments drives peptidoglycan synthesis and bacterial cell division. *Science* **355**: 739-743.

Blasios, V., A.W. Bisson-Filho, P. Castellen, M.L. Nogueira, J. Bettini, R.V. Portugal, A.C. Zeri & F.J. Gueiros-Filho, (2013) Genetic and biochemical characterization of the MinC-FtsZ interaction in *Bacillus subtilis*. *PLoS One* **8**: e60690.

Bloomfield, V.A., (1997) DNA condensation by multivalent cations. *Biopolymers* **44**: 269-282.

Bradshaw, N. & R. Losick, (2015) Asymmetric division triggers cell-specific gene expression through coupled capture and stabilization of a phosphatase. *Elife* **4**.

Bramhill, D. & A. Kornberg, (1988) Duplex opening by dnaA protein at novel sequences

in initiation of replication at the origin of the *E. coli* chromosome. *Cell* **52**: 743-755.

Bramkamp, M., R. Emmins, L. Weston, C. Donovan, R.A. Daniel & J. Errington, (2008) A novel component of the division-site selection system of *Bacillus subtilis* and a new mode of action for the division inhibitor MinCD. *Mol Microbiol* **70**: 1556-1569.

Breier, A.M. & A.D. Grossman, (2007) Whole-genome analysis of the chromosome partitioning and sporulation protein Spo0J (ParB) reveals spreading and origin-distal sites on the *Bacillus subtilis* chromosome. *Mol Microbiol* **64**: 703-718.

Britton, R.A., P. Eichenberger, J.E. Gonzalez-Pastor, P. Fawcett, R. Monson, R. Losick & A.D. Grossman, (2002) Genome-wide analysis of the stationary-phase sigma factor (sigma-H) regulon of *Bacillus subtilis*. *J Bacteriol* **184**: 4881-4890.

Britton, R.A. & A.D. Grossman, (1999) Synthetic lethal phenotypes caused by mutations affecting chromosome partitioning in *Bacillus subtilis*. *J Bacteriol* **181**: 5860-5864.

Britton, R.A., D.C. Lin & A.D. Grossman, (1998) Characterization of a prokaryotic SMC protein involved in chromosome partitioning. *Genes Dev* **12**: 1254-1259.

Brown, E.E., A.K. Miller, I.V. Krieger, R.M. Otto, J.C. Sacchettini & J.K. Herman, (2019) A DNA-binding protein tunes septum placement during *Bacillus subtilis* sporulation. *Journal of Bacteriology*: JB.00287-00219.

Browning, D.F., D.C. Grainger & S.J. Busby, (2010) Effects of nucleoid-associated proteins on bacterial chromosome structure and gene expression. *Curr Opin Microbiol* **13**: 773-780.

Burbulys, D., K.A. Trach & J.A. Hoch, (1991) Initiation of sporulation in *B. subtilis* is controlled by a multicomponent phosphorelay. *Cell* **64**: 545-552.

Burkholder, W.F., I. Kurtser & A.D. Grossman, (2001) Replication initiation proteins regulate a developmental checkpoint in *Bacillus subtilis*. *Cell* **104**: 269-279.

Burmann, F., A. Basfeld, R. Vazquez Nunez, M.L. Diebold-Durand, L. Wilhelm & S. Gruber, (2017) Tuned SMC arms drive chromosomal loading of prokaryotic Condensin.

Mol Cell **65**: 861-872 e869.

Burmann, F., H.C. Shin, J. Basquin, Y.M. Soh, V. Gimenez-Oya, Y.G. Kim, B.H. Oh & S. Gruber, (2013) An asymmetric SMC-kleisin bridge in prokaryotic condensin. *Nat Struct Mol Biol* **20**: 371-379.

Burton, B. & D. Dubnau, (2010) Membrane-associated DNA transport machines. *Cold Spring Harb Perspect Biol* **2**: a000406.

Burton, B.M., K.A. Marquis, N.L. Sullivan, T.A. Rapoport & D.Z. Rudner, (2007) The ATPase SpoIIIE transports DNA across fused septal membranes during sporulation in *Bacillus subtilis*. *Cell* **131**: 1301-1312.

Bush, N.G., K. Evans-Roberts & A. Maxwell, (2015) DNA Topoisomerases. *EcoSal Plus* **6**.

Butan, C., L.M. Hartnell, A.K. Fenton, D. Bliss, R.E. Sockett, S. Subramaniam & J.L. Milne, (2011) Spiral architecture of the nucleoid in *Bdellovibrio bacteriovorus*. *J Bacteriol* **193**: 1341-1350.

Bylund, J.E., M.A. Haines, P.J. Piggot & M.L. Higgins, (1993) Axial filament formation in *Bacillus subtilis*: induction of nucleoids of increasing length after addition of chloramphenicol to exponential-phase cultures approaching stationary phase. *J Bacteriol* **175**: 1886-1890.

Cabre, E.J., B. Monterroso, C. Alfonso, A. Sanchez-Gorostiaga, B. Reija, M. Jimenez, M. Vicente, S. Zorrilla & G. Rivas, (2015) The nucleoid occlusion SlmA protein accelerates the disassembly of the FtsZ protein polymers without affecting their GTPase activity. *PLoS One* **10**: e0126434.

Campo, N., K.A. Marquis & D.Z. Rudner, (2008) SpoIIQ anchors membrane proteins on both sides of the sporulation septum in *Bacillus subtilis*. *J Biol Chem* **283**: 4975-4982.

Carballido-Lopez, R., (2006) Orchestrating bacterial cell morphogenesis. *Mol Microbiol* **60**: 815-819.

Carniol, K., S. Ben-Yehuda, N. King & R. Losick, (2005) Genetic dissection of the sporulation protein SpoIIE and its role in asymmetric division in *Bacillus subtilis*. *J Bacteriol* **187**: 3511-3520.

Cattoni, D.I., S. Thakur, C. Godefroy, A. Le Gall, J. Lai-Kee-Him, P.E. Milhiet, P. Bron & M. Nollmann, (2014) Structure and DNA-binding properties of the *Bacillus subtilis* SpoIIIE DNA translocase revealed by single-molecule and electron microscopies. *Nucleic Acids Res* **42**: 2624-2636.

Chai, Y., R. Kolter & R. Losick, (2010) Reversal of an epigenetic switch governing cell chaining in *Bacillus subtilis* by protein instability. *Mol Microbiol* **78**: 218-229.

Chang, F. & K.C. Huang, (2014) How and why cells grow as rods. *BMC Biol* **12**: 54.

Chara, O., A. Borges, P.E. Milhiet, M. Nollmann & D.I. Cattoni, (2018) Sequence-dependent catalytic regulation of the SpoIIIE motor activity ensures directionality of DNA translocation. *Sci Rep* **8**: 5254.

Cho, H. & T.G. Bernhardt, (2013) Identification of the SlmA active site responsible for blocking bacterial cytokinetic ring assembly over the chromosome. *PLoS Genet* **9**: e1003304.

Cho, H., H.R. McManus, S.L. Dove & T.G. Bernhardt, (2011) Nucleoid occlusion factor SlmA is a DNA-activated FtsZ polymerization antagonist. *Proc Natl Acad Sci U S A* **108**: 3773-3778.

Chung, J.D., G. Stephanopoulos, K. Ireton & A.D. Grossman, (1994) Gene expression in single cells of *Bacillus subtilis*: evidence that a threshold mechanism controls the initiation of sporulation. *J Bacteriol* **176**: 1977-1984.

Claessen, D., R. Emmins, L.W. Hamoen, R.A. Daniel, J. Errington & D.H. Edwards, (2008) Control of the cell elongation-division cycle by shuttling of PBP1 protein in *Bacillus subtilis*. *Mol Microbiol* **68**: 1029-1046.

Cleverley, R. & R. Lewis, (2015) EzrA: a spectrin-like scaffold in the bacterial cell division machinery. *Microb Cell* **2**: 59-61.

Cleverley, R.M., J.R. Barrett, A. Basle, N.K. Bui, L. Hewitt, A. Solovyova, Z.Q. Xu, R.A. Daniel, N.E. Dixon, E.J. Harry, A.J. Oakley, W. Vollmer & R.J. Lewis, (2014) Structure and function of a spectrin-like regulator of bacterial cytokinesis. *Nat Commun* **5**: 5421.

Corn, J.E. & J.M. Berger, (2006) Regulation of bacterial priming and daughter strand synthesis through helicase-primase interactions. *Nucleic Acids Res* **34**: 4082-4088.

Corn, J.E., J.G. Pelton & J.M. Berger, (2008) Identification of a DNA primase template tracking site redefines the geometry of primer synthesis. *Nat Struct Mol Biol* **15**: 163-169.

Cowtan, K., (2006) The Buccaneer software for automated model building. 1. Tracing protein chains. *Acta Crystallogr D Biol Crystallogr* **62**: 1002-1011.

Cozzarelli, N.R., (1980) DNA topoisomerases. *Cell* **22**: 327-328.

Crowe, A.M., P.J. Stogios, I. Casabon, E. Evdokimova, A. Savchenko & L.D. Eltis, (2015) Structural and functional characterization of a ketosteroid transcriptional regulator of *Mycobacterium tuberculosis*. *J Biol Chem* **290**: 872-882.

Cunha, S., C.L. Woldringh & T. Odijk, (2001) Polymer-mediated compaction and internal dynamics of isolated *Escherichia coli* nucleoids. *J Struct Biol* **136**: 53-66.

Cunningham, K.A. & W.F. Burkholder, (2009) The histidine kinase inhibitor Sda binds near the site of autophosphorylation and may sterically hinder autophosphorylation and phosphotransfer to Spo0F. *Mol Microbiol* **71**: 659-677.

Cuthbertson, L. & J.R. Nodwell, (2013) The TetR family of regulators. *Microbiol Mol Biol Rev* **77**: 440-475.

Dajkovic, A., G. Lan, S.X. Sun, D. Wirtz & J. Lutkenhaus, (2008) MinC spatially controls bacterial cytokinesis by antagonizing the scaffolding function of FtsZ. *Curr Biol* **18**: 235-244.

de Boer, P.A., R.E. Crossley & L.I. Rothfield, (1989) A division inhibitor and a

topological specificity factor coded for by the minicell locus determine proper placement of the division septum in *E. coli*. *Cell* **56**: 641-649.

de Vries, R., (2001) Flexible polymer-induced condensation and bundle formation of DNA and F-actin filaments. *Biophys J* **80**: 1186-1194.

de Vries, R., (2010) DNA condensation in bacteria: Interplay between macromolecular crowding and nucleoid proteins. *Biochimie* **92**: 1715-1721.

Dervyn, E., C. Suski, R. Daniel, C. Bruand, J. Chapuis, J. Errington, L. Janniere & S.D. Ehrlich, (2001) Two essential DNA polymerases at the bacterial replication fork. *Science* **294**: 1716-1719.

Dillon, S.C. & C.J. Dorman, (2010) Bacterial nucleoid-associated proteins, nucleoid structure and gene expression. *Nat Rev Microbiol* **8**: 185-195.

Doan, T., K.A. Marquis & D.Z. Rudner, (2005) Subcellular localization of a sporulation membrane protein is achieved through a network of interactions along and across the septum. *Mol Microbiol* **55**: 1767-1781.

Dominguez-Escobar, J., A. Chastanet, A.H. Crevenna, V. Fromion, R. Wedlich-Soldner & R. Carballido-Lopez, (2011) Processive movement of MreB-associated cell wall biosynthetic complexes in bacteria. *Science* **333**: 225-228.

Dorman, C.J., (2014) Function of nucleoid-associated proteins in chromosome structuring and transcriptional regulation. *J Mol Microbiol Biotechnol* **24**: 316-331.

dos Santos, V.T., A.W. Bisson-Filho & F.J. Gueiros-Filho, (2012) DivIVA-mediated polar localization of ComN, a posttranscriptional regulator of *Bacillus subtilis*. *J Bacteriol* **194**: 3661-3669.

Du, S. & J. Lutkenhaus, (2014) SlmA antagonism of FtsZ assembly employs a two-pronged mechanism like MinCD. *PLoS Genet* **10**: e1004460.

Du, S. & J. Lutkenhaus, (2017) Assembly and activation of the *Escherichia coli* divisome. *Mol Microbiol* **105**: 177-187.

Duderstadt, K.E., K. Chuang & J.M. Berger, (2011) DNA stretching by bacterial initiators promotes replication origin opening. *Nature* **478**: 209-213.

Duderstadt, K.E., M.L. Mott, N.J. Crisona, K. Chuang, H. Yang & J.M. Berger, (2010) Origin remodeling and opening in bacteria rely on distinct assembly states of the DnaA initiator. *J Biol Chem* **285**: 28229-28239.

Duman, R., S. Ishikawa, I. Celik, H. Strahl, N. Ogasawara, P. Troc, J. Lowe & L.W. Hamoen, (2013) Structural and genetic analyses reveal the protein SepF as a new membrane anchor for the Z ring. *Proc Natl Acad Sci U S A* **110**: E4601-4610.

Duncan, L., S. Alper & R. Losick, (1994) Establishment of cell type specific gene transcription during sporulation in *Bacillus subtilis*. *Curr Opin Genet Dev* **4**: 630-636.

Duncan, L., S. Alper & R. Losick, (1996) SpoIIAA governs the release of the cell-type specific transcription factor sigma F from its anti-sigma factor SpoIIAB. *J Mol Biol* **260**: 147-164.

Duncan, L. & R. Losick, (1993) SpoIIAB is an anti-sigma factor that binds to and inhibits transcription by regulatory protein sigma F from *Bacillus subtilis*. *Proc Natl Acad Sci U S A* **90**: 2325-2329.

Dupaigne, P., N.K. Tonthat, O. Espeli, T. Whitfill, F. Boccard & M.A. Schumacher, (2012) Molecular basis for a protein-mediated DNA-bridging mechanism that functions in condensation of the *E. coli* chromosome. *Mol Cell* **48**: 560-571.

Dworkin, J. & R. Losick, (2001) Differential gene expression governed by chromosomal spatial asymmetry. *Cell* **107**: 339-346.

Egan, A.J. & W. Vollmer, (2013) The physiology of bacterial cell division. *Ann N Y Acad Sci* **1277**: 8-28.

Eichenberger, P., P. Fawcett & R. Losick, (2001) A three-protein inhibitor of polar septation during sporulation in *Bacillus subtilis*. *Mol Microbiol* **42**: 1147-1162.

El Najjar, N., J. El Andari, C. Kaimer, G. Fritz, T.C. Rosch & P.L. Graumann, (2018)

Single-molecule tracking of DNA translocases in *Bacillus subtilis* reveals strikingly different dynamics of SftA, SpoIIIE, and FtsA. *Appl Environ Microbiol* **84**.

Elmore, S., M. Muller, N. Vischer, T. Odijk & C.L. Woldringh, (2005) Single-particle tracking of *oriC*-GFP fluorescent spots during chromosome segregation in *Escherichia coli*. *J Struct Biol* **151**: 275-287.

Emsley, P., B. Lohkamp, W.G. Scott & K. Cowtan, (2010) Features and development of Coot. *Acta Crystallogr D Biol Crystallogr* **66**: 486-501.

Engohang-Ndong, J., D. Baillat, M. Aumercier, F. Bellefontaine, G.S. Besra, C. Locht & A.R. Baulard, (2004) EthR, a repressor of the TetR/CamR family implicated in ethionamide resistance in *mycobacteria*, octamerizes cooperatively on its operator. *Mol Microbiol* **51**: 175-188.

Eppinger, M., B. Bunk, M.A. Johns, J.N. Edirisinghe, K.K. Kutumbaka, S.S. Koenig, H.H. Creasy, M.J. Rosovitz, D.R. Riley, S. Daugherty, M. Martin, L.D. Elbourne, I. Paulsen, R. Biedendieck, C. Braun, S. Grayburn, S. Dhingra, V. Lukyanchuk, B. Ball, R. Ul-Qamar, J. Seibel, E. Bremer, D. Jahn, J. Ravel & P.S. Vary, (2011) Genome sequences of the biotechnologically important *Bacillus megaterium* strains QM B1551 and DSM319. *J Bacteriol* **193**: 4199-4213.

Errington, J. & L.J. Wu, (2017) Cell Cycle Machinery in *Bacillus subtilis*. *Subcell Biochem* **84**: 67-101.

Erzberger, J.P., M.L. Mott & J.M. Berger, (2006) Structural basis for ATP-dependent DnaA assembly and replication-origin remodeling. *Nat Struct Mol Biol* **13**: 676-683.

Espeli, O., R. Borne, P. Dupaigne, A. Thiel, E. Gigant, R. Mercier & F. Boccard, (2012) A MatP-divisome interaction coordinates chromosome segregation with cell division in *E. coli*. *EMBO J* **31**: 3198-3211.

Eswaramoorthy, P., D. Duan, J. Dinh, A. Dravis, S.N. Devi & M. Fujita, (2010) The threshold level of the sensor histidine kinase KinA governs entry into sporulation in *Bacillus subtilis*. *J Bacteriol* **192**: 3870-3882.

Eswaramoorthy, P., M.L. Erb, J.A. Gregory, J. Silverman, K. Pogliano, J. Pogliano &

K.S. Ramamurthi, (2011) Cellular architecture mediates DivIVA ultrastructure and regulates Min activity in *Bacillus subtilis*. *MBio* **2**.

Eswaramoorthy, P., P.W. Winter, P. Wawrzusin, A.G. York, H. Shroff & K.S. Ramamurthi, (2014) Asymmetric division and differential gene expression during a bacterial developmental program requires DivIVA. *PLoS Genet* **10**: e1004526.

Fawcett, P., P. Eichenberger, R. Losick & P. Youngman, (2000) The transcriptional profile of early to middle sporulation in *Bacillus subtilis*. *Proc Natl Acad Sci U S A* **97**: 8063-8068.

Feucht, A., T. Magnin, M.D. Yudkin & J. Errington, (1996) Bifunctional protein required for asymmetric cell division and cell-specific transcription in *Bacillus subtilis*. *Genes Dev* **10**: 794-803.

Fiche, J.B., D.I. Cattoni, N. Diekmann, J.M. Langerak, C. Clerte, C.A. Royer, E. Margeat, T. Doan & M. Nollmann, (2013) Recruitment, assembly, and molecular architecture of the SpoIIIE DNA pump revealed by superresolution microscopy. *PLoS Biol* **11**: e1001557.

Fisher, J.K., A. Bourniquel, G. Witz, B. Weiner, M. Prentiss & N. Kleckner, (2013) Four-dimensional imaging of *E. coli* nucleoid organization and dynamics in living cells. *Cell* **153**: 882-895.

Frandsen, N., I. Barak, C. Karmazyn-Campelli & P. Stragier, (1999) Transient gene asymmetry during sporulation and establishment of cell specificity in *Bacillus subtilis*. *Genes Dev* **13**: 394-399.

Fujita, M., J.E. Gonzalez-Pastor & R. Losick, (2005) High- and low-threshold genes in the Spo0A regulon of *Bacillus subtilis*. *J Bacteriol* **187**: 1357-1368.

Fujita, M. & R. Losick, (2005) Evidence that entry into sporulation in *Bacillus subtilis* is governed by a gradual increase in the level and activity of the master regulator Spo0A. *Genes Dev* **19**: 2236-2244.

Fuller, R.S., B.E. Funnell & A. Kornberg, (1984) The dnaA protein complex with the *E. coli* chromosomal replication origin (*oriC*) and other DNA sites. *Cell* **38**: 889-900.

Gamba, P., M.J. Jonker & L.W. Hamoen, (2015) A novel feedback loop that controls bimodal expression of genetic competence. *PLoS Genet* **11**: e1005047.

Gamba, P., J.W. Veening, N.J. Saunders, L.W. Hamoen & R.A. Daniel, (2009) Two-step assembly dynamics of the *Bacillus subtilis* divisome. *J Bacteriol* **191**: 4186-4194.

Garner, E.C., R. Bernard, W. Wang, X. Zhuang, D.Z. Rudner & T. Mitchison, (2011) Coupled, circumferential motions of the cell wall synthesis machinery and MreB filaments in *B. subtilis*. *Science* **333**: 222-225.

Gerdes, K., M. Howard & F. Szardenings, (2010) Pushing and pulling in prokaryotic DNA segregation. *Cell* **141**: 927-942.

Gholamhoseinian, A., Z. Shen, J.J. Wu & P. Piggot, (1992) Regulation of transcription of the cell division gene *ftsA* during sporulation of *Bacillus subtilis*. *J Bacteriol* **174**: 4647-4656.

Ghosal, D., D. Trambaiolo, L.A. Amos & J. Lowe, (2014) MinCD cell division proteins form alternating copolymeric cytomotive filaments. *Nat Commun* **5**: 5341.

Gibrat, J.F., T. Madej & S.H. Bryant, (1996) Surprising similarities in structure comparison. *Curr Opin Struct Biol* **6**: 377-385.

Gibson, D.G., L. Young, R.Y. Chuang, J.C. Venter, C.A. Hutchison, 3rd & H.O. Smith, (2009) Enzymatic assembly of DNA molecules up to several hundred kilobases. *Nat Methods* **6**: 343-345.

Gonzalez-Pastor, J.E., E.C. Hobbs & R. Losick, (2003) Cannibalism by sporulating bacteria. *Science* **301**: 510-513.

Gonzy-Treboul, G., C. Karmazyn-Campelli & P. Stragier, (1992) Developmental regulation of transcription of the *Bacillus subtilis ftsAZ* operon. *J Mol Biol* **224**: 967-979.

Graham, T.G., X. Wang, D. Song, C.M. Etson, A.M. van Oijen, D.Z. Rudner & J.J. Loparo, (2014) ParB spreading requires DNA bridging. *Genes Dev* **28**: 1228-1238.

Grainger, D.C., D. Hurd, M.D. Goldberg & S.J. Busby, (2006) Association of nucleoid proteins with coding and non-coding segments of the *Escherichia coli* genome. *Nucleic Acids Res* **34**: 4642-4652.

Grant, C.E., T.L. Bailey & W.S. Noble, (2011) FIMO: scanning for occurrences of a given motif. *Bioinformatics* **27**: 1017-1018.

Gregory, J.A., E.C. Becker & K. Pogliano, (2008) *Bacillus subtilis* MinC destabilizes FtsZ-rings at new cell poles and contributes to the timing of cell division. *Genes Dev* **22**: 3475-3488.

Grilley, M., K.M. Welsh, S.S. Su & P. Modrich, (1989) Isolation and characterization of the *Escherichia coli mutL* gene product. *J Biol Chem* **264**: 1000-1004.

Grkovic, S., M.H. Brown, M.A. Schumacher, R.G. Brennan & R.A. Skurray, (2001) The *Staphylococcal* QacR multidrug regulator binds a correctly spaced operator as a pair of dimers. *J Bacteriol* **183**: 7102-7109.

Gruber, S., (2018) SMC complexes sweeping through the chromosome: going with the flow and against the tide. *Curr Opin Microbiol* **42**: 96-103.

Gruber, S. & J. Errington, (2009) Recruitment of condensin to replication origin regions by ParB/SpoOJ promotes chromosome segregation in *B. subtilis*. *Cell* **137**: 685-696.

Gruber, S., J.W. Veening, J. Bach, M. Blettinger, M. Bramkamp & J. Errington, (2014) Interlinked sister chromosomes arise in the absence of condensin during fast replication in *B. subtilis*. *Curr Biol* **24**: 293-298.

Guberman, J.M., A. Fay, J. Dworkin, N.S. Wingreen & Z. Gitai, (2008) PSICIC: noise and asymmetry in bacterial division revealed by computational image analysis at sub-pixel resolution. *PLoS Comput Biol* **4**: e1000233.

Gueiros-Filho, F.J. & R. Losick, (2002) A widely conserved bacterial cell division protein that promotes assembly of the tubulin-like protein FtsZ. *Genes Dev* **16**: 2544-2556.

Gundogdu, M.E., Y. Kawai, N. Pavlendova, N. Ogasawara, J. Errington, D.J. Scheffers & L.W. Hamoen, (2011) Large ring polymers align FtsZ polymers for normal septum formation. *EMBO J* **30**: 617-626.

Guo, F. & S. Adhya, (2007) Spiral structure of *Escherichia coli* HUalphabeta provides foundation for DNA supercoiling. *Proc Natl Acad Sci U S A* **104**: 4309-4314.

Gutierrez, J., R. Smith & K. Pogliano, (2010) SpoIID-mediated peptidoglycan degradation is required throughout engulfment during *Bacillus subtilis* sporulation. *J Bacteriol* **192**: 3174-3186.

Hadizadeh Yazdi, N., C.C. Guet, R.C. Johnson & J.F. Marko, (2012) Variation of the folding and dynamics of the *Escherichia coli* chromosome with growth conditions. *Mol Microbiol* **86**: 1318-1333.

Haeusser, D.P. & W. Margolin, (2016) Splitsville: structural and functional insights into the dynamic bacterial Z ring. *Nat Rev Microbiol* **14**: 305-319.

Haeusser, D.P., R.L. Schwartz, A.M. Smith, M.E. Oates & P.A. Levin, (2004) EzrA prevents aberrant cell division by modulating assembly of the cytoskeletal protein FtsZ. *Mol Microbiol* **52**: 801-814.

Hajduk, I.V., C.D. Rodrigues & E.J. Harry, (2016) Connecting the dots of the bacterial cell cycle: Coordinating chromosome replication and segregation with cell division. *Semin Cell Dev Biol* **53**: 2-9.

Hale, C.A. & P.A. de Boer, (1997) Direct binding of FtsZ to ZipA, an essential component of the septal ring structure that mediates cell division in *E. coli*. *Cell* **88**: 175-185.

Hamoen, L.W., J.C. Meile, W. de Jong, P. Noirot & J. Errington, (2006) SepF, a novel FtsZ-interacting protein required for a late step in cell division. *Mol Microbiol* **59**: 989-999.

Hamon, M.A. & B.A. Lazazzera, (2001) The sporulation transcription factor Spo0A is required for biofilm development in *Bacillus subtilis*. *Mol Microbiol* **42**: 1199-1209.

Handler, A.A., J.E. Lim & R. Losick, (2008) Peptide inhibitor of cytokinesis during sporulation in *Bacillus subtilis*. *Mol Microbiol* **68**: 588-599.

Hansen, F.G. & T. Atlung, (2018) The DnaA Tale. *Front Microbiol* **9**: 319.

Hardy, C.D. & N.R. Cozzarelli, (2005) A genetic selection for supercoiling mutants of *Escherichia coli* reveals proteins implicated in chromosome structure. *Mol Microbiol* **57**: 1636-1652.

Harwood, C.R. & S.M. Cutting, (1990) *Molecular biological methods for Bacillus*. Wiley, New York, NY.

Harwood, C.R.a.C., S.M., (1990) *Molecular Biological Methods for Bacillus*. Wiley, New York.

Hilbert, D.W. & P.J. Piggot, (2004) Compartmentalization of gene expression during *Bacillus subtilis* spore formation. *Microbiol Mol Biol Rev* **68**: 234-262.

Hirano, T., (2006) At the heart of the chromosome: SMC proteins in action. *Nat Rev Mol Cell Biol* **7**: 311-322.

Hoch, J.A., (1991) Genetic analysis in *Bacillus subtilis*. *Methods Enzymol* **204**: 305-320.

Holmes, V.F. & N.R. Cozzarelli, (2000) Closing the ring: links between SMC proteins and chromosome partitioning, condensation, and supercoiling. *Proc Natl Acad Sci U S A* **97**: 1322-1324.

Hussain, S., C.N. Wivagg, P. Szwedziak, F. Wong, K. Schaefer, T. Izore, L.D. Renner, M.J. Holmes, Y. Sun, A.W. Bisson-Filho, S. Walker, A. Amir, J. Lowe & E.C. Garner, (2018) MreB filaments align along greatest principal membrane curvature to orient cell wall synthesis. *Elife* **7**.

Illing, N. & J. Errington, (1991) Genetic regulation of morphogenesis in *Bacillus subtilis*: roles of sigma E and sigma F in prespore engulfment. *J Bacteriol* **173**: 3159-3169.

Ioannou, C., P.M. Schaeffer, N.E. Dixon & P. Soultanas, (2006) Helicase binding to DnaI exposes a cryptic DNA-binding site during helicase loading in *Bacillus subtilis*. *Nucleic Acids Res* **34**: 5247-5258.

Ireton, K. & A.D. Grossman, (1994) A developmental checkpoint couples the initiation of sporulation to DNA replication in *Bacillus subtilis*. *EMBO J* **13**: 1566-1573.

Ireton, K., N.W.t. Gunther & A.D. Grossman, (1994) *spo0J* is required for normal chromosome segregation as well as the initiation of sporulation in *Bacillus subtilis*. *J Bacteriol* **176**: 5320-5329.

Ishikawa, S., L. Core & M. Perego, (2002) Biochemical characterization of aspartyl phosphate phosphatase interaction with a phosphorylated response regulator and its inhibition by a pentapeptide. *J Biol Chem* **277**: 20483-20489.

Ishikawa, S., Y. Kawai, K. Hiramatsu, M. Kuwano & N. Ogasawara, (2006) A new FtsZ-interacting protein, YlmF, complements the activity of FtsA during progression of cell division in *Bacillus subtilis*. *Mol Microbiol* **60**: 1364-1380.

Jameson, K.H. & A.J. Wilkinson, (2017) Control of initiation of DNA replication in *Bacillus subtilis* and *Escherichia coli*. *Genes (Basel)* **8**.

Jones, L.J., R. Carballido-Lopez & J. Errington, (2001) Control of cell shape in bacteria: helical, actin-like filaments in *Bacillus subtilis*. *Cell* **104**: 913-922.

Kahramanoglou, C., A.S. Seshasayee, A.I. Prieto, D. Ibberson, S. Schmidt, J. Zimmermann, V. Benes, G.M. Fraser & N.M. Luscombe, (2011) Direct and indirect effects of H-NS and Fis on global gene expression control in *Escherichia coli*. *Nucleic Acids Res* **39**: 2073-2091.

Kaimer, C., J.E. Gonzalez-Pastor & P.L. Graumann, (2009) SpoIIIE and a novel type of DNA translocase, SftA, couple chromosome segregation with cell division in *Bacillus subtilis*. *Mol Microbiol* **74**: 810-825.

Kaimer, C., K. Schenk & P.L. Graumann, (2011) Two DNA translocases synergistically affect chromosome dimer resolution in *Bacillus subtilis*. *J Bacteriol* **193**: 1334-1340.

Kar, S., R. Edgar & S. Adhya, (2005) Nucleoid remodeling by an altered HU protein: reorganization of the transcription program. *Proc Natl Acad Sci U S A* **102**: 16397-16402.

Karimova, G., J. Pidoux, A. Ullmann & D. Ladant, (1998) A bacterial two-hybrid system based on a reconstituted signal transduction pathway. *Proc Natl Acad Sci U S A* **95**: 5752-5756.

Kawai, Y. & N. Ogasawara, (2006) *Bacillus subtilis* EzrA and FtsL synergistically regulate FtsZ ring dynamics during cell division. *Microbiology* **152**: 1129-1141.

Kearns, D.B. & R. Losick, (2005) Cell population heterogeneity during growth of *Bacillus subtilis*. *Genes Dev* **19**: 3083-3094.

Khodursky, A.B., B.J. Peter, M.B. Schmid, J. DeRisi, D. Botstein, P.O. Brown & N.R. Cozzarelli, (2000) Analysis of topoisomerase function in bacterial replication fork movement: use of DNA microarrays. *Proc Natl Acad Sci U S A* **97**: 9419-9424.

Khvorova, A., V.K. Chary, D.W. Hilbert & P.J. Piggot, (2000) The chromosomal location of the *Bacillus subtilis* sporulation gene *spoIIR* is important for its function. *J Bacteriol* **182**: 4425-4429.

Khvorova, A., L. Zhang, M.L. Higgins & P.J. Piggot, (1998) The *spoIIE* locus is involved in the Spo0A-dependent switch in the location of FtsZ rings in *Bacillus subtilis*. *J Bacteriol* **180**: 1256-1260.

Kim, J., S.H. Yoshimura, K. Hizume, R.L. Ohniwa, A. Ishihama & K. Takeyasu, (2004) Fundamental structural units of the *Escherichia coli* nucleoid revealed by atomic force microscopy. *Nucleic Acids Res* **32**: 1982-1992.

King, N., O. Dreesen, P. Stragier, K. Pogliano & R. Losick, (1999) Septation, dephosphorylation, and the activation of sigmaF during sporulation in *Bacillus subtilis*. *Genes Dev* **13**: 1156-1167.

Kloosterman, T.G., R. Lenarcic, C.R. Willis, D.M. Roberts, L.W. Hamoen, J. Errington & L.J. Wu, (2016) Complex polar machinery required for proper chromosome segregation in vegetative and sporulating cells of *Bacillus subtilis*. *Mol Microbiol* **101**:

333-350.

Kowalski, D. & M.J. Eddy, (1989) The DNA unwinding element: a novel, *cis*-acting component that facilitates opening of the *Escherichia coli* replication origin. *EMBO J* **8**: 4335-4344.

Krol, E., A. de Sousa Borges, M. Kopacz & D.J. Scheffers, (2017) Metal-dependent SpoIIE oligomerization stabilizes FtsZ during asymmetric division in *Bacillus subtilis*. *PLoS One* **12**: e0174713.

Krzywinski, M., J. Schein, I. Birol, J. Connors, R. Gascoyne, D. Horsman, S.J. Jones & M.A. Marra, (2009) Circos: an information aesthetic for comparative genomics. *Genome Res* **19**: 1639-1645.

Kunkel, B., R. Losick & P. Stragier, (1990) The *Bacillus subtilis* gene for the development transcription factor sigma K is generated by excision of a dispensable DNA element containing a sporulation recombinase gene. *Genes Dev* **4**: 525-535.

Lan, G., B.R. Daniels, T.M. Dobrowsky, D. Wirtz & S.X. Sun, (2009) Condensation of FtsZ filaments can drive bacterial cell division. *Proc Natl Acad Sci U S A* **106**: 121-126.

Lee, P.S. & A.D. Grossman, (2006) The chromosome partitioning proteins Soj (ParA) and Spo0J (ParB) contribute to accurate chromosome partitioning, separation of replicated sister origins, and regulation of replication initiation in *Bacillus subtilis*. *Mol Microbiol* **60**: 853-869.

Lenarcic, R., S. Halbedel, L. Visser, M. Shaw, L.J. Wu, J. Errington, D. Marenduzzo & L.W. Hamoen, (2009) Localisation of DivIVA by targeting to negatively curved membranes. *EMBO J* **28**: 2272-2282.

Leonard, A.C. & J.E. Grimwade, (2015) The orisome: structure and function. *Front Microbiol* **6**: 545.

Levin, P.A., I.G. Kurtser & A.D. Grossman, (1999) Identification and characterization of a negative regulator of FtsZ ring formation in *Bacillus subtilis*. *Proc Natl Acad Sci U S A* **96**: 9642-9647.

Levin, P.A. & R. Losick, (1996) Transcription factor Spo0A switches the localization of the cell division protein FtsZ from a medial to a bipolar pattern in *Bacillus subtilis*. *Genes Dev* **10**: 478-488.

Levin, P.A., R. Losick, P. Stragier & F. Arigoni, (1997) Localization of the sporulation protein SpoIIE in *Bacillus subtilis* is dependent upon the cell division protein FtsZ. *Mol Microbiol* **25**: 839-846.

Levin, P.A., J.J. Shim & A.D. Grossman, (1998) Effect of minCD on FtsZ ring position and polar septation in *Bacillus subtilis*. *J Bacteriol* **180**: 6048-6051.

Levine, C., H. Hiasa & K.J. Marians, (1998) DNA gyrase and topoisomerase IV: biochemical activities, physiological roles during chromosome replication, and drug sensitivities. *Biochim Biophys Acta* **1400**: 29-43.

Levine, J.H., M.E. Fontes, J. Dworkin & M.B. Elowitz, (2012) Pulsed feedback defers cellular differentiation. *PLoS Biol* **10**: e1001252.

Lewis, P.J., S.D. Thaker & J. Errington, (2000) Compartmentalization of transcription and translation in *Bacillus subtilis*. *EMBO J* **19**: 710-718.

Lewis, P.J., L.J. Wu & J. Errington, (1998) Establishment of prespore-specific gene expression in *Bacillus subtilis*: localization of SpoIIE phosphatase and initiation of compartment-specific proteolysis. *J Bacteriol* **180**: 3276-3284.

Li, Y. & H. Araki, (2013) Loading and activation of DNA replicative helicases: the key step of initiation of DNA replication. *Genes Cells* **18**: 266-277.

Li, Y., B. Youngren, K. Sergueev & S. Austin, (2003) Segregation of the *Escherichia coli* chromosome terminus. *Mol Microbiol* **50**: 825-834.

Lim, H.C., I.V. Surovtsev, B.G. Beltran, F. Huang, J. Bewersdorf & C. Jacobs-Wagner, (2014) Evidence for a DNA-relay mechanism in ParABS-mediated chromosome segregation. *Elife* **3**: e02758.

Lin, D.C. & A.D. Grossman, (1998) Identification and characterization of a bacterial

chromosome partitioning site. *Cell* **92**: 675-685.

Lin, D.C., P.A. Levin & A.D. Grossman, (1997) Bipolar localization of a chromosome partition protein in *Bacillus subtilis*. *Proc Natl Acad Sci U S A* **94**: 4721-4726.

Lin, Z., C. Wang, X. Feng, M. Liu, J. Li & C. Bai, (1998) The observation of the local ordering characteristics of spermidine-condensed DNA: atomic force microscopy and polarizing microscopy studies. *Nucleic Acids Res* **26**: 3228-3234.

Lindow, J.C., R.A. Britton & A.D. Grossman, (2002) Structural maintenance of chromosomes protein of *Bacillus subtilis* affects supercoiling *in vivo*. *J Bacteriol* **184**: 5317-5322.

Lioy, V.S., A. Cournac, M. Marbouty, S. Duigou, J. Mozziconacci, O. Espeli, F. Boccard & R. Koszul, (2018) Multiscale structuring of the *E. coli* chromosome by nucleoid-associated and condensin proteins. *Cell* **172**: 771-783 e718.

Liu, L.F. & J.C. Wang, (1987) Supercoiling of the DNA template during transcription. *Proc Natl Acad Sci U S A* **84**: 7024-7027.

Livny, J., Y. Yamaichi & M.K. Waldor, (2007) Distribution of centromere-like *parS* sites in bacteria: insights from comparative genomics. *J Bacteriol* **189**: 8693-8703.

Loose, M. & T.J. Mitchison, (2014) The bacterial cell division proteins FtsA and FtsZ self-organize into dynamic cytoskeletal patterns. *Nat Cell Biol* **16**: 38-46.

Lopez, D. & R. Kolter, (2010) Extracellular signals that define distinct and coexisting cell fates in *Bacillus subtilis*. *FEMS Microbiol Rev* **34**: 134-149.

Lucchini, S., G. Rowley, M.D. Goldberg, D. Hurd, M. Harrison & J.C. Hinton, (2006) H-NS mediates the silencing of laterally acquired genes in bacteria. *PLoS Pathog* **2**: e81.

Lucet, I., A. Feucht, M.D. Yudkin & J. Errington, (2000) Direct interaction between the cell division protein FtsZ and the cell differentiation protein SpoIIE. *EMBO J* **19**: 1467-1475.

Lutkenhaus, J., (2007) Assembly dynamics of the bacterial MinCDE system and spatial regulation of the Z ring. *Annu Rev Biochem* **76**: 539-562.

Makowska-Grzyska, M. & J.M. Kaguni, (2010) Primase directs the release of DnaC from DnaB. *Mol Cell* **37**: 90-101.

Malik, M., A. Bensaid, J. Rouviere-Yaniv & K. Drlica, (1996) Histone-like protein HU and bacterial DNA topology: suppression of an HU deficiency by gyrase mutations. *J Mol Biol* **256**: 66-76.

Marchler-Bauer, A., S. Lu, J.B. Anderson, F. Chitsaz, M.K. Derbyshire, C. DeWeese-Scott, J.H. Fong, L.Y. Geer, R.C. Geer, N.R. Gonzales, M. Gwadz, D.I. Hurwitz, J.D. Jackson, Z. Ke, C.J. Lanczycki, F. Lu, G.H. Marchler, M. Mullokandov, M.V. Omelchenko, C.L. Robertson, J.S. Song, N. Thanki, R.A. Yamashita, D. Zhang, N. Zhang, C. Zheng & S.H. Bryant, (2011) CDD: a Conserved Domain Database for the functional annotation of proteins. *Nucleic Acids Res* **39**: D225-229.

Marston, A.L. & J. Errington, (1999) Dynamic movement of the ParA-like Soj protein of *B. subtilis* and its dual role in nucleoid organization and developmental regulation. *Mol Cell* **4**: 673-682.

Marston, A.L., H.B. Thomaides, D.H. Edwards, M.E. Sharpe & J. Errington, (1998) Polar localization of the MinD protein of *Bacillus subtilis* and its role in selection of the mid-cell division site. *Genes Dev* **12**: 3419-3430.

Massey, T.H., C.P. Mercogliano, J. Yates, D.J. Sherratt & J. Lowe, (2006) Double-stranded DNA translocation: structure and mechanism of hexameric FtsK. *Mol Cell* **23**: 457-469.

McGinness, T. & R.G. Wake, (1979) Completed *Bacillus subtilis* nucleoid as a doublet structure. *J Bacteriol* **140**: 730-733.

Meeske, A.J., C.D. Rodrigues, J. Brady, H.C. Lim, T.G. Bernhardt & D.Z. Rudner, (2016) High-throughput genetic screens identify a large and diverse collection of new sporulation genes in *Bacillus subtilis*. *PLoS Biol* **14**: e1002341.

Melby, T.E., C.N. Ciampaglio, G. Briscoe & H.P. Erickson, (1998) The symmetrical

structure of structural maintenance of chromosomes (SMC) and MukB proteins: long, antiparallel coiled coils, folded at a flexible hinge. *J Cell Biol* **142**: 1595-1604.

Mercier, R., M.A. Petit, S. Schbath, S. Robin, M. El Karoui, F. Boccard & O. Espeli, (2008) The MatP/*matS* site-specific system organizes the terminus region of the *E. coli* chromosome into a macrodomain. *Cell* **135**: 475-485.

Messer, W., F. Blaesing, J. Majka, J. Nardmann, S. Schaper, A. Schmidt, H. Seitz, C. Speck, D. Tungler, G. Wegrzyn, C. Weigel, M. Welzeck & J. Zakrzewska-Czerwinska, (1999) Functional domains of DnaA proteins. *Biochimie* **81**: 819-825.

Miermans, C.A. & C.P. Broedersz, (2018) Bacterial chromosome organization by collective dynamics of SMC condensins. *J R Soc Interface* **15**.

Migocki, M.D., M.K. Freeman, R.G. Wake & E.J. Harry, (2002) The Min system is not required for precise placement of the midcell Z ring in *Bacillus subtilis*. *EMBO Rep* **3**: 1163-1167.

Miller, A.K., E.E. Brown, B.T. Mercado & J.K. Herman, (2016) A DNA-binding protein defines the precise region of chromosome capture during Bacillus sporulation. *Mol Microbiol* **99**: 111-122.

Miller, D.T., J.E. Grimwade, T. Betteridge, T. Rozgaja, J.J. Torgue & A.C. Leonard, (2009) Bacterial origin recognition complexes direct assembly of higher-order DnaA oligomeric structures. *Proc Natl Acad Sci U S A* **106**: 18479-18484.

Minnen, A., L. Attaiech, M. Thon, S. Gruber & J.W. Veening, (2011) SMC is recruited to *oriC* by ParB and promotes chromosome segregation in *Streptococcus pneumoniae*. *Mol Microbiol* **81**: 676-688.

Minnen, A., F. Burmann, L. Wilhelm, A. Anchimiuk, M.L. Diebold-Durand & S. Gruber, (2016) Control of smc coiled coil architecture by the ATPase heads facilitates targeting to chromosomal ParB/*parS* and release onto flanking DNA. *Cell Rep* **14**: 2003-2016.

Modrich, P., (1989) Methyl-directed DNA mismatch correction. *J Biol Chem* **264**: 6597-6600.

Moeller, R., A.C. Schuerger, G. Reitz & W.L. Nicholson, (2012) Protective role of spore structural components in determining *Bacillus subtilis* spore resistance to simulated Mars surface conditions. *Appl Environ Microbiol* **78**: 8849-8853.

Molle, V., M. Fujita, S.T. Jensen, P. Eichenberger, J.E. Gonzalez-Pastor, J.S. Liu & R. Losick, (2003) The Spo0A regulon of *Bacillus subtilis*. *Mol Microbiol* **50**: 1683-1701.

Monahan, L.G., A. Robinson & E.J. Harry, (2009) Lateral FtsZ association and the assembly of the cytokinetic Z ring in bacteria. *Mol Microbiol* **74**: 1004-1017.

Montero Llopis, P., A.F. Jackson, O. Sliusarenko, I. Surovtsev, J. Heinritz, T. Emonet & C. Jacobs-Wagner, (2010) Spatial organization of the flow of genetic information in bacteria. *Nature* **466**: 77-81.

Mukherjee, A. & J. Lutkenhaus, (1998) Dynamic assembly of FtsZ regulated by GTP hydrolysis. *EMBO J* **17**: 462-469.

Mulder, E. & C.L. Woldringh, (1989) Actively replicating nucleoids influence positioning of division sites in *Escherichia coli* filaments forming cells lacking DNA. *J Bacteriol* **171**: 4303-4314.

Murat, D., M. Byrne & A. Komeili, (2010) Cell biology of prokaryotic organelles. *Cold Spring Harb Perspect Biol* **2**: a000422.

Murphy, L.D. & S.B. Zimmerman, (1995) Condensation and cohesion of lambda DNA in cell extracts and other media: implications for the structure and function of DNA in prokaryotes. *Biophys Chem* **57**: 71-92.

Murray, H. & J. Errington, (2008) Dynamic control of the DNA replication initiation protein DnaA by Soj/ParA. *Cell* **135**: 74-84.

Murray, H., H. Ferreira & J. Errington, (2006) The bacterial chromosome segregation protein Spo0J spreads along DNA from *parS* nucleation sites. *Mol Microbiol* **61**: 1352-1361.

Mysliwiec, T.H., J. Errington, A.B. Vaidya & M.G. Bramucci, (1991) The *Bacillus*

subtilis spo0J gene: evidence for involvement in catabolite repression of sporulation. *J Bacteriol* **173**: 1911-1919.

Nagler, K., C. Julius & R. Moeller, (2016) Germination of spores of astrobiologically relevant *Bacillus* species in high-salinity environments. *Astrobiology* **16**: 500-512.

Narula, J., S.N. Devi, M. Fujita & O.A. Igoshin, (2012) Ultrasensitivity of the *Bacillus subtilis* sporulation decision. *Proc Natl Acad Sci U S A* **109**: E3513-3522.

Narula, J., A. Kuchina, D.D. Lee, M. Fujita, G.M. Suel & O.A. Igoshin, (2015) Chromosomal arrangement of phosphorelay genes couples sporulation and DNA replication. *Cell* **162**: 328-337.

Narula, J., A. Kuchina, F. Zhang, M. Fujita, G.M. Suel & O.A. Igoshin, (2016) Slowdown of growth controls cellular differentiation. *Mol Syst Biol* **12**: 871.

Nasmyth, K. & C.H. Haering, (2005) The structure and function of SMC and kleisin complexes. *Annu Rev Biochem* **74**: 595-648.

Nicholson, W.L., N. Munakata, G. Horneck, H.J. Melosh & P. Setlow, (2000) Resistance of *Bacillus* endospores to extreme terrestrial and extraterrestrial environments. *Microbiol Mol Biol Rev* **64**: 548-572.

Nicolas, P., U. Mader, E. Dervyn, T. Rochat, A. Leduc, N. Pigeonneau, E. Bidnenko, E. Marchadier, M. Hoebeke, S. Aymerich, D. Becher, P. Bisicchia, E. Botella, O. Delumeau, G. Doherty, E.L. Denham, M.J. Fogg, V. Fromion, A. Goelzer, A. Hansen, E. Hartig, C.R. Harwood, G. Homuth, H. Jarmer, M. Jules, E. Klipp, L. Le Chat, F. Lecointe, P. Lewis, W. Liebermeister, A. March, R.A. Mars, P. Nannapaneni, D. Noone, S. Pohl, B. Rinn, F. Rugheimer, P.K. Sappa, F. Samson, M. Schaffer, B. Schwikowski, L. Steil, J. Stulke, T. Wiegert, K.M. Devine, A.J. Wilkinson, J.M. van Dijl, M. Hecker, U. Volker, P. Bessieres & P. Noirot, (2012) Condition-dependent transcriptome reveals high-level regulatory architecture in *Bacillus subtilis*. *Science* **335**: 1103-1106.

Niki, H., Y. Yamaichi & S. Hiraga, (2000) Dynamic organization of chromosomal DNA in *Escherichia coli*. *Genes Dev* **14**: 212-223.

Odijk, T., (1998) Osmotic compaction of supercoiled DNA into a bacterial nucleoid.

Biophys Chem **73**: 23-29.

Ogasawara, N. & H. Yoshikawa, (1992) Genes and their organization in the replication origin region of the bacterial chromosome. *Mol Microbiol* **6**: 629-634.

Ogura, M. & T. Tanaka, (2009) The *Bacillus subtilis* late competence operon *comE* is transcriptionally regulated by *yutB* and under post-transcription initiation control by *comN* (*yrzD*). *J Bacteriol* **191**: 949-958.

Ogura, Y., N. Ogasawara, E.J. Harry & S. Moriya, (2003) Increasing the ratio of Soj to Spo0J promotes replication initiation in *Bacillus subtilis*. *J Bacteriol* **185**: 6316-6324.

Ohlsen, K.L., J.K. Grimsley & J.A. Hoch, (1994) Deactivation of the sporulation transcription factor Spo0A by the Spo0E protein phosphatase. *Proc Natl Acad Sci U S A* **91**: 1756-1760.

Ojkic, N., J. Lopez-Garrido, K. Pogliano & R.G. Endres, (2016) Cell-wall remodeling drives engulfment during *Bacillus subtilis* sporulation. *Elife* **5**.

Oliva, M.A., S. Halbedel, S.M. Freund, P. Dutow, T.A. Leonard, D.B. Veprintsev, L.W. Hamoen & J. Lowe, (2010) Features critical for membrane binding revealed by DivIVA crystal structure. *EMBO J* **29**: 1988-2001.

Oshima, T., S. Ishikawa, K. Kurokawa, H. Aiba & N. Ogasawara, (2006) *Escherichia coli* histone-like protein H-NS preferentially binds to horizontally acquired DNA in association with RNA polymerase. *DNA Res* **13**: 141-153.

Otwinowski, Z. & W. Minor, (1997) [20] Processing of X-ray diffraction data collected in oscillation mode. *Methods Enzymol* **276**: 307-326.

Ouzounov, N., J.P. Nguyen, B.P. Bratton, D. Jacobowitz, Z. Gitai & J.W. Shaevitz, (2016) MreB orientation correlates with cell diameter in *Escherichia coli*. *Biophys J* **111**: 1035-1043.

Palecek, J.J. & S. Gruber, (2015) Kite proteins: a superfamily of SMC/Kleisin partners conserved across Bacteria, Archaea, and Eukaryotes. *Structure* **23**: 2183-2190.

Park, J.T. & T. Uehara, (2008) How bacteria consume their own exoskeletons (turnover and recycling of cell wall peptidoglycan). *Microbiol Mol Biol Rev* **72**: 211-227, table of contents.

Patrick, J.E. & D.B. Kearns, (2008) MinJ (YvjD) is a topological determinant of cell division in *Bacillus subtilis*. *Mol Microbiol* **70**: 1166-1179.

Pease, P.J., O. Levy, G.J. Cost, J. Gore, J.L. Ptacin, D. Sherratt, C. Bustamante & N.R. Cozzarelli, (2005) Sequence-directed DNA translocation by purified FtsK. *Science* **307**: 586-590.

Perez, A.R., A. Abanes-De Mello & K. Pogliano, (2000) SpoIIB localizes to active sites of septal biogenesis and spatially regulates septal thinning during engulfment in *Bacillus subtilis*. *J Bacteriol* **182**: 1096-1108.

Pichoff, S. & J. Lutkenhaus, (2005) Tethering the Z ring to the membrane through a conserved membrane targeting sequence in FtsA. *Mol Microbiol* **55**: 1722-1734.

Pichoff, S. & J. Lutkenhaus, (2007) Identification of a region of FtsA required for interaction with FtsZ. *Mol Microbiol* **64**: 1129-1138.

Piggot, P.J. & J.G. Coote, (1976) Genetic aspects of bacterial endospore formation. *Bacteriol Rev* **40**: 908-962.

Piggot, P.J. & D.W. Hilbert, (2004) Sporulation of *Bacillus subtilis*. *Curr Opin Microbiol* **7**: 579-586.

Pogliano, J., N. Osborne, M.D. Sharp, A. Abanes-De Mello, A. Perez, Y.L. Sun & K. Pogliano, (1999) A vital stain for studying membrane dynamics in bacteria: a novel mechanism controlling septation during *Bacillus subtilis* sporulation. *Mol Microbiol* **31**: 1149-1159.

Pogliano, J., M.D. Sharp & K. Pogliano, (2002) Partitioning of chromosomal DNA during establishment of cellular asymmetry in *Bacillus subtilis*. *J Bacteriol* **184**: 1743-1749.

Postow, L., C.D. Hardy, J. Arsuaga & N.R. Cozzarelli, (2004) Topological domain structure of the *Escherichia coli* chromosome. *Genes Dev* **18**: 1766-1779.

Predich, M., G. Nair & I. Smith, (1992) *Bacillus subtilis* early sporulation genes *kinA*, *spo0F*, and *spo0A* are transcribed by the RNA polymerase containing sigma H. *J Bacteriol* **174**: 2771-2778.

Prieto, A.I., C. Kahramanoglou, R.M. Ali, G.M. Fraser, A.S. Seshasayee & N.M. Luscombe, (2012) Genomic analysis of DNA binding and gene regulation by homologous nucleoid-associated proteins IHF and HU in *Escherichia coli* K12. *Nucleic Acids Res* **40**: 3524-3537.

Ptacin, J.L., M. Nollmann, E.C. Becker, N.R. Cozzarelli, K. Pogliano & C. Bustamante, (2008) Sequence-directed DNA export guides chromosome translocation during sporulation in *Bacillus subtilis*. *Nat Struct Mol Biol* **15**: 485-493.

Ptacin, J.L., M. Nollmann, C. Bustamante & N.R. Cozzarelli, (2006) Identification of the FtsK sequence-recognition domain. *Nat Struct Mol Biol* **13**: 1023-1025.

Ptacin, J.L. & L. Shapiro, (2013) Chromosome architecture is a key element of bacterial cellular organization. *Cellular microbiology* **15**: 45-52.

Rahn-Lee, L., B. Gorbatyuk, O. Skovgaard & R. Losick, (2009) The conserved sporulation protein YneE inhibits DNA replication in *Bacillus subtilis*. *J Bacteriol* **191**: 3736-3739.

Rajewska, M., K. Wegrzyn & I. Konieczny, (2012) AT-rich region and repeated sequences - the essential elements of replication origins of bacterial replicons. *FEMS Microbiol Rev* **36**: 408-434.

Ramamurthi, K.S. & R. Losick, (2009) Negative membrane curvature as a cue for subcellular localization of a bacterial protein. *Proc Natl Acad Sci U S A* **106**: 13541-13545.

Rannou, O., E. Le Chatelier, M.A. Larson, H. Nouri, B. Dalmais, C. Laughton, L. Janniere & P. Soultanas, (2013) Functional interplay of DnaE polymerase, DnaG primase and DnaC helicase within a ternary complex, and primase to polymerase hand-

off during lagging strand DNA replication in *Bacillus subtilis*. *Nucleic Acids Res* **41**: 5303-5320.

Rasband, W.S., (1997-2014) ImageJ. In. Bethesda, Maryland: U.S. National Institutes of Health, pp.

Raskin, D.M. & P.A. de Boer, (1999) Rapid pole-to-pole oscillation of a protein required for directing division to the middle of *Escherichia coli*. *Proc Natl Acad Sci U S A* **96**: 4971-4976.

Ricca, E., S. Cutting & R. Losick, (1992) Characterization of *bofA*, a gene involved in intercompartmental regulation of pro-sigma K processing during sporulation in *Bacillus subtilis*. *J Bacteriol* **174**: 3177-3184.

Rice, P.A., S. Yang, K. Mizuuchi & H.A. Nash, (1996) Crystal structure of an IHF-DNA complex: a protein-induced DNA U-turn. *Cell* **87**: 1295-1306.

Richardson, T.T., O. Harran & H. Murray, (2016) The bacterial DnaA-trio replication origin element specifies single-stranded DNA initiator binding. *Nature* **534**: 412-416.

Rodikova, E.A., O.V. Kovalevskiy, S.G. Mayorov, Z.I. Budarina, V.V. Marchenkov, B.S. Melnik, A.P. Leech, D.V. Nikitin, M.G. Shlyapnikov & A.S. Solonin, (2007) Two HlyIIR dimers bind to a long perfect inverted repeat in the operator of the hemolysin II gene from *Bacillus cereus*. *FEBS Lett* **581**: 1190-1196.

Rodrigues, C.D. & E.J. Harry, (2012) The Min system and nucleoid occlusion are not required for identifying the division site in *Bacillus subtilis* but ensure its efficient utilization. *PLoS Genet* **8**: e1002561.

Rossler, D., W. Ludwig, K.H. Schleifer, C. Lin, T.J. McGill, J.D. Wisotzkey, P. Jurtshuk, Jr. & G.E. Fox, (1991) Phylogenetic diversity in the genus *Bacillus* as seen by 16S rRNA sequencing studies. *Systematic and applied microbiology* **14**: 266-269.

Rowen, L. & A. Kornberg, (1978) Primase, the dnaG protein of *Escherichia coli*. An enzyme which starts DNA chains. *J Biol Chem* **253**: 758-764.

Rowland, S.L., W.F. Burkholder, K.A. Cunningham, M.W. Maciejewski, A.D. Grossman & G.F. King, (2004) Structure and mechanism of action of Sda, an inhibitor of the histidine kinases that regulate initiation of sporulation in *Bacillus subtilis*. *Mol Cell* **13**: 689-701.

Rowlett, V.W. & W. Margolin, (2015) The Min system and other nucleoid-independent regulators of Z ring positioning. *Front Microbiol* **6**: 478.

Ryter, A., P. Schaeffer & H. Ionesco, (1966) Cytologic classification, by their blockage stage, of sporulation mutants of *Bacillus subtilis* Marburg. *Ann Inst Pasteur (Paris)* **110**: 305-315.

Sanders, G.M., H.G. Dallmann & C.S. McHenry, (2010) Reconstitution of the *B. subtilis* replisome with 13 proteins including two distinct replicases. *Mol Cell* **37**: 273-281.

Schaeffer, P., J. Millet & J.P. Aubert, (1965) Catabolic repression of bacterial sporulation. *Proc Natl Acad Sci U S A* **54**: 704-711.

Scheffers, D.J. & J. Errington, (2004) PBP1 is a component of the *Bacillus subtilis* cell division machinery. *J Bacteriol* **186**: 5153-5156.

Schleiffer, A., S. Kaitna, S. Maurer-Stroh, M. Glotzer, K. Nasmyth & F. Eisenhaber, (2003) Kleisins: a superfamily of bacterial and eukaryotic SMC protein partners. *Mol Cell* **11**: 571-575.

Schneider, C.A., W.S. Rasband & K.W. Eliceiri, (2012) NIH Image to ImageJ: 25 years of image analysis. *Nat Methods* **9**: 671-675.

Scholefield, G., J. Errington & H. Murray, (2012) Soj/ParA stalls DNA replication by inhibiting helix formation of the initiator protein DnaA. *EMBO J* **31**: 1542-1555.

Scholefield, G., R. Whiting, J. Errington & H. Murray, (2011) Spo0J regulates the oligomeric state of Soj to trigger its switch from an activator to an inhibitor of DNA replication initiation. *Mol Microbiol* **79**: 1089-1100.

Schumacher, M.A., J. Lee & W. Zeng, (2016) Molecular insights into DNA binding and

anchoring by the *Bacillus subtilis* sporulation kinetochore-like RacA protein. *Nucleic Acids Res* **44**: 5438-5449.

Schumacher, M.A., M.C. Miller, S. Grkovic, M.H. Brown, R.A. Skurray & R.G. Brennan, (2001) Structural mechanisms of QacR induction and multidrug recognition. *Science* **294**: 2158-2163.

Schumacher, M.A., M.C. Miller, S. Grkovic, M.H. Brown, R.A. Skurray & R.G. Brennan, (2002) Structural basis for cooperative DNA binding by two dimers of the multidrug-binding protein QacR. *EMBO J* **21**: 1210-1218.

Sciochetti, S.A., P.J. Piggot & G.W. Blakely, (2001) Identification and characterization of the *dif* site from *Bacillus subtilis*. *J Bacteriol* **183**: 1058-1068.

Selber-Hnatiw, S., B. Rukundo, M. Ahmadi, H. Akoubi, H. Al-Bizri, A.F. Aliu, T.U. Ambeaghen, L. Avetisyan, I. Bahar, A. Baird, F. Begum, H. Ben Soussan, V. Blondeau-Ethier, R. Bordaries, H. Bramwell, A. Briggs, R. Bui, M. Carnevale, M. Chancharoen, T. Chevassus, J.H. Choi, K. Coulombe, F. Couvrette, S. D'Abreau, M. Davies, M.P. Desbiens, T. Di Maulo, S.A. Di Paolo, S. Do Ponte, P. Dos Santos Ribeiro, L.A. Dubuc-Kanary, P.K. Duncan, F. Dupuis, S. El-Nounou, C.N. Eyangos, N.K. Ferguson, N.R. Flores-Chinchilla, T. Fotakis, H.D.M. Gado Oumarou, M. Georgiev, S. Ghiassy, N. Glibetic, J. Gregoire Bouchard, T. Hassan, I. Huseen, M.F. Ibuna Quilatan, T. Iozzo, S. Islam, D.B. Jaunky, A. Jeyasegaram, M.A. Johnston, M.R. Kahler, K. Kaler, C. Kamani, H. Karimian Rad, E. Konidis, F. Konieczny, S. Kurianowicz, P. Lamothe, K. Legros, S. Leroux, J. Li, M.E. Lozano Rodriguez, S. Luponio-Yoffe, Y. Maalouf, J. Mantha, M. McCormick, P. Mondragon, T. Narayana, E. Neretin, T.T.T. Nguyen, I. Niu, R.B. Nkemazem, M. O'Donovan, M. Oueis, S. Paquette, N. Patel, E. Pecsi, J. Peters, A. Pettorelli, C. Poirier, V.R. Pompa, H. Rajen, R.O. Ralph, J. Rosales-Vasquez, D. Rubinshtein, S. Sakr, M.S. Sebai, L. Serravalle, F. Sidibe, A. Sinnathurai, D. Soho, A. Sundarakrishnan, V. Svistkova, T.E. Ugbeye, M.S. Vasconcelos, M. Vincelli, O. Voitovich, P. Vrabel, L. Wang, *et al.*, (2017) Human Gut Microbiota: Toward an Ecology of Disease. *Front Microbiol* **8**: 1265.

Setlow, B. & P. Setlow, (1993) Binding of small, acid-soluble spore proteins to DNA plays a significant role in the resistance of *Bacillus subtilis* spores to hydrogen peroxide. *Appl Environ Microbiol* **59**: 3418-3423.

Setlow, P., (2006) Spores of *Bacillus subtilis*: their resistance to and killing by radiation, heat and chemicals. *J Appl Microbiol* **101**: 514-525.

Sharp, M.D. & K. Pogliano, (2002) Role of cell-specific SpoIIIE assembly in polarity of DNA transfer. *Science* **295**: 137-139.

Sharpe, M.E. & J. Errington, (1996) The *Bacillus subtilis soj-spo0J* locus is required for a centromere-like function involved in prespore chromosome partitioning. *Mol Microbiol* **21**: 501-509.

Sheldrick, G.M., (2008) A short history of SHELX. *Acta Crystallogr A* **64**: 112-122.

Sherratt, D.J., B. Soballe, F.X. Barre, S. Filipe, I. Lau, T. Massey & J. Yates, (2004) Recombination and chromosome segregation. *Philos Trans R Soc Lond B Biol Sci* **359**: 61-69.

Shiu-Hin Chan, D., W.G. Seetoh, B.N. McConnell, D. Matak-Vinkovic, S.E. Thomas, V. Mendes, M. Blaszczyk, A.G. Coyne, T.L. Blundell & C. Abell, (2017) Structural insights into the EthR-DNA interaction using native mass spectrometry. *Chem Commun (Camb)* **53**: 3527-3530.

Sievers, J., B. Raether, M. Perego & J. Errington, (2002) Characterization of the *parB*-like *yyaA* gene of *Bacillus subtilis*. *J Bacteriol* **184**: 1102-1111.

Silhavy, T.J., D. Kahne & S. Walker, (2010) The bacterial cell envelope. *Cold Spring Harb Perspect Biol* **2**: a000414.

Singh, A.K., B. Manjasetty, G.L. Balasubramani, S. Koul, A. Kaushik, M.K. Ekka, V. Singh & S. Kumaran, (2015) Crystal Structure of Fad35R from *Mycobacterium tuberculosis* H37Rv in the Apo-State. *PLoS One* **10**: e0124333.

Singh, J.K., R.D. Makde, V. Kumar & D. Panda, (2007) A membrane protein, EzrA, regulates assembly dynamics of FtsZ by interacting with the C-terminal tail of FtsZ. *Biochemistry* **46**: 11013-11022.

Singh, S.S., N. Singh, R.P. Bonocora, D.M. Fitzgerald, J.T. Wade & D.C. Grainger, (2014) Widespread suppression of intragenic transcription initiation by H-NS. *Genes Dev* **28**: 214-219.

Smits, W.K., A.I. Goranov & A.D. Grossman, (2010) Ordered association of helicase loader proteins with the *Bacillus subtilis* origin of replication *in vivo*. *Mol Microbiol* **75**: 452-461.

Sobetzko, P., A. Travers & G. Muskhelishvili, (2012) Gene order and chromosome dynamics coordinate spatiotemporal gene expression during the bacterial growth cycle. *Proc Natl Acad Sci U S A* **109**: E42-50.

Soppa, J., K. Kobayashi, M.F. Noirot-Gros, D. Oesterhelt, S.D. Ehrlich, E. Dervyn, N. Ogasawara & S. Moriya, (2002) Discovery of two novel families of proteins that are proposed to interact with prokaryotic SMC proteins, and characterization of the *Bacillus subtilis* family members ScpA and ScpB. *Mol Microbiol* **45**: 59-71.

Soultanas, P., (2012) Loading mechanisms of ring helicases at replication origins. *Mol Microbiol* **84**: 6-16.

Speck, C. & W. Messer, (2001) Mechanism of origin unwinding: sequential binding of DnaA to double- and single-stranded DNA. *EMBO J* **20**: 1469-1476.

Stella, S., D. Cascio & R.C. Johnson, (2010) The shape of the DNA minor groove directs binding by the DNA-bending protein Fis. *Genes Dev* **24**: 814-826.

Stouf, M., J.C. Meile & F. Cornet, (2013) FtsK actively segregates sister chromosomes in *Escherichia coli*. *Proc Natl Acad Sci U S A* **110**: 11157-11162.

Stricker, J., P. Maddox, E.D. Salmon & H.P. Erickson, (2002) Rapid assembly dynamics of the *Escherichia coli* FtsZ-ring demonstrated by fluorescence recovery after photobleaching. *Proc Natl Acad Sci U S A* **99**: 3171-3175.

Sullivan, N.L., K.A. Marquis & D.Z. Rudner, (2009) Recruitment of SMC by ParB-*parS* organizes the origin region and promotes efficient chromosome segregation. *Cell* **137**: 697-707.

Surovtsev, I.V. & C. Jacobs-Wagner, (2018) Subcellular Organization: A critical feature of bacterial cell replication. *Cell* **172**: 1271-1293.

Surovtsev, I.V., H.C. Lim & C. Jacobs-Wagner, (2016) The slow mobility of the ParA partitioning protein underlies its steady-state patterning in *Caulobacter*. *Biophys J* **110**: 2790-2799.

Szwedziak, P., Q. Wang, S.M. Freund & J. Lowe, (2012) FtsA forms actin-like protofilaments. *EMBO J* **31**: 2249-2260.

Thiel, A., M. Valens, I. Vallet-Gely, O. Espeli & F. Boccard, (2012) Long-range chromosome organization in *E. coli*: a site-specific system isolates the Ter macrodomain. *PLoS Genet* **8**: e1002672.

Thomaides, H.B., M. Freeman, M. El Karoui & J. Errington, (2001) Division site selection protein DivIVA of *Bacillus subtilis* has a second distinct function in chromosome segregation during sporulation. *Genes Dev* **15**: 1662-1673.

Tocheva, E.I., J. Lopez-Garrido, H.V. Hughes, J. Fredlund, E. Kuru, M.S. Vannieuwenhze, Y.V. Brun, K. Pogliano & G.J. Jensen, (2013) Peptidoglycan transformations during *Bacillus subtilis* sporulation. *Mol Microbiol* **88**: 673-686.

Tonthat, N.K., S.T. Arold, B.F. Pickering, M.W. Van Dyke, S. Liang, Y. Lu, T.K. Beuria, W. Margolin & M.A. Schumacher, (2011) Molecular mechanism by which the nucleoid occlusion factor, SlmA, keeps cytokinesis in check. *EMBO J* **30**: 154-164.

Tonthat, N.K., S.L. Milam, N. Chinnam, T. Whitfill, W. Margolin & M.A. Schumacher, (2013) SlmA forms a higher-order structure on DNA that inhibits cytokinetic Z-ring formation over the nucleoid. *Proc Natl Acad Sci U S A* **110**: 10586-10591.

Tran, N.T., M.T. Laub & T.B.K. Le, (2017) SMC progressively aligns chromosomal arms in *Caulobacter crescentus* but is antagonized by convergent transcription. *Cell Rep* **20**: 2057-2071.

Updegrove, T.B. & K.S. Ramamurthi, (2017) Geometric protein localization cues in bacterial cells. *Curr Opin Microbiol* **36**: 7-13.

Ursell, T.S., J. Nguyen, R.D. Monds, A. Colavin, G. Billings, N. Ouzounov, Z. Gitai, J.W. Shaevitz & K.C. Huang, (2014) Rod-like bacterial shape is maintained by feedback between cell curvature and cytoskeletal localization. *Proc Natl Acad Sci U S A* **111**:

E1025-1034.

Valens, M., S. Penaud, M. Rossignol, F. Cornet & F. Boccard, (2004) Macrodomain organization of the *Escherichia coli* chromosome. *EMBO J* **23**: 4330-4341.

van Baarle, S. & M. Bramkamp, (2010) The MinCDJ system in *Bacillus subtilis* prevents minicell formation by promoting divisome disassembly. *PLoS One* **5**: e9850.

van Baarle, S., I.N. Celik, K.G. Kaval, M. Bramkamp, L.W. Hamoen & S. Halbedel, (2013) Protein-protein interaction domains of *Bacillus subtilis* DivIVA. *J Bacteriol* **195**: 1012-1021.

van den Ent, F., L. Amos & J. Lowe, (2001) Bacterial ancestry of actin and tubulin. *Curr Opin Microbiol* **4**: 634-638.

van Ruiten, M.S. & B.D. Rowland, (2018) SMC complexes: Universal DNA looping machines with distinct regulators. *Trends Genet* **34**: 477-487.

van Teeffelen, S. & L.D. Renner, (2018) Recent advances in understanding how rod-like bacteria stably maintain their cell shapes. *F1000Res* **7**: 241.

van Teeffelen, S., S. Wang, L. Furchtgott, K.C. Huang, N.S. Wingreen, J.W. Shaevitz & Z. Gitai, (2011) The bacterial actin MreB rotates, and rotation depends on cell-wall assembly. *Proc Natl Acad Sci U S A* **108**: 15822-15827.

Vecchiarelli, A.G., K. Mizuuchi & B.E. Funnell, (2012) Surfing biological surfaces: exploiting the nucleoid for partition and transport in bacteria. *Mol Microbiol* **86**: 513-523.

Veening, J.W., H. Murray & J. Errington, (2009) A mechanism for cell cycle regulation of sporulation initiation in *Bacillus subtilis*. *Genes Dev* **23**: 1959-1970.

Vega, D.E. & W. Margolin, (2019) Direct interaction between the two Z Ring membrane anchors FtsA and ZipA. *J Bacteriol* **201**.

Velten, M., S. McGovern, S. Marsin, S.D. Ehrlich, P. Noirot & P. Polard, (2003) A two-

protein strategy for the functional loading of a cellular replicative DNA helicase. *Mol Cell* **11**: 1009-1020.

Vos, S.M., E.M. Tretter, B.H. Schmidt & J.M. Berger, (2011) All tangled up: how cells direct, manage and exploit topoisomerase function. *Nat Rev Mol Cell Biol* **12**: 827-841.

Vreeland, R.H., W.D. Rosenzweig & D.W. Powers, (2000) Isolation of a 250 million-year-old halotolerant bacterium from a primary salt crystal. *Nature* **407**: 897-900.

Wagner, J.K., K.A. Marquis & D.Z. Rudner, (2009) SirA enforces diploidy by inhibiting the replication initiator DnaA during spore formation in *Bacillus subtilis*. *Mol Microbiol* **73**: 963-974.

Wagner-Herman, J.K., R. Bernard, R. Dunne, A.W. Bisson-Filho, K. Kumar, T. Nguyen, L. Mulcahy, J. Koullias, F.J. Gueiros-Filho & D.Z. Rudner, (2012) RefZ facilitates the switch from medial to polar division during spore formation in *Bacillus subtilis*. *J Bacteriol* **194**: 4608-4618.

Wagstaff, J. & J. Lowe, (2018) Prokaryotic cytoskeletons: protein filaments organizing small cells. *Nat Rev Microbiol* **16**: 187-201.

Walter, J.C., J. Dorignac, V. Lorman, J. Rech, J.Y. Bouet, M. Nollmann, J. Palmeri, A. Parmeggiani & F. Geniet, (2017) Surfing on protein waves: Proteophoresis as a mechanism for bacterial genome partitioning. *Phys Rev Lett* **119**: 028101.

Wang, J.C., (1991) DNA topoisomerases: why so many? *J Biol Chem* **266**: 6659-6662.

Wang, S.T., B. Setlow, E.M. Conlon, J.L. Lyon, D. Imamura, T. Sato, P. Setlow, R. Losick & P. Eichenberger, (2006) The forespore line of gene expression in *Bacillus subtilis*. *J Mol Biol* **358**: 16-37.

Wang, X., H.B. Brandao, T.B. Le, M.T. Laub & D.Z. Rudner, (2017) *Bacillus subtilis* SMC complexes juxtapose chromosome arms as they travel from origin to terminus. *Science* **355**: 524-527.

Wang, X., T.B. Le, B.R. Lajoie, J. Dekker, M.T. Laub & D.Z. Rudner, (2015)

Condensin promotes the juxtaposition of DNA flanking its loading site in *Bacillus subtilis*. *Genes Dev* **29**: 1661-1675.

Wang, X., P. Montero Llopis & D.Z. Rudner, (2014) *Bacillus subtilis* chromosome organization oscillates between two distinct patterns. *Proc Natl Acad Sci U S A* **111**: 12877-12882.

Wang, X. & D.Z. Rudner, (2014) Spatial organization of bacterial chromosomes. *Curr Opin Microbiol* **22**: 66-72.

Webb, C.D., A. Teleman, S. Gordon, A. Straight, A. Belmont, D.C. Lin, A.D. Grossman, A. Wright & R. Losick, (1997) Bipolar localization of the replication origin regions of chromosomes in vegetative and sporulating cells of *B. subtilis*. *Cell* **88**: 667-674.

Whitten, A.E., D.A. Jacques, B. Hammouda, T. Hanley, G.F. King, J.M. Guss, J. Trewhella & D.B. Langley, (2007) The structure of the KinA-Sda complex suggests an allosteric mechanism of histidine kinase inhibition. *J Mol Biol* **368**: 407-420.

Wilhelm, L., F. Burmann, A. Minnen, H.C. Shin, C.P. Toseland, B.H. Oh & S. Gruber, (2015) SMC condensin entraps chromosomal DNA by an ATP hydrolysis dependent loading mechanism in *Bacillus subtilis*. *Elife* **4**.

Winn, M.D., C.C. Ballard, K.D. Cowtan, E.J. Dodson, P. Emsley, P.R. Evans, R.M. Keegan, E.B. Krissinel, A.G. Leslie, A. McCoy, S.J. McNicholas, G.N. Murshudov, N.S. Pannu, E.A. Potterton, H.R. Powell, R.J. Read, A. Vagin & K.S. Wilson, (2011) Overview of the CCP4 suite and current developments. *Acta Crystallogr D Biol Crystallogr* **67**: 235-242.

Woldringh, C.L., E. Mulder, P.G. Huls & N. Vischer, (1991) Toporegulation of bacterial division according to the nucleoid occlusion model. *Res Microbiol* **142**: 309-320.

Woldringh, C.L., E. Mulder, J.A. Valkenburg, F.B. Wientjes, A. Zaritsky & N. Nanninga, (1990) Role of the nucleoid in the toporegulation of division. *Res Microbiol* **141**: 39-49.

Wu, H.Y., S.H. Shyy, J.C. Wang & L.F. Liu, (1988) Transcription generates positively and negatively supercoiled domains in the template. *Cell* **53**: 433-440.

Wu, L.J. & J. Errington, (1994) *Bacillus subtilis* SpoIIIE protein required for DNA segregation during asymmetric cell division. *Science* **264**: 572-575.

Wu, L.J. & J. Errington, (1997) Septal localization of the SpoIIIE chromosome partitioning protein in *Bacillus subtilis*. *EMBO J* **16**: 2161-2169.

Wu, L.J. & J. Errington, (1998) Use of asymmetric cell division and *spoIIIE* mutants to probe chromosome orientation and organization in *Bacillus subtilis*. *Mol Microbiol* **27**: 777-786.

Wu, L.J. & J. Errington, (2002) A large dispersed chromosomal region required for chromosome segregation in sporulating cells of *Bacillus subtilis*. *EMBO J* **21**: 4001-4011.

Wu, L.J. & J. Errington, (2003) RacA and the Soj-Spo0J system combine to effect polar chromosome segregation in sporulating *Bacillus subtilis*. *Mol Microbiol* **49**: 1463-1475.

Wu, L.J. & J. Errington, (2004) Coordination of cell division and chromosome segregation by a nucleoid occlusion protein in *Bacillus subtilis*. *Cell* **117**: 915-925.

Wu, L.J., S. Ishikawa, Y. Kawai, T. Oshima, N. Ogasawara & J. Errington, (2009) Noc protein binds to specific DNA sequences to coordinate cell division with chromosome segregation. *EMBO J* **28**: 1940-1952.

Wu, L.J., P.J. Lewis, R. Allmansberger, P.M. Hauser & J. Errington, (1995) A conjugation-like mechanism for prespore chromosome partitioning during sporulation in *Bacillus subtilis*. *Genes Dev* **9**: 1316-1326.

Wu, L.J.a.E., J., (2003) RacA and the Soj-Spo0J system combine to effect polar chromosome segregation in sporulating *Bacillus subtilis*. *Mol Microbiol* **49**: 1463-1475.

Yang, X., Z. Lyu, A. Miguel, R. McQuillen, K.C. Huang & J. Xiao, (2017) GTPase activity-coupled treadmilling of the bacterial tubulin FtsZ organizes septal cell wall synthesis. *Science* **355**: 744-747.

Yates, J., I. Zhekov, R. Baker, B. Eklund, D.J. Sherratt & L.K. Arciszewska, (2006)

Dissection of a functional interaction between the DNA translocase, FtsK, and the XerD recombinase. *Mol Microbiol* **59**: 1754-1766.

Yen Shin, J., J. Lopez-Garrido, S.H. Lee, C. Diaz-Celis, T. Fleming, C. Bustamante & K. Pogliano, (2015) Visualization and functional dissection of coaxial paired SpoIIIE channels across the sporulation septum. *Elife* **4**: e06474.

Young, K.D., (2006) The selective value of bacterial shape. *Microbiol Mol Biol Rev* **70**: 660-703.

Youngman, P.J., J.B. Perkins & R. Losick, (1983) Genetic transposition and insertional mutagenesis in *Bacillus subtilis* with *Streptococcus faecalis* transposon Tn*917*. *Proc Natl Acad Sci U S A* **80**: 2305-2309.

Youngren, B., H.J. Nielsen, S. Jun & S. Austin, (2014) The multifork *Escherichia coli* chromosome is a self-duplicating and self-segregating thermodynamic ring polymer. *Genes Dev* **28**: 71-84.

Yu, Z., S.E. Reichheld, A. Savchenko, J. Parkinson & A.R. Davidson, (2010) A comprehensive analysis of structural and sequence conservation in the TetR family transcriptional regulators. *J Mol Biol* **400**: 847-864.

Zhang, H.N., Z.W. Xu, H.W. Jiang, F.L. Wu, X. He, Y. Liu, S.J. Guo, Y. Li, L.J. Bi, J.Y. Deng, X.E. Zhang & S.C. Tao, (2017) Cyclic di-GMP regulates *Mycobacterium tuberculosis* resistance to ethionamide. *Sci Rep* **7**: 5860.

Zhang, X.Z. & Y. Zhang, (2011) Simple, fast and high-efficiency transformation system for directed evolution of cellulase in *Bacillus subtilis*. *Microb Biotechnol* **4**: 98-105.

Zwart, P.H., (2005) Anomalous signal indicators in protein crystallography. *Acta Crystallogr D Biol Crystallogr* **61**: 1437-1448.

APPENDIX A

CHAPTER II SUPPLEMENTAL

APPENDIX A TABLE A.1. STRAINS

Strain	Description	Reference
Parental		
B. subtilis PY79	*Bacillus subtilis* laboratory strain	(Youngman *et al.*, 1983)
B. subtilis 168	*Bacillus subtilis* laboratory strain 168 *trpC2*	Bacillus Genetic Stock Center (1A866)
WH320	Chemically mutagenized version of sequenced strain *B. megaterium DSM319*	MoBiTek
DH5α	*F- endA1 glnV44 thi-1 recA1 relA1 gyrA96 deoR nupG Φ80dlacZΔM15 Δ(lacZYA-argF)U169, hsdR17(r_K^- m_K^+), λ–*	
DHP1	*F-, cya-99, araD139, galE15, galK16, rpsL1 (Strr), hsdR2, mcrA1,mcrB1;*	Obtained from Thomas Bernhardt
AH109	*MATa, trp1-901, leu2-3, 112, ura3-52, his3-200, gal4D, gal80D, LYS2::GAL1UAS-GAL1TATA-HIS3, GAL2UAS-GAL2TATA-ADE2, URA3::MEL1UAS-MEL1TATA-lacZ, MEL1*	Clontech
WH320		
BAM073	P_{xylA}*-refZ*$_{Bsub}$ *(amp) (tet)*	Figure II.2A
B. subtilis 168		
BAM071	*amyE::*P_{hy}*-refZ*$_{Bmeq}$ *(spec)*	Figure II.2B
BJH205	RBM_{5mu}	This work
BJH241	*lacA::*P_{spoIIQ}*-cfp (erm)*	This work
BJW556	*ycgO::*P_{ftsW}*-tetR-cfp (spec),* $(tetO)_{48}$ *Ω* RBM_{L2} *region (cat)*	Figure II.6
BJH245	*lacA(-61°)::*P_{spoIIQ}*-cfp (erm), yycR(-7°)::*P_{spoIIQ}*-yfp (phleo), spoIIIE36-tet*	Figure II.8
BJH246	RBM_{5mu}*, lacA(-61°)::*P_{spoIIQ}*-cfp (erm), yycR(-7°)::*P_{spoIIQ}*-yfp (phleo), spoIIIE36-tet*	Figure II.8
BJH251	*refZ::cat, lacA(-61°)::*P_{spoIIQ}*-cfp (erm), yycR(-7°)::*P_{spoIIQ}*-yfp (phleo), spoIIIE36-tet*	Figure II.8
BJH253	*refZ::cat, amyE::*P_{refZ}*-refZ (spec), lacA(-61°)::*P_{spoIIQ}*-cfp (erm), yycR(-7°)::*P_{spoIIQ}*-yfp (phleo), spoIIIE36-tet*	Figure II.8
BJH292	RBM_{5mu}*, refZ::cat, lacA(-61°)::*P_{spoIIQ}*-cfp (erm), yycR(-7°)::*P_{spoIIQ}*-yfp (phleo), spoIIIE36-tet*	Figure II.8
BAM076	*+51°::*P_{spoIIQ}*-cfp (erm)*	This work
BAM077	RBM_{5mu}*, +51°::*P_{spoIIQ}*-cfp (erm), yycR(-7°)::*P_{spoIIQ}*-yfp (phleo), spoIIIE36-tet*	Figure II.8
BAM078	*+51°::*P_{spoIIQ}*-cfp (erm), yycR(-7°)::*P_{spoIIQ}*-yfp (phleo), spoIIIE36-tet*	Figure II.8
BAM079	*refZ::cat, +51°::*P_{spoIIQ}*-cfp (erm), yycR(-7°)::*P_{spoIIQ}*-yfp (phleo), spoIIIE36-tet*	Figure II.8
BAM080	RBM_{5mu}*, refZ::cat, +51°::*P_{spoIIQ}*-cfp (erm), yycR(-7°)::*P_{spoIIQ}*-yfp (phleo), spoIIIE36-tet*	Figure II.8
BAM081	*refZ::cat, amyE::*P_{refZ}*-refZ (spec), +51°::*P_{spoIIQ}*-cfp (erm), yycR(-7°)::*P_{spoIIQ}*-yfp (phleo), spoIIIE36-tet*	Figure II.8
BAM175	*+*RBM_{L1} *(wt), lacA(-61°)::*P_{spoIIQ}*-cfp (erm), yycR(-7°)::*P_{spoIIQ}*-yfp (phleo), spoIIIE36-tet*	Figure II.8
BAM176	*+*RBM_{L1} *(wt), +51°::*P_{spoIIQ}*-cfp (erm), yycR(-7°)::*P_{spoIIQ}*-yfp (phleo), spoIIIE36-tet*	Figure II.8
BAM185	*+*RBM_{L2} *(wt), lacA(-61°)::*P_{spoIIQ}*-cfp (erm), yycR(-7°)::*P_{spoIIQ}*-yfp (phleo), spoIIIE36-tet*	Figure II.8
BAM186	*+*RBM_{L2} *(wt), +51°::*P_{spoIIQ}*-cfp (erm), yycR(-7°)::*P_{spoIIQ}*-yfp (phleo), spoIIIE36-tet*	Figure II.8
BAM193	*+*RBM_{O} *(wt), lacA(-61°)::*P_{spoIIQ}*-cfp (erm), yycR(-7°)::*P_{spoIIQ}*-yfp (phleo), spoIIIE36-tet*	Figure II.8
BAM194	*+*RBM_{O} *(wt), +51°::*P_{spoIIQ}*-cfp (erm), yycR(-7°)::*P_{spoIIQ}*-yfp (phleo), spoIIIE36-tet*	Figure II.8
BAM183	*+*RBM_{R1} *(wt), lacA(-61°)::*P_{spoIIQ}*-cfp (erm), yycR(-7°)::*P_{spoIIQ}*-yfp (phleo), spoIIIE36-tet*	Figure II.8
BAM184	*+*RBM_{R1} *(wt), +51°::*P_{spoIIQ}*-cfp (erm), yycR(-7°)::*P_{spoIIQ}*-yfp (phleo), spoIIIE36-tet*	Figure II.8
BAM357	*+*RBM_{R2} *(wt) lacA(-61°)::*P_{spoIIQ}*-cfp (erm), yycR(-7°)::*P_{spoIIQ}*-yfp (phleo), spoIIIE36-tet*	Figure II.8
BAM358	*+*RBM_{R2} *(wt), +51°::*P_{spoIIQ}*-cfp (erm), yycR(-7°)::*P_{spoIIQ}*-yfp (phleo), spoIIIE36-tet*	Figure II.8
BAM108	*+*RBM_{L1} *(wt), +*RBM_{R2} *(wt), lacA(-61°)::*P_{spoIIQ}*-cfp (erm), yycR(-7°)::*P_{spoIIQ}*-yfp (phleo), spoIIIE36-tet*	Figure II.8

Appendix A Table A.1. Strains, continued

Strain	Description	Reference
BAM109	*+RBM_{L1} (wt), +RBM_{R2} (wt), +51°::P_{spoIIQ}-cfp (erm), yycR(-7°)::P_{spoIIQ}-yfp (phleo), spoIIIE36-tet*	Figure II.8
BAM117	*+RBM_{L2} (wt), +RBM_{R1} (wt), lacA(-61°)::P_{spoIIQ}-cfp (erm), yycR(-7°)::P_{spoIIQ}-yfp (phleo), spoIIIE36-tet*	Figure II.8
BAM116	*+RBM_{L2} (wt), +RBM_{R1} (wt), +51°::P_{spoIIQ}-cfp (erm), yycR(-7°)::P_{spoIIQ}-yfp (phleo), spoIIIE36-tet*	Figure II.8
BAM133	*+RBM_{L1} (wt), +RBM_{L2} (wt), lacA(-61°)::P_{spoIIQ}-cfp (erm), yycR(-7°)::P_{spoIIQ}-yfp (phleo), spoIIIE36-tet*	Figure II.8
BAM134	*+RBM_{L1} (wt), +RBM_{L2} (wt), +51°::P_{spoIIQ}-cfp (erm), yycR(-7°)::P_{spoIIQ}-yfp (phleo), spoIIIE36-tet*	Figure II.8
BAM140	*+RBM_{R1} (wt), +RBM_{R2} (wt), lacA(-61°)::P_{spoIIQ}-cfp (erm), yycR(-7°)::P_{spoIIQ}-yfp (phleo), spoIIIE36-tet*	Figure II.8
BAM141	*+RBM_{R1} (wt), +RBM_{R2} (wt), +51°::P_{spoIIQ}-cfp (erm), yycR(-7°)::P_{spoIIQ}-yfp (phleo), spoIIIE36-tet*	Figure II.8
BAM151	*+RBM_{L1} (wt), +RBM_{R1} (wt), +RBM_{R2} (wt), lacA(-61°)::P_{spoIIQ}-cfp (erm), yycR(-7°)::P_{spoIIQ}-yfp (phleo), spoIIIE36-tet*	Figure II.8
BAM152	*+RBM_{L1} (wt), +RBM_{R1} (wt), +RBM_{R2} (wt), +51°::P_{spoIIQ}-cfp (erm), yycR(-7°)::P_{spoIIQ}-yfp (phleo), spoIIIE36-tet*	Figure II.8
BAM156	*+RBM_{L2} (wt), +RBM_{R1} (wt), +RBM_{R2} (wt), lacA(-61°)::P_{spoIIQ}-cfp (erm), yycR(-7°)::P_{spoIIQ}-yfp (phleo), spoIIIE36-tet*	Figure II.8
BAM157	*+RBM_{L2} (wt), +RBM_{R1} (wt), +RBM_{R2} (wt), +51°::P_{spoIIQ}-cfp (erm), yycR(-7°)::P_{spoIIQ}-yfp (phleo), spoIIIE36-tet*	Figure II.8
***E. coli* DHP1**		
CAM247	*spoIIIE-T25 (kan), refZ-T18 (amp)*	Figure II.7
CAM243	*spoIIIE-T25 (kan), empty-T18 (amp)*	Figure II.7

APPENDIX A TABLE A.2. PLASMIDS

Plasmid	Description	Reference
pDR111	*$P_{hyperspank}$-empty (amp)(spec)*	David Z. Rudner
pJH048	*amyE::$P_{hyperspank}$-$refZ_{B.meg}$ (amp) (spec)*	Figure II.2A
pHIS1522	*P_{xylA}-empty (amp) (tet)*	MoBiTek
pYD029	*P_{xylA}-$refZ_{B.sub}$ (tet)*	Figure II.2B
pJH026	*pminiMAD – RBM_{Omu} (amp) (erm)*	Creating RBM_O point mutants
pJH027	*pminiMAD – RBM_{L2mu} (amp) (erm)*	Creating RBM_{L2} point mutants
pJH028	*pminiMAD – RBM_{L1mu} (amp) (erm)*	Creating RBM_{L1} point mutants
pJH029	*pminiMAD – RBM_{R2mu} (amp) (erm)*	Creating RBM_{R2} point mutants
pJH030	*pminiMAD – RBM_{R1mu} (amp) (erm)*	Creating RBM_{R1} point mutants
pJW119	*$(tetO)_{48}$ΩRBM$_{L2}$ region (amp) (cat)(Cambell vector)*	Figure II.6
pAM030	*SUMO-RefZ (amp)*	Figure II.5
pAM125	*spoIIIE-T25 (kan)*	Figure II.7
pJW101	*T18-refZ (amp)*	Figure II.7
pJW097	*refZ-T18 (amp)*	Figure II.7
pAM132	*T18-sftA (amp)*	Figure II.7
pAM131	*T25-sftA (kan)*	Figure II.7
pAM130	*sftA-T18 (amp)*	Figure II.7
pAM129	*sftA-T25 (kan)*	Figure II.7
pCH363	*empty-T18 (amp)*	Tom Bernhardt/B2H vector
pCH364	*T18-empty (amp)*	Tom Bernhardt/B2H vector
pKNT25	*empty-T25 (kan)*	Tom Bernhardt/B2H vector
pKT25	*T25-empty (kan)*	Tom Bernhardt/B2H vector
pER19	*Cambell vector*	(Ricca *et al.*, 1992)
pminiMAD	*ori^{BsTs} (amp) (erm)*	(Kearns & Losick, 2005)

APPENDIX TABLE A.3. OLIGOS

Oligo	Sequence 5' to 3'
OAM094	AAAAAGCTCTTCCGGTATGAAAGTAAGCACCAAAGACA
OAM095	TTTTTCTCGAGCTAGTTGGTGAGCGCCA
OAM098	CGATGGGAATTCATCATATTACAG
OAM099	TTAACGGGAGGAAATAATTCTATGAGTCGCTCATAGATGACATATAACGATCTGC
OAM100	TAATAAAACAGCGGAAGTCAGCATATACATTAATTTTTACGCTAAAAGCTTGG
OAM101	ATTCGAAAGTGGCTTGAGATTAC
OEB001	TCGACAATTAAAATCTGAATTCCTTC
OEB002	TATGGCTCGTCTTAAAGGCAGTTCTCGGTATCGTGGAGGTC
OEB003	GACCTCCACGATACCGAGAACTGCCTTTAAGACGAGCCATA
OEB004	CATCTTTGTTTCCCAGACAGC
OEB009	ATCAGCGCTCTGGTGATTG
OEB010	TTTTGCACAGCCTTAGCTTC
OEB012	GCGACACCTCATCATAACAA
OEB013	TTCCACCTCGCCGTAGATTC
OEB014	CCGCGCTTATGTACAGCATA
OEB015	AGCTTTAGCGGATCCGTGAT
OEB016	TTAAAGAACCGCTATGTCAG
OEB017	TGTATTCCTATACTACCACG
OEB018	TGGGCCATCTGCTCCATT
OEB019	GAGGACCCGTTTAAATGGAAGC
OEB020	GAAAACGAGAAATTTTCACACTC
OEB021	TTTTCTTCTTTTGACCGGCT
OEB027	ATTGAGAGTGCTAACAGAGGTGATG
OEB028	GTTGCAGAGCTAAATGTGATTTCATC
OEB029	GAAAACAAAACGATTAACTTTCCG
OEB030	GTGCTGTCTTAGGTACATGACAAC
OEB031	GCCTGAGTTCCATGATATCAC
OEB032	CTGCAATTTTCCATCTCTTCATA
OJH063	GGGAAATGTACAATGAAAGTAAGCACCAAAGACAAAATT
OJH064	GCCGGCATGCGGGTTGGTGAGCGCCACGTCTC
OJH112	CCATGGTACCGAAGCTGATTTGGTCAAGGTA
OJH113	GAGCTCGAGTGATTAAAACAAATAGCCCCC
OJH115	ACCGTAACAAGCTTTACACCA
OJH116	CCATGTCGACCAGGGAAAAAAAGTGCTCCTG
OJH117	CTCGAGCTCTTAACTGATCTGCTGCTT
OJH119	CCGAGCCGAATTCTTTCTCTA
OJH120	GGATCGGCCGGCTGGATTCAA
OJH121	GAGCTCGAGTCATTAAAAAAAGCCGTTCCC
OJH123	AATGGAATTCGCCATGATCAATAGCATTCA
OJH124	CATTCGGCCGCATCGGGATTCCTGCTGTAAC
OJH125	CTCGAGCTCTTAAGACTTTCCCGGCTT
OJH127	TCAAGAATTCCTTTCGTCATC
OJH128	CATTCGGCCGCTGGCAGGACTGGATGATCTC
OJH129	CTCGAGCTCTTAAGTGTTTCTATCCGC
OJH147	AATGGAATTCCGGCTGAGCTTTTGCACA
OJH152	TATTTGTTTTAATCACTCGAGCTCTCAAAACGAAAAGGCGGTCAA
OJH153	CAGATCAGTTAAGAGCTCGAGTAATCAAAGAAGACATTCCTTTAC
OJH154	TTTTTTTAATGACTCGAGCTCTTAAACATAATGAGCGTATTTTT
OJH155	GGAAAGTCTTAAGAGCTCGAGTGATGAAGGCTGTCTGGG
OJH156	AGAAACACTTAAGAGCTCGAGTGATTCACTTACAAATGCAGA
OJH201	GCGACTCATAGAATTATTTCCTCC
OJH202	ATGTATATGCTGACTTCCGCTGT

Appendix Table A.3. Oligos, continued

Oligo	Sequence 5' to 3'
OJW167	GCATGCATGCGTAACACACAGGAAACAGCTATGAAAGTAAGCACCAAAGACAAAATTA
OJW168	GCATGGATCCGAACCGCTACCGTTGGTGAGCGCCACGTCTCCT
OJW197	CGCGAATTCGCTGCTTAAAATTGGACCCATACG
OJW198	GCCGCTAGCTGCATGTCCGTTCTGTCAGCC
OKK034	CGCAAGCTTACATAAGGAGGAACTACTATGGCTGTACAGTCAAAAACG
OKK035	TTTGCTAGCCGGTGTTAGGATAATTGAACGCG
OKK060	GCATTCTAGAGTAACACACAGGAAACAGCTATGAGTGTGGCAAAGAAAAAA
OKK061	GCATGAATTCGAACCGCTACCGTTAGAAGAGAGCTCATCATATT
OKK064	GCATTCTAGAGTAACACACAGGAAACAGCTATGAGTTGGCTTCATAAATTT
OKK065	GCATGAATTCGAACCGCTACCGTTTTCGTTTATTAAATCACT
OKK066	GCATGGATCCGGGCAGCGGTATGAGTTGGCTTCATAAATTTTT
OKK067	GCATGAATTCTTATTCGTTTATTAAATCACTTGC

APPENDIX A METHODS A.1. STRAIN CONSTRUCTION

Right Arm (+51°) Reporter Construction

The *+51°::P_{spoIIQ}-cfp (erm)* reporter for the right arm trapping experiments (BAM076) was created by Gibson Assembly (Gibson *et al.*, 2009). Briefly, dsDNA in the *+51°* region were amplified from *Bs168* genomic DNA using primers sets OAM098/OAM099 ("UP") and OAM100/OAM101 ("DOWN"). The reporter portion was generated by PCR amplification of genomic DNA from BJH241, a strain harboring *lacA::PspoIIQ-cfp* (erm)(Sullivan *et al.*, 2009), using primer set OJH201/OJH202. The three products were combined in a one-step enzymatic assembly reaction and transformed directly into *B. subtilis 168* selecting for MLS resistance. The final strain was confirmed by PCR.

APPENDIX A METHODS A.2. PLASMID CONSTRUCTION

pAM030 was generated by cloning PCR product from OAM094 and OAM095 amplification of *Bs168* genomic into pTB146 (SapI-XhoI).

pAM125 was generated by cloning PCR product from OKK060 and OKK061 amplification of *Bs168* genomic into pKNT25 (XbaI-EcoRI).

pAM129 was generated by cloning PCR product from OKK064 and OKK065 amplification of *Bs168* genomic into pKNT25 (XbaI-EcoRI).

pAM130 was generated by cloning PCR product from OKK064 and OKK065 amplification of *Bs168* genomic into pCH363 (XbaI-EcoRI).

pAM131 was generated by cloning PCR product from OKK066 and OKK067 amplification of *Bs168* genomic into pKT25 (BamHI-EcoRI).

pAM132 was generated by cloning PCR product from OKK066 and OKK067 amplification of *Bs168* genomic into pCH364 (BamHI-EcoRI).

pJH026 was generated with overlap extension PCR. The "UP" product was amplified from *Bs168* genomic with primer pair OJH128/OJH129. The "DOWN" product was amplified from *Bs168* genomic with primer pair OJH156/ OJH147. The two PCR products were used as template for overlap extension PCR with primer pair OJH128/147. The amplified fragment was cut with EcoRI and KpnI and cloned into pminiMAD cut with the same enzymes.

pJH027 was generated with overlap extension PCR. The "UP" product was amplified from *Bs168* genomic with primer pair OJH112/OJH113. The "DOWN" product was amplified from *Bs168* genomic with primer pair OJH152/ OJH115. The two PCR products were used as template for overlap extension PCR with primer pair OJH112/115. The amplified fragment was cut with EcoRI and KpnI and cloned into pminiMAD cut with the same enzymes.

pJH028 was generated with overlap extension PCR. The "UP" product was amplified from *Bs168* genomic with primer pair OJH116/OJH117. The "DOWN" product was amplified from *Bs168* genomic with primer pair OJH153/ OJH119. The two PCR products were used as template for overlap extension PCR with primer pair OJH116/119. The amplified fragment was cut with SalI and EcoRI and cloned into pminiMAD cut with the same enzymes.

pJH029 was generated with overlap extension PCR. The "UP" product was amplified from *Bs168* genomic with primer pair OJH120/OJH121. The "DOWN" product was amplified from *Bs168* genomic with primer pair OJH154/ OJH123. The two PCR products were used as template for overlap extension PCR with primer pair OJH120/123. The amplified fragment was cut with EagI and EcoRI and cloned into pminiMAD cut with the same enzymes.

pJH030 was generated with overlap extension PCR. The "UP" product was amplified from *Bs168* genomic with primer pair OJH124/OJH125. The "DOWN" product was amplified from *Bs168* genomic with primer pair OJH155/ OJH127. The two PCR products were used as template for overlap extension PCR with primer pair OJH124/127. The amplified fragment was cut with EagI and EcoRI and cloned into pminiMAD cut with the same enzymes.

pJH047 was generated by was generated by cloning PCR product from OKK034 and OKK035 amplification of *Bacillus megaterium* WH320 genomic into pDR111 (HindIII-EcoRI).

pJW087 was generated by was generated by cloning PCR product from OJW152 and OJW153 amplification of PY79 genomic into pGADT7 (EcoRI-BamHI).

pJW089 was generated by was generated by cloning PCR product from OJW152 and OJW153 amplification of PY79 genomic into pGBKT7 (EcoRI-BamHI).

pJW096 was generated by cloning PCR product from OJW167 and OJW168 amplification of PY79 genomic into pKNT25 (SphI-BamHI).

pJW097 was generated by cloning PCR product from OJW167 and OJW168 amplification of PY79 genomic into pCH363 (SphI-BamHI).

pJW101 was generated by cloning PCR product from OJW171 and OJW172 amplification of PY79 genomic into pCH363 (EcoRI-BamHI).

pJW119 was generated by cloning PCR product from OJW197 and OJW198 amplification of PY79 genomic into (EcoRI-NheI) into pER19 harboring a $(tetO)_{48}$ fragment at NheI-HindIII site.

pYD029 was generated by cloning PCR product from OJH063 and OJH064 amplification of *Bs168* genomic into pHIS1522 (BsrGI-SphI).

APPENDIX A METHODS A.3. BIOINFORMATICS ANALYSIS OF *RBM*S ACROSS *BACILLUS*

Using FIMO each complete *Bacillus* genome record in Genbank with an annotated *dnaA* was used to search for the *RBM* sequence using the following motif file:

MEME version 4

ALPHABET= ACGT

strands: + -

MOTIF refZ

letter-probability matrix: alength= 4 w= 20 nsites= 5 E= 2.8e-005

0.000000 0.000000 0.000000 1.000000
0.000000 0.000000 0.000000 1.000000
0.800000 0.000000 0.200000 0.000000
1.000000 0.000000 0.000000 0.000000
1.000000 0.000000 0.000000 0.000000
0.000000 1.000000 0.000000 0.000000
1.000000 0.000000 0.000000 0.000000
1.000000 0.000000 0.000000 0.000000
1.000000 0.000000 0.000000 0.000000
0.000000 1.000000 0.000000 0.000000
0.000000 0.000000 1.000000 0.000000
0.000000 0.000000 0.000000 1.000000
0.000000 0.000000 0.000000 1.000000
0.000000 0.000000 0.000000 1.000000
0.200000 0.200000 0.600000 0.000000
1.000000 0.000000 0.000000 0.000000
0.000000 0.000000 0.000000 1.000000
0.000000 0.200000 0.200000 0.600000
0.800000 0.200000 0.000000 0.000000
1.000000 0.000000 0.000000 0.000000

Every hit that had a P-value less than $1x10^{-10}$ and contained the central palindrome was sorted by distance from the annotated origin. Some genomes (for example, *Bacillus anthracis* A2012) appeared to have misannotated start sites. The raw data entered in GenBank was used for our analysis unless indicated otherwise. The $1x10^{-10}$ cutoff was based on the fact that this value did not eliminate any of the five *oriC*-proximal *RBM*s (*Bacillus subtilis* PY79 and 168) characterized in this study. Due to the stringency of the P-value cutoff, it is likely that that not all bona fide *RBM* sites were identified in the analysis.

In some of the cases, the putative *RBM* is a perfect palindrome, resulting in the production of two records for a single *RBM* (one for each DNA strand). These were easily identifiable due to the identical coordinates. In order to graphically represent this data, each genome size and *RBM* coordinate was normalized to 360 degrees (-180 and +180 from the annotated *oriC*)(see APPENDIX A Figure A.1). Below are the coordinates and sequences for a subset of the strains represented graphically, including all of those displayed in Figure II.1D (highlighted in yellow).

B. amyloliquefaciens

Strain: FZB42

Accession: CP000560

Size: 3,918,589

Start	Stop	Angle(°)	Strand	p-value	Gene (Strand)	Sequence
393,046	393,064	36.11	+	1.00e-11	yxeP (+)	TTAAACAAACGTTTAATCAA
3,464,227	3,464,246	318.26	-	8.19e-11	ywqE (-)	TTAAACAAACGTTTGAATAA

Strain: TA208

Accession: CP002627

Size: 3,937,511

Start	Stop	Angle(°)	Strand	p-value	Gene (Strand)	Sequence
288,100	288,119	26.34	+	3.09e-11	aroK (+)/cah (+)	TTAAACAAACGTTTGATAAA
357,782	357,801	32.71	+	1.00e-11	yxeP (+)	TTAAACAAACGTTTAATCAA
3,497,498	3,497,517	319.77	-	8.19e-11	ptpZ (-)	TTAAACAAACGTTTGAATAA

Strain: LL3

Accession: CP002634

Size: 3,995,227

Start	Stop	Angle(°)	Strand	p-value	Gene (Strand)	Sequence
292,778	292,797	26.38	+	3.09e-11	aroK (+)/cah (+)	TTAAACAAACGTTTGATAAA
362,458	362,477	32.66	+	1.00e-11	yxeP (+)	TTAAACAAACGTTTAATCAA
3,544,320	3,544,339	319.37	-	8.19e-11	ptpZ (-)	TTAAACAAACGTTTGAATAA

Strain: XH7

Accession: CP002927

Size: 3,939,203

Start	Stop	Angle(°)	Strand	p-value	Gene (Strand)	Sequence
294,010	294,029	26.87	+	3.09e-11	aroK (+)/cah (+)	TTAAACAAACGTTTGATAAA
363,692	363,711	33.24	+	1.00e-11	yxeP (+)	TTAAACAAACGTTTAATCAA
3,499,161	3,499,180	315.22	-	8.19e-11	ywqE (-)	TTAAACAAACGTTTGAATAA

Strain: Y2

Accession: CP003332

Size: 4,238,624

Start	Stop	Angle(°)	Strand	p-value	Gene (Strand)	Sequence
375,752	375,771	31.91	+	1.00e-11	yxeP (+)	TTAAACAAACGTTTAATCAA
3,773,857	3,773,876	320.54	-	8.19e-11	ywqE (-)	TTAAACAAACGTTTGAATAA

Strain: DSM7

Accession: FN597644

Size: 3,980,199

Start	Stop	Angle(°)	Strand	p-value	Gene (Strand)	Sequence
310,978	310,997	28.13	+	3.09e-11	aroK (+)/cah (+)	TTAAACAAACGTTTGATAAA
380,507	380,526	34.42	+	1.00e-11	yxeP (+)	TTAAACAAACGTTTAATCAA
3,530,326	3,530,354	319.11	-	8.19e-11	ptpZ (-)	TTAAACAAACGTTTGAATAA

Strain: subsp. plantarum CAU B946

Accession: HE617159

Size: 4,019,861

Start	Stop	Angle(°)	Strand	p-value	Gene (Strand)	Sequence
377,029	377,048	33.77	+	1.00e-11	yxeP (+)	TTAAACAAACGTTTAATCAA
3,584,864	3,584,883	321.05	-	8.19e-11	ywqE (-)	TTAAACAAACGTTTGAATAA

Strain: subsp. plantarum YAU B9601-Y2

Accession: HE774679
Size: 4,242,774

Start	Stop	Angle(°)	Strand	p-value	Gene (Strand)	Sequence
377,481	377,500	32.03	+	1.00e-11	yxeP (+)	TTAAACAAACGTTTAATCAA
3,777,734	3,777,753	320.54	-	8.19e-11	ywqE (-)	TTAAACAAACGTTTGAATAA

B. anthracis

Strain: Ames

Accession: AE016879

Size: 5,227,293

Start	Stop	Angle(°)	Strand	p-value	Gene (Strand)	Sequence
395,632	395,651	27.25	+	9.09e-13	thiE (+)/BA_0378 (-)	TTAAACAAACGTTTGATTAA
329,879	329,898	22.72	-	9.09e-13	gatB (+)/BA_0323 (+)	TTAAACAAACGTTTGATTAA
329,914	329,933	22.72	+	9.09e-13	gatB (+)/BA_0323 (+)	TTAAACAAACGTTTGATTAA
408,014	408,033	28.10	+	8.19e-11	BA_0388 (+)/BA_0389 (+)	TTAAACAAACGTTTGATTAG
408,059	408,078	28.10	+	8.19e-11	BA_0388 (+)/BA_0389 (+)	TTAAACAAACGTTTGTTTAA
408,059	408,078	28.10	-	8.19e-11	BA_0388 (+)/BA_0389 (+)	TTAAACAAACGTTTGTTTAA
4,742,752	4,742,771	326.63	+	9.09e-13	BA_5229 (-)/BA_5230 (-)	TTAAACAAACGTTTGATTAA
4,742,834	4,742,853	326.64	+	9.09e-13	BA_5229 (-)/BA_5230 (-)	TTAAACAAACGTTTGATTAA
4,955,850	4,955,869	341.31	+	9.09e-13	BA_5466 (+)/BA_5497 (-)	TTAAACAAACGTTTGATTAA

Strain: Ames Ancestor

Accession: AE017334
Size: 5,227,419

Start	Stop	Angle(°)	Strand	p-value	Gene (Strand)	Sequence
395,632	395,651	27.25	+	9.09e-13	thiE (+)/GBAA_0378 (-)	TTAAACAAACGTTTGATTAA
329,879	329,898	22.72	-	9.09e-13	gatB (+)/GBAA_0323 (+)	TTAAACAAACGTTTGATTAA
329,914	329,933	22.72	+	9.09e-13	gatB (+)/GBAA_0323 (+)	TTAAACAAACGTTTGATTAA
408,014	408,033	28.10	+	8.19e-11	GBAA_0388 (+)/GBAA_0389 (+)	TTAAACAAACGTTTGATTAG
408,059	408,078	28.10	+	8.19e-11	GBAA_0388 (+)/GBAA_0389 (+)	TTAAACAAACGTTTGTTTAA
408,059	408,078	28.10	-	8.19e-11	GBAA_0388 (+)/GBAA_0389 (+)	TTAAACAAACGTTTGTTTAA
4,955,976	4,955,995	341.31	+	9.09e-13	GBAA_5466 (+)/GBAA_5467 (-)	TTAAACAAACGTTTGATTAA
4,742,878	4,742,897	326.63	+	9.09e-13	GBAA_5229 (-)/GBAA_5230 (-)	TTAAACAAACGTTTGATTAA
4,742,960	4,742,979	326.64	+	9.09e-13	GBAA_5229 (-)/GBAA_5230 (-)	TTAAACAAACGTTTGATTAA

Strain: CDC 684

Accession: CP001215
Size: 5,230,115

Start	Stop	Angle(°)	Strand	p-value	Gene (Strand)	Sequence
330,233	330,252	22.73	-	9.09e-13	gatB (+)/BAMEG_0382 (+)	TTAAACAAACGTTTGATTAA
330,268	330,287	22.73	+	9.09e-13	gatB (+)/BAMEG_0382 (+)	TTAAACAAACGTTTGATTAA
395,985	396,004	27.19	+	9.09e-13	thiE (+)/BAMEG_0444 (-)	TTAAACAAACGTTTGATTAA
408,463	408,482	28.12	+	8.19e-11	BAMEG_0456 (+)/BAMEG_0457 (+)	TTAAACAAACGTTTGATTAG
408,508	408,527	28.12	+	8.19e-11	BAMEG_456 (+)/BAMEG_0457 (+)	TTAAACAAACGTTTGTTTAA
408,508	408,527	28.12	-	8.19e-11	BAMEG_456 (+)/BAMEG_0457 (+)	TTAAACAAACGTTTGTTTAA
4,745,201	4,745,220	326.62	+	9.09e-13	BAMEG_5285 (-)/BAMEG_5286 (-)	TTAAACAAACGTTTGATTAA
4,745,283	4,745,302	326.63	+	9.09e-13	BAMEG_5285 (-)/BAMEG_5286 (-)	TTAAACAAACGTTTGATTAA
4,958,300	4,958,319	341.29	+	9.09e-13	BAMEG_5514 (+)/BAMEG_5515 (-)	TTAAACAAACGTTTGATTAA

Strain: A0248

Accession: CP001598
Size: 5,227,419

Start	Stop	Angle(°)	Strand	p-value	Gene (Strand)	Sequence
329,779	329,798	22.71	-	9.09e-13	gatB (+)/BAA_0379 (+)	TTAAACAAACGTTTGATTAA
329,814	329,833	22.71	+	9.09e-13	gatB (+)/BAA_0379 (+)	TTAAACAAACGTTTGATTAA
395,532	595,551	27.24	+	9.09e-13	thiE (+)/BAA_0441 (-)	TTAAACAAACGTTTGATTAA
407,914	407,933	28.09	+	8.19e-11	BAA_0452 (+)/BAA_0453 (+)	TTAAACAAACGTTTGATTAG
407,959	407,978	28.10	+	8.19e-11	BAA_0452 (+)/BAA_0453 (+)	TTAAACAAACGTTTGTTTAA
407,959	407,978	28.10	-	8.19e-11	BAA_0453 (+)/BAA_0453 (+)	TTAAACAAACGTTTGTTTAA
4,955,876	4,955,895	341.30	+	9.09e-13	BAA_5494 (+)/BAA_5495 (-)	TTAAACAAACGTTTGATTAA
4,742,778	4,742,797	326.56	+	9.09e-13	BAA_5264 (-)/BAA_5264 (-)	TTAAACAAACGTTTGATTAA
4,742,860	4,742,879	326.56	+	9.09e-13	BAA_5264 (-)/BAA_5264 (-)	TTAAACAAACGTTTGATTAA

B. atrophaeus

Strain: 1942

Accession: CP002207
Size: 4,168,266

Start	Stop	Angle(°)	Strand	p-value	Gene (Strand)	Sequence
368,215	369,234	31.89	-	4.55e-13	BATR1942_20340 (+)/BATR1942_20345(-)	TTAAACAAACGTTTCATTAA
431,516	431,535	37.27	+	4.55e-12	BATR1942_20570 (+)	TTAAACAAACGTTTAATTAA
3,642,884	3,642,903	314.62	-	8.19e-13	BATR1942_15800 (-)/BATR1942_15805(-)	TTAAACAAACGTTTGATTAT
3,730,800	3,730,819	322.22	+	6.37e-13	ureA (-)/BATR1942_16290(-)	TTGAACAAACGTTTGATTAA

Note: dnaA is annoted at the 313.4° position in the genbank file. I've adjusted the coordinates by the appropriate amount.

B. cereus

Strain: ATCC10987

Accession: AE017194
Size: 5,224,283

Start	Stop	Angle(°)	Strand	p-value	Gene (Strand)	Sequence
370,834	370,853	25.55	-	9.09e-13	gatB (+)/BCE_0352 (+)	TTAAACAAACGTTTGATTAA
370,869	370,888	25.56	+	9.09e-13	gatB (+)/BCE_0352 (+)	TTAAACAAACGTTTGATTAA
502,625	502,644	34.64	+	9.09e-13	thiE (+)/BCE_0488 (-)	TTAAACAAACGTTTGATTAA
515,844	515,863	35.55	+	8.19e-11	BCE_0501 (+)	TTAAACAAACGTTTGATTAG
515,889	515,908	35.55	+	9.09e-13	BCE_0501 (+)/BCE_0502 (+)	TTAAACAAACGTTTGATTAA
4,735,175	4,735,194	326.30	+	8.19e-11	BCE_5131 (-)/BCE_5132 (-)	TTAAACAAACATTTGATTAA
4,735,256	4,735,275	326.30	+	9.09e-13	BCE_5231 (-)/BCE_5132 (-)	TTAAACAAACGTTTGATTAA
4,735,337	4,735,356	326.31	+	9.09e-13	BCE_5131 (-)/BCE_5132)	TTAAACAAACGTTTGATTAA
4,933,421	4,933,440	344.09	+	9.09e-13	BCE_5344 (+)/BCE_5345 (-)	TTAAACAAACGTTTGATTAA

Strain: E33L

Accession: CP000001
Size: 5,300,915

Start	Stop	Angle(°)	Strand	p-value	Gene (Strand)	Sequence
343,657	343,676	23.34	-	9.09e-13	gatB (+)/BCE33L0294 (+)	TTAAACAAACGTTTGATTAA
343,692	343,711	23.34	+	9.09e-13	gatB (+)/BCE33L0294 (+)	TTAAACAAACGTTTGATTAA
413,006	413,025	27.89	+	9.09e-13	BCE33L0350	TTAAACAAACGTTTGATTAA
426,236	426,255	28.95	+	8.19e-11	BCE33L0362 (+)/BCE33L0363(+)	TTAAACAAACGTTTGATTAG
426,281	426,300	28.95	+	9.09e-13	BCE33L0362	TTAAACAAACGTTTGATTAA
4,811,502	4,811,524	326.76	+	9.09e-13	arsC (-)/BCE33L4718 (-)	TTAAACAAACGTTTGATTAA
4,811,583	4,811,,602	326.77	+	9.09e13	arsC (-)/BCE33L4718 (-)	TTAAACAAACGTTTGATTAA
5,017,010	5,017,029	340.72	+	9.09e-13	BCE33L4926 (+)/BCE33L4926(-)	TTAAACAAACGTTTGATTAA

Strain: Q1

Accession: CP000227

Size: 5,214,195

Start	Stop	Angle(°)	Strand	p-value	Gene (Strand)	Sequence
350,211	350,230	24.18	-	9.09e-13	gatB (+)/BCQ_0373 (+)	TTAAACAAACGTTTGATTAA
350,246	350,265	24.18	+	9.09e-13	gatB (+)/BCQ_0373 (+)	TTAAACAAACGTTTGATTAA
461,423	461,442	21.86	+	9.09e-13	BCQ_0463 (+)	TTAAACAAACGTTTGATTAA
474,631	474,650	32.77	+	8.19e-11	BCQ_0475 (+)/BCQ_0476 (+)	TTAAACAAACGTTTGATTAG
474,676	474,695	32.78	+	9.09e-13	BCQ_0475 (+)/BCQ_0476 (+)	TTAAACAAACGTTTGATTAA
4,676,918	4,676,937	322.91	+	9.09e-13	arsC (-)/BCQ_4810 (-)	TTAAACAAACGTTTGATTAA
4,676,999	4,677,018	322.91	+	9.09e-13	arsC (-)/BCQ_4810 (-)	TTAAACAAACGTTTGATTAA
4,922,341	4,922,360	339.85	+	9.09e-13	BCQ_5057 (+)/BCQ_5058 (-)	TTAAACAAACGTTTGATTAA

Strain: B4264

Accession: CP001176

Size: 5,419,036

Start	Stop	Angle(°)	Strand	p-value	Gene (Strand)	Sequence
343,173	343,192	22.78	-	9.09e-13	gatB (+)/BCB4264_A0368 (+)	TTAAACAAACGTTTGATTAA
343,208	343,227	22.80	+	9.09e-13	gatB (+)/BCB4264_A0368 (+)	TTAAACAAACGTTTGATTAA
424,715	424,734	28.21	+	8.19e-11	thiE (+)/BCB4264_A0441 (-)	TTAAACAAACATTTGATTAA
439,129	439,148	29.17	+	8.19e-13	BCB4264_A0453 (+)/BCB4264_A0454(+)	TTAAACAAACGTTTGATTAG
439,174	439,193	29.18	+	9.09e-13	BCB4264_A0453 (+)/BCB4264_A0454(+)	TTAAACAAACGTTTGATTAA
4,941,440	4,941,459	328.27	+	8.19e-11	BCB4264_A5136 (-)/BCB4264_A5137(-)	TTAAACAAGCGTTTGATTAA
4,941,520	4,941,539	328.28	+	9.09e-13	BCB4264_A5136 (-)/BCB4264_A5137(-)	TTAAACAAACGTTTGATTAA
4,941,601	4,941,620	328.28	+	9.09e-13	BCB4264_A5136 (-)/BCB4264_A5137(-)	TTAAACAAACGTTTGATTAA
5,148,932	5,148,951	342.06	+	8.19e-11	BCB4264_A5350 (+)/BCB4264_A5351(-)	TTAAACAAACGTTTGTTTAA
5,148,932	5,148,951	342.06	-	8.19e-11	BCB4264_A5350 (+)/BCB4264_A5351(-)	TTAAACAAACGTTTGTTTAA

Strain: AH187

Accession: CP001177

Size: 5,269,030

Start	Stop	Angle(°)	Strand	p-value	Gene (Strand)	Sequence
353,407	353,426	24.15	-	9.09e-13	gatB (+)/BCAH187_A0396 (+)	TTAAACAAACGTTTGATTAA
353,442	353,461	24.15	+	9.09e-13	gatB (+)/BCAH187_A0396 (+)	TTAAACAAACGTTTGATTAA
462,406	462,425	31.80	+	9.09e-13	BCAH187_A0488 (+)	TTAAACAAACGTTTGATTAA
475,614	475,633	32.50	+	8.19e-11	BCAH187_A0501 (+)/BCAH187_A0502(+)	TTAAACAAACGTTTGATTAG
475,659	475,678	32.50	+	9.09e-13	BCAH187_A0501 (+)BCAH187_A0502(+)	TTAAACAAACGTTTGATTAA
4,736,033	4,736,052	323.59	+	9.09e-13	BCAH187_A5135 (-)/BCAH187_A5136	TTAAACAAACGTTTGATTAA
4,736,114	4,736,133	323.59	+	9.09e-13	BCAH187_A5135 (-)/BCAH187_A5136	TTAAACAAACGTTTGATTAA
4,987,367	4,987,386	340.78	+	8.19e-11	BCAH187_A5401 (+)/BCAH187_A5402(-)	TTAAACAAGCGTTTGATTAA

Strain: G9842

Accession: CP001186

Size: 5,387,334

Start	Stop	Angle(°)	Strand	p---value	Gene (Strand)	Sequence
329,376	329,395	22.01	---	9.09e---13	gatB (+)/BCG9842_B4952 (+)	TTAAACAAACGTTTGATTAA
329,411	329,430	22.01	+	9.09e---13	gatB (+)/BCG9842_B4952 (+)	TTAAACAAACGTTTGATTAA
402,839	402,858	26.92	+	8.19e---11	thiE (+)/BCG9842_B4883 (---)	TTAAACAAACATTTGATTAA
418,997	419,016	28.00	+	8.19e---11	BCG9842_B4871 (+)/BCG9842_B4870 (+)	TTAAACAAACGTTTGATTAG
419,042	419,061	28.00	+	9.09e---13	BCG9842_B4871 (+)/BCG9842_B4870 (+)	TTAAACAAACGTTTGATTAA
4,895,992	4,896,011	327.17	+	8.19e---11	BCG9842_B0104 (---)/BCG9842_B0103 (---)	TTAAACAAGCGTTTGATTAA
4,896,073	4,896,072	327.17	+	9.09e---13	BCG9842_B0104 (---)/BCG9842_B0103 (---)	TTAAACAAACGTTTGATTAA
5,095,530	5,095,549	340.50	+	8.19e---11	BCG9842_B5609 (+)/BCG9842_B5608 (---)	TTAAACAAACGTTTGTTTAA
5,095,549	5,095,530	340.50	---	8.19e---11	BCG9842_B5609 (+)/BCG9842_B5608 (---)	TTAAACAAACGTTTGTTTAA

Strain: AH820

Accession: CP001283

Size: 5,302,683

Start	Stop	Angle(°)	Strand	p-value	Gene (Strand)	Sequence
338,974	338,993	23.01	+	9.09e-13	gatB (+)/BCAH820_0355	TTAAACAAACGTTTGATTAA
411,930	411,949	27.97	+	9.09e-13	thiE (+)/BCAH820_0421 (-)	TTAAACAAACGTTTGATTAA
424,399	424,418	28.81	+	8.19e-11	BCAH820_0431 (+)/BCAH820_0342(+)	TTAAACAAACGTTTGATTAG
424,444	424,463	28.81	+	9.09e-13	BCAH_820_0431 (+)/BCAH820_0432(+)	TTAAACAAACGTTTGATTAA
4,803,230	4,803,249	326.09	+	9.09e-13	BCAH820_5098 (-)/BCAH820_5099(-)	TTAAACAAACGTTTGATTAA
4,803,312	4,803,331	326.10	+	9.09e-13	BCAH820_5098 (-)(/BCAH820_5099(-)	TTAAACAAACGTTTGATTAA
5,015,228	5,015,247	340.48	+	9.09e-13	BCAH820_5318 (+)/BCAH820_5319(-)	TTAAACAAACGTTTGATTAA

Strain: 03BB102

Accession: CP001407

Size: 5,269,628

Start	Stop	Angle(°)	Strand	p-value	Gene (Strand)	Sequence
349,705	349,724	23.89	+	9.09e-13	gatB (+)/BCA_0396 (+)	TTAAACAAACGTTTGATTAA
415,035	415,054	28.35	+	9.09e-13	thiE (+)/BCA_0456 (-)	TTAAACAAACGTTTGATTAA
428,290	428,309	29.26	+	9.09e-13	BCA_0468 (+)/BCA_0469 (+)	TTAAACAAACGTTTGATTAA
4,764,769	4,764,788	325.51	+	9.09e-13	BCA_5127 (-)/BCA_5128 (-)	TTAAACAAACGTTTGATTAA
4,764,851	4,764,870	325.52	+	9.09e-13	BCA_5127 (-)/BCA_5128 (-)	TTAAACAAACGTTTGATTAA
4,989,793	4,989,812	350.88	+	9.09e-13	BCA_5367 (+)/BCA_5368 (-)	TTAAACAAACGTTTGATTAA

Strain: biovar anthracis str biovar anthracis str. CI

Accession: CP001746

Size: 5,196,054

Start	Stop	Angle(°)	Strand	p-value	Gene (Strand)	Sequence
326,571	326,590	22.63	-	9.09e-13	gatB (+)/BACI_c03690 (+)	TTAAACAAACGTTTGATTAA
326,606	326,625	22.63	+	9.09e-13	gatB (+)/BACI_c03690 (+)	TTAAACAAACGTTTGATTAA
392,139	392,158	27.17	+	9.09e-13	thiE1 (+)/dcuB (-)	TTAAACAAACGTTTGATTAA
404,581	404,600	28.03	+	8.19e-11	BACI_c04410 (+)/BACI_c04420 (+)	TTAAACAAACGTTTGATTAG
404,626	404,645	28.03	+	9.09e-13	BACI_c04410 (+)/BACI_c04420 (+)	TTAAACAAACGTTTGATTAA
4,696,219	4,696,238	325.37	+	9.09e-13	BACI_c50000 (-)/BACI_c50010 (-)	TTAAACAAACGTTTGATTAA
4,696,301	4696320	325.38	+	9.09e-13	BACI_c50000 (-)/BACI_c50010 (-)	TTAAACAAACGTTTGATTAA
4,907,380	4,907,399	340.00	+	9.09e-13	BACI_c52190 (+)/BACI_c52200 (-)	TTAAACAAACGTTTGATTAA

B. clausii

Strain: KSM-K16

Accession: AP006627

Size: 4,303,871

Start	Stop	Angle(°)	Strand	p-value	Gene (Strand)	Sequence
3,868,562	3,868,581	323.59	+	4.55e-12	ABC3710 (+)/ABC3711 (+)	TTAAACAAACGTTTAATTAA

B. coagulans

Strain: 2-6

Accession: CP002472

Size: 3,073,079

Start	Stop	Angle(°)	Strand	p-value	Gene (Strand)	Sequence
201,692	201,711	23.63	+	8.19e-11	BCO26_0190 (+)/BCO26_0191 (+)	TTAATCAAACGTTTGATTAA
201,711	201,692	23.63	-	8.19e-11	BCO26_0190 (+)/ykvR (+)	TTAATCAAACGTTTGATTAA

B. halodurans

Strain: C-125

Accession: BA000004

Size: 4,202,352

Start	Stop	Angle(°)	Strand	p-value	Gene (Strand)	Sequence
3,459,650	3,459,669	296.28	+	8.19e-11	BH3341 (-)/BH3342 (+)	TTAAACAAACGTTTGATTAG
3,542,689	3,542,708	303.49	-	4.55e-12	BH3430 (-)	TTAAACAAACGTTTGATCAA

B. licheniformis

Strain: DSM 13 = ATCC 14580
Accession: AE017333

Size: 4,222,645

Start	Stop	Angle(°)	Strand	p-value	Gene (Strand)	Sequence
172,255	172,274	11.87	+	1.00e-11	murP (-)	TTAAACAAACGTTTAATCAA
348,621	348,640	29.72	+	4.55e-13	aroK (+)	TTAAACAAACGTTTAATTAA
3,620,770	3,620,789	308.69	+	3.82e-11	BLi03803 (-)	TTAAACAAACGTTTGATTGA
3,955,326	3,955,345	337.21	+	4.55e-13	yxkO (-)/cydD (-)	TTAAACAAACGTTTAATTAA

B. megaterium

Strain: DSM 319

Accession: CP001982
Size: 5,097,447

Start	Stop	Angle (°)	Strand	p-value	Gene	Sequence
491,457	491,476	34.71	-	8.19e-11	BMD_0522	TTAAACAAACGTTTGATTAT
568,619	568,638	40.16	+	3.82e-11	hemH	TTAAACAAACGTTTGATTTA
4,793,265	4,793,284	338.52	-	3.09e-11	sufB	TTAAACAAACGTTTGATAAA
4,801,051	4,801,070	339.07	+	8.19e-11	BMD_4985	TTAAACAAACGTTTGATTAT

Strain: QM B1551
Accession: CP001983
Size: 5,097,129

Start	Stop	Angle(°)	Strand	p-value	Gene	Sequence
483,873	483,892	34.17	-	8.19e-11	BMQ_0519	TTAAACAAACGTTTGATTAT
561,167	561,186	39.63	+	3.82e-11	hemH	TTAAACAAACGTTTGATTTA
4,636,603	4,636,622	327.47	+	8.19e-11	BMQ_4808	TTAAACAAACGTTTGATTAG
4,796,232	4,796,251	338.75	-	3.09e-11	sufB	TTAAACAAACGTTTGATAAA
4,804,018	4,804,037	339.70	+	8.19e-11	BMQ_5000	TTAAACAAACGTTTGATTAT

Strain: WSH-002

Accession: CP003017
Size: 4,983,975

Start	Stop	Angle(°)	Strand	p-value	Gene	Sequence
288,473	288,492	17.35	-	8.19e-11	BMWSH_0274	TTAAACAAACGTTTGATTAT
296,258	296,277	21.40	+	3.09e-11	yurU	TTAAACAAACGTTTGATAAA
455,612	455,631	32.91	-	8.19e-11	BMWSH_0439	TTAAACAAACGTTTGATTAG
4,409,442	4,409,461	318.50	-	3.82e-11	hemH	TTAAACAAACGTTTGATTTA
4,487,428	4,487,447	324.13	+	8.19e-11	lldP2	TTAAACAAACGTTTGATTAT

Note: At the time of analysis, *dnaA* was the last sequence feature listed in the GenBank file. This effectively creates a mirror of the annotation of the other two B. megaterium strains. The coordinates were left as annotated for the analysis.

B. pseudofirmus

Strain: OF4
Accession: CP001878

Size: 3,858,997

Start	Stop	Angle(°)	Strand	p-value	Gene (Strand)	Sequence
213,646	213,665	19.93	+	4.55e-13	BpOF4_09005 (+)/BpOF4_09010 (-)	TTAAACAAACGTTTAATTAA
383,078	383,097	35.74	-	4.55e-12	Psd (+)/BpOF4_09815 (-)	TTAAACAAACGTTTAATTAA
455,892	455,911	42.53	-	4.55e-12	BpOF4_10145 (+)/BpOF4_10150 (+)	TTAAACAAACGTTTAATTAA
3,135,675	3,135,694	292.52	-	4.55e-12	BpOF4_04245 (+)/dgk (+)	TTAAACAAACGTTTAATTAA
3,239,819	3,239,838	302.24	+	4.55e-12	BpOF4_04910 (-)	TTAAACAAACGTTTAATTAA

B. pumilus

Strain: SAFR-032

Accession: CP000813

Size: 3,704,465

Start	Stop	Angle(°)	Strand	p-value	Gene (Strand)	Sequence
293,898	293,917	28.56	+	4.55e-12	ycgK (+)	TTAAACAAACGTTTAATTAA
390,289	390,317	37.93	+	4.55e-12	yxeP (+)	TTAAACAAACGTTTAATTAA
3,180,019	3,180,038	309.03	+	3.82e-11	galE2 (-)	TTAAACAAACGTTTGATTGA
3,237,609	3,237,590	314.63	-	1.00e-11	BPUM_3251 (-)	TTAAACAAACGTTTAATCAA

B. subtilis

Strain: 168

Accession: AL009126

Size: 4,215,606

Start	Stop	Angle(°)	Strand	p-value	Gene (Strand)	Sequence
38,594	38,613	3.26	+	6.37e-12	yaaO (+)	TTAAACAAACGTTTGATTCA
342,414	342,433	29.24	+	4.55e-12	ycgK (+)	TTAAACAAACGTTTGATGAA
367,289	367,289	31.37	-	4.55e-12	zinT (+)/yckA (-)	TTAAACAAACGTTTCATTAA
3,731,586	3,731,567	318.67	-	1.00e-11	ywqE (-)	TTAAACAAACGTTTAATCAA
3,769,501	3,769,520	321.90	+	6.37e-12	ywzE (-)/ywzF (-)	TTGAACAAACGTTTGATTAA

Strain: subsp. natto BEST195

Accession: AP011541
Size: 4,091,591

Start	Stop	Angle(°)	Strand	p-value	Gene (Strand)	Sequence
38,454	38,473	3.38	+	6.37e-12	yaaO (+)	TTAAACAAACGTTTGATTCA
362,839	362,820	23.21	-	4.55e-12	BSNT_00595 (+)/yckA (-)	TTAAACAAACGTTTCATTAA
337,981	338,000	29.74	+	4.55e-12	ycgK (+)	TTAAACAAACGTTTGATGAA
3,594,502	3,594,483	316.26	-	1.00e-11	ywqE (-)	TTAAACAAACGTTTAATCAA
3,634,221	3,634,240	319.76	+	6.37e-12	BSNT_05594 (-)/BSNT_05595 (-)	TTGAACAAACGTTTGATTAA

Strain: subsp. spizizenii str. W23

Accession: CP002183
Size: 4,027,676

Start	Stop	Angle(°)	Strand	p-value	Gene (Strand)	Sequence
38,689	38,708	3.46	+	3.82e-11	yaaO (+)	TTAAACAAACGTTTGATTTA
327,327	327,346	29.26	+	3.09e-11	ycgK (+)	TTAAACAAACGTTTGATAAA
352,830	352,849	31.54	-	4.55e-12	yciC (+)/yckA (-)	TTAAACAAACGTTTCATTAA
3,525,664	3,525,693	315.13	-	1.00e-11	ywqE (-)	TTAAACAAACGTTTAATCAA
3,575,500	3,575,519	319.58	+	6.37e-12	urtE (-)	TTGAACAAACGTTTGATTAA

Strain: BSn5

Accession: CP002468

Size: 4,093,599

Start	Stop	Angle(°)	Strand	p-value	Gene (Strand)	Sequence
673,176	673,195	59.20	+	6.37e-12	BSn5_11705	TTAAACAAACGTTTGATTCA
675,712	675,731	59.42	+	4.55e-12	BSn5_13165 (+)	TTAAACAAACGTTTGATGAA
700,713	700,732	61.62	-	4.55e-12	BSn5_13265 (+)/BSn5_13270 (-)	TTAAACAAACGTTTCATTAA
3,945,316	3,945,335	346.96	-	1.00e-11	BSn5_09040 (-)	TTAAACAAACGTTTAATCAA
3,983,282	3,983,301	350.30	+	6.37e-12	ureA (-)/BSn5_09275 (-)	TTGAACAAACGTTTGATTAA

Note: *dnaA* was annotated at the 189.3° position in the GenBank file at the time of analysis. This coordinate was manually adjusted before normalizing the genome size and coordinates for this strain.

Strain: subsp. spizizenii TU-B-10

Accession: CP002905
Size: 4,207,222

Start	Stop	Angle(°)	Strand	p-value	Gene (Strand)	Sequence
38,663	38,682	3.31	+	6.37e-12	GYO_0036 (+)	TTAAACAAACGTTTGATTCA
455,491	455,510	38.96	+	4.55e-12	GYO_0522 (+)	TTAAACAAACGTTTGATGAA
481,325	481,344	41.19	-	3.09e-11	GYO_0544 (+)/GYO_0545 (-)	TTAAACAAACGTTTTATTAA
3,702,639	3,702,658	316.82	-	1.00e-11	GYO_3985 (-)	TTAAACAAACGTTTAATCAA
3,752,559	3,752,578	321.10	+	6.37e-12	urtE (-)	TTGAACAAACGTTTGATTAA

Strain: subsp. subtilis RO-NN-1

Accession: CP002906
Size: 4,011,949

Start	Stop	Angle(°)	Strand	p-value	Gene (Strand)	Sequence
38,451	38,470	3.45	+	6.37e-12	I33_0038 (+)	TTAAACAAACGTTTGATTCA
332,377	332,396	29.82	+	4.55e-12	I33_0362 (+)	TTAAACAAACGTTTGATGAA
357,365	357,384	32.07	-	4.55e-12	I33_0383 (+)/I33_0384 (-)	TTAAACAAACGTTTCATTAA
481,344	481,325	43.19	-	3.09e-11	GYO_0544 (+)/GYO_0545 (-)	TTAAACAAACGTTTTATTAA
3,523,963	3,523,982	316.21	-	1.00e-11	I33_3755 (-)	TTAAACAAACGTTTAATCAA
3,572,638	3,572,657	320.58	+	6.37e-12	I33_3804 (-)	TTGAACAAACGTTTGATTAA

B. thuringiensis

Strain: serovar konkukian str. 97-27

Accession: AE017355
Size: 5,237,682

Start	Stop	Angle(°)	Strand	p-value	Gene (Strand)	Sequence
344,074	334,093	23.65	-	9.09e-13	gatB (+)/BT9727_0291 (+)	TTAAACAAACGTTTGATTAA
344,109	344,128	23.65	+	9.09e-13	gatB (+)/BT9727_0291 (+)	TTAAACAAACGTTTGATTAA
419,614	419,633	28.84	+	9.09e-13	thiE (+)/dcuB (-)	TTAAACAAACGTTTGATTAA
432,881	432,900	29.75	+	9.09e-13	BT9727_0365 (+)/BT9727_0366 (+)	TTAAACAAACGTTTGATTAA
473,836	742,855	32.57	+	8.19e-11	BT9727_0365 (+)/BT9727_0366 (+)	TTAAACAAACGTTTGATTAG
4,752,383	4,752,402	326.64	+	9.09e-13	arsC (-)/BT9727_4702 (-)	TTAAACAAACGTTTGATTAA
4,752,465	4,752,484	326.65	+	9.09e-13	arsC (-)/BT9727_4702 (-)	TTAAACAAACGTTTGATTAA
4,961,731	4,961,750	341.03	+	9.09e-13	BT9727_4910 (+)/BT9727_4911 (-)	TTAAACAAACGTTTGATTAA

Strain: Al
Accession: CP000485

Size: 5,257,091

Start	Stop	Angle(°)	Strand	p-value	Gene (Strand)	Sequence
360,646	360,665	24.70	-	9.09e-13	gatB (+)/BALH_0315 (+)	TTAAACAAACGTTTGATTAA
360,681	360,700	24.70	+	9.09e-13	gatB (+)/BALH_0315 (+)	TTAAACAAACGTTTGATTAA
433,728	433,747	29.70	+	9.09e-13	thiE (+)/dcuA (-)	TTAAACAAACGTTTGATTAA
446,943	446,962	31.98	+	8.19e-11	BALH_0388 (+)/BALH_0389 (+)	TTAAACAAACGTTTGATTAG
466,988	477,007	31.98	+	9.09e-13	BALH_0388 (+)/BALH_0389 (+)	TTAAACAAACGTTTGATTAA
4,761,639	4,761,658	326.07	+	9.09e-13	arsC (-)/BALH_4525 (-)	TTAAACAAACGTTTGATTAA
4,761,720	4,761,739	326.08	+	9.09e-13	arsC (-)/BALH_4525 (-)	TTAAACAAACGTTTGATTAA
4,979,518	4,979,537	341.00	+	9.09e-13	BALH_4727 (-)/BALH_4728 (-)	TTAAACAAACGTTTGATTAA

Strain: BMB171
Accession: CP001903
Size: 5,330,088

Start	Stop	Angle(°)	Strand	p-value	Gene (Strand)	Sequence
351,867	351,886	23.77	-	9.09e-13	gatB (+)/BMB171_C0298 (+)	TTAAACAAACGTTTGATTAA
351,902	351,921	23.77	+	9.09e-13	gatB (+)/BMB171_C0298 (+)	TTAAACAAACGTTTGATTAA
426,851	426,870	28.83	+	8.19e-11	thiE (+)/BMB171_C0362 (-)	TTAAACAAACATTTGATTAA
441,269	441,288	29.80	+	8.19e-11	BMB171_C0373 (+)	TTAAACAAACGTTTGATTAG
441,314	441,333	29.81	+	9.09e-13	BMB171_C0373 (+)/BMB171_C0374 (+)	TTAAACAAACGTTTGATTAA
4,809,711	4,809,730	234.85	+	8.19e-11	BMB171_C4601(-)/BMB171_C4602 (-)	TTAAACAAGCGTTTGATTAA
4,809,791	4,809,810	234.86	+	9.09e-13	BMB171_C4601 (-)/BMB171_C4602 (-)	TTAAACAAACGTTTGATTAA
4,809,872	4,989,891	234.86	+	9.09e-13	BMB171_C4601 (-)/BMB171_C4602 (-)	TTAAACAAACGTTTGATTAA
5,044,522	5,044,541	340.71	+	8.19e-11	BMB171_C4824 (+)/BMB171_C4825 (-)	TTAAACAAACGTTTGTTTAA
5,044,541	5,044,522	340.71	-	8.19e-11	BMB171_C4824 (+)BMB171_)C4825 (-)	TTAAACAAACGTTTGTTTAA

Strain: serovar chinensis CT-43

Accession: CP001907
Size: 5,486,830

Start	Stop	Angle(°)	Strand	p-value	Gene (Strand)	Sequence
343,712	343,731	22.55	-	9.09e-13	gatB (+)/CT43_CH0298 (+)	TTAAACAAACGTTTGATTAA
343,747	343,766	22.55	+	9.09e-13	gatB (+)/CT43_CH0298 (+)	TTAAACAAACGTTTGATTAA
419,678	419,697	27.54	+	9.09e-13	thiE (+)/CT43_CH0364 (-)	TTAAACAAACGTTTGATTAA
435,848	435,867	28.60	+	8.19e-11	CT43_CH0375 (+)/CT43_CH0376 (+)	TTAAACAAACGTTTGATTAG
435,893	435,912	28.60	+	9.09e-13	CT43_CH0375 (+)/CT43_CH0376 (+)	TTAAACAAACGTTTGATTAA
4,993,764	4,993,783	327.65	+	8.19e-11	CT43_CH5051 (-)/CT43_CH5052 (-)	TTAAACAAGCGTTTGATTAA
4,993,845	4,993,864	327.66	+	9.09e-13	CT43_CH5051 (-)/CT43_CH5052 (-)	TTAAACAAACGTTTGATTAA
4,993,926	4,993,945	327.66	+	9.09e-13	CT43_CH5051 (-)/CT43_CH5052 (-)	TTAAACAAACGTTTGATTAA

Strain: serovar finitimus YBT-020

Accession: CP002508

Size: 5,355,490

Start	Stop	Angle(°)	Strand	p-value	Gene (Strand)	Sequence
364,780	365,799	17.80	-	9.09e-13	gatB (+)/YBT020_01655 (+)	TTAAACAAACGTTTGATTAA
365,815	365,834	24.60	+	9.09e-13	gatB (+)/YBT020_01655 (+)	TTAAACAAACGTTTGATTAA
506,370	506,389	34.04	+	9.09e-13	YBT020_02415 (+)	TTAAACAAACGTTTGATTAA
519,632	519,651	34.93	+	9.09e-13	YBT020_02475 (+)/YBT020_02480 (+)	TTAAACAAACGTTTGATTAA
4,810,271	4,810,290	323.35	+	9.09e-13	YBT020_24785 (-)/YBT020_24790 (-)	TTAAACAAACGTTTGATTAA
4,810,353	4,810,372	323.36	+	9.09e-13	YBT020_24785 (-)/YBT020_24790 (-)	TTAAACAAACGTTTGATTAA
4,810,434	4,810,453	323.36	+	9.09e-13	YBT020_24785 (-)/YBT020_24790 (-)	TTAAACAAACGTTTGATTAA
5,074,172	5,074,191	341.89	+	9.09e-13	YBT020_26060 (+)/YBT020_26065 (-)	TTAAACAAACGTTTGATTAA

APPENDIX A Figure A.1 Graphical representation of *RBM*s across the *Bacillus* genus.

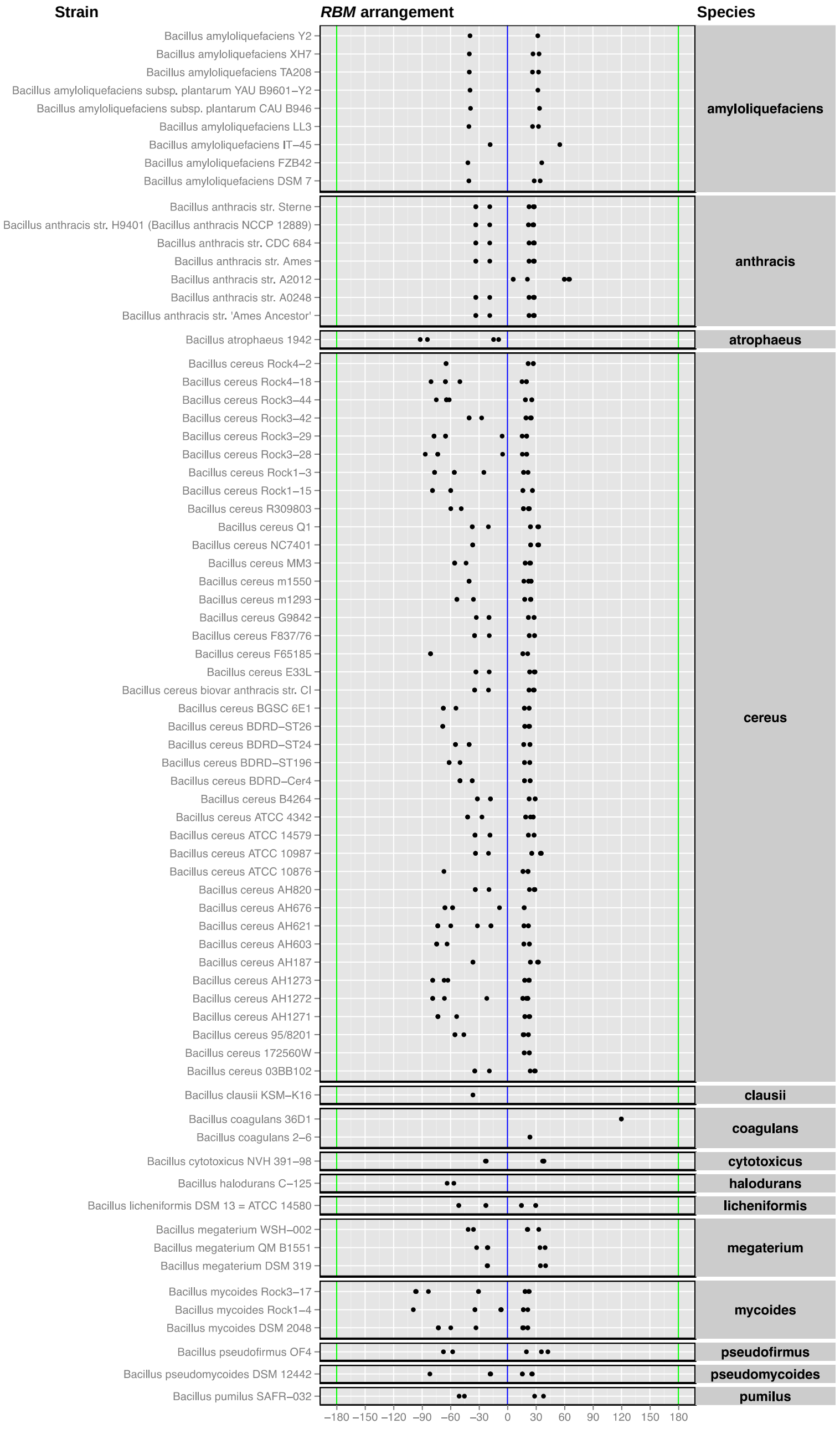

APPENDIX A Figure A.1, continued…

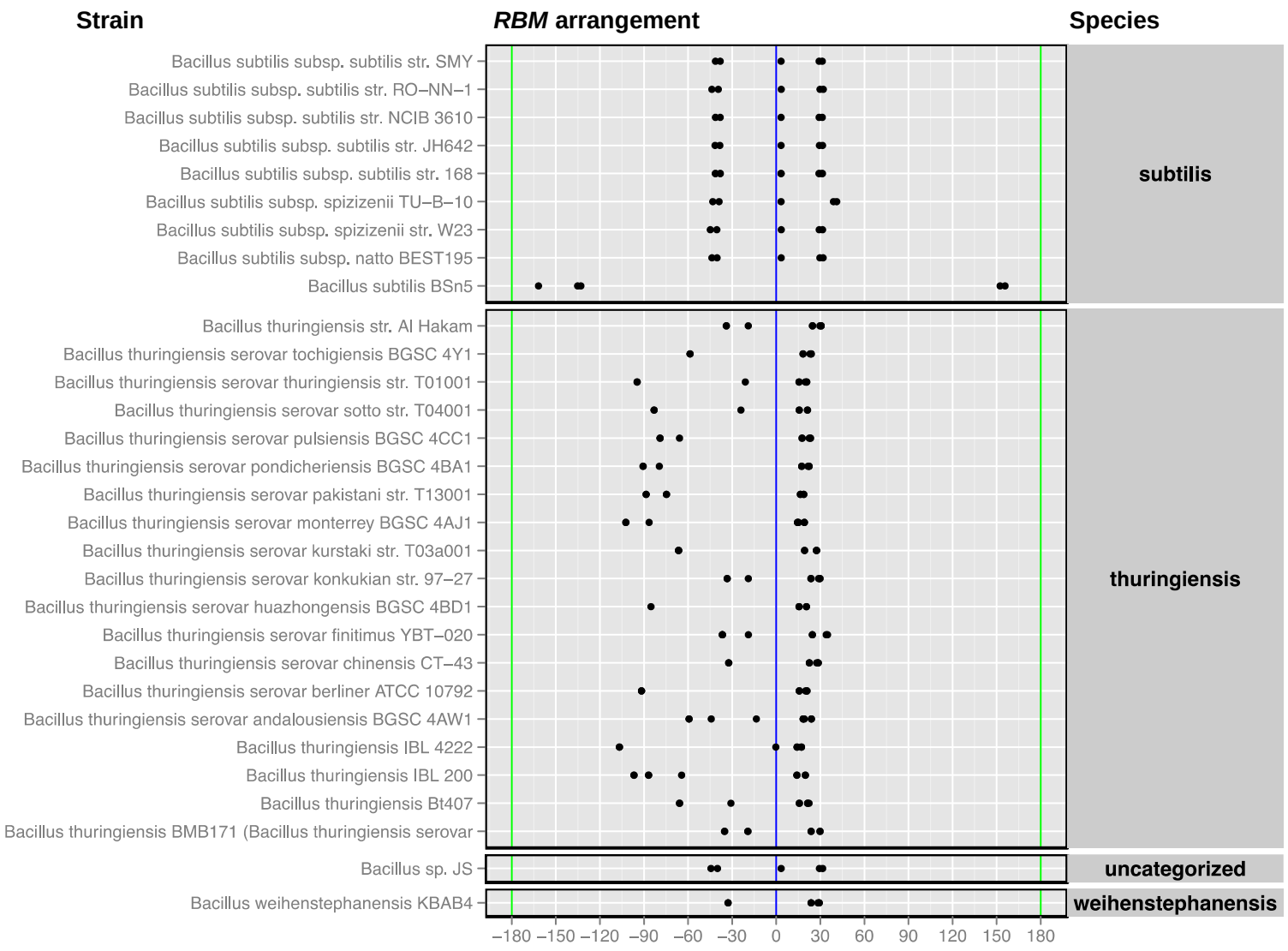

APPENDIX A Figure A.1 Graphical representation of *RBM*s across the *Bacillus* genus.
*RBM*s identified by FIMO mapped to chromosomes of strains for the indicated *Bacillus* species. Since genome sizes differed, all positions were normalized to a 360° circular chromosome linearized at 180° (x-axis) for the indicated *Bacillus* strain. Closely spaced *RBM*s are not resolvable, but coordinates are provided in APPENDIX A Methods A.3 (above).

APPENDIX B

CHAPTER III SUPPLEMENTAL

APPENDIX B TABLE B.1. STRAINS

Strain	Description	Reference
B. subtilis 168	*Bacillus subtilis* laboratory strain 168 *trpC2*	Bacillus Genetic Stock Center (1A866)
BL21 (DE3)	*BL21 (DE3) pLysS (cat)*	Expression host
DH5α	*F-, endA1, glnV44, thi-1, recA1, relA1, gyrA96, deoR, nupG, Φ80dlacZΔM15, Δ(lacZYA-argF)U169, hsdR17(r_K^- m_K^+), λ–*	
DHP1	*F-, cya-99, araD139, galE15, galK16, rpsL1 (Strr), hsdR2, mcrA1,mcrB1*	Obtained from Thomas Bernhardt
B. subtilis subsp. subtilis		
BJH188	*Em his nprE18 aprE3 eglS(DELTA)102 bglT/bglS(DELTA)EV lacA::P_{xylA}-comK (ERM)*	Bacillus Genetic Stock Center (1A976)
PY79		
BDR2353	*minD::kan*	David Rudner
BJH042	*minD::kan, amyE::P_{hy}-refZ (spec)*	This work
BJW123	*amyE::P_{hy}-empty (spec)*	(Wagner-Herman *et al.*, 2012)
B. subtilis 168		
BAM043	*minD::kan*	This work
BAM075	*amyE::P_{hy}-empty (spec)*	This work
BAM077	*RBM_{5mu}, yycR(-7°)::P_{spoIIQ}-yfp (phleo), +51°::P_{spoIIQ}-cfp (erm), spoIIIE36-tet*	(Miller *et al.*, 2016)
BAM078	*yycR(-7°)::P_{spoIIQ}-yfp (phleo), +51°::P_{spoIIQ}-cfp (erm), spoIIIE36-tet*	(Miller *et al.*, 2016)
BAM079	*refZ::cat, yycR(-7°)::P_{spoIIQ}-yfp (phleo), +51°::P_{spoIIQ}-cfp (erm), spoIIIE36-tet*	(Miller *et al.*, 2016)
BAM110	*yhdG::P_{hy}-empty (phleo)*	This work
BAM111	*yhdG::P_{hy}-refZ (WT) (phleo)*	This work
BAM142	*lacA::P_{xylA}-comK (erm)*	This work
BAM168	*sacA::P_{spremo}-lacZ (cat), refZ::tet, lacA::P_{xylA}-comK (erm), minD::kan*	This work
BAM229	*sacA::P_{spremo}-lacZ (cat)*	This work
BAM248	*sacA::P_{spremo}-lacZ (cat), refZ::tet*	This work
BAM266	*sacA::P_{spremo}-lacZ (cat), refZ::tet, lacA::P_{xylA}-comK (erm)*	This work
BAM374	*sacA::P_{spremo}-lacZ (cat), refZ::tet, lacA::P_{xylA}-comK (erm), minD::kan, amyE::P_{hy}-refZ (spec)*	Figure III.1B
BAM390	*sacA::P_{spremo}-lacZ (cat), refZ::tet, lacA::P_{xylA}-comK (erm), minD::kan, amyE::P_{hy}-empty (spec)*	Figure III.1B
BAM400	*sacA::P_{spremo}-lacZ (cat), refZ::tet, lacA::P_{xylA}-comK (erm), minD::kan, amyE::P_{hy}-refZ (E179K) (spec)*	Figure III.1B
BAM403	*sacA::P_{spremo}-lacZ (cat), refZ::tet, lacA::P_{xylA}-comK (erm), minD::kan, amyE::P_{hy}-refZ (E117G) (spec)*	Figure III.1B
BAM407	*sacA::P_{spremo}-lacZ (cat), refZ::tet, lacA::P_{xylA}-comK (erm), minD::kan, amyE::P_{hy}-refZ (R102C) (spec)*	Figure III.1B
BAM409	*sacA::P_{spremo}-lacZ (cat), refZ::tet, lacA::P_{xylA}-comK (erm), minD::kan, amyE::P_{hy}-refZ (R102S) (spec)*	Figure III.1B
BAM411	*sacA::P_{spremo}-lacZ (cat), refZ::tet, lacA::P_{xylA}-comK (erm), minD::kan, amyE::P_{hy}-refZ (L153R) (spec)*	Figure III.1B
BAM428	*amyE::P_{hy}-refZ (E179K) (spec)*	Figure III.1C & D
BAM431	*amyE::P_{hy}-refZ (E117G) (spec)*	Figure III.1C & D
BAM434	*amyE::P_{hy}-refZ (R102C) (spec)*	Figure III.1C & D

Appendix B Table B.1. Strains, continued…

Strain	Description	Reference
BAM436	*amyE::P_{hy}-refZ (R102S) (spec)*	Figure III.1C & D
BAM440	*sacA::P_{spremo}-lacZ (cat), refZ::tet, lacA::P_{xylA}-comK (erm), minD::kan, amyE::P_{hy}-refZ (R116W) (spec)*	Figure III.1B
BAM443	*sacA::P_{spremo}-lacZ (cat), refZ::tet, lacA::P_{xylA}-comK (erm), minD::kan, amyE::P_{hy}-refZ (R116S) (spec)*	Figure III.1B
BAM444	*sacA::P_{spremo}-lacZ (cat), refZ::tet, lacA::P_{xylA}-comK (erm), minD::kan, amyE::P_{hy}-refZ (E117D) (spec)*	Figure III.1B
BAM449	*sacA::P_{spremo}-lacZ (cat), refZ::tet, lacA::P_{xylA}-comK (erm), minD::kan, amyE::P_{hy}-refZ (E53K) (spec)*	Figure III.1B
BAM450	*amyE::P_{hy}-refZ (L153R) (spec)*	Figure III.1C & D
BAM451	*amyE::P_{hy}-refZ (R116W) (spec)*	Figure III.1C & D
BAM454	*amyE::P_{hy}-refZ (R116S) (spec)*	Figure III.1C & D
BAM455	*amyE::P_{hy}-refZ (E117D) (spec)*	Figure III.1C & D
BAM457	*amyE::P_{hy}-refZ (E53K) (spec)*	Figure III.1C & D
BAM462	*sacA::P_{spremo}-lacZ (cat), refZ::tet, lacA::P_{xylA}-comK (erm), minD::kan, amyE::P_{hy}-refZ (E61K) (spec)*	Figure III.1B
BAM490	*amyE::P_{hy}-refZ (E61K) (spec)*	Figure III.1C & D
BAM1006	*refZ::refZ (WT) (cat), yycR(-7°)::P_{spoIIQ}-yfp (phleo), lacA(-61°)::P_{spoIIQ}-cfp (erm), spoIIIE36-tet*	Figure III.2
BAM1007	*refZ::refZ (WT) (cat), yycR(-7°)::P_{spoIIQ}-yfp (phleo), +51°::P_{spoIIQ}-cfp (erm), spoIIIE36-tet*	Figure III.2
BAM1008	*refZ::refZ (E179K) (cat), yycR(-7°)::P_{spoIIQ}-yfp (phleo), lacA(-61°)::P_{spoIIQ}-cfp (erm), spoIIIE36-tet*	Figure III.2
BAM1009	*refZ::refZ (E179K) (cat), yycR(-7°)::P_{spoIIQ}-yfp (phleo), +51°::P_{spoIIQ}-cfp (erm), spoIIIE36-tet*	Figure III.2
BAM1010	*refZ::refZ (E117G) (cat), yycR(-7°)::P_{spoIIQ}-yfp (phleo), lacA(-61°)::P_{spoIIQ}-cfp (erm), spoIIIE36-tet*	Figure III.2
BAM1011	*refZ::refZ (E117G) (cat), yycR(-7°)::P_{spoIIQ}-yfp (phleo), +51°::P_{spoIIQ}-cfp (erm), spoIIIE36-tet*	Figure III.2
BAM1012	*refZ::refZ (R012C) (cat), yycR(-7°)::P_{spoIIQ}-yfp (phleo), lacA(-61°)::P_{spoIIQ}-cfp (erm), spoIIIE36-tet*	Figure III.2
BAM1013	*refZ::refZ (R102C) (cat), yycR(-7°)::P_{spoIIQ}-yfp (phleo), +51°::P_{spoIIQ}-cfp (erm), spoIIIE36-tet*	Figure III.2
BAM1014	*refZ::refZ (R102S) (cat), yycR(-7°)::P_{spoIIQ}-yfp (phleo), lacA(-61°)::P_{spoIIQ}-cfp (erm), spoIIIE36-tet*	Figure III.2
BAM1015	*refZ::refZ (R102S) (cat), yycR(-7°)::P_{spoIIQ}-yfp (phleo), +51°::P_{spoIIQ}-cfp (erm), spoIIIE36-tet*	Figure III.2
BAM1016	*refZ::refZ (L153R) (cat), yycR(-7°)::P_{spoIIQ}-yfp (phleo), lacA(-61°)::P_{spoIIQ}-cfp (erm), spoIIIE36-tet*	Figure III.2
BAM1017	*refZ::refZ (L153R) (cat), yycR(-7°)::P_{spoIIQ}-yfp (phleo), +51°::P_{spoIIQ}-cfp (erm), spoIIIE36-tet*	Figure III.2
BAM1018	*refZ::refZ (R116W) (cat), yycR(-7°)::P_{spoIIQ}-yfp (phleo), lacA(-61°)::P_{spoIIQ}-cfp (erm), spoIIIE36-tet*	Figure III.2
BAM1019	*refZ::refZ (R116W) (cat), yycR(-7°)::P_{spoIIQ}-yfp (phleo), +51°::P_{spoIIQ}-cfp (erm), spoIIIE36-tet*	Figure III.2
BAM1020	*refZ::refZ (R116S) (cat), yycR(-7°)::P_{spoIIQ}-yfp (phleo), lacA(-61°)::P_{spoIIQ}-cfp (erm), spoIIIE36-tet*	Figure III.2
BAM1021	*refZ::refZ (R116S) (cat), yycR(-7°)::P_{spoIIQ}-yfp (phleo), +51°::P_{spoIIQ}-cfp (erm), spoIIIE36-tet*	Figure III.2
BAM1022	*refZ::refZ (E117D) (cat), yycR(-7°)::P_{spoIIQ}-yfp (phleo), lacA(-61°)::P_{spoIIQ}-cfp (erm), spoIIIE36-tet*	Figure III.2
BAM1023	*refZ::refZ (E117D) (cat), yycR(-7°)::P_{spoIIQ}-yfp (phleo), +51°::P_{spoIIQ}-cfp (erm), spoIIIE36-tet*	Figure III.2

Appendix B Table B.1. Strains, continued…

Strain	Description	Reference
BAM1024	*refZ::refZ (E53K) (cat), yycR(-7°)::P_{spoIIQ}-yfp (phleo), lacA(-61°)::P_{spoIIQ}-cfp (erm), spoIIIE36-tet*	Figure III.2
BAM1025	*refZ::refZ (E53K) (cat), yycR(-7°)::P_{spoIIQ}-yfp (phleo), +51°::P_{spoIIQ}-cfp (erm), spoIIIE36-tet*	Figure III.2
BAM1026	*refZ::refZ (E61K) (cat), yycR(-7°)::P_{spoIIQ}-yfp (phleo), lacA(-61°)::P_{spoIIQ}-cfp (erm), spoIIIE36-tet*	Figure III.2
BAM1027	*refZ::refZ (E61K) (cat), yycR(-7°)::P_{spoIIQ}-yfp (phleo), +51°::P_{spoIIQ}-cfp (erm), spoIIIE36-tet*	Figure III.2
BAM1060	*sacA::P_{spremo}-lacZ (cat), refZ::tet, lacA::P_{xylA}-comK (erm), minD::kan, amyE::P_{hy}-refZ (E53K) (spec)*	Original rLOF isolate
BAM1061	*sacA::P_{spremo}-lacZ (cat), refZ::tet, lacA::P_{xylA}-comK (erm), minD::kan, amyE::P_{hy}-refZ (E61K) (spec)*	Original rLOF isolate
BAM1062	*sacA::P_{spremo}-lacZ (cat), refZ::tet, lacA::P_{xylA}-comK (erm), minD::kan, amyE::P_{hy}-refZ (R102C) (spec)*	Original rLOF isolate
BAM1063	*sacA::P_{spremo}-lacZ (cat), refZ::tet, lacA::P_{xylA}-comK (erm), minD::kan, amyE::P_{hy}-refZ (R102S) (spec)*	Original rLOF isolate
BAM1064	*sacA::P_{spremo}-lacZ (cat), refZ::tet, lacA::P_{xylA}-comK (erm), minD::kan, amyE::P_{hy}-refZ (R116S) (spec)*	Original rLOF isolate
BAM1065	*sacA::P_{spremo}-lacZ (cat), refZ::tet, lacA::P_{xylA}-comK (erm), minD::kan, amyE::P_{hy}-refZ (R116W) (spec)*	Original rLOF isolate
BAM1066	*sacA::P_{spremo}-lacZ (cat), refZ::tet, lacA::P_{xylA}-comK (erm), minD::kan, amyE::P_{hy}-refZ (E117D) (spec)*	Original rLOF isolate
BAM1067	*sacA::P_{spremo}-lacZ (cat), refZ::tet, lacA::P_{xylA}-comK (erm), minD::kan, amyE::P_{hy}-refZ (E117G) (spec)*	Original rLOF isolate
BAM1068	*sacA::P_{spremo}-lacZ (cat), refZ::tet, lacA::P_{xylA}-comK (erm), minD::kan, amyE::P_{hy}-refZ (L153R) (spec)*	Original rLOF isolate
BAM1069	*sacA::P_{spremo}-lacZ (cat), refZ::tet, lacA::P_{xylA}-comK (erm), minD::kan, amyE::P_{hy}-refZ (E179K) (spec)*	Original rLOF isolate
BAM1662	*sacA::P_{spremo}-lacZ (cat), refZ::tet, lacA::P_{xylA}-comK (erm), minD::kan, amyE::P_{hy}-empty (spec), yhdG::P_{hy}-empty (phleo)*	This work
BAM1663	*sacA::P_{spremo}-lacZ (cat), refZ::tet, lacA::P_{xylA}-comK (erm), minD::kan, yhdG::P_{hy}-refZ (WT) (phleo)*	This work
BAM1664	*sacA::P_{spremo}-lacZ (cat), refZ::tet, lacA::P_{xylA}-comK (erm), minD::kan, amyE::P_{hy}-empty (spec), yhdG::P_{hy}-refZ (WT) (phleo)*	This work
BAM1665	*sacA::P_{spremo}-lacZ (cat), refZ::tet, lacA::P_{xylA}-comK (erm), minD::kan, amyE::P_{hy}-refZ (spec), yhdG::P_{hy}-empty (phleo)*	This work
BAM1666	*sacA::P_{spremo}-lacZ (cat), refZ::tet, lacA::P_{xylA}-comK (erm), minD::kan, amyE::P_{hy}-refZ (spec), yhdG::P_{hy}-refZ (WT) (phleo)*	This work
BAM1667	*sacA::P_{spremo}-lacZ (cat), refZ::tet, lacA::P_{xylA}-comK (erm), minD::kan, amyE::P_{hy}-refZ (E53K) (spec), yhdG::P_{hy}-refZ (WT) (phleo)*	This work
BAM1668	*sacA::P_{spremo}-lacZ (cat), refZ::tet, lacA::P_{xylA}-comK (erm), minD::kan, amyE::P_{hy}-refZ (E61K) (spec), yhdG::P_{hy}-refZ (WT) (phleo)*	This work
BAM1669	*sacA::P_{spremo}-lacZ (cat), refZ::tet, lacA::P_{xylA}-comK (erm), minD::kan, amyE::P_{hy}-refZ (R102C) (spec), yhdG::P_{hy}-refZ (WT) (phleo)*	This work
BAM1670	*sacA::P_{spremo}-lacZ (cat), refZ::tet, lacA::P_{xylA}-comK (erm), minD::kan, amyE::P_{hy}-refZ (R102S) (spec), yhdG::P_{hy}-refZ (WT) (phleo)*	This work
BAM1671	*sacA::P_{spremo}-lacZ (cat), refZ::tet, lacA::P_{xylA}-comK (erm), minD::kan, amyE::P_{hy}-refZ (R116S) (spec), yhdG::P_{hy}-refZ (WT) (phleo)*	This work
BAM1672	*sacA::P_{spremo}-lacZ (cat), refZ::tet, lacA::P_{xylA}-comK (erm), minD::kan, amyE::P_{hy}-refZ (R116W) (spec), yhdG::P_{hy}-refZ (WT) (phleo)*	This work
BAM1673	*sacA::P_{spremo}-lacZ (cat), refZ::tet, lacA::P_{xylA}-comK (erm), minD::kan, amyE::P_{hy}-refZ (E117D) (spec), yhdG::P_{hy}-refZ (WT) (phleo)*	This work

Appendix B Table B.1. Strains, continued…

Strain	Description	Reference
BAM1674	*sacA::P_{spremo}-lacZ (cat), refZ::tet, lacA::P_{xylA}-comK (erm), minD::kan, amyE::P_{hy}-refZ (E117G) (spec), yhdG::P_{hy}-refZ (WT) (phleo)*	This work
BAM1675	*sacA::P_{spremo}-lacZ (cat), refZ::tet, lacA::P_{xylA}-comK (erm), minD::kan, amyE::P_{hy}-refZ (L153R) (spec), yhdG::P_{hy}-refZ (WT) (phleo)*	This work
BAM1676	*sacA::P_{spremo}-lacZ (cat), refZ::tet, lacA::P_{xylA}-comK (erm), minD::kan, amyE::P_{hy}-refZ (E179K) (spec), yhdG::P_{hy}-refZ (WT) (phleo)*	This work
BJH205	*RBM_{5mu}*	(Miller *et al.*, 2016)
BJH228	*amyE::P_{hy}-refZ (spec)*	Figure III.1C & D
BJH245	*yycR(-7°)::P_{spoIIQ}-yfp (phleo), lacA(-61°)::P_{spoIIQ}-cfp (erm), spoIIIE36-tet*	(Miller *et al.*, 2016)
BJH246	*RBM_{5mu}, yycR(-7°)::P_{spoIIQ}-yfp (phleo), lacA(-61°)::P_{spoIIQ}-cfp (erm), spoIIIE36-tet*	(Miller *et al.*, 2016)
BJH251	*refZ::cat, yycR(-7°)::P_{spoIIQ}-yfp (phleo), lacA(-61°)::P_{spoIIQ}-cfp (erm), spoIIIE36-tet*	(Miller *et al.*, 2016)

APPENDIX B TABLE B.2. PLASMIDS

Plasmid	Description	Reference
pAM037	*yycR::P_{spremo} (cat)(amp)*	This work
pAM046	*sacA::cat (amp)*	This work
pAM080	*sacA::P_{spremo} (cat)(amp)*	This work
pAM083	*sacA::P_{spremo}-lacZ (cat)(amp)*	This work
pAM139	*refZ(Y43A)-T25 (kan)*	This work
pAM141	*refZ(R106A)-T25 (kan)*	This work
pAM144	*refZ(Y43A)-T18 (amp)*	This work
pAM146	*refZ(R106A)-T18 (amp)*	This work
pAM152	*refZ(E53K)-T18 (amp)*	This work
pAM153	*refZ(E61K)-T18 (amp)*	This work
pAM154	*refZ(R102C)-T18 (amp)*	This work
pAM155	*refZ(R102S)-T18 (amp)*	This work
pAM156	*refZ(R116S)-T18 (amp)*	This work
pAM157	*refZ(R116W)-T18 (amp)*	This work
pAM158	*refZ(E117D)-T18 (amp)*	This work
pAM159	*refZ(E117G)-T18 (amp)*	This work
pAM160	*refZ(L153R)-T18 (amp)*	This work
pAM161	*refZ(E179K)-T18 (amp)*	This work
pAM162	*refZ(E53K)-T25 (kan)*	This work
pAM163	*refZ(E61K)-T25 (kan)*	This work
pAM164	*refZ(R102C)-T25 (kan)*	This work
pAM165	*refZ(R102S)-T25 (kan)*	This work
pAM166	*refZ(R116S)-T25 (kan)*	This work
pAM167	*refZ(R116W)-T25 (kan)*	This work
pAM168	*refZ(E117D)-T25 (kan)*	This work
pAM169	*refZ(E117G)-T25 (kan)*	This work
pAM170	*refZ(L153R)-T25 (kan)*	This work
pAM171	*refZ(E179K)-T25 (kan)*	This work
pCH363	*empty-T18 (amp)*	Tom Bernhardt
pDR111	*amyE::P_{hy} (spec)(amp)*	David Rudner
pEB013	*refZ(R116S)-His6 (kan)*	This work

Appendix B Table B.2. Plasmids, continued…

Plasmid	Description	Reference
pEB014	*refZ(E117G)-His6 (kan)*	This work
pEB015	*refZ(E117D)-His6 (kan)*	This work
pEB016	*refZ(E179K)-His6 (kan)*	This work
pEB017	*refZ(R102C)-His6 (kan)*	This work
pEB018	*refZ(R102S)-His6 (kan)*	This work
pEB019	*refZ(E53K)-His6 (kan)*	This work
pEB020	*refZ(E61K)-His6 (kan)*	This work
pEB021	*refZ(L153R)-His6 (kan)*	This work
pEB022	*refZ(R116W)-His6 (kan)*	This work
pET24b (+)	*C-terminal His6-tag*	
pJH036	*sacA::P_{hy}-lacZ (erm)(amp)*	This work
pJK013	*amyE::P_{hy}-refZ (spec)(amp)*	(Wagner-Herman *et al.*, 2012)
pJW004	*yhdG::P_{hy}-empty (phleo)(amp)*	(Wagner-Herman *et al.*, 2012)
pJW014	*yhdG::P_{hy}-refZ (WT) (phleo)(amp)*	(Wagner-Herman *et al.*, 2012)
pJW034	*yycR::P_{hy} (cat)(amp)*	This work
pJW096	*refZ(WT)-T25 (kan)*	This work
pJW097	*refZ(WT)-T18 (amp)*	(Miller *et al.*, 2016)
pJW098	*ftsZ-T25 (kan)*	This work
pJW099	*ftsZ-T18 (kan)*	This work
pJW100	*T25-refZ(WT) (kan)*	This work
pJW101	*T18-refZ(WT) (kan)*	This work
pJW102	*T25-ftsZ (kan)*	This work
pJW103	*T25-ftsZ (kan)*	This work
pKM062	*sacA::erm (amp)*	David Rudner
pKM074	*MCS1+2 (cat)(amp)*	David Rudner
pKNT25	*empty-T25 (kan)*	Tom Bernhardt
pLM025	*refZ(WT)-His6 (kan)*	David Rudner
pRD001	*amyE::P_{hy}-refZ(R106A) (spec)(amp)*	David Rudner
pRD010	*amyE::P_{hy}-refZ(Y43A) (spec)(amp)*	(Miller *et al.*, 2016)

APPENDIX B TABLE B.3. OLIGONUCLEOTIDES

Oligo	Sequence 5' to 3'
OAM001	AGAAGCGTTAGCGGCAGCAAGTGAT
OAM010	ATGGACACAACAACAGCAAAACAGGC
OAM012	GCTAGCCGCATGCAAGCTAATT
OAM013	AGTAGTTCCTCCTTATGTAAGC
OAM122	ATTAAGCTTACATAAGGAGGAACTACTATG
OAM124	GTCGCACTGGCTGTTACTTC
OAM125	CACATGACCAGGAGCTTCGT
OAM139	TCGAGGGTCATTTTGCAAAAGTTGTTGACTTGAACAAACGTTTGATTCATAATGTGTGTA
OAM140	AGCTTACACACATTATGAATCAAACGTTTGTTCAAGTCAACAACTTTTGCAAAATGACCC
OAM148	GCATGCATGCGTAACACACAGGAAACAGCTATGAAAGTAAGCACCAAAGACAAAATTA
OAM149	GCATGGATCCGAACCGCTACCGTTGGTGAGCGCCACGTCT
OAM165	ACCGAATTAGCTTGCATGCGGCTAGCTCTAGTTGGTGAGCGCCAC

Appendix B Table B.3. Oligonucleotides, continued…

Oligo	Sequence 5' to 3'
OAM166	ACCGAATTAGCTTGCATGCGGCTAGCTCTA
OAM200	CAATGAATGATCTGGCTGTGAG
OAM201	GCTTACTTTCATACGGCTCACTC
OAM202	TAGTATCAAGAGGAAGGAGTGAGCCGTATGAAAGTAAGCACCAAAGACAA
OAM203	TATCTAGAGGGAAACCGTTGTGGTCTAGTTGGTGAGCGCCAC
OAM204	AGGAGGAACTATATCCGGATCTGGACCAACTAGCACCGTTCCAA
OAM205	TTCAAGGCTGTCATAAAGCTC
OEB009	ATCAGCGCTCTGGTGATTG
OEB010	TTTTGCACAGCCTTAGCTTC
OEB024	ATACATATGAAAGTAAGCACCAAAGACA
OEB025	CGTTTTGAACAAACGTTTGATTAA
OEB026	TTAATCAAACGTTTGTTCAAAACG
OEB041	TATGGCTAGCATGAAAGTAAGCACCAAAGACA
OEB042	GGTGCTCGAGGTTGGTGAGCGCCACGTCTC
OEB092	Biotin-GCCTTTTCGTTTTGAACAAACGTTTGATTAAAACAAATAGC
OEB093	GCTATTTGTTTTAATCAAACGTTTGTTCAAAACGAAAAGGC
OJH001	CATATGTAAGATTTAAATGCAACCG
OJH002	CTACAAGGTGTGGCATAATGTGT
OJH133	GCAGGAATTCGACTCTCTAGCTTGAGG
OJH179	CCAGATCCGGATATAGTTCCTCCT
OJH180	ACCACAACGGTTTCCCTCTAGATA
OJH185	CAGGAATTCGACTCTCTAGC
OJH186	CTCAGCTAGCTAACTCACATTAATTGCGTTGC
OJW167	GCATGCATGCGTAACACACAGGAAACAGCTATGAAAGTAAGCACCAAAGACAAAATTA
OJW168	GCATGGATCCGAACCGCTACCGTTGGTGAGCGCCACGTCTCCT
OJW169	GCATGCATGCGTAACACACAGGAAACAGCTATGTTGGAGTTCGAAACAAACATAGAC
OJW170	GCATGGATCCGAACCGCTACCGCCGCGTTTATTACGGTTTCTTAAGA
OJW171	GCATGGATCCGGGCAGCGGTATGAAAGTAAGCACCAAAGACAAAATTA
OJW172	GCATGGATCCCTAGTTGGTGAGCGCCACGTC
OJW173	GCATGGATCCGGGCAGCGGTATGTTGGAGTTCGAAACAAACATAGAC
OJW174	GCATGGATCCTTAGCCGCGTTTATTACGGTTTCTTAA
OLM048	GCCGCTAGCATGAAAGTAAGCACCAAAGAC
OLM049	GCGCTCGAGGTTGGTGAGCGCCACGTC
OYD070	GTGTGGAATTGTGAGCGGATAAC

APPENDIX B METHODS B.1. STRAIN CONSTRUCTION

Solid medium plates used for selections were made from lysogeny broth (LB, Lennox) with 1.5% (w/v) Bacto™ agar supplemented with the indicated concentrations of antibiotics/supplements. Integration into the *amyE* locus was assayed for by loss of amylase activity following growth on LB plates supplemented with 1% (w/v) soluble potato starch (EMD) and overlayed with Gram's Iodine (Ricca Chemical Company). Where appropriate, transformants were screened for parental background resistances and on LB plates supplemented with 40 µg ml^{-1} X-gal to visually screen for *lacZ* expression from the P_{spremo} promoter.

BAM043 was created by transformation of *B. subtilis* 168 with genomic DNA isolated from BJH042 selecting for *minD* deletion on 10 µg ml^{-1} kanamycin plates.

BAM075 was created by transformation of *B. subtilis* 168 with linearized pDR111 (P_{hy}-*empty*), selecting for integration at the *amyE* locus on 100 µg ml^{-1} spectinomycin plates.

BAM110 was created by transformation of BJH294 with pJW004 selecting for integration of P_{hy}-*empty* at the *yhdG* locus on 0.8 µg ml^{-1} phleomycin plates and patched on 7.5 µg ml^{-1} chloramphenicol plates to confirm loss of parental resistance.

BAM111 was created by transformation of BJH294 with pJW014 selecting for integration of P_{hy}-*refZ* at the *yhdG* locus on 0.8 µg ml^{-1} phleomycin plates and patched on 7.5 µg ml^{-1} chloramphenicol plates to confirm loss of parental resistance.

BAM142 was created by transformation of *B. subtilis* 168 with genomic DNA isolated from BJH188 selecting for integration of P_{xylA}-*comK* at the *lacA* locus on 1 µg ml^{-1} erythromycin (erm) plus 25 µg ml^{-1} lincomycin (MLS) plates.

BAM168 (selection-screen background) was created by transformation of BAM266 with genomic DNA isolated from BAM043 (*minD::kan)* selecting for integration on 10 µg ml^{-1} kanamycin plates.

BAM229 was created by transformation of *B. subtilis* 168 with linearized pAM083 (Plasmid Construction), selecting for P_{spremo}-*lacZ* integration at the *sacA* locus on 7.5 µg ml^{-1} chloramphenicol plates. The *sacA* locus was screened for size by PCR with OAM124 and OAM125. PCR products of the expected size were sequenced with OJH133 to confirm promoter fusion.

BAM248 was created by transformation of BAM229 with genomic DNA isolated from BJH247 (*refZ::tet*) selecting for integration on 10 µg ml^{-1} tetracycline plates.

BAM266 was created by transformation of BAM248 with genomic DNA isolated from BAM142 selecting for integration of P_{xylA}-*comK* at the *lacA* locus on 1 µg ml^{-1} erythromycin (erm) plus 25 µg ml^{-1} lincomycin (MLS) plates.

BAM374 (P_{hy}-*refZ* in selection-screen background) was created by transformation of super-competent BAM168 cells with genomic DNA isolated from BJH228 (pJW013 integrated at *amyE*) selecting for integration of P_{hy}-*refZ* at the *amyE* locus on 100 µg ml^{-1} spectinomycin plates supplemented with 0.2% (v/v) glucose to repress leaky expression from the P_{hy} promoter (even moderate expression of wildtype *refZ* produces a growth defect in a Δ*minD* background).

BAM390 (P_{hy}-*empty* in the selection-screen background) was created by transformation of super-competent BAM168 cells with genomic DNA isolated from BAM075 (pDR111 integrated at *amyE*) selecting for integration of P_{hy}-*empty* at the *amyE* locus on 100 µg ml^{-1} spectinomycin plates.

BAM400, 403, 407, 409, 411, 440, 443, 444, 449, 462 (P_{hy}-*rLOF* mutants in clean selection-screen background) were created similar to BAM374, except genomic DNA prepared from the original *rLOF* mutant strains (BAM1060-1069) was transformed into super-competent BAM168 cells selecting for integration of P_{hy}-*rLOF* at the *amyE* locus on 100 µg ml^{-1} spectinomycin plates supplemented with 0.2% (v/v) glucose.

BAM428, 431, 434, 436, 450, 451, 454, 455, 457, 490 (P_{hy}-*rLOF* in wildtype background) were created by transformation of *B. subtilis* 168 with genomic DNA prepared from the original *rLOF* mutant strains (BAM1060-1069) selecting for integration of P_{hy}-*rLOF* at the *amyE* locus on 100 µg ml^{-1} spectinomycin plates.

BAM1006-BAM1027 (P_{refZ}-*refZ* and P_{refZ}-*rLOF* Reporter Trapping Strains) were created by transformation of BJH245 and BAM078 (the left and right arm reporter backgrounds, respectively) with linear DNA constructs [UP_{refZ} + P_{refZ}-*rLOF* (or P_{refZ}-*refZ*) + (cat^R) + $DOWN_{refZ}$] generated by assembly (Gibson *et al.*, 2009) of the following DNA fragments:

<u>UP_{refZ}</u>
The upstream chromosomal region flanking the *refZ* gene, including the native promoter, was amplified by PCR with OAM200 and OAM201 from genomic DNA prepared from *B. subtilis* 168, to create a large region of homology for double crossover integration at the native *refZ* locus.

<u>P_{refZ}-*rLOF* (or P_{refZ}-*refZ*)</u>
The wildtype *refZ* sequence and the 10 *rLOF* mutant sequences were amplified by PCR with OAM202 and OAM203 from genomic DNA prepared from BJH228 (pJW013 integrated at *amyE*) and BAM1060-1069 (original *rLOF* mutant strains), respectively. PCR reactions were resolved on 0.8% agarose gels and purified following extraction.

OAM202 introduces 27 bp to the 5' end with homology to the 3' end of the "UP_{refZ}" fragment (see above). OAM203 introduces 24 bp to the 3' end with homology to the 5' end of the "*(cat^R)*" fragment (below).

(cat^R)
A chloramphenicol resistance gene (*cat^R*) and its associated promoter were amplified by PCR with OJH179 and OJH180 from plasmid pKM074, to provide a selectable marker for assembly integration of the assembled construct at the native *refZ* locus.

$DOWN_{refZ}$
The downstream chromosomal region flanking the *refZ* gene was amplified by PCR with OAM204 and OAM205 from genomic DNA prepared from *B. subtilis* 168, to create a large region of homology for double crossover integration at the native *refZ* locus. OAM204 introduces homology to the 3' end of the "*(cat^R)*" fragment.

Assembly reactions (20 µl each) were transformed into 0.2 ml of competent cells with selection for integration at the native *refZ* locus on 7.5 µg ml^{-1} chloramphenicol plates. Genomic DNA was isolated and *refZ* chromosomal regions were screened for size by PCR with OAM200 and OAM205. Fragments of expected size were sequenced with OEB041 or OEB042 to confirm the presence of the *rLOF* mutation.

BAM1060-1069 (P_{hy}-*rLOF* mutants obtained in the selection-screen) were isolated following transformation of super-competent BAM168 cells with linear DNA constructs [UP_{amyE}-*($spec^R$)*-P_{hy} + *refZ** + *lacI-*$DOWN_{amyE}$] generated by Gibson assembly(Gibson *et al.*, 2009) of the following DNA fragments:

UP_{amyE}-*($spec^R$)*-P_{hy}
The upstream chromosomal region flanking the *amyE* gene, the spectinomycin resistance gene and its associated promoter, and the P_{hy} promoter were amplified by PCR with OAM010 and OAM013 from genomic DNA isolated from BJH228 (pJW013 integrated at *amyE*).

*refZ**
refZ open-reading frame was PCR amplified from pJW013 with Phusion High-Fidelity polymerase using OAM122 and OAM165 to create the template for mutagenesis. The resulting template was mutagenized by error-prone PCR with OAM122 and OAM166 using the GeneMorph II Random Mutagenesis Kit according to the manufacturer's protocol (Agilent Technologies #200550) to generate a pool of mutant *refZ* PCR fragments (*refZ**). OAM122 introduces 5' sequence homology to the P_{hy} promoter (see above) and OAM166 introduces 3' sequence homology to the *lacI-*$DOWN_{amyE}$ fragment.

lacI-DOWN$_{amyE}$

The *lacI* repressor gene and the downstream chromosomal region flanking the *amyE* gene were amplified by PCR with OAM001 and OAM012 from genomic DNA isolated from BJH228 (pJW013 integrated at *amyE*).

Assembly reactions were placed on ice and transformed directly into super-competent BAM168, selecting for integration at *amyE* on 100 µg ml^{-1} spectinomycin plates supplemented with 1 mM IPTG. Super-competent BAM168 cells were prepared and transformed as described in *Selection of rLOF mutants* (Experimental Procedures).

BAM1662 and 1663 were created by transformation of the corresponding P$_{hy}$-*rLOF* mutants in a clean selection-screen background with genomic DNA prepared from BAM110 selecting for integration at *yhdG* on 0.8 µg ml^{-1} phleomycin plates supplemented with 0.2% glucose at 30°C overnight.

BAM1664-1676 were created by transformation of the corresponding P$_{hy}$-*rLOF* mutants in a clean selection-screen background with genomic DNA prepared from BAM111 selecting for integration at *yhdG* on 0.8 µg ml^{-1} phleomycin plates supplemented with 0.2% glucose at 30°C overnight.

BJH042 was created by transformation of BDR2353 (*minD::kan*) with linearized pJK013 selecting for integration of P$_{hy}$-*refZ* at the *amyE* locus on 100 µg ml^{-1} spectinomycin plates.

BJH228 was created by transformation of *B. subtilis* 168 with genomic DNA isolated from BJW123 selecting for integration of P$_{hy}$-*refZ* at the *amyE* locus on 100 µg ml^{-1} spectinomycin plates.

BJH294 was created by transformation of *B. subtilis* 168 with genomic DNA isolated from BJH083 (BDR2260) selecting for integration of the chloramphenicol resistance gene at the *yhdG* locus on 5 µg ml^{-1} chloramphenicol plates.

APPENDIX B METHODS B.2. PLASMID CONSTRUCTION

pAM037 [*yycR::*P$_{spremo}$ *(cat)*] was generated by cloning the annealed product of oligos OAM139 and OAM140 into pJW034 between XhoI-HindIII.

pAM046 [*sacA::(cat)*] was generated by subcloning the *cat* (chloramphenicol) resistance cassette from pKM074 into the backbone of pKM062 between SalI-BamHI.

pAM080 [*sacA::*P$_{spremo}$ *(cat)*] was generated by cloning PCR product of OJH133 and OJH001 amplified from pAM037 into pAM046 between EcoRI-HindIII.

pAM083 [*sacA::*P$_{spremo}$-*lacZ (cat)*] was generated by cloning PCR product of OJH185 and OJH186 amplified from pJH036 into pAM080 between HindIII-NheI.

pAM139 (RefZ^{Y43A}-T25) was generated by cloning the PCR product of OAM148 and OAM149 amplified from pRD010 into pKNT25 (empty-T25 plasmid) between SphI-BamHI. Plasmids were confirmed by PCR with OYD070 and OAM149 and products were sequenced to confirm the presence of the *rLOF* mutation.

pAM141 (RefZ^{R106A}-T25) was generated by cloning the PCR product of OAM148 and OAM149 amplified from pRD001 into pKNT25 (empty-T25 plasmid) between SphI-BamHI. Plasmids were confirmed by PCR with OYD070 and OAM149 and products were sequenced to confirm the presence of the *rLOF* mutation.

pAM144 (RefZ^{Y43A}-T18) was generated by cloning the PCR product of OAM148 and OAM149 amplified from pRD010 into pCH363 (empty-T18 plasmid) between SphI-BamHI. Plasmids were confirmed by PCR with OYD070 and OAM149 and products were sequenced to confirm the presence of the *rLOF* mutation.

pAM146 (RefZ^{R106A}-T18) was generated by cloning the PCR product of OAM148 and OAM149 amplified from pRD001 into pCH363 (empty-T18 plasmid) between SphI-BamHI. Plasmids were confirmed by PCR with OYD070 and OAM149 and products were sequenced to confirm the presence of the *rLOF* mutation.

pAM152-161 (rLOF-T18 B2H plasmids) were generated by cloning the PCR products of OAM148 and OAM149 from genomic DNA prepared from corresponding left arm rLOF Reporter Trapping strains (BAM1006-1026, even numbered strains) into pCH363 (empty-T18 plasmid) between SphI-BamHI. Plasmids were confirmed by PCR with OYD070 and OAM149 and products were sequenced to confirm the presence of the *rLOF* mutations.

pAM162-171 (rLOF-T25 B2H plasmids) were generated by cloning the PCR products of OAM148 and OAM149 from genomic DNA prepared from corresponding left arm rLOF Reporter Trapping strains (BAM1006-1026, even numbered strains) into pKNT25 (empty-T25 plasmid) between SphI-BamHI. Plasmids were confirmed by PCR with OYD070 and OAM149 and products were sequenced to confirm the presence of the *rLOF* mutations.

pEB013 (RefZ^{R116S}-His6) was generated by cloning the PCR product from OEB041 and OEB042 amplification of genomic DNA from BAM1064 into pET-24b (+) (NheI and XhoI). Confirmed by sequencing.

pEB014 (RefZ^{E117G}-His6) was generated by cloning PCR product from OEB041 and OEB042 amplification of genomic DNA from BAM1067 into pET-24b (+) (NheI and XhoI). Confirmed by sequencing.

pEB015 (RefZ^{E117D}-His6) was generated by cloning PCR product from OEB041 and OEB042 amplification of genomic DNA from BAM1066 into pET-24b (+) (NheI and XhoI). Confirmed by sequencing.

pEB016 (RefZ^{E179K}-His6) was generated by cloning PCR product from OEB041 and OEB042 amplification of genomic DNA from BAM1069 into pET-24b (+) (NheI and XhoI). Confirmed by sequencing.

pEB017 (RefZ^{R102C}-His6) was generated by cloning PCR product from OEB041 and OEB042 amplification of genomic DNA from BAM1062 into pET-24b (+) (NheI and XhoI). Confirmed by sequencing.

pEB018 (RefZ^{R102S}-His6) generated by cloning PCR product from OEB041 and OEB042 amplification of genomic DNA from BAM1063 into pET-24b (+) (NheI and XhoI). Confirmed by sequencing.

pEB019 (RefZ^{E53K}-His6) generated by cloning PCR product from OEB041 and OEB042 amplification of genomic DNA from BAM1060 into pET-24b (+) (NheI and XhoI). Confirmed by sequencing.

pEB020 (RefZ^{E61K}-His6) was generated by cloning PCR product from OEB041 and OEB042 amplification of genomic DNA from BAM1061 into pET-24b (+) (NheI and XhoI). Confirmed by sequencing.

pEB021 (RefZ^{L153R}-His6) was generated by cloning PCR product from OEB041 and OEB042 amplification of genomic DNA from BAM1068 into pET-24b (+) (NheI and XhoI). Confirmed by sequencing.
pEB022 (RefZ^{R116W}-His6) was generated by cloning PCR product from OEB041 and OEB042 amplification of genomic DNA from BAM1065 into pET-24b (+) (NheI and XhoI). Confirmed by sequencing.

pJW096 (RefZ-T25) was generated by cloning PCR product from OJW167 and OJW168 amplification of genomic DNA from *B. subtilis* wild-type PY79 into pKNT25 (SphI and BamHI). Confirmed by restriction enzyme digestion.

pJW097 (RefZ-T18) was generated by cloning PCR product from OJW167 and OJW168 amplification of genomic DNA from *B. subtilis* wild-type PY79 into pCH363 (SphI and BamHI). Confirmed by restriction enzyme digestion.

pJW098 (FtsZ-T25) was generated by cloning PCR product from OJW169 and OJW170 amplification of genomic DNA from *B. subtilis* wild-type PY79 into pKNT25 (SphI and BamHI). Confirmed by restriction enzyme digestion.

pJW099 (FtsZ-T18) was generated by cloning PCR product from OJW169 and OJW170 amplification of genomic DNA from *B. subtilis* wild-type PY79 into pCH363 (SphI and BamHI). Confirmed by restriction enzyme digestion.

pJW100 (T25-RefZ) was generated by cloning PCR product from OJW171 and OJW172 amplification of genomic DNA from *B. subtilis* wild-type PY79 into pKT25 (EcoRI and BamHI). Confirmed by restriction enzyme digestion.

pJW101 (T18-RefZ) was generated by cloning PCR product from OJW171 and OJW172 amplification of genomic DNA from *B. subtilis* wild-type PY79 into pCH364 (EcoRI and BamHI). Confirmed by restriction enzyme digestion.

pJW102 (T25-FtsZ) was generated by cloning PCR product from OJW173 and OJW174 amplification of genomic DNA from *B. subtilis* wild-type PY79 into pKT25 (EcoRI and BamHI). Confirmed by restriction enzyme digestion.

pJW103 (T18-FtsZ) was generated by cloning PCR product from OJW173 and OJW174 amplification of genomic DNA from *B. subtilis* wild-type PY79 into pCH364 (EcoRI and BamHI). Confirmed by restriction enzyme digestion.

pLM025 ($RefZ^{WT}$-His6) was generated by cloning PCR product from OLM048 and OLM049 amplification of genomic DNA from PY79 into pET-24b (+) (NheI and XhoI). Confirmed by sequencing.

APPENDIX C

CHAPTER IV SUPPLEMENTAL

APPENDIX C TABLE C.1. STRAINS

Strain	Description	Reference/Figure
B. subtilis 168	*Bacillus subtilis* laboratory strain 168 *trpC2*	Bacillus Genetic Stock Center (1A866)
B. subtilis PY79	Laboratory strain	(Youngman *et al.*, 1983)
DH5α	*F-, endA1, glnV44, thi-1, recA1, relA1, gyrA96, deoR, nupG, Φ80dlacZΔM15, Δ(lacZYA-argF)U169, hsdR17(r_K^- m_K^+), λ–*	
DHP1	*F-, cya-99, araD139, galE15, galK16, rpsL1 (Strr), hsdR2, mcrA1,mcrB1*	Obtained from Thomas Bernhardt
PY79		
BAM1560	*refZ::erm*	
BAM1561	*ΔrefZ*	
BAM1580	*refZ::refZ (WT)-gfp (Cambell) (spec)*	Figure IV.1
BAM1581	*refZ::refZ (E53K)-gfp (Cambell) (spec)*	Figure IV.1
BAM1582	*refZ::refZ (E61K)-gfp (Cambell) (spec)*	Figure IV.1
BAM1583	*refZ::refZ (R102C)-gfp (Cambell) (spec)*	Figure IV.1
BAM1584	*refZ::refZ (R102S)-gfp (Cambell) (spec)*	Figure IV.1
BAM1585	*refZ::refZ (R116S)-gfp (Cambell) (spec)*	Figure IV.1
BAM1586	*refZ::refZ (R116W)-gfp (Cambell) (spec)*	Figure IV.1
BAM1587	*refZ::refZ (E117D)-gfp (Cambell) (spec)*	Figure IV.1
BAM1588	*refZ::refZ (E117G)-gfp (Cambell) (spec)*	Figure IV.1
BAM1589	*refZ::refZ (L153R)-gfp (Cambell) (spec)*	Figure IV.1
BAM1590	*refZ::refZ (E179K)-gfp (Cambell) (spec)*	Figure IV.1
BAM1591	*refZ::refZ (Y43A)-gfp (Cambell) (spec)*	Figure IV.1
BAM1592	*refZ::refZ (Y44A)-gfp (Cambell) (spec)*	Figure IV.1
BAM1593	*refZ::refZ (R106A)-gfp (Cambell) (spec)*	Figure IV.1
BAM1594	*refZ::refZ (E107A)-gfp (Cambell) (spec)*	Figure IV.1
BDR2128	*amyE::P_{spoIIE}-gfp (spec)*	Figure IV.5A
BJW329	*amyE::P_{spoIIE}-gfp (spec), noc::erm*	Figure IV.5A
BJW330	*amyE::P_{spoIIE}-gfp (spec), refZ::tet, noc::erm*	Figure IV.5A
BRB447	*amyE::P_{spoIIE}-gfp (spec), refZ::tet*	Figure IV.5A
***B. subtilis* 168**		
BAM067	*amyE::P_{spoIIQ}-cfp (cat)*	Figure IV.8
BAM908	*RBM_{5mu}, noc::erm*	
BAM909	*RBM_{5mu}, amyE::P_{spoIIG}-cfp (spec)*	Figure IV.4
BAM912	*amyE::P_{spoIIG}-cfp (spec), noc::erm*	Figure IV.4
BAM920	*RBM_{5mu}, amyE::P_{spoIIG}-cfp (spec), noc::erm*	Figure IV.4
BAM1280	*noc::erm, refZ::refZ (WT) (cat)*	Figure IV.6B

Appendix C Table C.1. Strains, continued…

Strain	Description	Reference/Figure
BAM1281	*noc::erm, refZ::refZ (E53K) (cat)*	Figure IV.6B
BAM1282	*noc::erm, refZ::refZ (E61K) (cat)*	Figure IV.6B
BAM1283	*noc::erm, refZ::refZ (R102C) (cat)*	Figure IV.6B
BAM1284	*noc::erm, refZ::refZ (R102S) (cat)*	Figure IV.6B
BAM1285	*noc::erm, refZ::refZ (R116S) (cat)*	Figure IV.6B
BAM1286	*noc::erm, refZ::refZ (R116W) (cat)*	Figure IV.6B
BAM1287	*noc::erm, refZ::refZ (E117D) (cat)*	Figure IV.6B
BAM1288	*noc::erm, refZ::refZ (E117G) (cat)*	Figure IV.6B
BAM1289	*noc::erm, refZ::refZ (L153R) (cat)*	Figure IV.6B
BAM1290	*noc::erm, refZ::refZ (E179K) (cat)*	Figure IV.6B
BAM1291	*noc::erm, refZ::refZ (Y43A) (cat)*	Figure IV.6B
BAM1292	*noc::erm, refZ::refZ (Y44A) (cat)*	Figure IV.6B
BAM1293	*noc::erm, refZ::refZ (R106A) (cat)*	Figure IV.6B
BAM1294	*noc::erm, refZ::refZ (E107A) (cat)*	Figure IV.6B
BAM1295	*refZ::cat, noc::erm*	Figure IV.6B
BAM1296	*refZ::erm*	
BAM1305	*noc::erm, refZ::refZ (WT) (cat), amyE::P_{cotD}-lacZ (spec)*	Figure IV.5
BAM1306	*noc::erm, refZ::refZ (E53K) (cat), amyE::P_{cotD}-lacZ (spec)*	Figure IV.6A
BAM1307	*noc::erm, refZ::refZ (E61K) (cat), amyE::P_{cotD}-lacZ (spec)*	Figure IV.6A
BAM1308	*noc::erm, refZ::refZ (R102C) (cat), amyE::P_{cotD}-lacZ (spec)*	Figure IV.6A
BAM1309	*noc::erm, refZ::refZ (R102S) (cat), amyE::P_{cotD}-lacZ (spec)*	Figure IV.6A
BAM1310	*noc::erm, refZ::refZ (R116S) (cat), amyE::P_{cotD}-lacZ (spec)*	Figure IV.6A
BAM1311	*noc::erm, refZ::refZ (R116W) (cat), amyE::P_{cotD}-lacZ (spec)*	Figure IV.6A
BAM1312	*noc::erm, refZ::refZ (E117D) (cat), amyE::P_{cotD}-lacZ (spec)*	Figure IV.6A
BAM1313	*noc::erm, refZ::refZ (E117G) (cat), amyE::P_{cotD}-lacZ (spec)*	Figure IV.6A
BAM1314	*noc::erm, refZ::refZ (L153R) (cat), amyE::P_{cotD}-lacZ (spec)*	Figure IV.6A
BAM1315	*noc::erm, refZ::refZ (E179K) (cat), amyE::P_{cotD}-lacZ (spec)*	Figure IV.6A
BAM1316	*noc::erm, refZ::refZ (Y43A) (cat), amyE::P_{cotD}-lacZ (spec)*	Figure IV.6A
BAM1317	*noc::erm, refZ::refZ (Y44A) (cat), amyE::P_{cotD}-lacZ (spec)*	Figure IV.6A
BAM1318	*noc::erm, refZ::refZ (R106A) (cat), amyE::P_{cotD}-lacZ (spec)*	Figure IV.6A
BAM1319	*noc::erm, refZ::refZ (E107A) (cat), amyE::P_{cotD}-lacZ (spec)*	Figure IV.6A
BAM1321	*noc::erm, amyE::P_{cotD}-lacZ (spec)*	Figure IV.6A
BAM1323	*amyE::P_{cotD}-lacZ (spec)*	Figure IV.6A
BAM1324	*refZ::refZ (WT) (cat), amyE::P_{cotD}-lacZ (spec)*	Figure IV.6A
BAM1325	*refZ::refZ (E53K) (cat), amyE::P_{cotD}-lacZ (spec)*	Figure IV.6A
BAM1326	*refZ::refZ (E61K) (cat), amyE::P_{cotD}-lacZ (spec)*	Figure IV.6A
BAM1327	*refZ::refZ (R102C) (cat), amyE::P_{cotD}-lacZ (spec)*	Figure IV.6A
BAM1328	*refZ::refZ (R102S) (cat), amyE::P_{cotD}-lacZ (spec)*	Figure IV.6A
BAM1329	*refZ::refZ (R116S) (cat), amyE::P_{cotD}-lacZ (spec)*	Figure IV.6A
BAM1330	*refZ::refZ (R116W) (cat), amyE::P_{cotD}-lacZ (spec)*	Figure IV.6A

Appendix C Table C.1. Strains, continued…

Strain	Description	Reference/Figure
BAM1331	*refZ::refZ (E117D) (cat), amyE::P_{cotD}-lacZ (spec)*	Figure IV.6A
BAM1332	*refZ::refZ (E117G) (cat), amyE::P_{cotD}-lacZ (spec)*	Figure IV.6A
BAM1333	*refZ::refZ (L153R) (cat), amyE::P_{cotD}-lacZ (spec)*	Figure IV.6A
BAM1334	*refZ::refZ (E179K) (cat), amyE::P_{cotD}-lacZ (spec)*	Figure IV.6A
BAM1335	*refZ::refZ (Y43A) (cat), amyE::P_{cotD}-lacZ (spec)*	Figure IV.6A
BAM1336	*refZ::refZ (Y44A) (cat), amyE::P_{cotD}-lacZ (spec)*	Figure IV.6A
BAM1337	*refZ::refZ (R106A) (cat), amyE::P_{cotD}-lacZ (spec)*	Figure IV.6A
BAM1338	*refZ::refZ (E107A) (cat), amyE::P_{cotD}-lacZ (spec)*	Figure IV.6A
BAM1339	*ΔrefZ*	
BAM1359	*ΔrefZ, noc::erm*	Figure IV.6B
BAM1409	*ΔrefZ, minD::kan*	Figure IV.5B
BAM1460	*RBM_{Tmu}, refZ::refZ-gfp (Cambell) (spec)*	Figure IV.2
BAM1463	*RBM_{6mu}, refZ::refZ-gfp (Cambell) (spec)*	Figure IV.2
BAM1550	*ΔrefZ, amyE::P_{cotD}-lacZ (spec)*	Figure IV.3A
BAM1557	*ΔrefZ, sepF::erm*	Figure IV.5B
BAM1558	*ΔrefZ, Δ(soj-spo0J)::cat*	
BAM1559	*ΔrefZ, ezrA::kan, amyE::P_{cotD}-lacZ (spec)*	Figure IV.3A
BAM1562	*RBM_{5mu}, noc::erm, amyE::P_{cotD}-lacZ (spec)*	Figure IV.3A
BAM1563	*ezrA::kan, amyE::P_{cotD}-lacZ (spec)*	Figure IV.3A
BAM1564	*RBM_{5mu}, ezrA::kan, amyE::P_{cotD}-lacZ (spec)*	Figure IV.3A
BAM1565	*RBM_{5mu}, Δ(soj-spo0J)::cat*	
BAM1566	*ΔrefZ, Δ(soj-spo0J)::cat, pelB::spo0J (kan)*	Figure IV.5B
BAM1567	*RBM_{5mu}, Δ(soj-spo0J)::cat, pelB::spo0J (kan)*	Figure IV.5B
BAM1568	*ΔrefZ, Δ(soj-spo0J)::cat, pelB::spo0J (kan), amyE::P_{cotD}-lacZ (spec)*	Figure IV.3A
BAM1569	*RBM_{5mu}, Δ(soj-spo0J)::cat, pelB::spo0J (kan), amyE::P_{cotD}-lacZ (spec)*	Figure IV.3A
BAM1573	*RBM_{5mu}, amyE::P_{cotD}-lacZ (spec)*	Figure IV.3A
BAM1577	*ΔrefZ, sepF::erm, amyE::P_{cotD}-lacZ (spec)*	Figure IV.3A
BAM1600	*amyE::P_{spoIIQ}-cfp (cat), refZ::tet*	Figure IV.8
BAM1601	*RBM_{5mu}, amyE::P_{spoIIQ}-cfp (cat)*	Figure IV.8
BAM1602	*amyE::P_{spoIIQ}-cfp (cat), noc::erm*	Figure IV.8
BAM1604	*amyE::P_{spoIIG}-cfp (spec), noc::erm, refZ::tet*	Figure IV.4
BAM1605	*RBM_{5mu}, amyE::P_{spoIIG}-cfp (spec), refZ::tet*	Figure IV.4
BAM1609	*RBM_{5mu}, amyE::P_{spoIIG}-cfp (spec), refZ::tet, noc::erm*	Figure IV.4
BAM1610	*amyE::P_{spoIIQ}-cfp (cat), refZ::tet, noc::erm*	Figure IV.8
BAM1611	*RBM_{5mu}, amyE::P_{spoIIQ}-cfp (cat), noc::erm*	Figure IV.8
BAM1612	*RBM_{5mu}, amyE::P_{spoIIQ}-cfp (cat), refZ::tet*	Figure IV.8
BAM1613	*RBM_{5mu}, amyE::P_{spoIIQ}-cfp (cat), refZ::tet, noc::erm*	Figure IV.8
BJH205	*RBM_{5mu}*	(Miller *et al.*, 2016)
BJH214	*refZ::refZ-gfp (Cambell) (spec)*	Figure IV.2
BJH215	*RBM_{5mu}, refZ::refZ-gfp (Cambell) (spec)*	Figure IV.2

Appendix C Table C.1. Strains, continued…

Strain	Description	Reference/Figure
BJH255	*refZ::cat*	(Miller *et al.*, 2016)
BKE15390	*sepF::erm*	Bacillus Genetic Stock Center
BKE29630	*refZ::erm*	Bacillus Genetic Stock Center
BAM1654	*amyE::P_{spoIIQ}-cfp (cat)*	Figure IV.9
BAM1655	*amyE::P_{spoIIQ}-cfp (cat), refZ::tet*	Figure IV.9
BAM1656	*RBM_{5mu}, amyE::P_{spoIIQ}-cfp (cat)*	Figure IV.9
BAM1657	*amyE::P_{spoIIQ}-cfp (cat), noc::erm*	Figure IV.9
BAM1658	*amyE::P_{spoIIQ}-cfp (cat), refZ::tet, noc::erm*	Figure IV.9
BAM1659	*RBM_{5mu}, amyE::P_{spoIIQ}-cfp (cat), noc::erm*	Figure IV.9
BAM1660	*RBM_{5mu}, amyE::P_{spoIIQ}-cfp (cat), refZ::tet*	Figure IV.9
BAM1661	*RBM_{5mu}, amyE::P_{spoIIQ}-cfp (cat), refZ::tet, noc::erm*	Figure IV.9
BAM1688	*yycR::tetO(48)(cat), ycgO::P_{ftsW}-tetR-cfp (phleo)*	Figure IV.10
BAM1692	*yycR::tetO(48)(cat), ycgO::P_{ftsW}-tetR-cfp (phleo), refZ::tet*	Figure IV.10
BAM1693	*yycR::tetO(48)(cat), ycgO::P_{ftsW}-tetR-cfp (phleo), noc::erm*	Figure IV.10
BAM464	*Δ(soj-spo0J)::cat, pelB::spo0J (kan)*	Figure IV.5B
BAM043	*minD::kan*	Figure IV.5B
BAM102	*ezrA::kan*	Figure IV.5B

APPENDIX C TABLE C.2. PLASMIDS

Plasmid	Description	Reference/Figure/Use
pAM177	*refZ(E53K)-gfp (amp)*	This work
pAM178	*refZ(E61K)-gfp (amp)*	This work
pAM179	*refZ(R102C)-gfp (amp)*	This work
pAM180	*refZ(R102S)-gfp (amp)*	This work
pAM181	*refZ(R116S)-gfp (amp)*	This work
pAM182	*refZ(R116W)-gfp (amp)*	This work
pAM183	*refZ(E117D)-gfp (amp)*	This work
pAM184	*refZ(E117G)-gfp (amp)*	This work
pAM185	*refZ(L153R)-gfp (amp)*	This work
pAM186	*refZ(E179K)-gfp (amp)*	This work
pAM187	*refZ(Y43A)-gfp (amp)*	This work
pAM188	*refZ(Y44A)-gfp (amp)*	This work
pAM189	*refZ(R106A)-gfp (amp)*	This work
pAM190	*refZ(E107A)-gfp (amp)*	This work